Aus der
Hals-, Nasen-, Ohren-Klinik und Poliklinik –
Plastische Operationen der
Universitätsmedizin der Johannes Gutenberg-Universität Mainz

Identifizierung Krankheits-relevanter Mechanismen in Kopf-Hals-Tumoren

Neuartige Biomarker und diagnostische Hilfsmittel

Habilitationsschrift
zur Erlangung der venia legendi
für das Fach
„Molekulare Medizin“

Universitätsmedizin der Johannes Gutenberg-Universität Mainz

Vorgelegt von

Dr. Désirée Gül
aus Wiesbaden

Mainz, 2022

WISSENSCHAFTLICHE ORIGINALPUBLIKATIONEN DER KUMULATIVEN HABILITATIONSSCHRIFT (ERST- UND LETZTAUTORENSCHAFTEN)

INDEX OF SCIENTIFIC PUBLICATIONS SUMMARIZED IN THIS PROFESSORIAL DISSERTATION (FIRST AND SENIOR AUTHORSHIP)

I. Gribko, A.; Hahlbrock, A.; Strieth, S.; Becker, S.; Hagemann, J.; Deichelbohrer, M.; Hildebrandt, A.; Habtemichael, N.; **Wunsch, D**. Disease-relevant signalling-pathways in head and neck cancer: Taspase1's proteolytic activity fine-tunes TFIIA function. *Sci Rep* 2017, 7, 14937, doi:10.1038/s41598-017-14814-x.

II. Kiweler, N.*; **Wunsch, D.***; Wirth, M.; Mahendrarajah, N.; Schneider, G.; Stauber, R.H.; Brenner, W.; Butter, F.; Kramer, O.H. Histone deacetylase inhibitors dysregulate DNA repair proteins and antagonize metastasis-associated processes. *J Cancer Res Clin Oncol* 2020, *146*, 343-356, doi:10.1007/s00432-019-03118-4.*equal first author contribution

III. **Gül, D.** , Habtemichael , N., Dietrich, D., Dietrich, J., Gößwein, D., Khamis, A., Deuss, E., Künzel, J., Schneider, G., Strieth, S., Stauber RH. Identification of cytokeratin24 as a tumor suppressor for the management of head and neck cancer. *Biological Chemistry* 2021. doi:doi:10.1515/hsz-2021-0287.

IV. **Gül D.,** Schweitzer A., Khamis A., Knauer S. K., Ding G. B., Freudelsperger L., Karampinis I., Strieth S., Hagemann J., Stauber R. H. Impact of Secretion-Active Osteoblast-Specific Factor 2 in Promoting Progression and Metastasis of Head and Neck Cancer. Cancers (Basel). 2022;14(9).

V. Gribko, A.; Stiefel, J.; Liebetanz, L.; Nagel, S.M.; Künzel, J.; Wandrey, M.; Hagemann, J.; Stauber, R.H.; Freese, C.; **Gül, D**. IsoMAG—An Automated System for the Immunomagnetic Isolation of Squamous Cell Carcinoma-Derived Circulating Tumor Cells. *Diagnostics* 2021, *11*, 2040.

INHALT

1. ZUSAMMENFASSUNG

Maligne Erkrankungen des Kopf-Hals Bereiches zählen zu den häufigsten Tumorerkrankungen weltweit. Mit mindestens 890.000 Neuerkrankungen pro Jahr zählen die Plattenepithelkarzinome der Kopf-Hals Region (*head and neck squamous cell carcinoma*, HNSCC) zur sechshäufigsten Krebserkrankung weltweit, und machen den Hauptanteil der Kopf-Hals-Tumore aus. Trotz voranschreitender Forschung hat sich die Prognose für einen Großteil der Patienten mit Kopf-Hals-Tumoren in den letzten Jahrzehnten kaum verbessert. Die hohe Sterblichkeitsrate kann dabei sowohl auf eine späte Diagnose, als auch auf das Fehlen von verlässlichen *Biomarkern*, und dem bruchstückhaften Verständis Krankheits-relevanter Signalwege zurückgeführt werden. Obwohl der Einsatz von Kinase-Inhibitoren und neuartigen Antikörpern zunehmend an klinischer Relevanz gewonnen hat, besteht nach wie vor ein dringender Bedarf an wirksamen Therapien und neuen Wirkstoffzielen.

Übergeordnetes Ziel der hier zusammengefassten Studien war die Erforschung und Entschlüsselung molekularer Mechanismen, welche kausal an der Entstehung, Rezidivbildung und Metastasierung von Kopf-Hals-Tumoren beteiligt sind. Dabei steht ein translationaler Ansatz im Fokus, welcher darauf abzielt, gewonnene Erkenntnisse in therapeutisch nutzbare Biomarker und neue diagnostische Hilfsmittel zu übersetzen (*„from bench to bedside"*). Durch die bioinformatische Auswertung von klinischen Patientendaten kombiniert mit Expressionsanalysen, sowie molekularbiologische Untersuchungen (siehe *Figure 1*) konnten Krankheits-relevante (Protease-)Netzwerke detailliert charakterisiert, sowie die (extra)zellulären Strukturproteine Zytokeratin24 und Periostin/OSF-2 als mögliche prediktive Biomarker für HNSCC identifiziert werden. Ein weiterer Fokus lag zudem auf der Analyse von Metastase-Signalwegen, sowie dem Einfluss möglicher Chemotherapeutika (HDAC-Inhibitoren) auf diesen Prozess.

Die Protease Threonin Aspartase 1 (Taspase1) spielt eine entscheidende Rolle bei der Entstehung verschiedener Tumorerkrankungen, so auch bei HNSCC. Durch genomweite Expressionsuntersuchungen konnten wir eine vermehrte Taspase1-Expression in Kopf-Hals-Primärtumoren und korrespondierenden Metastasen zeigen (I, Gribko *et al*. 2017). Interessanterweise ergaben molekularbiologische Untersuchungen des Taspase1-Substrats TFIIA ein evolutionär konserviertes nukleäres Exportsignal (NES), welches einer Kernlokalisierung und damit der Transkriptionsaktivität von TFIIA entgegenwirkt. Durch die Taspase1-vermittelte

proteolytische Prozessierung von TFIIA wird das NES maskiert, wodurch die Kernlokalisierung und transkriptionelle Aktivierung von TFIIA-Zielgenen, wie CDKN2A, verstärkt wird. Zusammenfassend konnten wir einen bisher unbekannten Mechanismus beschreiben, wie es durch zelluläre Lokalisierung und Taspase1-Spaltung zur Feinregulation der transkriptionellen Aktivität von TFIIA in HNSCC kommt (I, Gribko *et al*. 2017).

Die Entstehung von lokalen und Fernmetastasen stellt eine klinisch relevante Herausforderung bei einer Vielzahl von Tumorerkrankungen, so auch HNSCC dar. Durch den Einsatz von Histondeacetylase-Inhibitoren (HDACi) konnten wir zeigen, dass die damit einhergehende vermehrte Acetylierung von zellulären Proteinen, Metastasierungsprozessen entgegen wirken kann (II, Kiweler, Wünsch *et al.* 2020). Unsere Daten verdeutlichen, dass HDACi allein und in Kombination mit etablierten Chemotherapeutika die Expression von DNA-Reparaturproteinen verändern und dadurch DNA-Schäden und Apoptose auslösen. HDACi unterdrücken die epithelial-mesenchymale Transition und beeinträchtigen die DNA-Integrität von Krebszellen (II, Kiweler, Wünsch *et al.* 2020).

Anhand unserer Daten aus den Expressionsstudien haben wir weitere Signalnetzwerke rekonstruiert, welche in Tumoren im Vergleich zu Metastasen unterschiedlich aktiviert werden, wie z. B. mesenchymal-epitheliale Transition, und strukturelle Integritätsnetzwerke (III, Gül *et al.* 2021). Als *Proof-of-Principle*-Studie führten wir funktionelle Analysen eines neuartigen Zytokeratins, Zytokeratin24 (cKRT24), durch, welches bislang noch nicht als Biomarker für Tumore beschrieben wurde. Die umfangreichen Ergebnisse der Studie, wie die mit einer schlechten Prognose korrelierende verminderte Expression von cKRT24 in Primärtumoren und Metastasen, sowie der negative Effekt von cKRT24-Überexpression auf die Viabilität von HNSCC Zellen *in vitro* und *in vivo*, unterstützen unsere Hypothese, welche cKRT24 eine Funktion als Tumorsuppressor zuschreibt (III, Gül *et al.* 2021).

Ein weiterer vielversprechender Biomarker Kandidat, welcher unter den Top 3 der am stärksten überexprimierten Proteine in den untersuchten Tumoren und Metastasen identifiziert werden konnte, ist Periostin/OSF-2. Ein hoher OSF-2-Level korrelierte hier besonders bei HPV-negativen HNSCC-Patienten mit dem Auftreten von Metastasen und einem reduzierten Gesamtüberleben (IV, Gül *et al.* 2022). Unsere Ergebnisse weisen OSF-2 als potenziellen prognostischen Biomarker und Wirkstoffziel aus, welches die Metastasierung fördert, indem es

primär das zelluläre Überleben in der Mikroumgebung des Tumors und in (Lymphknoten-) Metastasen unterstützt (IV, Gül *et al.* 2022).

Um die Früherkennung und Behandlung (metastasierender) Tumorerkrankungen zu verbessern, sowie um neue Kandidaten für HNSCC-spezifische Biomarker zu identifizieren, gilt die Detektion und Untersuchung von zirkulierenden Tumor-Zellen („circulating tumor cells“, CTCs) als erfolgversprechender Ansatz. Unter Verwendung verschiedener Plattenepithelkarzinom-Zelllinien haben wir ein immunmagnetisches Isolationsprotokoll etabliert, welches basierend auf der Expression tumor-spezifischer Oberflächenmarker (EpCAM, CSV) eine hocheffiziente, automatisierte CTC-Anreicherung durch das *Fraunhofer IsoMAG IMS*-System erlaubt (V, Gribko *et al.* 2021). Zusammenfassend konnten wir zeigen, dass das IsoMAG-System den Nachweis und die Isolation von CTCs aus HNSCC-Patientenblut bei gleichzeitiger signifikanter Verringerung der Leukozytenkontamination ermöglicht. Zukünftige Entwicklungen zielen darauf ab, das IsoMAG IMS-System in einen vollautomatisierten mikrofluidischen Isolationsworkflow zu integrieren, und somit die Einzelzell-Detektion auch in der klinischen Routine weiter zu erleichtern (*Figure 1*) (V, Gribko *et al.* 2021).

Zusammenfassend konnten im Rahmen dieser Arbeit entscheidende Einblicke in Krankheits-relevante Signalwege und Mechanismen der Tumorbiologie von Kopf-Hals-Tumoren gewonnen werden. Die Bedeutung dieser neuen Erkenntnisse ist dabei nicht nur im grundlagenwissenschaftlichen Bereich der Krebsentstehung zu sehen, sondern sie besitzen zudem eine hohe translationale Relevanz für ihre zukünftige klinische Anwendung.

1. SUMMARY

Head and neck cancers (HNC) are among the most common malignant neoplasms in humans. The most common entity of HNC is solid squamous cell carcinoma (HNSCC) which is the sixth most malignant tumor worldwide with yearly 890.000 new cases. Due to the late disease presentation of the patient, lack of suitable biomarkers, and corresponding drugs for individually targeted therapy approaches, survival rates for HNSCC have not improved significantly within the last years. Although the use of kinase inhibitors or antibodies has gained increasing clinical relevance, there is still urgent need for more effective therapies, innovative predictive tools, and relevant drug targets.

Therefore, the aim of the summarized studies was the investigation and decoding of molecular mechanisms involved in the development, relapse, and metastasis of HNC. Studies were conducted following a translational, interdisciplinary approach which aims at translation of gained knowledge into clinically applicable biomarkers and new diagnostic tools ("from bench to bedside"). By bioinformatic evaluation of clinical patient data combined with expression analyzes and molecularbiological experiments (Figure 1), we uncovered and characterized disease-relevant (protease)networks, and identified novel predictive biomarkers for HNC, such as the (extra)cellular structural proteins cytokeratin24 and periostin/OSF-2. The studies also focused on the analysis of metastasis pathways, as well as the influence of potential chemotherapeutic agents (HDAC inhibitors) on this process.

The protease threonine aspartase 1 (Taspase1) plays a crucial role in the development of various tumor diseases including HNC. Genome-wide expression profiling of matched HNC samples revealed significant upegulation of Taspase1 in primary tumors and metastases (I, Gribko *et al*. 2017). Unexpectedly, we identified an evolutionary conserved nuclear export signal (NES) counteracting nuclear localization and thus, transcriptional activity of TFIIA. Notably, proteolytic processing of TFIIA by Taspase1 was found to mask the NES, thereby promoting nuclear localization and transcriptional activation of TFIIA target genes, such as CDKN2A. Collectively, we here describe a hitherto unknown mechanism how cellular localization and Taspase1 cleavage fine-tunes transcriptional activity of TFIIA in HNSCC (I, Gribko *et al*. 2017).

The development of local and distant metastases is a clinically relevant challenge in a variety of tumor diseases, including HNSCC. By using histone deacetylase inhibitors (HDACi)

we were able to show that HDACi-induced increased acetylation of cellular proteins antagonize metastasis-associated processes (II, Kiweler, Wünsch *et al.* 2020). We show that HDACi interfere with DNA repair protein expression and trigger DNA damage and apoptosis alone and in combination with established chemotherapeutics. HDACi suppress the epithelial-mesenchymal-transition (EMT) and compromise the DNA integrity of cancer cells (II, Kiweler, Wünsch *et al.* 2020).

Based on our expression datasets, we provided additional signaling networks differentially activated in tumors *versus* metastases, such as mesenchymal-epithelial transition, and structural integrity networks (III, Gül *et al.* 2021). As a proof of principle study, we exploited the data sets and performed functional analyses of a novel cytokeratin, cytokeratin24 (cKRT24), which had not been described as biomarker for tumors before. The extensive results of the study, such as correlation of low cKRT24 expression with poor overall survival in HNSCC, as well as the negative effect of cKRT24 overexpression on the viability of HNSCC cells in vitro and in vivo, support our hypothesis describing cKRT24 as a tumor suppressor in HNSCC (III, Gül *et al.* 2021).

As another promising biomarker candidate we identified osteoblast-specific factor 2 (OSF-2) as significantly overexpressed in metastases and primary tumors compared to normal tissue (IV, Gül *et al.* 2022). High OSF-2 levels correlate with metastatic disease and reduced overall survival of predominantly HPV-negative HNC patients. The fact that OSF-2 was strongly expressed in tumor-associated fibroblasts, and we could identify a functional protein secretion signal suggests its tumor microenvironment-promoting function. Collectively, we suggest OSF-2 as a potential prognostic biomarker and drug target, promoting metastasis by supporting the tumor microenvironment and cellular survival of (lymph node) metastases rather than by influencing primary cancer cell proliferation or therapy resistance (IV, Gül *et al.* 2022).

To improve early detection and treatment of (metastatic) tumor diseases, as well as to identify novel candidates for HNC biomarkers, the detection and analysis of circulating tumor cells (CTCs) is a promising approach. By using different squamous cell carcinoma cell lines, we developed an isolation protocol for automated immunomagnetic CTC enrichment based on tumor-specific cell surface markers (EpCAM, CSV) by the *Fraunhofer IsoMAG IMS* system (V, Gribko *et al.* 2021). In summary, we demonstrate that the IsoMAG system allows the detection

and isolation of CTCs from HNSCC patient blood in an automated process with a significant leukocyte count reduction. Future developments seek to integrate the IsoMAG IMS system into a fully-automated microfluidic-based isolation workflow to further facilitate single CTC detection also in clinical routine (Figure 1) (V, Gribko *et al.* 2021).

Collectively, this work discovered new insights into disease-relevant signaling pathways and mechanisms relevant, but not limited to head and neck tumors. These findings not only improve our understanding of basic tumor biology, but can be translational exploited for future clinical applications.

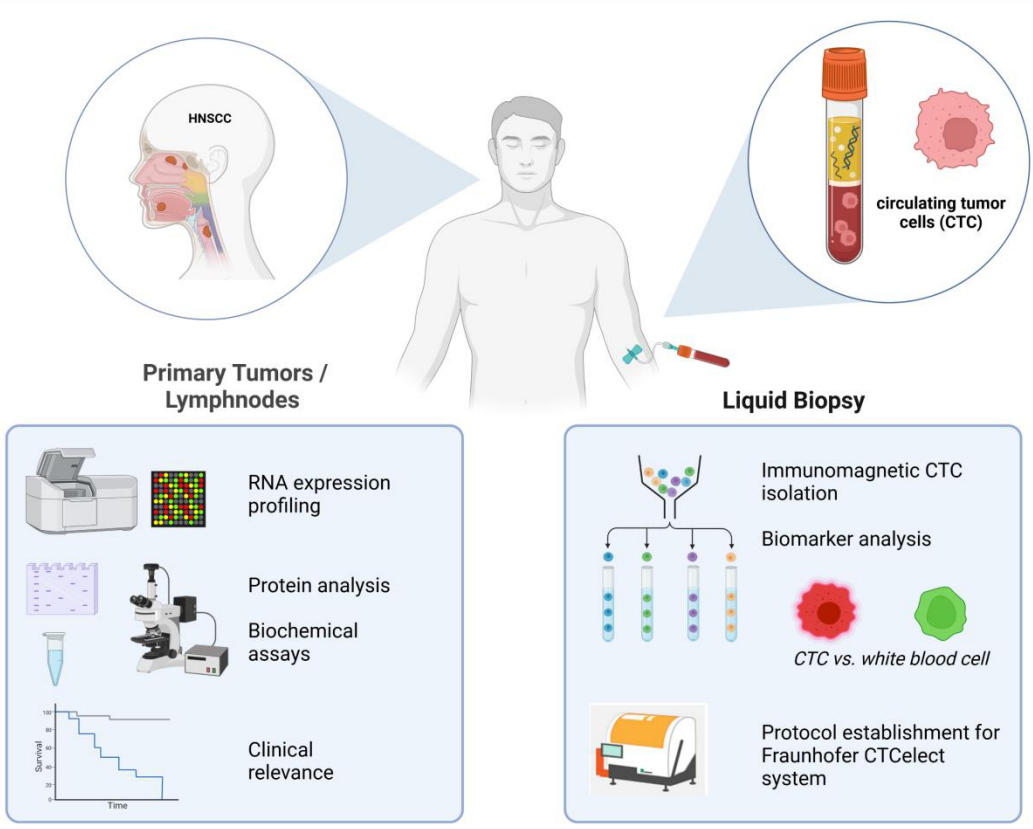

Figure 1. Summary of the workflow performed in this habilitation project. For further details, see text. Created with BioRender.com

2. INTRODUCTION

Despite improved preventive checkups and innovative therapy strategies, cancer is one of the main causes of death in industrial nations. Although initial treatment is often successful, patients frequently develop tumor recurrences due to therapy resistances (Siemer et al. 2021). Patients receiving completely homogeneous treatment may respond differently to anti-cancer therapy due to cellular resistance mechanisms. Therefore, a molecular understanding of the underlying mechanisms is of high clinical and basic scientific interest, and thus, could also contribute to improved treatment strategies. Here, the identification and establishment of novel biomarkers and innovative diagnostic tools play a key role to improve the prognosis of cancer patients.

2.1 Head and neck cancer

Head and neck cancers (HNC) are among the most common malignant neoplasms in humans (Stauber et al. 2012). HNCs include tumors of the throat (lat.: pharynx), the larynx, the lips, and the oral cavity which predominantly emerge from mucous membranes. This so-called solid squamous cell carcinoma (HNSCC) represents the most common entity of HNC, and is the sixth most malignant tumor worldwide with yearly 890.000 new cases, and 450,000 deaths in 2018 (Figure 2)(Ferlay et al. 2019). In Germany, a total of around 17,000 people developed a tumor in the head and neck area in 2014; about 3 out of 4 people affected were men (12,660). Here, tumors of the oral cavity and lips as well as oropharyngeal carcinomas were diagnosed most frequently (Wienecke and Kraywinkel 2019). The median age of onset for men was 63 years, for women 65 years. Five-year survival rates show wide variability mainly depending on sex, tumor localisation, and staging. Whereas patients with laryngeal cancer show highest relative survival rates (about 60%), tumors of the hypopharynx lead to lowest survival rates of about 30%. In general, epidemiological studies show that overall survival rates for most HNC sites are higher in women than in men. Here, several factors come into play, such as earlier diagnoses in women, biological factors, and status of human papilloma virus infection (HPV). Typically, in about 30% of patients tumor is detected at an early stage (I or II), and a large proportion of patients can be cured. If the tumor is not detected until an advanced stage (III or IV), the prognosis is significantly worse (Braakhuis, Brakenhoff, and Leemans 2005). Despite significant improvements in local tumor control, patient survival has changed

little over the past two decades (Johnson et al. 2020). One reason for this is the high number of recurrences - 10 - 30% of patients with advanced HNC develop local recurrences, while regional recurrences occur in 10% and distant metastases in 15-25% (Johnson et al. 2020; Sacco and Cohen 2015).

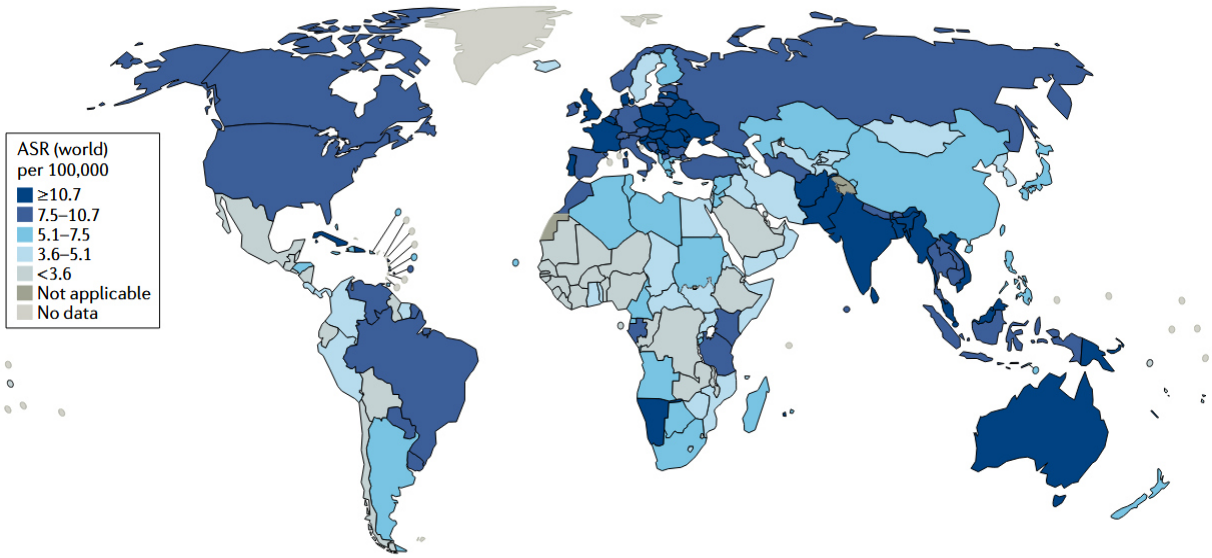

Figure 2: Global incidence of HNSCC. The estimated age-standardized rates (ASRs) of head and neck squamous cellc arcinoma (HNSCC) incidence worldwide are shown for men and women combined (taken from (Johnson et al. 2020)).

Major risk factors associated with the development of HNSCC include exogenous noxae, such as tobacco use, alcohol consumption, and especially the combination of both whereby high-proof alcohol probably serves as a solvent for carcinogens found in cigarette smoke (Pai and Westra 2009). As the use of electronic cigarettes is recently increasing, it will be important to evaluate their effect on HNSCC risk in the coming decades. Apart from these classical risk factors, high-risk human papilloma virus infections (HPV) is emerging as a risk factor of HNSCC (Aggarwal et al. 2020). HPV is a member of the double-stranded DNA virus family papillomaviridae including more than 200 different types of papillomaviruses. Based on their occurrence in malignant or benign lesions of uterine cervix, HPV is grouped as high-risk or low-risk types, respectively (Shukla et al. 2009). In HNSCCs, the high-risk HPV type 16 represents the most prominent infection, whereas low-risks HPV types, such as type 6 and 11, are associated with benign lesions like papillomas and warts (Aggarwal et al. 2020).

High-risk HPV infection is considered to be responsible in particular for the development of tumors of the tongue base, the oropharynx, and the pharyngeal tonsils (Gillison et al. 2012), whereas tobacco and alcohol consumption represent the main risk factors for all other tumor locations. Sunlight also plays a role in the formation of lip tumors, and occupational exposure to certain chemicals and wood dust in formation of tumors of the nasopharynx (Wienecke and Kraywinkel 2019). Thus, the increasing occurrence of oropharyngeal carcinomas probably indicate an increasing etiological importance of HPV infections. The fact that women exhibit higher survival rates may be at least partially caused by the higher amount of HPV-positive tumors in women. HPV-positive tumors usually show enhanced response to chemo- and radiotherapy, and thus have a better prognosis (Fakhry et al. 2008).

Currently, the main prognostic parameters of HNSCC are the size and location of the tumour, the presence of distant metastasis and cervical lymph node metastases, which is not sufficient to evaluate the disease outcome (Hamoir, Schmitz, and Gregoire 2014; Sessions et al. 2002; Gregoire et al. 2010). In the 8th edition of the *Union for International Cancer Control* (UICC) staging system the HPV status was also considered as a relevant biomarker for disease outcome (Beltz et al. 2019).

Although 95% of head and neck tumors are classified as squamous cell carcinomas (HNSCC), it represents a very heterogeneous tumor entity. This fact complicates prognosis, treatment, and identification of the molecular basis of carcinogenesis. HNCs can be classified on histological, or on molecular level (Chung et al. 2004). Based on expression analyses, at least four groups have already been identified (Chung et al. 2004). As mentioned before, one of the most important classification here is the differentiation of HPV-positive and HPV-negative tumors. Additionally, karyotyping and ploidy analysis revealed that a majority of tumors are aneuploid (Hermsen et al. 2001; Jin et al. 2006).

Precise staging of the tumor according to the TNM classification is of great importance not only for prognosis, but also for therapeutic treatment (Johnson et al. 2020; Marur and Forastiere 2016). Since there are still no reliable biomarkers for head and neck tumors, such as Her2/neu for breast cancer, treatment decisions are mostly based on the TNM classification (Chung et al. 2004). Usually, treatment of HNCs include surgery, radiation, and chemotherapy or a combination of treatments. If the tumor is detected at an early stage, it is usually surgically removed and/or irradiated (Lee et al. 2018). In case of advanced tumors additional

complex treatments are applied consisting of chemo-/radiotherapy and targeted therapy (Johnson et al. 2020). Here, chemotherapeutic treatment is mainly cisplatin/carboplatin- and 5-FU (5-fluorouracil)-based. For unresectable tumors, chemotherapy is often combined with radiation therapy (radiochemotherapy), whereby drugs and radiation may be given simultaneously or sequentially (Marur and Forastiere 2016). The sole use of chemotherapeutic agents mainly takes place for distant metastases or recurrent HNC and depends on the age and physical condition of the patient (Johnson et al. 2020). Targeted therapeutics, such as the EGFR-inhibitor cetuximab, or the immune checkpoint inhibitors pembrolizumab and nivolumab specifically interfere with cell signaling processes and are used in addition to radio- or chemotherapy. Pembrolizumab and nivolumab are approved by the FDA especially for treatment of unresectable, recurrent, and/or metastatic HNSCCs (Johnson et al. 2020). Other targeted therapeutics, mostly applied in combination to (radio)chemotherapy are currently under clinical investigation (Johnson et al. 2020).

Despite these advances in therapy, the treatment of HNSCC still often comes along with functional impairment and cosmetic deformity of vital functions of the aerodigestive tract, such as breathing, swallowing, speech, hearing and smell (Gregoire et al. 2010). Although the use of kinase inhibitors, immuntherapy, and antibodies has gained increasing clinical relevance, there is still urgent need for effective therapies and novel drug targets (Deuss et al. 2020; Gul et al. 2021; Gul et al. 2022).

2.2 Molecular pathways of cancer: The oncologically relevant protease Taspase1

Beside unspecific functions in intra- and intercellular “waste management”, proteases have fundamental roles in multiple biological processes and are associated with a wide variety of pathological conditions including cancer. Thus, proteases represent a promising starting point to study molecular cancer pathways and identify novel biomarkers (Wünsch et al. 2016).

Intra- and extracellular proteases catalyze the highly selective cleavage of specific substrates, which in turn influence cell metabolism, tissue remodeling, apoptosis, proliferation and migration (Koblinski, Ahram, and Sloane 2000; Malek et al. 2001). Thus, proteases need to be strictly regulated, as deregulated protease activity might cause pathological conditions, including neoplastic diseases like cancer (Turk 2006; Lopez-Otin and Bond 2008; Lopez-Otin and Matrisian 2007; Overall and Dean 2006; Dall and Brandstetter

2016). Hence, any attempt to understand the biological and pathological relevance of proteases must take into account the large diversity of proteolytic systems operating in cells, tissues and organs (Unruhe et al. 2016). Identification and characterization of the responsible endopeptidase furthermore provides targets for the intervention of diseases involving specific pathways (Saklatvala 2002).

The Threonine Aspartase-1 or Taspase1 (*MEROPS* database: T02.004) was initially identified as protease responsible for the processing and therefore activation of the Mixed Lineage Leukemia (MLL) protein (Hsieh, Cheng, and Korsmeyer 2003). The human *Taspase1* gene encodes a protein of 420 amino acids (aa) resembling the Taspase1 proenzyme. Whereas comparison of crystal structures of Taspase1 and several type 2 asparaginases suggest the formation of an asymmetric αββα-heterotetramer (Khan, Dunn, and Tong 2005), our studies revealed that Taspase1 is already active as αβ monomer in living cells (Bier, Hecht, et al. 2012; Bier, Knauer, et al. 2012). In contrast to the exclusively *cis*-active type 2 asparaginases, only Taspase1 is also able to cleave other substrates in *trans* by hydrolyzing its target proteins at conserved ($Q^{3}[FILV]^{2}D^{1}\downarrow G^{1'}x^{2'}D^{3'}D^{4'}$) sites (Bier, Knauer, Klapthor, et al. 2011; Hsieh, Cheng, and Korsmeyer 2003). Mutation of the catalytic nucleophile, Thr^{234}, abolishes Taspase1's proteolytic activity (Hsieh, Cheng, and Korsmeyer 2003; Khan, Dunn, and Tong 2005). Besides MLL other essential proteins, such as the precursor of the general transcription factor IIA (TFIIA) (Zhou et al. 2006; Schrenk et al. 2018) or the Upstream Stimulatory Factor 2 (USF2) (Bier, Knauer, Klapthor, et al. 2011) could be identified by us as native Taspase1 targets. The generation of knockout mice deficient for Taspase1 revealed that MLL and TFIIA processing occurs exclusively in presence of Taspase1 (Takeda et al. 2006; Takeda et al. 2015). Taspase1-deficient mice are viable, but smaller in size and show profound skeletal abnormalities (Takeda et al. 2006), craniofacial malformations (Takeda et al. 2015), and male infertility (Oyama et al. 2013). Taken together, Taspase1 plays an important role in the regulation of correct segmental identities, head morphogenesis and spermatogenesis. However, the molecular mechanisms how Taspase1 may affect substrate functions through site-specific proteolysis still remain to be determined (Wunsch, Hahlbrock, Heiselmayer, Backer, Heun, et al. 2015; Wunsch, Hahlbrock, Heiselmayer, Backer, Schrenk, et al. 2015). Moreover, the full repertoire of physiological or pathological pathways regulated in humans by Taspase1 remains still to be understood (Wünsch et al. 2016).

As summarized in our reviews, Taspase1 is an oncologically relevant protease playing essential roles in the development of aggressive infant leukemias, as well as in a variety of solid tumors, including head and neck cancer (Figure 3) (Wünsch et al. 2016; Hahlbrock et al. 2016; Stauber et al. 2016). An initial indication of a possible role for Taspase1 during tumorigenesis was provided by the observation that Taspase1-deficient cells exhibit significantly increased resistance to Ras-, Myc-, and DNp53-induced oncogenic transformation *in vitro* (Takeda et al. 2006). Moreover, Taspase1 is found overexpressed in several solid tumor entities (Bier, Knauer, Docter, et al. 2011; Chen et al. 2010; Takeda et al. 2006). Taspase1 is also required for the maintenance of a complete cancer phenotype (Chen et al. 2010). While Taspase1 is not an oncogene in the classical sense, it activates typical cancer properties in cells, and thus can be classified as a "non-oncogene addiction protease" (Luo, Solimini, and Elledge 2009). Furthermore, Taspase1 is involved in cell cycle regulation (at least) by modulating the expression of various cyclins (Takeda et al. 2006). The study of Dong *et al.* describes the importance of the Taspase1-dependent cyclin E activation for the development of HER2/neu-positive breast tumors (Dong et al. 2014).

In summary, Taspase1 is involved in a number of biological functions executing its proteolytic activity on various target proteins. These include not only differentiation processes during development, but also cell proliferation and apoptosis which are important pathways during tumorigenesis. The underlying mechanisms and how deregulated Taspase1 activity may promote the development of malignancies, especially of HNSCC, requires further investigation. Importantly, no specific small molecule or genetic inhibitors are available worldwide, hampering not only to further dissect Taspase1's disease mechanisms, but also precluding the full assessment of its clinical impact (Bier, Hecht, et al. 2012; Stauber, Bier, and Knauer 2012; Wünsch et al. 2012).

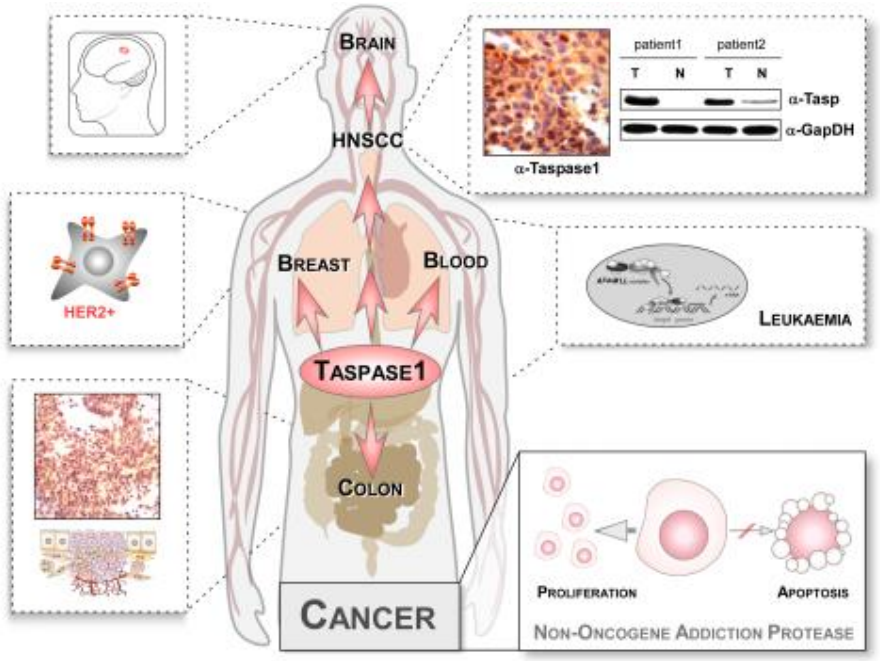

Figure 3: Taspase1 is an oncologically relevant protease. Taspase1 is overexpressed in several solid as well as liquid malignancies. Thus, Taspase1 was characterized as non-oncogene addiction protease which per se does not represent a classical oncogene, but is crucial for the maintenance of the complete cancer phenotype due to proliferative and anti-apoptotic characteristics (down right). Taspase1-associated tumor development and maintenance could be shown in colon, glioblastoma and HER2-positive breast cancer models as well as in patients suffering from head and neck squamous cell carcinoma (HNSCC; top right) (Wünsch et al. 2016).

2.3 Molecular pathways of cancer: intra- and extracellular structural proteins

The structural integrity of eukaryotic cells and tissues is maintained by the cytoskeleton composed microfilaments, intermediate filaments (IF), and microtubules. Among these three different groups, the intermediate filaments (IF) make up the largest family, and have been characterized as important effectors of tumorigenesis and metastasis. The highly conserved family of cytokeratin proteins (cKRTs) are the major IF structural proteins of epithelial cells and consists of more than 25 members which are critical for cell stabilization, shape, intracellular signaling and transport (Moll et al. 1982). Usually keratins are expressed as specific heterodimeric pairs consisting of the acidic type I (K9-K24 and Ha1-8) and the neutral-basic type II (K1-K8 and Hb1-6) polypeptides, both of which are essential for filament formation and function (Moll, Divo, and Langbein 2008). During malignant transformation, original signature expressions of IF proteins are largely retained. Since the majority of tumor cells originate from epithelial cells, cKRTs are well suited to stratify carcinomas into site of origin, and tumor subtype (Sharma et al. 2019), as well as to predict clinical outcome and therapy response (Mehrpouya et al. 2019; Fillies et al. 2006; Toyoshima et al. 2008). Especially

cKRTs 8, 18, and 19 being the most abundant subtypes in epithelial cells are well established as biomarkers for epithelial tumors, such as HNC (Fillies et al. 2006). Apart from their use as diagnostic tools, the relevance of cytokeratins as prognostic markers as well as their role in epithelial tumorigenesis and treatment responsiveness is not well understood (Karantza 2011).

In recent years, it becomes more an more clear that besides intracellular (structural) proteins, the tumor microenvironment plays a decisive role in development and progression of tumors. The tumor microenvironment can be defined as everything that surrounds tumor cells except the tumor cells themselves, and thus is composed of stroma cells, such as cancer-associated fibroblasts, immune cells, extracellular matrix (ECM) proteins, and small components such as hormones, growth factor, or cytokines (Figure 4) (Gonzalez-Gonzalez and Alonso 2018). Belonging to the group of ECM-glycoproteins, the osteoblast-specific factor-2 (OSF-2, periostin) is part of the tumor microenvironment. Originally, OSF-2 was described as a homophilic adhesion molecule in bone formation (Takeshita et al. 1993), and plays an important role in ECM structure and organization, particularly in collagen assembly (Gonzalez-Gonzalez and Alonso 2018). Over the past years, OSF-2 was proposed to be a novel therapeutic target for cancer (Kudo et al. 2007). Indeed, OSF-2/*POSTN* was found to be overexpressed in various human cancers including oral squamous cell carcinoma (Siriwardena et al. 2006; Gonzalez et al. 2003), breast (Shao et al. 2004), and lung (Sasaki, Dai, et al. 2001), and higher *POSTN* expression levels were correlated with increased tumor aggressiveness and/or poorer survival in these entities. The functional role of OSF-2 in (head and neck) cancer, as well as the origin of OSF-2 expression is controversially discussed. Here, tumor-promoting and tumor-suppressing activity have been reported (e.g. (Shao et al. 2004; Siriwardena et al. 2006; Kim et al. 2005), and OSF-2 production has been shown by tumor cells, as well as non-tumor cells, such as cancer-associated fibroblasts (Erkan et al. 2007; Sasaki, Lo, et al. 2001). In summary, OSF-2 is a multifunctional protein executing various biological functions in health and disease, including cancer/metastasis, and thus represents a potential biomarker for HNC.

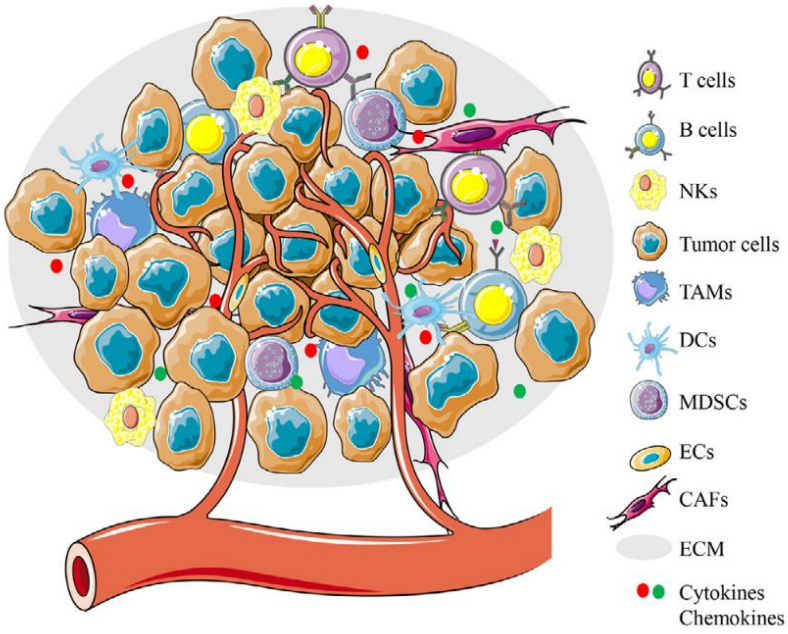

Figure 4: Components of the tumor microenvironment (from (Shi, Tang, and Miao 2020)). CAFs, cancer-associated fibroblasts; DCs, dendritic cells; ECs, endothelial cells; ECM, extracellular matrix; MDSCs, myeloid-derived suppressor cells; NKs, natural killer cells; TAMs, tumor-associated macrophages.

2.4 Circulating tumor cells – an early-systemic tumor component indicative for metastasis

Despite the aggressive protocols in first-line treatment, invasion and metastasis occur in over 50% in HNSCC patients (Ferlito et al. 2001) resulting in a 5-year survival rate of only 4 to 35% depending on the number of metastatic sites (Beckham et al. 2019). Most deaths from this class of tumors are caused by lymph-/haematogenous spread of cancer cells into distant organs and their subsequent growth to overt metastases. The classical view is that metastatic spread is a late process in malignant progression, but work of the last decade strongly suggested that dissemination of primary cancer cells to distant sites is already an early event (Rocken 2010; Hu et al. 2017). Today, it is accepted that circulating tumor cells (CTCs) which are released into the blood circulation from the primary tumor play an important role in the formation of metastases according to the “seed and soil theory” (Figure 5) (Gribko et al. 2019; Kunzel et al. 2019). Moreover, tumor cells in the bone marrow seem to form an important reservoir of cancer cells from which they may re-circulate into other distant organs.

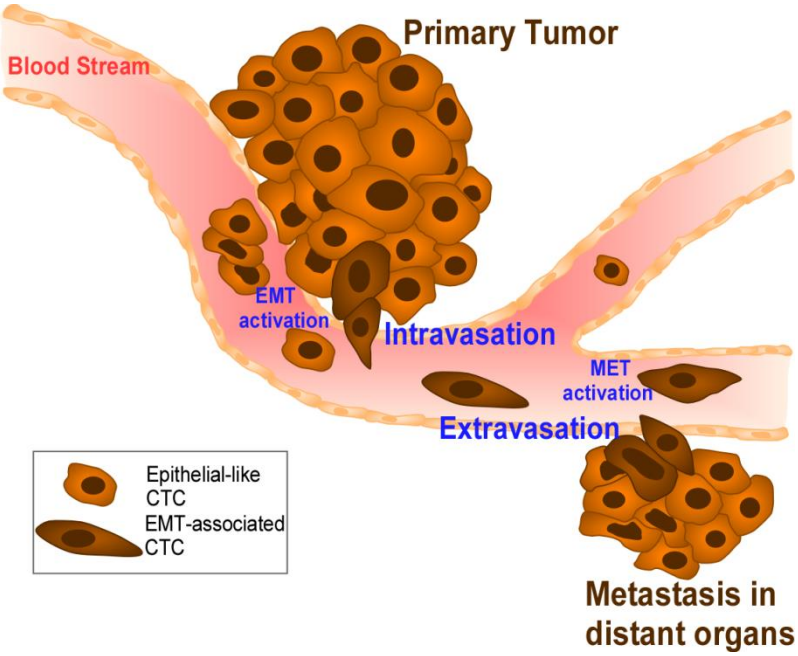

Figure 5: Characteristic stages of tumor cell dissemination during metastasis. Cells from primary tumor undergo epithelial-mesenchymal transition (EMT) leading to the loss of cell-cell adhesion and promoting local invasion into the blood vessels (intravasation). The produced CTCs are able to escape from blood vessels into distant organs of future metastasis (extravasation) after the reverse process, MET, induced by interaction with the local microenvironment (from (Gribko et al. 2019)).

Several studies have indicated that the presence of CTCs in the blood is a poor prognostic indicator of overall and progression-free survival in patients with colorectal (Huang et al. 2015), breast (Lianidou and Markou 2011), or HNSCC (Cho et al. 2018). Compared to other entities, the impact of CTCs in HNSCC patients is still unclear and not applied in clinical routine (Kulasinghe et al. 2018). To date only little data exist evaluating the prognostic value of CTC in HNSCC (Wollenberg et al. 2004; Jatana et al. 2010; Wikner et al. 2014; Mockelmann et al. 2014; Partridge et al. 2003; Nichols et al. 2012; Winter et al. 2009; Tinhofer and Staudte 2018; Kulasinghe et al. 2018). But also in HNSCC circulating tumor cells appear to represent a potential prognostic factor for the early onset of drug resistance, metastasis and disease-free survival (Grobe et al. 2014; Thalgott, Heck, and Pantel 2014). Patients diagnosed with identical cancers and given similar treatments from the standard repertoire of surgery, radiation and chemotherapies often respond very differently (Heath, Davis, and Hood 2009). Therefore, there is a great demand for a less invasive method, for example a simple bed-side blood test, to determine the state of disease including possible treatment resistance.

The fact that tumor cells are detectable in the peripheral blood of cancer patients months to years after complete removal of the primary tumor indicates that these cells might indeed circulate between metastatic sites. Hence, the detection and characterization of tumor cells in the peripheral blood has therefore gained (pre)clinical considerable attention as so-called "liquid biopsy" (Cristofanilli et al. 2007; Tinhofer and Staudte 2018). In addition, profiling of the geno- and phenotype of CTCs is considered to provide new insights into the biology of tumor cells in cancer patients and might open new perspectives for early detection of metastatic spread and its successful treatment. However, so far detection methods vary significantly across studies, ranging from RT-PCR, immunocytochemistry to immunomagnetic/immunofluoresence, targeting either tumor-associated genes or proteins. Thus, the optimal cut-off value and clinically relevant predictive power of CTCs' is still debated. Currently, the most common methods for CTC isolation are fluorescence activated cell sorting (FACS) or immunomagnetic separation in order to sort out cells that present the desired surface profile after fluorescent/magnetic labeling. Since establishment of the FDA-approved *CellSearch* system, an automated immunomagnetic enrichment and staining system, the sensitivity of CTC detection has markedly improved (Nichols et al. 2012; Riethdorf et al. 2007). Besides FACS, also the CellSearch System relies on the expression of the epithelial cell adhesion molecule (EpCAM) for the quantification of CTCs, although ERBB2 or the EGFR are also investigated for different tumor types.

As technical approach, the Fraunhofer-IMM Mainz aims at the establishment of a fully automated, software-based platform for CTC detection and isolation, named CTCelect. This magnetic flow cytometry (MFC) system consists of a immunomagnetic enrichment module, the IsoMAG, and microfluidic detection/dispensing unit. In contrast to the current gold standard CellSearch®, CTCelect is an all-in-one benchtop system and requires no fixation or sample transfer between different devices, which reduces manual errors, contamination and cell stress, as well as costs and hands-on time (Gribko et al. 2021).

In summary, basic and cost-efficient methods for the detection, isolation, and molecular understanding of CTCs are of high scientific and clinical relevance. Therefore, the development of minimal-invasive methods which specifically and sensitively detect these tumor components in patient blood are urgently needed (Siemer et al. 2020; Gribko et al. 2019;

Kunzel et al. 2019). Furthermore, downstream molecular characterization of isolated structures is mandatory for the establishment of novel cancer biomarkers.

3. AIMS OF THIS WORK

Due to their heterogeneity, and high number of recurrences, head and neck cancers (HNC) belong to the most common malignant neoplasms, and there is still high need for novel treatment options including new drug targets. In this field, mRNA expression profiling technologies allow the use of the entire transcriptome landscape to define new molecular cancer subtypes, identify disease-relevant signaling pathways and stratify patient clusters (Goesswein et al. 2018).

By systematic gene expression analyses combined with a tiered experimental pipeline we identified and confirmed a variety of genes which are differentially expressed in head and neck primary tumors, as well as (lymph node) metastases. Among these proteins, the unique protease Taspase1 has been shown to be significantly upregulated in HNCs. However, the detailed molecular mechanisms how Taspase1 executes it´s functions in cancer cells remain to be fully understood. Based on these previous studies, this work includes analyses and decoding of disease-relevant signaling pathways that are causally involved in the development, recurrence, and metastasis of head and neck tumors. Besides established methods, novel diagnostic tools of “liquid biopsy” were used to increase the spectrum of analyzed tumor components. **Consequently, major aims of this work were:**

I. the detailed characterization of Taspase1´s role in head and neck cancer cells,
II. identification of new potential biomarkers for HNC, and their clinical and molecular characterization, and
III. establishment and application of a "magnetic flow cytometry" based on the principle of immunomagnetic separation using antibody-conjugated ferromagnetic micro/nanoparticles for quantification and molecular characterization of tumor components from blood of head and neck tumor patients.

Finally, we expect not only to reveal and understand the clinical relevance of known and novel HNC biomarker proteins, but also to provide evidence allowing biomedical translation of these findings into the clinics.

4. RESULTS

4.1 Disease-relevant signalling-pathways in head and neck cancer: Taspase1's proteolytic activity fine-tunes TFIIA function

Alena Gribko, Angelina Hahlbrock, Sebastian Strieth, Sven Becker, Jan Hagemann, Maximilian Deichelbohrer, Andreas Hildebrandt, Negusse Habtemichael, and **Désirée Wünsch**

Head and neck cancer (HNC) is the seventh most common malignancy in the world and its prevailing form, the head and neck squamous cell carcinoma (HNSCC), is characterized as aggressive and invasive cancer type. The transcription factor II A (TFIIA), initially described as general regulator of RNA polymerase II-dependent transcription, is part of complex transcriptional networks also controlling mammalian head morphogenesis. Posttranslational cleavage of the TFIIA precursor by the oncologically relevant protease Taspase1 is crucial in this process. In contrast, the relevance of Taspase1-mediated TFIIA cleavage during oncogenesis of HNSCC is not characterized yet.

Here, we performed genome-wide expression profiling of HNSCC which revealed significant downregulation of the TFIIA downstream target CDKN2A. To identify potential regulatory mechanisms of TFIIA on cellular level, we characterized nuclear-cytoplasmic transport and Taspase1-mediated cleavage of TFIIA variants. Unexpectedly, we identified an evolutionary conserved nuclear export signal (NES) counteracting nuclear localization and thus, transcriptional activity of TFIIA. Notably, proteolytic processing of TFIIA by Taspase1 was found to mask the NES, thereby promoting nuclear localization and transcriptional activation of TFIIA target genes, such as CDKN2A. Collectively, we here describe a hitherto unknown mechanism how cellular localization and Taspase1 cleavage fine-tunes transcriptional activity of TFIIA in HNSCC.

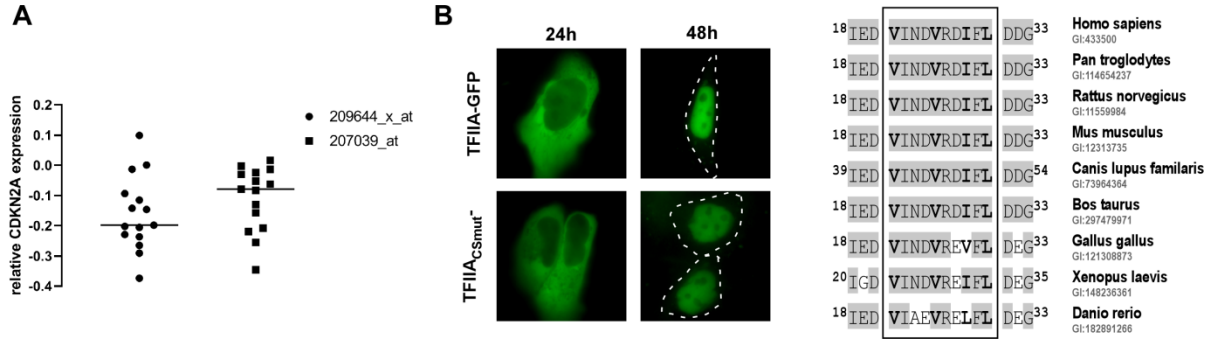

Figure 4.1: TFIIA-associated functions are regulated by Taspase1-mediated cleavage and a conserved nuclear export signal. (A) TFIIA downstream target CDKN2A is downregulated in HNSCC patients. (B) Taspase1-mediated cleavage of TFIIA results in masking of the NES (right), thereby promoting nuclear localization (left).

4.2 Histone deacetylase inhibitors dysregulate DNA repair proteins and antagonize metastasis-associated processes

Nicole Kiweler*, **Désirée Wünsch***, Matthias Wirth, Nisintha Mahendrarajah, Gunter Schneider, Roland H Stauber, Walburgis Brenner, Falk Butter, Oliver H Kramer.
*equal first author contribution

We set out to determine whether clinically relevant epigenetic drugs against class I histone deacetylases (HDACs) affect hallmarks of the metastatic process. We treated permanent and primary renal, lung, and breast cancer cells with the class I histone deacetylase inhibitors (HDACi) entinostat (MS-275) and valproic acid (VPA), the replicative stress inducer hydroxyurea (HU), the DNA-damaging agent cis-platinum (L-OHP), and the cytokine transforming growth factor-β (TGFβ). We used proteomics, quantitative PCR, immunoblot, single cell DNA damage assays, and flow cytometry to analyze cell fate after drug exposure. We show that HDACi interfere with DNA repair protein expression and trigger DNA damage and apoptosis alone and in combination with established chemotherapeutics. Furthermore, HDACi disrupt the balance of cell adhesion protein expression and abrogate TGFβ-induced cellular plasticity of transformed cells.

HDACi suppress the epithelial-mesenchymal-transition (EMT) and compromise the DNA integrity of cancer cells. These data encourage further testing of HDACi against tumor cells.

4.3 Identification of cytokeratin24 as a tumor suppressor for the management of head and neck cancer

Désirée Gül, Negusse Habtemichael, Dimo Dietrich, Jörg Dietrich, Dorothée Gößwein, Aya Khamis, Eric Deuss, Julian Künzel, Günter Schneider, Sebastian Strieth, and Roland H. Stauber

To improve management of head and neck squamous cell carcinoma patients, we need to increase our understanding of carcinogenesis, to identify biomarkers, and drug targets. This study aimed to identify novel biomarkers by providing transcriptomics profiles of matched primary tumors, lymph node metastasis, and non-malignant tissue of 20 HNSCC patients as well as by bioinformatic analyses of a *TCGA* HNSCC cohort, comprising 554 patients. We provide cancer cell signaling networks differentially expressed in tumors *versus* metastases, such as mesenchymal-epithelial transition, and structural integrity networks. As a proof of principle study, we exploited the data sets and performed functional analyses of a novel cytokeratin, cytokeratin24 (cKRT24), which had not been described as biomarker for tumors before. Survival analysis revealed that low cKRT24 expression correlated with poor overall survival in HNSCC. Experimentally, downregulation of cKRT24 in primary tumors, metastases, and HNSCC cell lines was verified on mRNA and protein level. Cloning and ectopic overexpression of cKRT24 not only affected viability and growth of HNSSC cell lines, but also inhibited tumor growth in murine xenograft studies. We conclude that cKRT24 functions as a tumor suppressor in HNSCC, and may serve as an additional prognostic biomarker and novel target to support current HNSCC treatments.

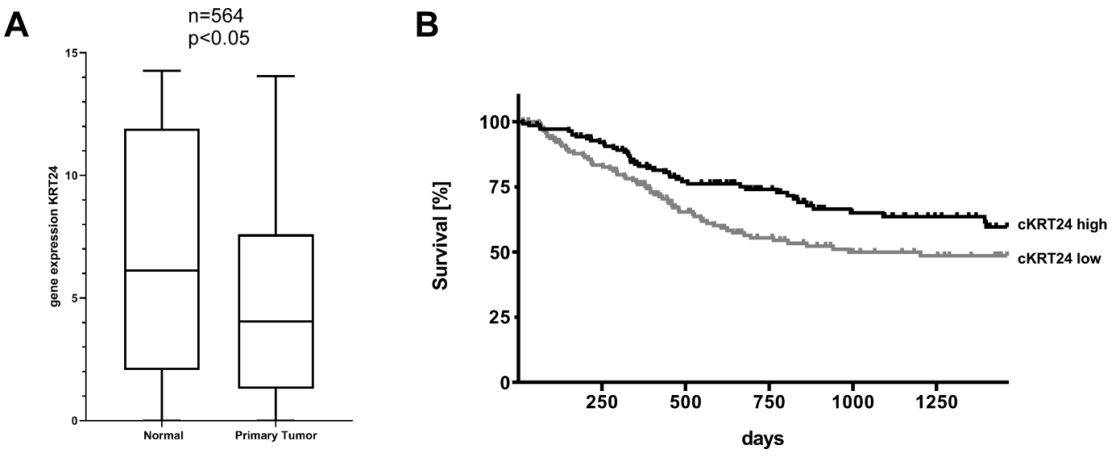

Figure 4.2: cKRT24 is significantly downregulated in primary head and neck tumors (A) exhibiting poor overall survival (B).

4.4 Impact of secretion-active osteoblast-specific factor 2 in promoting progression and metastasis of head and neck cancer

Désirée Gül, Andrea Schweitzer, Aya Khamis, Shirley Knauer, Guo-Bin Ding, Laura Freudelsperger, Ioannis Karampinis, Sebastian Strieth, Jan Hagemann, and Roland H. Stauber

Treatment success of head and neck cancer (HNC) is still hampered by tumor relapse due to metastases. Our study aimed to identify biomarkers by exploiting transcriptomics profiles of patient-matched metastases, primary tumors, and normal tissue mucosa as well as the *TCGA* HNC cohort data sets. Analyses identified osteoblast-specific factor 2 (OSF-2) as significantly overexpressed in lymph node metastases and primary tumors compared to normal tissue. High OSF-2 levels correlate with metastatic disease and reduced overall survival of predominantly HPV-negative HNC patients. No significant correlation was observed with tumor localization or therapy response. These findings were supported by the fact that OSF-2 expression was not elevated in cisplatin-resistant HNC cell lines. OSF-2 was strongly expressed in tumor-associated fibroblasts, suggesting a tumor microenvironment-promoting function. Molecular cloning and expression studies of OSF-2 variants from patients identified an evolutionary conserved bona fide protein secretion signal (^{1}MIPFLPMFSLLLLLIVNPINA^{21}). OSF-2 enhanced cell migration and cellular survival under stress conditions, which could be mimicked by the extracellular administration of recombinant protein. Here, OSF-2 executes its functions via ß1 integrin, resulting in the phosphorylation of PI3K and activation of the Akt/PKB signaling pathway. Collectively, we suggest OSF-2 as a potential prognostic biomarker and drug target, promoting metastases by supporting the tumor microenvironment and lymph node metastases survival rather than by enhancing primary tumor proliferation or therapy resistance.

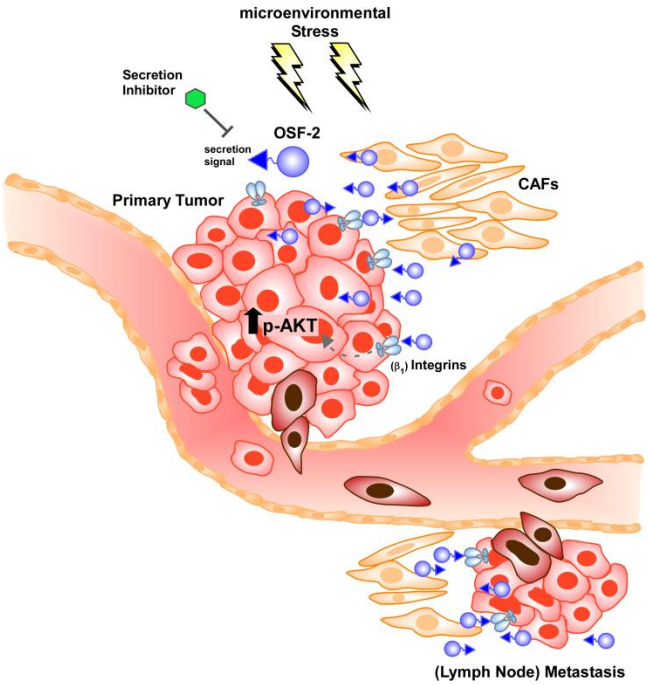

Figure 4.3: OSF-2 promotes metastasis by regulating the tumor microenvironment and cellular survival in HNC. Due to the conserved N-terminal secretion signal, OSF-2 seems to execute its tumor-promoting functions not mainly intracellularly, but extracellularly in the tumor microenvironment. OSF-2 modulates the tumor microenvironment by integrin-dependent activation of Akt/PKB pathways and downstream signaling, particularly critical under stress conditions.

4.5 IsoMAG—An Automated System for the Immunomagnetic Isolation of Squamous Cell Carcinoma-Derived Circulating Tumor Cells

Alena Gribko, Janis Stiefel, Lana Liebetanz, Sophie-Madeleine Nagel, Julian Künzel, Madita Wandrey, Jan Hagemann, Roland H. Stauber, Christian Freese, and **Désirée Gül**

Detailed information about circulating tumor cells (CTCs) as an indicator of therapy response and cancer metastasis is crucial not only for basic research but also for diagnostics and therapeutic approaches. Here, we showcase a newly developed IsoMAG IMS system with an optimized protocol for fully automated immunomagnetic enrichment of CTCs, also revealing rare CTC subpopulations. Using different squamous cell carcinoma cell lines, we developed an isolation protocol exploiting highly efficient EpCAM-targeting magnetic beads for automated CTC enrichment by the IsoMAG IMS system. By FACS analysis, we analyzed white blood contamination usually preventing further downstream analysis of enriched cells. 1 µm magnetic beads with tosyl-activated hydrophobic surface properties were found to be optimal for automated CTC enrichment. More than 86.5 and 95% of spiked cancer cells were recovered from both cell culture media and human blood employing our developed protocol. In addition, contamination with white blood cells was minimized to about 1200 cells starting from 7.5 mL blood. Finally, we showed that the system is applicable for HNSCC patient samples and characterized isolated CTCs by immunostaining using a panel of tumor markers. Herein, we demonstrate that the IsoMAG system allows the detection and isolation of CTCs from HNSCC patient blood for disease monitoring in a fully-automated process with a significant leukocyte count reduction. Future developments seek to integrate the IsoMAG IMS system into an automated microfluidic-based isolation workflow to further facilitate single CTC detection also in clinical routine.

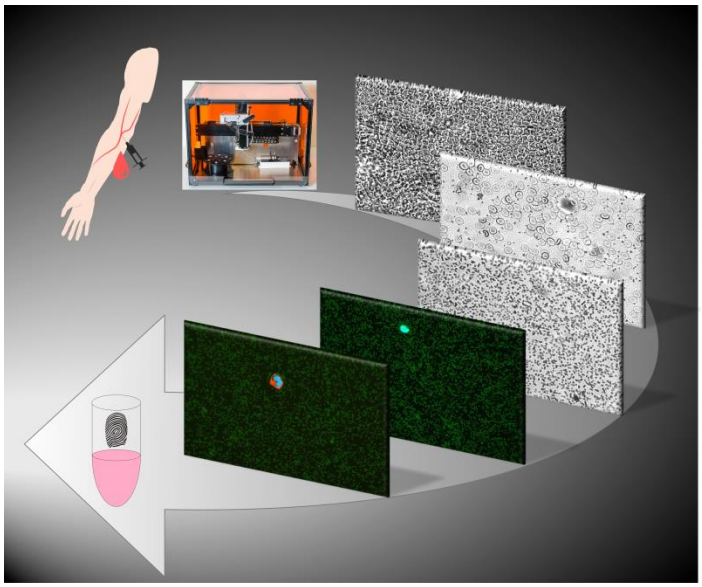

Figure 4.4: Schematic workflow of IsoMAG IMS system to isolate CTCs of cancer patient blood.

5. ACHIEVEMENTS OF THIS WORK AND OUTLOOK

Cancer is still one of the most common causes of death, and thus represents one of the greatest challenges facing the health care system in industrialized nations. Tumors of the head and neck region (HNC) represent a particular challenge due to the often late diagnosis associated with poor prognosis. Surprisingly, despite new findings and the development of novel (immune)therapeutic options, the prognosis of HNC patients has hardly improved over the last decades. Consequently, further knowledge of underlying mechanism, and cancer-relevant pathways giving rise to potential new biomarkers and drug targets are urgently needed.

Therefore, the aim of this professional dissertation entitled "*Identification of disease-relevant mechanisms in head and neck tumors - novel biomarkers and diagnostic tools*" was the discovery and characterization of molecular mechanisms involved in the development, recurrence, and metastasis of HNC. By a tiered experimental pipeline containing bioinformatic evaluation of clinical patient data, expression analyzes, and molecularbiological experiments, we characterized disease-relevant (protease)networks in detail, and identified the (extra)cellular structural proteins cytokeratin24 and periostin/OSF-2 as potential predictive biomarkers for HNC. The studies also focused on the analysis of metastasis pathways, as well as the influence of potential chemotherapeutic agents (HDAC inhibitors) on this process.

Through this work, it has been shown that all analyzed proteins and drugs are specifically involved in modulating hallmarks of cancer cells according to Hanahan and Weinberg (Figure 6). By regulating cell cycle and apoptotic pathways, overexpression of the protease Taspase1 in tumors results in resistance to cell death, and increased proliferation. Underlying signaling pathways include localization and Taspase1-mediated cleavage of TFIIA (I, Gribko *et al*. 2017). By identifying this unique mechanism of fine-tuning Taspase1´s oncological activity in HNC, we contributed to a more detailed understanding of Taspase1 (patho)biology in general. Since there are still no efficient Taspase1 inhibitors available for clinical use, further efforts should be made in this direction. We and others already suggested the application of nanoparticles (van den Boom et al. 2020), and supramolecular ligands (Pasch et al. 2021; Hoing et al. 2022) to block the oncological activity of Taspase1. The coming years will show whether such

alternative strategies will lead to success, and if Taspase1 can be established as novel therapeutic target in the clinic.

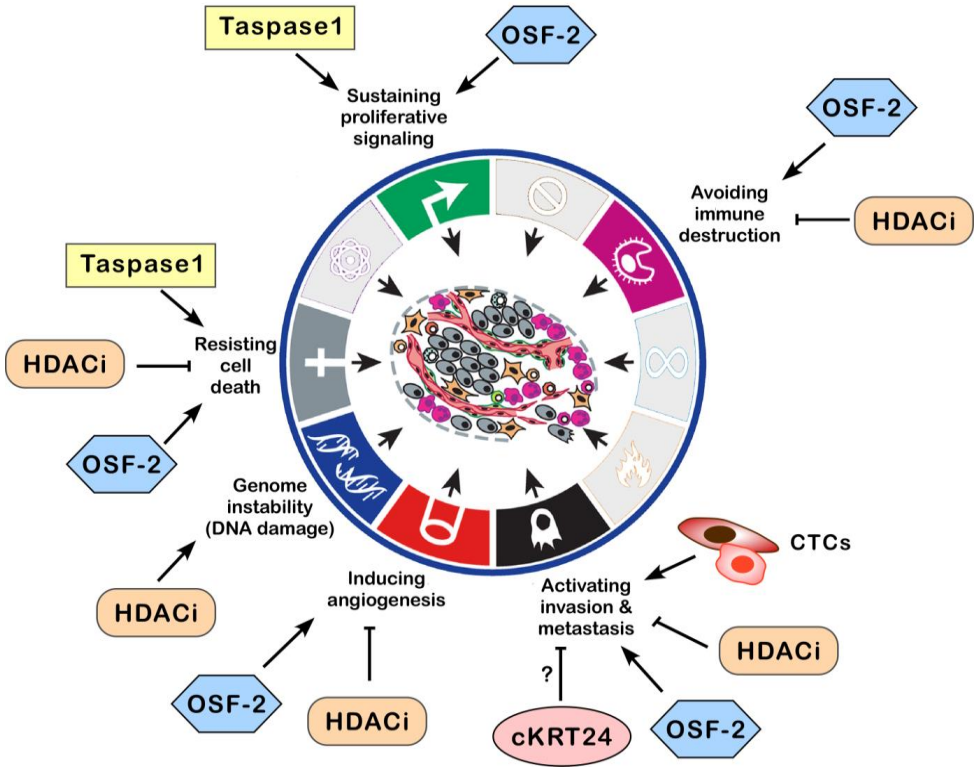

Figure 6: Roles of characterized potential biomarkers, and drugs in carcinogenesis illustrated based on postulated hallmarks of cancer (modified from (Hanahan and Weinberg 2011)). Arrows represent enhancing, blunt lines inhibiting effect. For further details, see text.

The application of HDAC inhibitors (HDACi) as anti-cancer drugs is based on the induction of cell death and DNA damage, the reduction of angiogenesis, and modulation of immune response (Figure 6). Furthermore, we could show that (at least) by suppression of epithelial-mesenchymal-transition (EMT) HDACi can prevent metastatic processes (II, Kiweler, Wünsch *et al.* 2020). Although the Food and Drug Administration has approved four HDACi for the treatment of hematological malignancies, there is still need to further evaluate their potential applicability for solid cancers including HNC. In context of the discussion on the impact of DNA repair and EMT on metastasis, our study provided important evidence suggesting further evaluation of HDACi treatment for (solid) malignancies (Kiweler et al. 2020).

By expressional analyses combined with *in vitro* and *in vivo* experiments, we identified the intracellular structural protein cytokeratin24 (cKRT24) as tumor suppressor

downregulated in HNC (III, Gül *et al.* 2021). As we found reduced expression in metastases, cKRT24 downregulation may activate invasion and thus favor metastasis. However, the underlying mechanisms how cKRT24 executes its tumorsuppressive function are not yet understood in detail. Here, we feel that our study may stimulate the field to examine cKRT24's pathological and clinical relevance concerning disease progression and therapy responses in large prospective studies. Such retro-/prospective studies also addressing the HPV-status and treatments may lead to consideration of cKRT24 as an additional biomarker for HNC.

Representing another protein identified via expressional analyses of a HNC patient cohort, the osteoblast-specific factor 2 (OSF-2) mainly executes its function via activation of metastasis (IV, Gül *et al.* 2022). In previous studies, OSF-2 expression has been associated with the induction of proliferation and angiogenesis, and inhibition of cell death and modulation of immune response (Gonzalez-Gonzalez and Alonso 2018). Importantly, we could show that OSF-2 promotes metastases by supporting the tumor microenvironment and lymph node metastases survival rather than by enhancing primary tumor proliferation or therapy resistance. By identifying a secretion signal, we suggest not only exploiting OSF-2 as a potential prognostic biomarker for head and neck cancers, but also targeting its tumor microenvironment reservoir by secretion inhibitors.

Finally, circulating tumor cells (CTCs) are an early-systemic tumor component indicative for metastasis, and thus their detection can be an important tool for diagnosis and treatment of HNCs. In our pilot study using the *Fraunhofer IsoMAG* system, we successfully established a protocol allowing detection and isolation of CTCs from HNC patient blood for disease monitoring in a fully-automated process with a significant leukocyte count reduction (V, Gribko *et al.* 2021). Importantly, the system was shown to allow the use of variable cancer/CTC markers since expression of epithelial markers can change during process of circulation (EMT/MET). Future challenge will be to implement the system an automated microfluidic-based isolation workflow tofurther facilitate single CTC detection also in clinical routine (Gribko et al. 2021; Stiefel et al. 2022).

Collectively, this work discovered new insights into disease-relevant signaling pathways and mechanisms relevant, but not limited to head and neck tumors. Applicability of the tiered experimental pipeline consisting of bioinformatics, expression analyzes, and molecularbiological experiments was demonstrated, and resulted in the identification of at

least three potential new biomarkers for HNC. Especially the use of novel diagnostic tools for the determination of biomarkers in the form of liquid biopsies is a particularly promising approach to improve diagnosis and prognosis of HNC tumors. These findings not only improve our understanding of basic tumor biology, but can be translationally exploited for future clinical applications.

6. REFERENCES (OWN IN BOLD)

Aggarwal, N., J. Yadav, K. Thakur, R. Bibban, A. Chhokar, T. Tripathi, A. Bhat, T. Singh, M. Jadli, U. Singh, M. K. Kashyap, and A. C. Bharti. 2020. 'Human Papillomavirus Infection in Head and Neck Squamous Cell Carcinomas: Transcriptional Triggers and Changed Disease Patterns', *Front Cell Infect Microbiol*, 10: 537650.

Beckham, T. H., J. E. Leeman, P. Xie, X. Li, D. A. Goldman, Z. Zhang, E. Sherman, S. McBride, N. Riaz, N. Lee, and C. J. Tsai. 2019. 'Long-term survival in patients with metastatic head and neck squamous cell carcinoma treated with metastasis-directed therapy', *Br J Cancer*, 121: 897-903.

Beltz, A., D. Gosswein, S. Zimmer, I. Limburg, D. Wunsch, A. Gribko, M. Deichelbohrer, J. Hagemann, R. H. Stauber, and J. Kunzel. 2019. 'Staging of oropharyngeal squamous cell carcinoma of the head and neck: Prognostic features and power of the 8th edition of the UICC staging manual', *Eur J Surg Oncol*, 45: 1046-53.

Bier, C., R. Hecht, L. Kunst, S. Scheiding, D. Wunsch, D. Goesswein, G. Schneider, O. H. Kramer, S. K. Knauer, and R. H. Stauber. 2012. 'Overexpression of the catalytically impaired Taspase1 T234V or Taspase1 D233A variants does not have a dominant negative effect in T(4;11) leukemia cells', *PLoS One*, 7: e34142.

Bier, C., S. K. Knauer, D. Docter, G. Schneider, O. H. Kramer, and R. H. Stauber. 2011. 'The importin-alpha/nucleophosmin switch controls taspase1 protease function', *Traffic*, 12: 703-14.

Bier, C., S. K. Knauer, A. Klapthor, A. Schweitzer, A. Rekik, O. H. Kramer, R. Marschalek, and R. H. Stauber. 2011. 'Cell-based Analysis of Structure-Function Activity of Threonine Aspartase 1', *J Biol Chem*, 286: 3007-17.

Bier, C., S. K. Knauer, D. Wunsch, L. Kunst, S. Scheiding, M. Kaiser, C. Ottmann, O. H. Kramer, and R. H. Stauber. 2012. 'Allosteric inhibition of Taspase1's pathobiological activity by enforced dimerization in vivo', *FASEB J*, 26: 3421-9.

Braakhuis, B. J., R. H. Brakenhoff, and C. R. Leemans. 2005. 'Head and neck cancer: molecular carcinogenesis', *Ann Oncol*, 16 Suppl 2: ii249-50.

Chen, D. Y., H. Liu, S. Takeda, H. C. Tu, S. Sasagawa, B. A. Van Tine, D. Lu, E. H. Cheng, and J. J. Hsieh. 2010. 'Taspase1 functions as a non-oncogene addiction protease that coordinates cancer cell proliferation and apoptosis', *Cancer Res*, 70: 5358-67.

Cho, J. K., G. J. Lee, H. D. Kim, U. Y. Moon, M. J. Kim, S. Kim, K. H. Baek, and H. S. Jeong. 2018. 'Differential impact of circulating tumor cells on disease recurrence and survivals in patients with head and neck squamous cell carcinomas: An updated meta-analysis', *PLoS One*, 13: e0203758.

Chung, C. H., J. S. Parker, G. Karaca, J. Wu, W. K. Funkhouser, D. Moore, D. Butterfoss, D. Xiang, A. Zanation, X. Yin, W. W. Shockley, M. C. Weissler, L. G. Dressler, C. G. Shores, W. G. Yarbrough, and C. M. Perou. 2004. 'Molecular classification of head and neck squamous cell carcinomas using patterns of gene expression', *Cancer Cell*, 5: 489-500.

Cristofanilli, M., K. R. Broglio, V. Guarneri, S. Jackson, H. A. Fritsche, R. Islam, S. Dawood, J. M. Reuben, S. W. Kau, J. M. Lara, S. Krishnamurthy, N. T. Ueno, G. N. Hortobagyi, and V. Valero. 2007. 'Circulating tumor cells in metastatic breast cancer: biologic staging beyond tumor burden', *Clin Breast Cancer*, 7: 471-9.

Dall, E., and H. Brandstetter. 2016. 'Structure and function of legumain in health and disease', *Biochimie*, 122: 126-50.

Deuss, E., D. Gosswein, D. Gul, S. Zimmer, S. Foersch, C. S. Eger, I. Limburg, R. H. Stauber, and J. Kunzel. 2020. 'Growth Factor Receptor Expression in Oropharyngeal Squamous Cell Cancer: Her1-4 and c-Met in Conjunction with the Clinical Features and Human Papillomavirus (p16) Status', *Cancers (Basel)*, 12.

Dong, Y., B. A. Van Tine, T. Oyama, P. I. Wang, E. H. Cheng, and J. J. Hsieh. 2014. 'Taspase1 cleaves MLL1 to activate cyclin E for HER2/neu breast tumorigenesis', *Cell Res*.

Erkan, M., J. Kleeff, A. Gorbachevski, C. Reiser, T. Mitkus, I. Esposito, T. Giese, M. W. Buchler, N. A. Giese, and H. Friess. 2007. 'Periostin creates a tumor-supportive microenvironment in the pancreas by sustaining fibrogenic stellate cell activity', *Gastroenterology*, 132: 1447-64.

Fakhry, C., W. H. Westra, S. Li, A. Cmelak, J. A. Ridge, H. Pinto, A. Forastiere, and M. L. Gillison. 2008. 'Improved survival of patients with human papillomavirus-positive head and neck squamous cell carcinoma in a prospective clinical trial', *J Natl Cancer Inst*, 100: 261-9.

Ferlay, J., M. Colombet, I. Soerjomataram, C. Mathers, D. M. Parkin, M. Pineros, A. Znaor, and F. Bray. 2019. 'Estimating the global cancer incidence and mortality in 2018: GLOBOCAN sources and methods', *Int J Cancer*, 144: 1941-53.

Ferlito, A., A. R. Shaha, C. E. Silver, A. Rinaldo, and V. Mondin. 2001. 'Incidence and sites of distant metastases from head and neck cancer', *ORL J Otorhinolaryngol Relat Spec*, 63: 202-7.

Fillies, T., R. Werkmeister, J. Packeisen, B. Brandt, P. Morin, D. Weingart, U. Joos, and H. Buerger. 2006. 'Cytokeratin 8/18 expression indicates a poor prognosis in squamous cell carcinomas of the oral cavity', *BMC Cancer*, 6: 10.

Gillison, M. L., L. Alemany, P. J. Snijders, A. Chaturvedi, B. M. Steinberg, S. Schwartz, and X. Castellsague. 2012. 'Human papillomavirus and diseases of the upper airway: head and neck cancer and respiratory papillomatosis', *Vaccine*, 30 Suppl 5: F34-54.

Goesswein, D., N. Habtemichael, A. Gerhold-Ay, J. Mazur, D. Wunsch, S. K. Knauer, J. Kunzel, C. Matthias, S. Strieth, and R. H. Stauber. 2018. 'Expressional analysis of disease-relevant signalling-pathways in primary tumours and metastasis of head and neck cancers', *Sci Rep*, 8: 7326.

Gonzalez-Gonzalez, L., and J. Alonso. 2018. 'Periostin: A Matricellular Protein With Multiple Functions in Cancer Development and Progression', *Front Oncol*, 8: 225.

Gonzalez, H. E., M. Gujrati, M. Frederick, Y. Henderson, J. Arumugam, P. W. Spring, K. Mitsudo, H. W. Kim, and G. L. Clayman. 2003. 'Identification of 9 genes differentially expressed in head and neck squamous cell carcinoma', *Arch Otolaryngol Head Neck Surg*, 129: 754-9.

Gregoire, V., J. L. Lefebvre, L. Licitra, E. Felip, and Ehns-Esmo-Estro Guidelines Working Group. 2010. 'Squamous cell carcinoma of the head and neck: EHNS-ESMO-ESTRO Clinical Practice Guidelines for diagnosis, treatment and follow-up', *Ann Oncol*, 21 Suppl 5: v184-6.

Gribko, A., J. Kunzel, D. Wunsch, Q. Lu, S. M. Nagel, S. K. Knauer, R. H. Stauber, and G. B. Ding. 2019. 'Is small smarter? Nanomaterial-based detection and elimination of circulating tumor cells: current knowledge and perspectives', *Int J Nanomedicine*, 14: 4187-209.

Gribko, Alena, Janis Stiefel, Lana Liebetanz, Sophie Madeleine Nagel, Julian Künzel, Madita Wandrey, Jan Hagemann, Roland H. Stauber, Christian Freese, and Désirée Gül. 2021. 'IsoMAG—An Automated System for the Immunomagnetic Isolation of Squamous Cell Carcinoma-Derived Circulating Tumor Cells', *Diagnostics*, 11: 2040.

Grobe, A., M. Blessmann, H. Hanken, R. E. Friedrich, G. Schon, J. Wikner, K. E. Effenberger, L. Kluwe, M. Heiland, K. Pantel, and S. Riethdorf. 2014. 'Prognostic relevance of circulating tumor cells in blood and disseminated tumor cells in bone marrow of patients with squamous cell carcinoma of the oral cavity', *Clin Cancer Res*, 20: 425-33.

Gul, D., N. Habtemichael, D. Dietrich, J. Dietrich, D. Gosswein, A. Khamis, E. Deuss, J. Kunzel, G. Schneider, S. Strieth, and R. H. Stauber. 2021. 'Identification of cytokeratin24 as a tumor suppressor for the management of head and neck cancer', *Biol Chem*, 0.

Gul, D., A. Schweitzer, A. Khamis, S. K. Knauer, G. B. Ding, L. Freudelsperger, I. Karampinis, S. Strieth, J. Hagemann, and R. H. Stauber. 2022. 'Impact of Secretion-Active Osteoblast-Specific Factor 2 in Promoting Progression and Metastasis of Head and Neck Cancer', *Cancers (Basel)*, 14.

Hahlbrock, A., D. Goesswein, J. Kunzel, D. Wunsch, and R. H. Stauber. 2016. 'Threonine Aspartase1: An unexplored protease with relevance for oral oncology?', *Oral Oncol*, 54: e10-2.

Hamoir, M., S. Schmitz, and V. Gregoire. 2014. 'The role of neck dissection in squamous cell carcinoma of the head and neck', *Curr Treat Options Oncol*, 15: 611-24.

Hanahan, D., and R. A. Weinberg. 2011. 'Hallmarks of cancer: the next generation', *Cell*, 144: 646-74.

Heath, J. R., M. E. Davis, and L. Hood. 2009. 'Nanomedicine targets cancer', *Sci Am*, 300: 44-51.

Hermsen, M., M. A. Guervos, G. Meijer, J. Baak, P. van Diest, C. A. Marcos, and A. Sampedro. 2001. 'New chromosomal regions with high-level amplifications in squamous cell carcinomas of the larynx and pharynx, identified by comparative genomic hybridization', *J Pathol*, 194: 177-82.

Hoing, A., A. Zimmermann, L. Moews, M. Killa, M. Heimann, A. Hensel, J. Voskuhl, and S. K. Knauer. 2022. 'A Bivalent Supramolecular GCP Ligand Enables Blocking of the Taspase1/Importin alpha Interaction', *ChemMedChem*, 17: e202100640.

Hsieh, J. J., E. H. Cheng, and S. J. Korsmeyer. 2003. 'Taspase1: a threonine aspartase required for cleavage of MLL and proper HOX gene expression', *Cell*, 115: 293-303.

Hu, Y., X. Yu, G. Xu, and S. Liu. 2017. 'Metastasis: an early event in cancer progression', *J Cancer Res Clin Oncol*, 143: 745-57.

Huang, X., P. Gao, Y. Song, J. Sun, X. Chen, J. Zhao, H. Xu, and Z. Wang. 2015. 'Meta-analysis of the prognostic value of circulating tumor cells detected with the CellSearch System in colorectal cancer', *BMC Cancer*, 15: 202.

Jatana, K. R., P. Balasubramanian, J. C. Lang, L. Yang, C. A. Jatana, E. White, A. Agrawal, E. Ozer, D. E. Schuller, T. N. Teknos, and J. J. Chalmers. 2010. 'Significance of circulating tumor cells in patients with squamous cell carcinoma of the head and neck: initial results', *Arch Otolaryngol Head Neck Surg*, 136: 1274-9.

Jin, C., Y. Jin, D. Gisselsson, J. Wennerberg, T. S. Wah, B. Stromback, Y. L. Kwong, and F. Mertens. 2006. 'Molecular cytogenetic characterization of the 11q13 amplicon in head and neck squamous cell carcinoma', *Cytogenet Genome Res*, 115: 99-106.

Johnson, D. E., B. Burtness, C. R. Leemans, V. W. Y. Lui, J. E. Bauman, and J. R. Grandis. 2020. 'Head and neck squamous cell carcinoma', *Nat Rev Dis Primers*, 6: 92.

Karantza, V. 2011. 'Keratins in health and cancer: more than mere epithelial cell markers', *Oncogene*, 30: 127-38.

Khan, J. A., B. M. Dunn, and L. Tong. 2005. 'Crystal structure of human Taspase1, a crucial protease regulating the function of MLL', *Structure*, 13: 1443-52.

Kim, C. J., N. Yoshioka, Y. Tambe, R. Kushima, Y. Okada, and H. Inoue. 2005. 'Periostin is down-regulated in high grade human bladder cancers and suppresses in vitro cell invasiveness and in vivo metastasis of cancer cells', *Int J Cancer*, 117: 51-8.

Kiweler, N., D. Wunsch, M. Wirth, N. Mahendrarajah, G. Schneider, R. H. Stauber, W. Brenner, F. Butter, and O. H. Kramer. 2020. 'Histone deacetylase inhibitors dysregulate DNA repair proteins and antagonize metastasis-associated processes', *J Cancer Res Clin Oncol*, 146: 343-56.

Koblinski, J. E., M. Ahram, and B. F. Sloane. 2000. 'Unraveling the role of proteases in cancer', *Clin Chim Acta*, 291: 113-35.

Kudo, Y., B. S. Siriwardena, H. Hatano, I. Ogawa, and T. Takata. 2007. 'Periostin: novel diagnostic and therapeutic target for cancer', *Histol Histopathol*, 22: 1167-74.

Kulasinghe, A., J. Kapeleris, R. Kimberley, S. R. Mattarollo, E. W. Thompson, J. P. Thiery, L. Kenny, K. O'Byrne, and C. Punyadeera. 2018. 'The prognostic significance of circulating tumor cells in head and neck and non-small-cell lung cancer', *Cancer Med*, 7: 5910-19.

Kunzel, J., A. Gribko, Q. Lu, R. H. Stauber, and D. Wunsch. 2019. 'Nanomedical detection and downstream analysis of circulating tumor cells in head and neck patients', *Biol Chem*, 400: 1465-79.

Lee, N. C. J., J. R. Kelly, H. S. Park, Y. An, B. L. Judson, B. A. Burtness, and Z. A. Husain. 2018. 'Patterns of failure in high-metastatic node number human papillomavirus-positive oropharyngeal carcinoma', *Oral Oncol*, 85: 35-39.

Lianidou, E. S., and A. Markou. 2011. 'Circulating tumor cells in breast cancer: detection systems, molecular characterization, and future challenges', *Clin Chem*, 57: 1242-55.

Lopez-Otin, C., and J. S. Bond. 2008. 'Proteases: multifunctional enzymes in life and disease', *J Biol Chem*, 283: 30433-7.

Lopez-Otin, C., and L. M. Matrisian. 2007. 'Emerging roles of proteases in tumour suppression', *Nat Rev Cancer*, 7: 800-8.

Luo, J., N. L. Solimini, and S. J. Elledge. 2009. 'Principles of cancer therapy: oncogene and non-oncogene addiction', *Cell*, 136: 823-37.

Malek, N. P., H. Sundberg, S. McGrew, K. Nakayama, T. R. Kyriakides, and J. M. Roberts. 2001. 'A mouse knock-in model exposes sequential proteolytic pathways that regulate p27Kip1 in G1 and S phase', *Nature*, 413: 323-7.

Marur, S., and A. A. Forastiere. 2016. 'Head and Neck Squamous Cell Carcinoma: Update on Epidemiology, Diagnosis, and Treatment', *Mayo Clin Proc*, 91: 386-96.

Mehrpouya, M., Z. Pourhashem, N. Yardehnavi, and M. Oladnabi. 2019. 'Evaluation of cytokeratin 19 as a prognostic tumoral and metastatic marker with focus on improved detection methods', *J Cell Physiol*, 234: 21425-35.

Mockelmann, N., S. Laban, K. Pantel, and R. Knecht. 2014. 'Circulating tumor cells in head and neck cancer: clinical impact in diagnosis and follow-up', *Eur Arch Otorhinolaryngol*, 271: 15-21.

Moll, R., M. Divo, and L. Langbein. 2008. 'The human keratins: biology and pathology', *Histochem Cell Biol*, 129: 705-33.

Moll, R., W. W. Franke, D. L. Schiller, B. Geiger, and R. Krepler. 1982. 'The catalog of human cytokeratins: patterns of expression in normal epithelia, tumors and cultured cells', *Cell*, 31: 11-24.

Nichols, A. C., L. E. Lowes, C. C. Szeto, J. Basmaji, S. Dhaliwal, C. Chapeskie, B. Todorovic, N. Read, V. Venkatesan, A. Hammond, D. A. Palma, E. Winquist, S. Ernst, K. Fung, J. H. Franklin, J. Yoo, J. Koropatnick, J. S. Mymryk, J. W. Barrett, and A. L. Allan. 2012. 'Detection of circulating tumor cells in advanced head and neck cancer using the CellSearch system', *Head Neck*, 34: 1440-4.

Overall, C. M., and R. A. Dean. 2006. 'Degradomics: systems biology of the protease web. Pleiotropic roles of MMPs in cancer', *Cancer Metastasis Rev*, 25: 69-75.

Oyama, T., S. Sasagawa, S. Takeda, R. A. Hess, P. M. Lieberman, E. H. Cheng, and J. J. Hsieh. 2013. 'Cleavage of TFIIA by Taspase1 activates TRF2-specified mammalian male germ cell programs', *Dev Cell*, 27: 188-200.

Pai, S. I., and W. H. Westra. 2009. 'Molecular pathology of head and neck cancer: implications for diagnosis, prognosis, and treatment', *Annu Rev Pathol*, 4: 49-70.

Partridge, M., R. Brakenhoff, E. Phillips, K. Ali, R. Francis, R. Hooper, K. Lavery, A. Brown, and J. Langdon. 2003. 'Detection of rare disseminated tumor cells identifies head and neck cancer patients at risk of treatment failure', *Clin Cancer Res*, 9: 5287-94.

Pasch, P., A. Hoing, S. Ueclue, M. Killa, J. Voskuhl, S. K. Knauer, and L. Hartmann. 2021. 'PEGylated sequence-controlled macromolecules using supramolecular binding to target the Taspase1/Importin alpha interaction', *Chem Commun (Camb)*, 57: 3091-94.

Riethdorf, S., H. Fritsche, V. Muller, T. Rau, C. Schindlbeck, B. Rack, W. Janni, C. Coith, K. Beck, F. Janicke, S. Jackson, T. Gornet, M. Cristofanilli, and K. Pantel. 2007. 'Detection of circulating tumor cells in peripheral blood of patients with metastatic breast cancer: a validation study of the CellSearch system', *Clin Cancer Res*, 13: 920-8.

Rocken, M. 2010. 'Early tumor dissemination, but late metastasis: insights into tumor dormancy', *J Clin Invest*, 120: 1800-3.

Sacco, A. G., and E. E. Cohen. 2015. 'Current Treatment Options for Recurrent or Metastatic Head and Neck Squamous Cell Carcinoma', *J Clin Oncol*, 33: 3305-13.

Saklatvala, J., Nagase, H., and Salvesen, G. 2002. 'Biochemical Society Symposia vol. 70: Proteases and the regulation of biological processes.', *Portland Press, London*.

Sasaki, H., M. Dai, D. Auclair, I. Fukai, M. Kiriyama, Y. Yamakawa, Y. Fujii, and L. B. Chen. 2001. 'Serum level of the periostin, a homologue of an insect cell adhesion molecule, as a prognostic marker in nonsmall cell lung carcinomas', *Cancer*, 92: 843-8.

Sasaki, H., K. M. Lo, L. B. Chen, D. Auclair, Y. Nakashima, S. Moriyama, I. Fukai, C. Tam, M. Loda, and Y. Fujii. 2001. 'Expression of Periostin, homologous with an insect cell adhesion molecule, as a prognostic marker in non-small cell lung cancers', *Jpn J Cancer Res*, 92: 869-73.

Schrenk, C., V. Fetz, C. Vallet, C. Heiselmayer, E. Schroder, A. Hensel, A. Hahlbrock, D. Wunsch, D. Goesswein, C. Bier, N. Habtemichael, G. Schneider, R. H. Stauber, and S. K. Knauer. 2018. 'TFIIA transcriptional activity is controlled by a 'cleave-and-run' Exportin-1/Taspase 1-switch', *J Mol Cell Biol*, 10: 33-47.

Sessions, D. G., G. J. Spector, J. Lenox, B. Haughey, C. Chao, and J. Marks. 2002. 'Analysis of treatment results for oral tongue cancer', *Laryngoscope*, 112: 616-25.

Shao, R., S. Bao, X. Bai, C. Blanchette, R. M. Anderson, T. Dang, M. L. Gishizky, J. R. Marks, and X. F. Wang. 2004. 'Acquired expression of periostin by human breast cancers promotes tumor angiogenesis through up-regulation of vascular endothelial growth factor receptor 2 expression', *Mol Cell Biol*, 24: 3992-4003.

Sharma, P., S. Alsharif, A. Fallatah, and B. M. Chung. 2019. 'Intermediate Filaments as Effectors of Cancer Development and Metastasis: A Focus on Keratins, Vimentin, and Nestin', *Cells*, 8.

Shi, R., Y. Q. Tang, and H. Miao. 2020. 'Metabolism in tumor microenvironment: Implications for cancer immunotherapy', *MedComm (2020)*, 1: 47-68.

Shukla, S., A. C. Bharti, S. Mahata, S. Hussain, R. Kumar, S. Hedau, and B. C. Das. 2009. 'Infection of human papillomaviruses in cancers of different human organ sites', *Indian J Med Res*, 130: 222-33.

Siemer, S., T. Fauth, P. Scholz, Y. Al-Zamel, A. Khamis, D. Gul, L. Freudelsperger, B. Wollenberg, S. Becker, R. H. Stauber, and J. Hagemann. 2021. 'Profiling Cisplatin Resistance in Head and Neck Cancer: A Critical Role of the VRAC Ion Channel for Chemoresistance', *Cancers (Basel)*, 13.

Siemer, S., D. Wunsch, A. Khamis, Q. Lu, A. Scherberich, M. Filippi, M. P. Krafft, J. Hagemann, C. Weiss, G. B. Ding, R. H. Stauber, and A. Gribko. 2020. 'Nano Meets Micro-Translational Nanotechnology in Medicine: Nano-Based Applications for Early Tumor Detection and Therapy', *Nanomaterials (Basel)*, 10.

Siriwardena, B. S., Y. Kudo, I. Ogawa, M. Kitagawa, S. Kitajima, H. Hatano, W. M. Tilakaratne, M. Miyauchi, and T. Takata. 2006. 'Periostin is frequently overexpressed and enhances invasion and angiogenesis in oral cancer', *Br J Cancer*, 95: 1396-403.

Stauber, R. H., C. Bier, and S. K. Knauer. 2012. 'Targeting Taspase1 for cancer therapy--letter', *Cancer Res*, 72: 2912; author reply 13.

Stauber, R. H., A. Hahlbrock, S. K. Knauer, and D. Wunsch. 2016. 'Cleaving for growth: threonine aspartase 1--a protease relevant for development and disease', *FASEB J*, 30: 1012-22.

Stauber, R. H., S. K. Knauer, N. Habtemichael, C. Bier, B. Unruhe, S. Weisheit, S. Spange, F. Nonnenmacher, V. Fetz, T. Ginter, S. Reichardt, C. Liebmann, G. Schneider, and O. H. Kramer. 2012. 'A combination of a ribonucleotide reductase inhibitor and histone deacetylase inhibitors downregulates EGFR and triggers BIM-dependent apoptosis in head and neck cancer', *Oncotarget*, 3: 31-43.

Stiefel, J., C. Freese, A. Sriram, S. Alebrand, N. Srinivas, C. Sproll, M. Wandrey, D. Gul, J. Hagemann, J. C. Becker, and M. Bassler. 2022. 'Characterization of a novel microfluidic platform for the isolation of rare single cells to enable CTC analysis from head and neck squamous cell carcinoma patients', *Eng Life Sci*, 22: 391-406.

Takeda, S., D. Y. Chen, T. D. Westergard, J. K. Fisher, J. A. Rubens, S. Sasagawa, J. T. Kan, S. J. Korsmeyer, E. H. Cheng, and J. J. Hsieh. 2006. 'Proteolysis of MLL family proteins is essential for taspase1-orchestrated cell cycle progression', *Genes Dev*, 20: 2397-409.

Takeda, S., S. Sasagawa, T. Oyama, A. C. Searleman, T. D. Westergard, E. H. Cheng, and J. J. Hsieh. 2015. 'Taspase1-dependent TFIIA cleavage coordinates head morphogenesis by limiting Cdkn2a locus transcription', *J Clin Invest*.

Takeshita, S., R. Kikuno, K. Tezuka, and E. Amann. 1993. 'Osteoblast-specific factor 2: cloning of a putative bone adhesion protein with homology with the insect protein fasciclin I', *Biochem J*, 294 (Pt 1): 271-8.

Thalgott, M., M. M. Heck, and K. Pantel. 2014. '[Detection of circulating tumor cells from peripheral blood in prostate cancer]', *Urologe A*, 53: 509-13.

Tinhofer, I., and S. Staudte. 2018. 'Circulating tumor cells as biomarkers in head and neck cancer: recent advances and future outlook', *Expert Rev Mol Diagn*, 18: 897-906.

Toyoshima, T., E. Vairaktaris, E. Nkenke, K. A. Schlegel, F. W. Neukam, and J. Ries. 2008. 'Cytokeratin 17 mRNA expression has potential for diagnostic marker of oral squamous cell carcinoma', *J Cancer Res Clin Oncol*, 134: 515-21.

Turk, B. 2006. 'Targeting proteases: successes, failures and future prospects', *Nat Rev Drug Discov*, 5: 785-99.

Unruhe, B., E. Schroder, D. Wunsch, and S. K. Knauer. 2016. 'An Old Flame Never Dies: Survivin in Cancer and Cellular Senescence', *Gerontology*, 62: 173-81.

van den Boom, J., A. Hensel, F. Trusch, A. Matena, S. Siemer, D. Guel, D. Docter, A. Hoing, P. Bayer, R. H. Stauber, and S. K. Knauer. 2020. 'The other side of the corona: nanoparticles inhibit the protease taspase1 in a size-dependent manner', *Nanoscale*, 12: 19093-103.

Wienecke, A., and K. Kraywinkel. 2019. 'Epidemiologie von Kopf-Hals-Tumoren in Deutschland', *Onkologe*, 25 190–200.

Wikner, J., A. Grobe, K. Pantel, and S. Riethdorf. 2014. 'Squamous cell carcinoma of the oral cavity and circulating tumour cells', *World J Clin Oncol*, 5: 114-24.

Winter, S. C., S. A. Stephenson, S. K. Subramaniam, V. Paleri, K. Ha, C. Marnane, S. Krishnan, and G. Rees. 2009. 'Long term survival following the detection of circulating tumour cells in head and neck squamous cell carcinoma', *BMC Cancer*, 9: 424.

Wollenberg, B., A. Walz, K. Kolbow, C. Pauli, S. Chaubal, and M. Andratschke. 2004. 'Clinical relevance of circulating tumour cells in the bone marrow of patients with SCCHN', *Onkologie*, 27: 358-62.

Wünsch, D., V. Fetz, D. Heider, S. Tenzer, C. Bier, L. Kunst, S. Knauer, and R. Stauber. 2012. 'Chemico-genetic strategies to inhibit the leukemic potential of threonine aspartase-1', *Blood Cancer J*, 2: e77.

Wunsch, D., A. Hahlbrock, C. Heiselmayer, S. Backer, P. Heun, D. Goesswein, W. Stocker, T. Schirmeister, G. Schneider, O. H. Kramer, S. K. Knauer, and R. H. Stauber. 2015. 'Fly versus man: evolutionary impairment of nucleolar targeting affects the degradome of Drosophila's Taspase1', *FASEB J*, 29: 1973-85.

Wunsch, D., A. Hahlbrock, C. Heiselmayer, S. Backer, C. Schrenk, F. Benne, O. Schilling, and S. K. Knauer. 2015. 'Evolutionary divergence of Threonine Aspartase1 leads to species-specific substrate recognition', *Biol Chem*, 396: 367-76.

Wünsch, D., A. Hahlbrock, S. Jung, T. Schirmeister, J. van den Boom, O. Schilling, S. K. Knauer, and R. H. Stauber. 2016. 'Taspase1: a 'misunderstood' protease with translational cancer relevance', *Oncogene*, 35: 3351-64.

Zhou, H., S. Spicuglia, J. J. Hsieh, D. J. Mitsiou, T. Hoiby, G. J. Veenstra, S. J. Korsmeyer, and H. G. Stunnenberg. 2006. 'Uncleaved TFIIA is a substrate for taspase 1 and active in transcription', *Mol Cell Biol*, 26: 2728-35.

7. PUBLICATIONS OF CUMULATIVE WORK

I. Gribko, A.; Hahlbrock, A.; Strieth, S.; Becker, S.; Hagemann, J.; Deichelbohrer, M.; Hildebrandt, A.; Habtemichael, N.; **Wunsch, D**. Disease-relevant signalling-pathways in head and neck cancer: Taspase1's proteolytic activity fine-tunes TFIIA function. *Sci Rep* 2017, 7, 14937, doi:10.1038/s41598-017-14814-x.

II. Kiweler, N.*; **Wunsch, D.***; Wirth, M.; Mahendrarajah, N.; Schneider, G.; Stauber, R.H.; Brenner, W.; Butter, F.; Kramer, O.H. Histone deacetylase inhibitors dysregulate DNA repair proteins and antagonize metastasis-associated processes. *J Cancer Res Clin Oncol* 2020, *146*, 343-356, doi:10.1007/s00432-019-03118-4.*equal first author contribution

III. **Gül, D.** , Habtemichael , N., Dietrich, D., Dietrich, J., Gößwein, D., Khamis, A., Deuss, E., Künzel, J., Schneider, G., Strieth, S., Stauber RH. Identification of cytokeratin24 as a tumor suppressor for the management of head and neck cancer. *Biological Chemistry* 2021. doi:doi:10.1515/hsz-2021-0287.

IV. **Gül D.,** Schweitzer A., Khamis A., Knauer S. K., Ding G. B., Freudelsperger L., Karampinis I., Strieth S., Hagemann J., Stauber R. H. Impact of Secretion-Active Osteoblast-Specific Factor 2 in Promoting Progression and Metastasis of Head and Neck Cancer. Cancers (Basel). 2022;14(9).

V. Gribko, A.; Stiefel, J.; Liebetanz, L.; Nagel, S.M.; Künzel, J.; Wandrey, M.; Hagemann, J.; Stauber, R.H.; Freese, C.; **Gül, D**. IsoMAG—An Automated System for the Immunomagnetic Isolation of Squamous Cell Carcinoma-Derived Circulating Tumor Cells. *Diagnostics* 2021, *11*, 2040.

I.

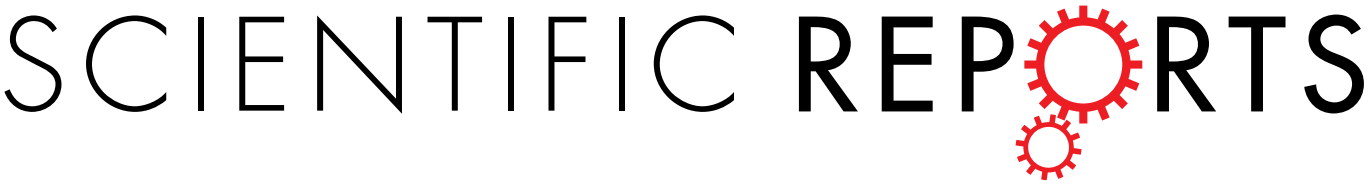

OPEN

Disease-relevant signalling-pathways in head and neck cancer: Taspase1's proteolytic activity fine-tunes TFIIA function

Received: 14 July 2017
Accepted: 16 October 2017
Published online: 02 November 2017

Alena Gribko[1], Angelina Hahlbrock[1], Sebastian Strieth[1], Sven Becker[1], Jan Hagemann[1], Max Deichelbohrer[1], Andreas Hildebrandt[2], Negusse Habtemichael[1] & Désirée Wünsch[1]

Head and neck cancer (HNC) is the seventh most common malignancy in the world and its prevailing form, the head and neck squamous cell carcinoma (HNSCC), is characterized as aggressive and invasive cancer type. The transcription factor II A (TFIIA), initially described as general regulator of RNA polymerase II-dependent transcription, is part of complex transcriptional networks also controlling mammalian head morphogenesis. Posttranslational cleavage of the TFIIA precursor by the oncologically relevant protease Taspase1 is crucial in this process. In contrast, the relevance of Taspase1-mediated TFIIA cleavage during oncogenesis of HNSCC is not characterized yet. Here, we performed genome-wide expression profiling of HNSCC which revealed significant downregulation of the TFIIA downstream target CDKN2A. To identify potential regulatory mechanisms of TFIIA on cellular level, we characterized nuclear-cytoplasmic transport and Taspase1-mediated cleavage of TFIIA variants. Unexpectedly, we identified an evolutionary conserved nuclear export signal (NES) counteracting nuclear localization and thus, transcriptional activity of TFIIA. Notably, proteolytic processing of TFIIA by Taspase1 was found to mask the NES, thereby promoting nuclear localization and transcriptional activation of TFIIA target genes, such as CDKN2A. Collectively, we here describe a hitherto unknown mechanism how cellular localization and Taspase1 cleavage fine-tunes transcriptional activity of TFIIA in HNSCC.

Head and neck cancers (HNC) are among the most common malignant neoplasms in humans[1]. HNC is typically diagnosed at advanced stages with metastases resulting in a 5-year survival rate of less than 50%[2]. The prevailing form of HNC, head and neck squamous cell carcinoma (HNSCC), is characterized as a very aggressive and invasive cancer type affecting multiple sites of the upper aerodigestive tract like the nasal cavity, mouth, salivary glands, larynx and pharynx[2,3]. Major risk factors associated with the development of HNSCC are tobacco use, alcohol consumption and high-risk human papilloma virus infections (HPV)[4]. Due to the late disease presentation of the patient, lack of suitable biomarkers, and corresponding drugs for individually targeted therapy approaches, survival rates for HNSCC have not improved significantly within the last years[5–7]. Currently, the main prognostic parameters of HNSCC are the size and location of the tumour, the presence of distant metastasis and cervical lymph node metastases, which is not sufficient to evaluate the disease outcome[3,8,9]. Despite advances in therapy, the treatment of HNSCC still often comes along with functional impairment and cosmetic deformity of vital functions of the aerodigestive tract, such as breathing, swallowing, speech, hearing and smell[3]. Although the use of kinase inhibitors or antibodies has gained increasing clinical relevance, there is still urgent need for effective therapies and novel drug targets.

The protease Threonine Aspartase1 or Taspase1 has been identified as a promising new anti-cancer target which is critically involved in the development of aggressive infant leukaemias and HER2-associated breast cancer via its substrate MLL[10,11]. In addition, Taspase1 is overexpressed in a variety of solid tumours, including HNSCC[12]. The human *Taspase1* gene encodes a protein of 420 amino acids (aa) resembling the Taspase1 proenzyme. Based on structural similarities Taspase1 was classified as a type 2 asparaginase exhibiting several specific

[1]Department of Otorhinolaryngology, Molecular and Cellular Oncology, University Hospital of Mainz, Langenbeckstrasse 1, Mainz, 55101, Germany. [2]Scientific Computing and Bioinformatics, Johannes Gutenberg University, Staudingerweg 9, Mainz, 55128, Germany. Correspondence and requests for materials should be addressed to D.W. (email: desiree.wuensch@unimedizin-mainz.de)

characteristics[13]. In contrast to the exclusively *cis*-active type 2 asparaginases, only Taspase1 is able to cleave distinct substrates in *trans* by hydrolyzing its target proteins at conserved ($Q^3[FILV]^2D^1\downarrow G^{1'}x^{2'}D^{3'}D^{4'}$) sites[14,15]. During mammalian development, Taspase1 plays an important role in the regulation of correct segmental identities, head morphogenesis and spermatogenesis[16–19]. However, the molecular mechanisms how Taspase1 may affect substrate functions through site-specific proteolysis still remain to be determined. Importantly, no specific small molecule or genetic inhibitors are available worldwide, hampering not only to further dissect Taspase1's disease mechanisms, but also precluding the full assessment of its clinical impact[20–22].

Besides MLL other essential proteins, such as the precursor of the transcription factor IIA (TFIIA) have been identified as native Taspase1 targets[23]. TFIIA has been initially characterized as part of the preinitiation complex initiating RNA polymerase II transcription[24]. TFIIA is composed of three subunits, α, β, and γ encoded by two separated genes, TFIIAαβ and TFIIAγ. The γ-subunit is conserved among different species, whereas sequence similarity in TFIIAαβ is limited mostly to the N-terminal region of the α-subunit and the C terminus covering most of the β-subunit[25]. TFIIAαβ is posttranslationally processed by Taspase1 at an evolutionary conserved cleavage site QVDG (aa 272 to 275)[23]. Interestingly, both uncleaved αβ and the cleaved α- and β-subunits can be found in association with the TFIIAγ subunit *in vivo*[26,27]. Additionally, both complexes interact with the TATA-binding protein (TBP) on DNA and support transcription to similar extents *in vitro* and in reporter assays[28,29]. Therefore, uncleaved and cleaved forms of TFIIA may have distinct gene regulatory functions in differentiation. The observation that cleavage is the prerequisite for proteasome mediated degradation of TFIIA[28] indicates that cleavage regulates TFIIA stability and thus, transcriptional activity. This hypothesis was supported by a study showing that Taspase1-mediated cleavage of TFIIA ensures proper head formation during mouse development[18]. It has been suggested that TFIIAαβ cleavage by Taspase1 results in suppression of CDKN2A expression and finally, in proper head formation[18]. The CDKN2A gene locus encodes for the cell cycle regulators $p16^{INK4a}$, $p19^{ARF}$ and $p21^{CIP}$, blocking cell cycle progress in G1 and S phase[30]. Especially the tumour suppressor $p16^{INK4a}$ is in focus of interest as putative biomarker for HNSCC.

Controlled distribution of macromolecules within different cellular compartments is an elaborated way of controlling protein activity. In eukaryotic cells, spatial and functional division is ensured by the nuclear envelope separating the nucleus from the cytoplasm[31]. Nucleocytoplasmic transport takes place through nuclear pores and is tightly regulated by specific signals and transport receptors[31]. In general, active nuclear import is mediated by short stretches of basic amino acids, termed nuclear localization signals (NLS), which interact with specific import receptors[12]. In contrast, signal mediated nuclear export pathways are less understood[32]. A well-characterized class of nuclear export signals (NES) consist of short leucine-rich stretches interacting with the export receptor Crm1[33]. Leucine-rich NES have been identified in an increasing number of cellular and viral proteins executing heterogeneous biological functions. Especially for transcription factors, executing their biological function within the cell nucleus, such regulated subcellular localization provides an attractive way to control their activity[34]. This indeed has been demonstrated for several key players of signal transduction cascades[35,36].

Besides its relevance during normal head development, the molecular mechanisms how Taspase1 may affect TFIIA functions in malignant tissue of HNSCCs still remain to be determined. In order to close this knowledge gap, we combined gene expression analysis of HNSCC tumours with cell-based analysis of TFIIA localization and proteolytic cleavage. Although TFIIA was initially described as a nuclear transcriptional regulator[37], we identified a significant fraction of TFIIA accumulating to the cytoplasm due to a highly efficient nuclear export signal. TFIIA´s ability to also reside in the cytoplasm not only counteracts its nuclear localization but also affects its transcriptional activity together with the proteolytic cleavage by Taspase1. Collectively, by regulating the nuclear availability of TFIIA, the interplay of nuclear export and Taspase1-mediated cleavage fine-tunes transcriptional regulation of TFIIA target genes, such as CDKN2A.

Results

Genome-wide expression profiling identifies CDKN2A downregulation in HNSCC tumours. To identify genes differentially expressed in HNSCC primary tumours (PT) *versus* lymph node metastasis (M) and the corresponding non-malignant tissue (N), tissues were obtained from 20 patients undergoing surgical resection. In contrast to other studies, in which genetic and epigenetic variations of individual patients require the analysis of large patient cohorts to increase the relevance of the obtained data sets, our study design focused on a patient cohort from which N, PT as well as M could be surgically recovered from the same patient. All cases were diagnosed histopathologically and staged according to the TNM classification recommended by the UICC (for clinical parameters see Supplementary Table S1). RNA was isolated from snap-frozen biopsies and all samples were assayed using the *Affymetrix U133A 2.0* gene array. We excluded 5 patients from the study due to insufficient mRNA quality. Primarily a qualitative tool, we performed unsupervised average-linkage hierarchical clustering using the *GeneSpring* software and identified several groups/subtypes within the unfiltered cluster dendrogram (Fig. 1A, Supplementary Fig. S1). Non-malignant tissue and carcinomas grouped separately on a clustering dendrogram employing the complete datasets. Thus, HNSCC tumour tissue can be distinguished from corresponding non-malignant tissue and non-malignant tissue from lymph node metastases using even unsupervised RNA expression signatures. The comparison of PT versus N revealed 650 deregulated genes (Fig. 1A), whereas lymph node metastasis (M) versus N resulted in 1579 differentially expressed genes, and 393 genes in M versus PT (Supplementary Fig. S1).

As mentioned before, Taspase1-mediated cleavage of TFIIAαβ ensures proper head morphogenesis by suppressing expression of CDKN2A[18]. In order to investigate the relevance of Taspase1-TFIIA-CDKN2A signalling also in malignant tissue of the head, gene expression was compared in PT versus N as well as M versus N (Fig. 1). Interestingly, in 14 out of 15 patients CDKN2A was significantly downregulated in PT versus N represented by two probe sets (Fig. 1C; mean $\log_2 FC = 0.65$, p value < 0.0001). Similar results were obtained for M versus N. Here, 11 out of 15 patients showed downregulation of CDKN2A (Fig. 1D; p value < 0.05). In contrast, expression

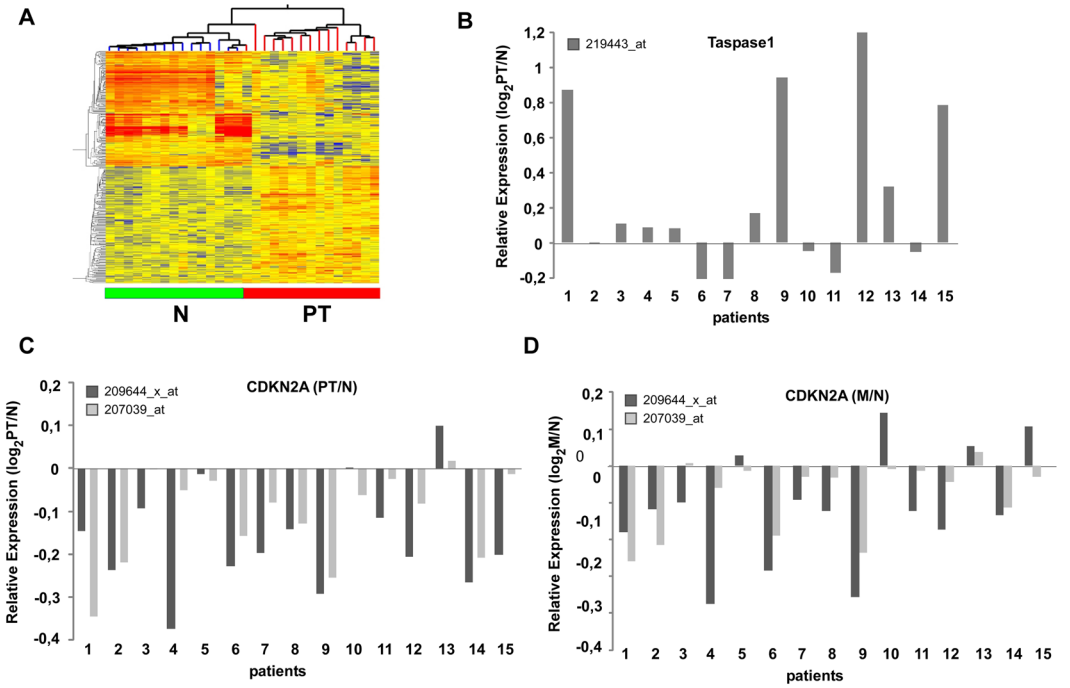

Figure 1. Genome-wide expression profiling of HNSCC primary tumours (PT) and lymph node metastases (M) versus normal tissue (N). (**A**) Intrinsic gene set cluster analysis of 45 HNSCC samples. Unsupervised two-way hierarchical clustering and gene tree representation of differentially regulated genes (fold change ≥ 2.0 and p-value < 0.05) allows to separate N and PT. X-axis represents patient samples; y-axis represents the list of probe sets grouped by similarity using Pearson correlation. The comparison of PT versus N revealed 650 deregulated genes. (**B**–**D**) Differential expression of Taspase1 (**B**) and CDKN2A (**C,D**) in 15 HNSCC tumours. Whereas the protease Taspase1 is overexpressed in primary tumours, CDKN2A expression is significantly downregulated in most PT (p-value < 0.0001) as well as M compared to N (p-value < 0.05). Relative expression levels (log_2PT/N; log_2M/N) obtained by *Affymetrix* microarray analysis are shown. CDKN2A locus is represented by two probe sets as indicated.

of TFIIA was not significantly altered in the analysed cohort (data not shown). Another member of the signalling pathway, the protease Taspase1, was found to be overexpressed in the majority of the analysed patients (Fig. 1B), as demonstrated before[12]. However, the variation of Taspase1 gene expression was elevated in the present cohort including individual patients showing no regulation or even slight downregulation of Taspase1.

Upstream analyses of CDKN2A associated pathways using the Ingenuity Pathway Analysis tool support our hypothesis that in HNSCC patients CDKN2A pathways are inactivated which is attended by silencing of the negative cell cycle regulator RB1, the CDK inhibitor CDKN1A, and the tumour suppressor TP53 (Supplementary Fig. S2A). Of note, conflicting data involving TP53 as indicated by yellow lines in the network analysis may be explained by mutations of the TP53 gene frequently occurring in HNSCC tumours[38]. In concordance, upstream analysis of cell cycle-associated genes revealed that these genes are mainly activated (Supplementary Fig. S2B).

Conclusively, genome-wide expression analysis indicates that HNSCC carcinogenesis involves deregulated signalling pathways including Taspase1 and CDKN2A.

TFIIA dynamically localizes in epithelial tumour cells. Although we found a significant downregulation of TFIIA-regulated CDKN2A locus in HNSCC patients, expression of TFIIA itself seems to be not altered. Besides transcriptional regulation, protein function could be also controlled by cellular localization and intracellular transport[39–41]. A prominent example is the group of nuclear factor-κB (NF-κB) proteins which regulate a variety of biological processes by translocating between cytoplasm and the nucleus[42]. Remarkably, TFIIA was initially described as a nuclear protein by the UniProtKB/Swiss-Prot database [P52655-TF2AA_HUMAN], but was also assigned to the cytoplasmic compartment by gene ontology [GO:0005737]. Here, we aim at the resolution of this inconsistency and the detailed characterization of TFIIA's cellular localization in epithelial tumour cells.

To dissect the mechanisms regulating TFIIA's intracellular localization, we cloned the *TFIIA*αβ open reading frame (ORF) from total RNA isolated from head and neck tumour tissue and confirmed its consistency with the ORF provided by official databases (UniProtKB - P52655). Since binding of the conserved TFIIAγ subunit does not differ dramatically between cleaved and uncleaved TFIIA forms, we focused on the analyses only of the TFIIAαβ precursor protein which will be termed TFIIA for convenience in the following text. In contrast to the reported nuclear localization, transient expression of TFIIA-GFP fusion protein revealed a predominant cytoplasmic localization in living interphase A431 cells after 24 h (Fig. 2A). Interestingly, TFIIA-GFP translocates from cytoplasm to nucleus within 48 h after transfection. As proteolytic cleavage by Taspase1 may play a critical role for TFIIA localization, we also analysed a cleavage-deficient TFIIA variant ($TFIIA_{CSmut}$, ^{272}QVDGTGD^{278} changed

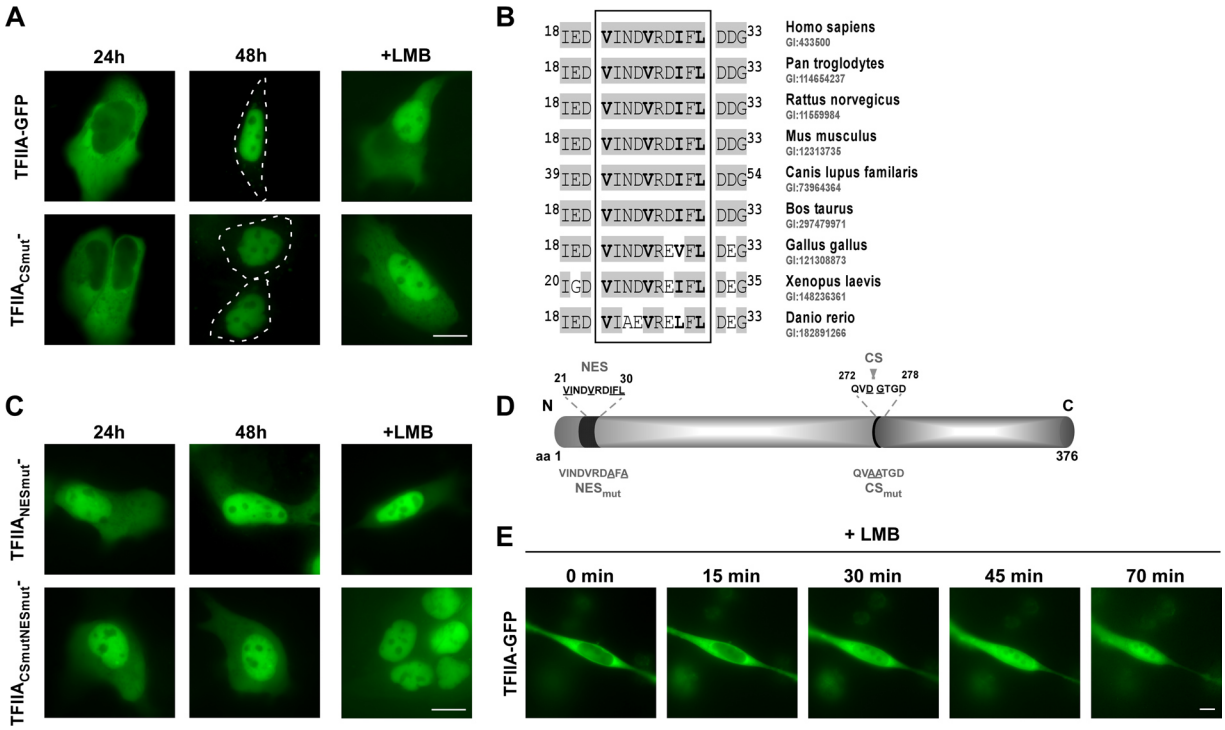

Figure 2. TFIIA dynamically localizes in epithelial tumour cells. (**A**) Transient transfection of A431 cells with wt TFIIA-GFP as well as the uncleaved mutant $TFIIA_{CSmut}$-GFP revealed initial cytoplasmic localization after 24 h. TFIIA variants translocate to the nucleus within 48 h. Treatment with the nuclear export inhibitor LMB for 3 h leads to a rapid nuclear accumulation of TFIIA wt and $TFIIA_{CSmut}$ variant. (**B**) TFIIA contains a putative nuclear export signal (aa ^{21}**VI**ND**V**RD**IFL**[30]; hydrophobic aa in bold) which is evolutionary conserved among TFIIA orthologs. (**C**) In contrast to wt TFIIA, the TFIIANESmut- and CSmutNESmut-GFP fusion variants showed nuclear accumulation already 24 h after transfection which was neither significantly changed at later time points (48 h) nor by LMB treatment. (**D**) Schematic illustration of TFIIA domain organization indicating position and sequence of nuclear export signal (NES) and Taspase1 cleavage site (CS). For used mutants changes in the aa sequence are underlined. Size not drawn to scale. (**E**) TFIIA translocates from cytoplasm to nucleus after LMB treatment within 70 min. A431 cells were transfected with wt TFIIA-GFP and treated with the export inhibitor LMB 24 h after transfection. A single cell was captured every 5 minutes for at least 70 minutes. Scale bar, 10 µm.

into ^{272}QV**AA**TGD^{278}, Fig. 2D). $TFIIA_{CSmut}$-GFP showed similar localization characterized by initial cytoplasmic localization, which changed after 48 h to nuclear (Fig. 2A). As proteins larger than 40 kDa are unable to enter or exit the nucleus by passive diffusion but depend on active nuclear transport[43], we analysed whether the dynamic translocation might be caused by active nuclear transport (Fig. 2B). Therefore, A431 cells were treated with the nuclear export inhibitor Leptomycin B (LMB) which specifically binds to the export receptor Crm1 and prevents its interaction with leucine-rich export signals[44]. Indeed, treatment with LMB lead to a rapid nuclear accumulation of TFIIA wt and $TFIIA_{CSmut}$ suggesting the presence of an active, Crm1-dependent NES. Time-lapse experiments confirmed rapid nuclear accumulation of wt TFIIA within 70 minutes induced by LMB treatment (Fig. 2E). *In silico* analysis identified a hydrophobic region of the classical type (aa^{21}**VI**ND**V**RD**IFL**[30]; hydrophobic aa in bold). Additionally, this motif is highly conserved in known TFIIA homologs (Fig. 2B), indicating a functional relevance of this putative NES.

To experimentally verify the activity of the NES, we cloned a TFIIA mutant ($TFIIA_{NESmut}$) in which two essential hydrophobic amino acid residues in the putative export signal were changed into Ala (aa^{21}**VI**ND**V**RD**AFA**[30], changed aa underlined, Fig. 2D). Transient expression of $TFIIA_{NESmut}$-GFP in A431 cells demonstrated that this mutation resulted in a nuclear accumulation of TFIIA directly after transfection, which was neither altered by prolonged transient expression nor by treatment with LMB (Fig. 2C). Combination of both mutations in the cleavage site and the NES ($TFIIA_{CSmutNESmut}$) induces nuclear accumulation comparable to the single NES mutation (Fig. 2C). Importantly, dynamic localization of TFIIA variants could be also confirmed in the HNSCC cell line Fadu (Supplementary Fig. S3) and by automated cell analysis using the Cellomics ArrayScan Imaging Platform (Supplementary Fig. S4).

To finally prove that the predicted sequence indeed functions as a *bona fide* nuclear export signal, we performed microinjection experiments of recombinant transport substrates containing the described sequence (Supplementary Fig. S5). Whereas the N-terminal 40 aa residues of TFIIA mediated very fast and efficient export into the cytoplasm, mutation of the NES (aa^{21}VINDVRDAFA^{30}) prevented nuclear export for at least 6 h. Collectively, these experiments unambiguously identified a leucine-rich NES in the α-subunit of TFIIA.

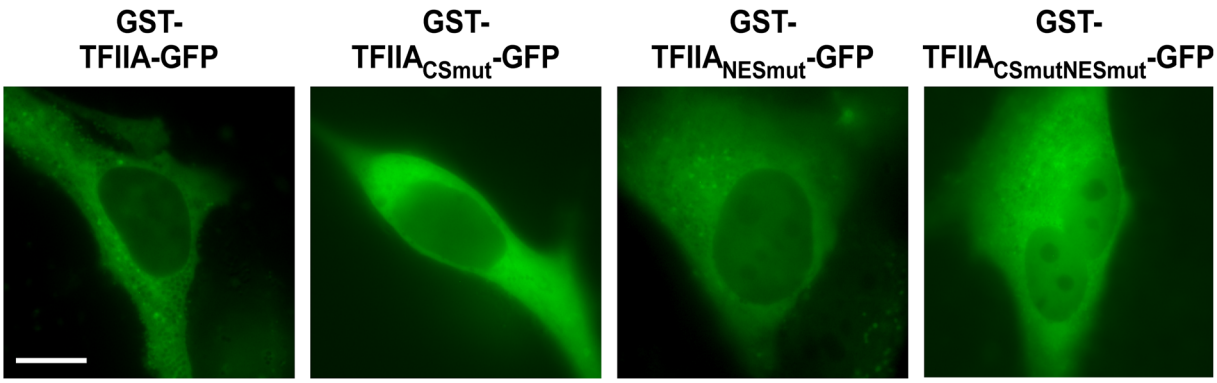

Figure 3. TFIIA is lacking an active nuclear import signal. Preventing passive diffusion of TFIIA-GFP variants by adding an N-terminal GST fusion tag results in an almost exclusively cytoplasmic localization. A431 cells were transfected with indicated constructs and visualized by fluorescence microscopy after 24 h. Scale bar, 10 µm.

Besides active nuclear export, nuclear accumulation of TFIIA might be enabled by an active nuclear localization signal (NLS) mediating importin-dependent nuclear import. In contrast to the results for the NES, bioinformatic analyses (NLStradamus, cNLS mapper, PredictProtein) employing regions of clustered basic amino acid residues as consensus sequence for NLS, did not indicate the presence of an active NLS in TFIIA (data not shown). In order to finally prove the absence of active nuclear import processes, we cloned diffusion-deficient TFIIA variants adding an N-terminal GST-tag to our constructs (Fig. 3). The resulting fusion proteins of approx. 88 kDa are not able to distribute within the cell by passive diffusion revealing active transport processes. Notably, for both NES-deficient mutants, TFIIA$_{NESmut}$-GFP, TFIIA$_{CSmutNESmut}$-GFP, a change of their prior nuclear localization to a cytoplasmic localization was detected, indicating deficiency in active nuclear access. In the absence of nuclear export, only active import signals could result in a nuclear accumulation of the diffusion-deficient GST fusion constructs. In summary, our results suggest that the dynamic cellular localization of TFIIA is actively regulated by its NES, but not by active nuclear import.

TFIIA cleavage by Taspase1 regulates its subcellular localization and transcriptional activity. Although the cleavage-deficient TFIIA mutant showed localization similar to wt TFIIA, we wanted to undoubtedly characterize the dependence of TFIIA's cellular localization on its proteolytic processing by Taspase1. Therefore, we co-expressed active Taspase1-mCherry (Fig. 4A) or its inactive mutant Tasp$_{T234V}$-mCherry (Fig. 4B) with TFIIA-GFP variants. Transient co-expression of TFIIA-GFP with the fluorescently labelled active protease resulted in a nuclear accumulation of TFIIA already after 24 h (Fig. 3A). In contrast, the catalytically inactive mutant (Tasp$_{T234V}$) did not alter TFIIA's predominant cytoplasmic localization. As a control, co-expression of Taspase1 or its inactive mutant did not affect the cytoplasmic localization of the cleavage-deficient mutant TFIIA$_{CSmut}$-GFP. Interestingly, the double mutant TFIIA$_{CSmutNESmut}$ also did not change its localization neither by co-expression of active nor inactive Taspase1 (Fig. 4A,B). Cleavage of all TFIIA variants was also confirmed by immunoblot analysis (Fig. 4C). Of note, we observed that the expression of wt Tasp and the Tasp$_{T234V}$ mutant could differ among samples. Since the expression plasmids are under the control of the same regulatory elements, these differences might be caused by altered protein stability of the uncleaved protease compared to cleaved subunits. However, the molecular details need to be confirmed in follow up studies.

It has been reported that Taspase1-mediated cleavage of TFIIA reduces expression of the CDK inhibitors p16^{INK4a} and p19^{ARF} encoded by the CDKN2A locus[18]. Since our results indicate that TFIIA cleavage by Taspase1 also diminishes active nuclear export of TFIIA, it is highly relevant if there is a link between TFIIA cleavage, subcellular localization and transcriptional activation of target genes, such as CDKN2A. To experimentally investigate such a putative link, we performed reporter gene studies using a p16^{INK4a}-luciferase reporter construct (Fig. 4D). Therefore, A431 cells were co-transfected with TFIIA variants and reporter construct, and luciferase activity was measured with a dual luciferase assay using renilla luciferase for normalization. As expected, TFIIA wt efficiently induced transcription of the p16^{INK4a} reporter compared to co-transfection with an empty vector control. Furthermore, p16^{INK4a} expression was even more increased by the engineered TFIIA mutants exhibiting enhanced nuclear localization. Especially the combination of NES inactivation and Taspase1 cleavage-deficiency (TFIIA$_{CSmutNESmut}$) resulted in a significant increase in reporter gene activation. Taken together, we could show that not only Taspase1-mediated cleavage of TFIIA, but also the integrity of its NES is able to regulate transcriptional activity of CDKN2A in epithelial cancer cells.

Discussion

Focusing on disease-relevant signalling-pathways in head and neck cancer, the Taspase1-TFIIA-CDKN2A axis is an interesting and potentially druggable target for HNSCC. In the past it could be demonstrated that Taspase1 uses different strategies to regulate biological processes like proliferation, cell cycle, differentiation and apoptosis[11,19]. Interestingly, our data support the hypothesis that Taspase1 fine-tunes the transcriptional activity of TFIIA via its subcellular localization and proteolytic cleavage. Our study revealed that the TFIIAαβ precursor contains a biologically active nuclear export signal (NES, aa ^{21}**V**IND**V**RD**I**F**L**^{30}), but lacking a nuclear localization signal

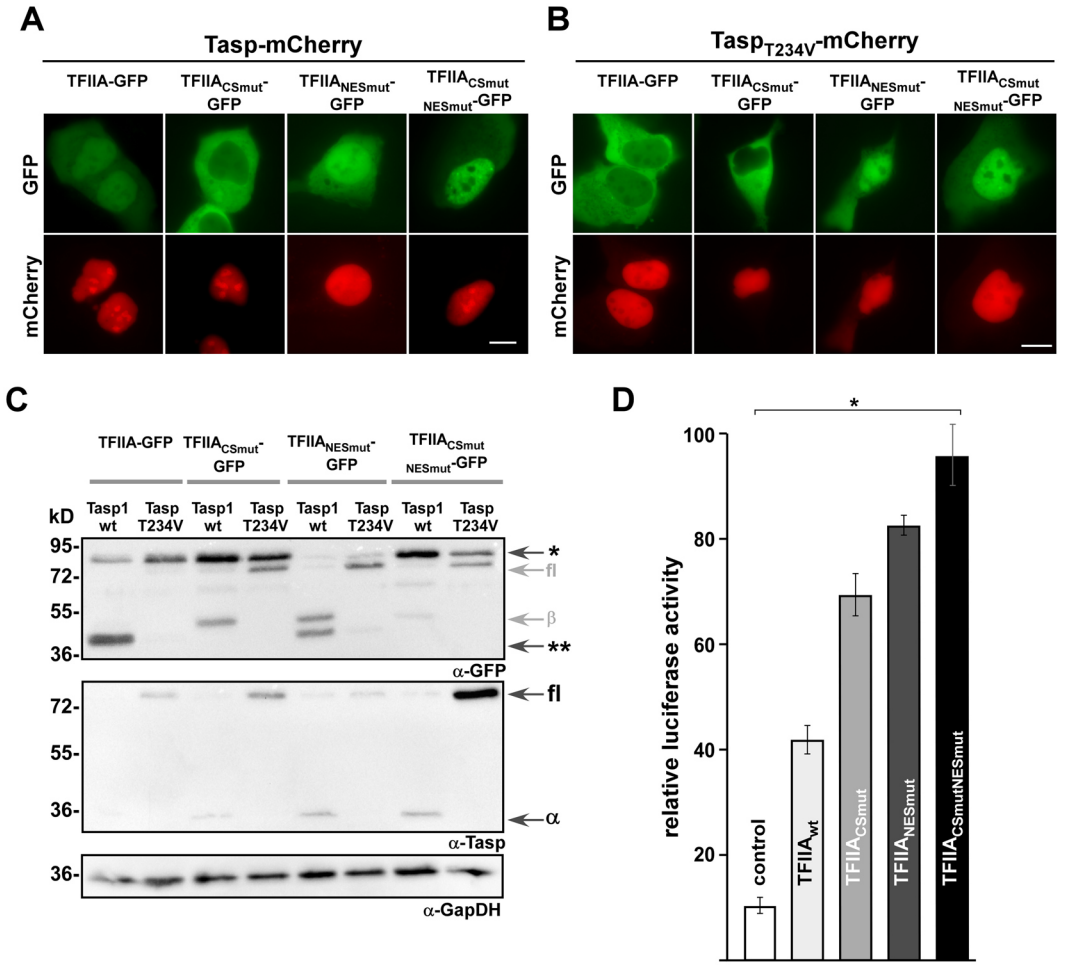

Figure 4. TFIIA cleavage by Taspase1 regulates its subcellular localization and transcriptional activity. (**A,B**) A431 cells were transfected with indicated TFIIA-GFP variants together with the active Taspase1- (**A**) or inactive Taspase$_{T243V}$-mCherry (**B**) expression plasmid. Localization was analysed by fluorescence microscopy after 24 h. TFIIA-GFP is translocated from cytoplasm to nucleus after expression of active Taspase1 but not of inactive Taspase1$_{T234V}$ mutant. In contrast the cleavage-deficient mutant TFIIA$_{CSmut}$-GFP did not relocalize in presence of Taspase1. The export-deficient TFIIA variants did not alter their subcellular localization upon Taspase1 expression. Scale bars, 10 µm. (**C**) Proteolytic cleavage of TFIIA-GFP variants as shown by immunoblot analysis of whole-cell lysates. A431 cells were transfected with indicated TFIIA-GFP together the active Taspase1- (wt) or inactive Taspase1(T234V)- BFP expression plasmids. In contrast to TFIIA- and TFIIA$_{NESmut}$-GFP, the TFIIA$_{CSmut}$-GFP could not be cleaved by active wildtype (wt) Taspase1. The inactive Taspase1$_{T234V}$ mutant neither showed self-cleavage in two active subunits nor *trans* cleavage activity of TFIIA. Expression of proteins and cleavage products in cell lysates was visualized using α-GFP and α-Taspase1 Abs. α-GapDH served as loading control. *Uncleaved TFIIA-GFP, **cleaved TFIIA-GFP, fl: Taspase1-BFP full length protein, α/β: Taspase1 α-/β-subunit. Of note, the α-GFP antibody is as well detecting the related BFP and thus full-length Tasp-BFP and the β-subunit containing the fusion tag. α-Taspase1 Ab is recognizing the full-length (75 kDa) as well as the α-subunit (28 kDa) of Taspase1. Shown blots are cropped. Full-length blots are shown in Supplementary Fig. S6. (**D**) Expression of the cell cycle regulator p16^{INK4a} is induced by impaired TFIIA export and proteolytic cleavage. A431 cells were co-transfected with either pGL3 basic or pGL3 basic-wt p16^{INK4a} 5′-UTR reporter, pRLSV40 and the respective TFIIA variant or pc3-GFP as negative control. Relative light units (RLU) were measured 48 h later, and plotted after normalization for transfection efficiency (pRLSV40). Bars, means of triplicates used to calculate standard deviations. Results of one representative experiment are shown, n = 3. Significance, *$p < 0.005$.

(NLS). The fact that transiently transfected, unprocessed TFIIA localized predominantly to the cytoplasm which was counteracted by treatment with the nuclear export inhibitor LMB, but unaffected by genetic inactivation of the Taspase1 cleavage site suggests accessibility of the NES in the uncleaved, full-length protein. On the other hand, nuclear import of TFIIA might be mediated via interaction with other proteins capable of nuclear import. For TFIIAγ, no NLS and thus no active nuclear import has been described so far. But there is evidence for other proteins to be shuttled inside different cellular compartments albeit lacking active transport signals. We discovered a comparable shuttling mechanism for the nuclear export of Taspase1 itself, making use of the NES of its interaction partner NPM1[12,45].

With respect to proteolytic processing, overexpression of Taspase1 but not of catalytically inactive variants enhanced TFIIA's direct nuclear accumulation, and uncleaved TFIIA mutants revealed an enhanced and elongated cytoplasmic localization. This leads us to the conclusion that processing of TFIIA by Taspase1 might mask the NES, albeit lacking support by the incomplete structural data available so far (pdb 1NVP). Possible scenarios include conformational changes in the α-subunit, which would shift the relative position of the subunit assembly and in turn lead to a complete masking of the NES. This could also be the result of interactions between TFIIA and other transcriptional factors, such as TBP.

Besides its crucial role for regulating the MLL-CyclinE axis in HER2/neu-positive breast cancer[10], Taspase1 controls the expression of CDK inhibitors encoded by CDKN2A locus ($p16^{INK4a}$ and $p19^{ARF}$)[11,16,18,46]. Reporter gene studies revealed a transcriptional activation of $p16^{INK4a}$ by TFIIA which was most prominent in TFIIA variants with genetically enforced nuclear localization in combination with impaired proteolytic cleavage. $p16^{INK4a}$ is an important tumour suppressor gene, involved in the p16/cyclin-dependent kinase/retinoblastoma gene pathway of cell cycle control[47]. The gene encodes an inhibitor of CDK4 and CDK6, which regulate the phosphorylation of retinoblastoma gene and the G1 to S phase transition of the cell cycle[30]. $p16^{INK4a}$ expression has been characterized in several tumour types ranging from its loss or downregulation to significant overexpression[48]. In head and neck cancer, $p16^{INK4a}$ overexpression has been suggested to have a major impact on treatment response and survival in patients with HPV-positive tumours[49]. HPV-related cancers presenting $p16^{INK4a}$ overexpression are very sensitive to radiotherapy, and have a better prognosis than HPV-negative tumours[50]. On the other hand, loss of CDKN2A expression by deletion, mutation, or hypermethylation is common in HNSCC and has been suggested as druggable target[51]. Although loss of $p16^{INK4a}$ could not be validated as prognostic factor for HNSCC patients, it was suggested that it may be used to predict overall patient survival in early-stage head and neck tumours[30]. While genetic inactivation of $p16^{INK4a}$ has been one of the most prominent genetic changes identified in human cancers to date, it has been reported that $p16^{INK4a}$ function can be regulated via other complex cellular events, such as oncogene activation[52]. In our present study containing only HPV-negative HNSCC tumours, we found a moderate but highly significant downregulation of $p16^{INK4a}$ suggesting rather expressional downregulation than complete loss or silencing of the CDKN2A gene. It has been reported that Taspase1-mediated cleavage of TFIIA affects the conformation of TFIID/TFIIA promoter complexes and thus, enables assembly with TFIID and other tissue-specific transcription factors[53]. Thereby, Taspase1-mediated cleavage of TFIIA regulates tissue-specific expression profiles, e.g. during spermatogenesis[16] and mammalian head morphogenesis[18], and is moreover essential for subsequent proteasomal degradation. The regulation of TFIIA protein levels via Taspase1-mediated cleavage is another regulatory key in this network allowing differential gene expression. In summary, this supports the hypothesis that in contrast to uncleaved TFIIAαβ/γ inducing bulk transcription, Taspase1 cleavage is regulating the switch between general and very specific transcriptional patterns and allows developmental fine-tuning. In undifferentiated cancer cells, Taspase1 activity might be regained and thus, originally developmental regulation processes might be reactivated. In summary, we propose a hitherto unknown mechanism how CDKN2A expression could be fine-tuned via the Taspase1-TFIIA signalling-pathway in head and neck tumours.

Materials and Methods

Antibodies (Ab), reagents and compounds. Ab used: α-TFIIA (sc-5314/sc-5315/sc-5311; Santa Cruz Biotechnology, Heidelberg, Germany); α-GAPDH (sc-47724; Santa Cruz Biotechnology, Heidelberg, Germany); α-GFP (sc-8334; Santa Cruz Biotechnology, Heidelberg, Germany); α-Taspase1 (sc-85945; Santa Cruz Biotechnology, Heidelberg, Germany). Appropriate HRP-, Cy3- or FITC-conjugated secondary antibodies (Sigma Aldrich, Munich, Germany; Santa Cruz Biotechnology, Heidelberg, Germany) were used. Reagents were from Sigma Aldrich (Sigma Aldrich, Munich, Germany) unless stated otherwise. Cells were treated with the export inhibitor Leptomycin B (LMB) (10 nM) as described[54].

Patient characteristics and material. Tissue samples were obtained from patients undergoing surgical resection at the departments of otolaryngology of the Universities of Frankfurt and Mainz. Investigation has been conducted in accordance with the ethical standards according to the Declaration of Helsinki and according to national and international guidelines. The study protocol has been approved by the ethics committees "Ethik-Kommission des Fachbereichs Medizin, Universitätsklinikum der Goethe-Universität" (#83756604) and "Ethik-Kommission der Landesärztekammer Rheinland-Pfalz" (#83748515) after obtaining the patients' informed consent to participate in the study and was processed anonymously. All cases were diagnosed histopathologically as HNSCC and staged according to the TNM classification of malignant tumours recommended by the 'Union International Contre le Cancer' UICC. In this study, tumour specimens, corresponding non-malignant tissue, and lymph node metastasis were analysed. Specimens included oropharyngeal and laryngopharyngeal carcinoma of different tumour size (T1-T4), lymph node status (N0-2), no distant metastasis (M0) and grading G1-G3. Upon resection samples were immediately placed on ice and snap-frozen in liquid nitrogen within 30 min. Histological analyses were performed to ensure that each specimen contained >70% tumour tissue and <10% necrotic debris. Samples not meeting these criteria were rejected.

RNA extraction. Frozen tissue samples (30–50 mg) were collected in 1ml Trizol (Invitrogen, Karlsruhe, Germany) and dispersed using an Ultra-Turrax T25 tissue homogenizer (IKA Werke, Staufen, Germany). Total RNA was extracted according to the recommendations given by the manufacturer's Trizol protocol and further purified on RNeasy Mini spin columns (Qiagen, Hilden, Germany). Integrity and purity of total RNA were assessed on a Bioanalyzer 2100 (Agilent Technologies, Boeblingen, Germany) using a RNA 6000 Nano LabChip Kit (Agilent) according to the manufacturer's instructions[55].

Target preparation and hybridization for Affymetrix GeneChip Arrays. Total RNA (5 µg) was used to prepare biotinylated cRNAs for hybridization, following the guidelines given in the Affymetrix GeneChip Expression Analysis Technical Manual. cRNA clean-up was performed on RNeasy Mini filters (Qiagen). In all, 10 µg of fragmented, labelled cRNA were hybridized to Affymetrix HG-U133A arrays (Affymetrix, Santa Clara, CA, USA) using standard conditions (16 h, 45 °C). Arrays were washed and stained in a Fluidics Station 400 (Affymetrix) and scanned on a Gene Array Scanner 2500 (Agilent), as recommended by Affymetrix. Raw fluorescence intensities from all hybridizations were normalized applying variance stabilization with additional scaling. Additionally, MAS5 as well as gcRMA expression values were calculated.

Microarray data processing, pathway analysis and statistical analysis. Data and cluster analyses were performed using Affymetrix Microarray Suite 5.0 (MAS5) and GeneSpring GX software (Agilent Technologies, Santa Clara, USA). All samples were normalized to the median of control samples. Each measurement for each gene in those specific samples was divided by the median of that gene's measurements in the corresponding control samples. The gene list was subjected to a student's t-test (p-value < 0.05). The resulting list was further filtered for confidence using a Benjamini-Hochberg false discovery rate correction. A 2.0-fold cut-off filter was then applied to identify genes that were preferentially up- or downregulated. Heat-plots are used for visualizing gene expression: yellow indicates no change in expression, red enhanced expression (upregulated), and blue suppressed expression (downregulated).

The Ingenuity Pathway Analysis (IPA) tool (Ingenuity Systems) was used to identify pathways related to differentially expressed genes in primary tumours (PT*vs*.N). Data was filtered to meet the criteria $p < 0.05$ in our comparison analysis.

Analysis of the data was performed using R 2.15.2 with the *limma* package 3.14.4. Raw fluorescence intensities from all hybridizations were normalized, applying robust multichip average (RMA) normalization for the.CEL data, followed by a quantile normalization to compare expression results across specimens. For the comparison of primary tumours to normal mucosa (PT*vs*.N), and metastasis to normal mucosa (M*vs*.N) of differentially expressed genes, we also utilized the *limma* package. For multiple testing a Bonferroni correction was performed.

Cell culture, microscopy fluorescence imaging of cells and computer-assisted microinjection. Cell lines used in the study were maintained and transfected as described[20,56]. Twelve-bit black and white images were captured using a digital Axiocam CCD camera (Carl Zeiss, Jena, Germany). Quantitation, image analysis and presentation were performed as described[33,57]. All assays were performed in triplicates. Purification and microinjection of recombinant GST-GFP transport substrates were performed as described in detail[33]. Automated analysis of the molecular translocation assay was performed using the Cellomics ArrayScan® VTI Imaging Platform (Thermo Fisher Scientific Inc., Berkshire, UK) as described[58]. Scans were performed sequentially with settings to give sub-saturating fluorescence intensity, and a minimum of 400 valid objects per well was recorded.

Plasmids. Expression constructs encoding TFIIA, Taspase1 and Taspase1$_{T234V}$ as untagged or fusions with autofluorescent proteins were described[12]. Plasmids encoding TFIIA variants were amplified from full length TFIIA cDNA and cloned into pc3-GFP or pGex-GFP using BamHI/NheI-restriction sites. Plasmid TFIIA$_{CSmut}$-, TFIIA$_{NESmut}$-, and pGex_TFIIA$_{NESmut}$-GFP were generated by splice overlap extension polymerase chain reaction as reported[59]. pF143 were described[60]. Plasmids were verified by sequence analysis[57].

Protein extraction, immunoblot analysis and immunofluorescence. Preparation of whole cell lysates was carried out as described using a physiological lysis buffer (50 mM Tris pH 8.0, 150 mM NaCl, 5 mM EDTA, 0.5% NP-40, 1 mM DTT, 1 mM PMSF, Complete Protease Inhibitory Cocktail from Roche Diagnostics, Mannheim, Germany). Equal loading of lysates was controlled by reprobing blots for GAPDH as described[61]. Immunofluorescence was performed as reported in detail[14,36]. Western blot data shown are representative for at least three independent experiments ($n = 3$).

Reporter gene assays. For luciferase reporter gene assays, 5×10^4 293T cells seeded in 24-well plates 24 h before transfection. Cells were transfected at 80% confluence using PEI (2.7 µl PEI per µg DNA) as described[1]. Specifically, 350 ng of either the empty pGL3 basic or the pGL3 basic reporter vector containing the wild-type p16INK4a 5'-UTR were used along with 50 ng of the control pRLSV40 plasmid introduced to normalize transfection efficiency and 200 ng of the respective TFIIA variants or pc3-GFP as negative control. Cells were harvested 24 h after transfection, and luciferase assays were carried out using the dual-luciferase reagent (Promega, Madison, WI, USA). Briefly, relative light units (RLU) were measured for both luciferases, firefly and renilla, normalized for transfection efficiency and plotted as relative luciferase activity for each TFIIA variant. Assays were performed in triplicate, and data shown are representative for at least three independent experiments ($n = 3$).

Bioinformatics. TFIIA proteins were analysed using NES-Finder (http://research.nki.nl/fornerodlab/NES-Finder.htm)[54]. Alignments and clustalW analyses were performed using BLAST (http://www.blast.ncbi.nlm.nih.gov/) and the BioEdit sequence alignment editor (http://www.mbio.ncsu.edu/BioEdit) with the human TFIIA amino acid sequence on NCBI databases (homo sapiens [GI: 433500]; bos taurus [GI: 297479971]; canis lupus familaris [GI: 73964364]; danio rerio [182891266]; gallus gallus [GI: 121308873]; mus musculus [GI: 12313735]; pan troglodytes [GI: 114654237]; rattus norvegicus [GI: 11559984]; xenopus laevis [GI: 148236361. Unless stated otherwise, data were obtained from three independent experiments done in triplicate.

Data availability statement. The datasets generated during and/or analysed during the current study are available from the corresponding author on reasonable request.

References

1. Stauber, R. H. *et al*. A combination of a ribonucleotide reductase inhibitor and histone deacetylase inhibitors downregulates EGFR and triggers BIM-dependent apoptosis in head and neck cancer. *Oncotarget* **3**, 31–43 (2012).
2. Leemans, C. R., Braakhuis, B. J. & Brakenhoff, R. H. The molecular biology of head and neck cancer. *Nature reviews* **11**, 9–22 (2011).
3. Gregoire, V., Lefebvre, J. L., Licitra, L., Felip, E. & Group, E.-E.-E. G. W. Squamous cell carcinoma of the head and neck: EHNS-ESMO-ESTRO Clinical Practice Guidelines for diagnosis, treatment and follow-up. *Ann Oncol* **21**(Suppl 5), v184–186, https://doi.org/10.1093/annonc/mdq185 (2010).
4. Benson, E., Li, R., Eisele, D. & Fakhry, C. The clinical impact of HPV tumor status upon head and neck squamous cell carcinomas. *Oral Oncol* **50**, 565–574, https://doi.org/10.1016/j.oraloncology.2013.09.008 (2014).
5. Cohen, R. B. Current challenges and clinical investigations of epidermal growth factor receptor (EGFR)- and ErbB family-targeted agents in the treatment of head and neck squamous cell carcinoma (HNSCC). *Cancer treatment reviews* **40**, 567–577, https://doi.org/10.1016/j.ctrv.2013.10.002 (2014).
6. Rothenberg, S. M. & Ellisen, L. W. The molecular pathogenesis of head and neck squamous cell carcinoma. *The Journal of clinical investigation* **122**, 1951–1957 (2012).
7. Denaro, N., Russi, E. G., Adamo, V. & Merlano, M. C. State-of-the-art and emerging treatment options in the management of head and neck cancer: news from 2013. *Oncology* **86**, 212–229, https://doi.org/10.1159/000357712 (2014).
8. Hamoir, M., Schmitz, S. & Gregoire, V. The role of neck dissection in squamous cell carcinoma of the head and neck. *Curr Treat Options Oncol* **15**, 611–624, https://doi.org/10.1007/s11864-014-0311-7 (2014).
9. Sessions, D. G. *et al*. Analysis of treatment results for oral tongue cancer. *Laryngoscope* **112**, 616–625, https://doi.org/10.1097/00005537-200204000-00005 (2002).
10. Dong, Y. *et al*. Taspase1 cleaves MLL1 to activate cyclin E for HER2/neu breast tumorigenesis. *Cell research* (2014).
11. Wünsch, D. *et al*. Taspase1: a 'misunderstood' protease with translational cancer relevance. *Oncogene* **35**, 3351–3364, https://doi.org/10.1038/onc.2015.436 (2016).
12. Bier, C. *et al*. The importin-alpha/nucleophosmin switch controls taspase1 protease function. *Traffic (Copenhagen, Denmark)* **12**, 703–714 (2011).
13. Khan, J. A., Dunn, B. M. & Tong, L. Crystal structure of human Taspase1, a crucial protease regulating the function of MLL. *Structure* **13**, 1443–1452 (2005).
14. Bier, C. *et al*. Cell-based Analysis of Structure-Function Activity of Threonine Aspartase 1. *The Journal of biological chemistry* **286**, 3007–3017 (2011).
15. Hsieh, J. J., Cheng, E. H. & Korsmeyer, S. J. Taspase1: a threonine aspartase required for cleavage of MLL and proper HOX gene expression. *Cell* **115**, 293–303 (2003).
16. Oyama, T. *et al*. Cleavage of TFIIA by Taspase1 activates TRF2-specified mammalian male germ cell programs. *Developmental cell* **27**, 188–200 (2013).
17. Takeda, S. *et al*. *Proteolysis of MLL fam*ily proteins is essential for taspase1-orchestrated cell cycle progression. *Genes & development* **20**, 2397–2409 (2006).
18. Takeda, S. *et al*. Taspase1-dependent TFIIA cleavage coordinates head morphogenesis by limiting Cdkn2a locus transcription. *The Journal of clinical investigation* (2015).
19. Stauber, R. H., Hahlbrock, A., Knauer, S. K. & Wünsch, D. Cleaving for growth: threonine aspartase 1–a protease relevant for development and disease. *FASEB J* **30**, 1012–1022, https://doi.org/10.1096/fj.15-270611 (2016).
20. Bier, C. *et al*. Allosteric inhibition of Taspase1's pathobiological activity by enforced dimerization *in vivo*. *FASEB J* **26**, 3421–3429, https://doi.org/10.1096/fj.11-202432 (2012).
21. Stauber, R. H., Bier, C. & Knauer, S. K. Targeting Taspase1 for cancer therapy–letter. *Cancer research* **72**, 2912; author reply 2913 (2012).
22. Wünsch, D. *et al*. Chemico-genetic strategies to inhibit the leukemic potential of threonine aspartase-1. *Blood cancer journal* **2**, e77, https://doi.org/10.1038/bcj.2012.22 (2012).
23. Zhou, H. *et al*. Uncleaved TFIIA is a substrate for taspase 1 and active in transcription. *Molecular and cellular biology* **26**, 2728–2735 (2006).
24. Yokomori, K. *et al*. *Drosophila TFIIA direct*s cooperative DNA binding with TBP and mediates transcriptional activation. *Genes & development* **8**, 2313–2323 (1994).
25. Ranish, J. A., Yudkovsky, N. & Hahn, S. Intermediates in formation and activity of the RNA polymerase II preinitiation complex: holoenzyme recruitment and a postrecruitment role for the TATA box and TFIIB. *Genes & development* **13**, 49–63 (1999).
26. Mitsiou, D. J. & Stunnenberg, H. G. TAC, a TBP-sans-TAFs complex containing the unprocessed TFIIAalphabeta precursor and the TFIIAgamma subunit. *Molecular cell* **6**, 527–537 (2000).
27. Mitsiou, D. J. & Stunnenberg, H. G. p300 is involved in formation of the TBP-TFIIA-containing basal transcription complex, TAC. *The EMBO journal* **22**, 4501–4511 (2003).
28. Hoiby, T. *et al*. Cleavage and proteasome-mediated degradation of the basal transcription factor TFIIA. *The EMBO journal* **23**, 3083–3091 (2004).
29. Sun, X., Ma, D., Sheldon, M., Yeung, K. & Reinberg, D. Reconstitution of human TFIIA activity from recombinant polypeptides: a role in TFIID-mediated transcription. *Genes & development* **8**, 2336–2348 (1994).
30. Ai, L. *et al*. Thep16 (CDKN2a/INK4a) tumor-suppressor gene in head and neck squamous cell carcinoma: a promoter methylation and protein expression study in 100 cases. *Mod Pathol* **16**, 944–950, https://doi.org/10.1097/01.MP.0000085760.74313.DD (2003).
31. Gorlich, D. & Kutay, U. Transport between the cell nucleus and the cytoplasm. *Annual review of cell and developmental biology* **15**, 607–660 (1999).
32. Lei, E. P. & Silver, P. A. Protein and RNA export from the nucleus. *Developmental cell* **2**, 261–272 (2002).
33. Knauer, S. K., Carra, G. & Stauber, R. H. Nuclear export is evolutionarily conserved in CVC paired-like homeobox proteins and influences protein stability, transcriptional activation, and extracellular secretion. *Molecular and cellular biology* **25**, 2573–2582 (2005).
34. Whiteside, S. T. & Goodbourn, S. Signal transduction and nuclear targeting: regulation of transcription factor activity by subcellular localisation. *Journal of cell science* **104**(Pt 4), 949–955 (1993).
35. Cartwright, P. & Helin, K. Nucleocytoplasmic shuttling of transcription factors. *Cell Mol Life Sci* **57**, 1193–1206 (2000).
36. Knauer, S. K. *et al*. Translocation biosensors to study signal-specific nucleo-cytoplasmic transport, protease activity and protein-protein interactions. *Traffic (Copenhagen, Denmark)* **6**, 594–606 (2005).
37. Hoiby, T., Zhou, H., Mitsiou, D. J. & Stunnenberg, H. G. A facelift for the general transcription factor TFIIA. *Biochimica et biophysica acta* **1769**, 429–436 (2007).
38. Zhou, G., Liu, Z. & Myers, J. N. TP53 Mutations in Head and Neck Squamous Cell Carcinoma and Their Impact on Disease Progression and Treatment Response. *Journal of cellular biochemistry* **117**, 2682–2692, https://doi.org/10.1002/jcb.25592 (2016).
39. Schweitzer, A., Knauer, S. K. & Stauber, R. H. Nuclear receptors in head and neck cancer: current knowledge and perspectives. *Int J Cancer* **126**, 801–809 (2010).
40. Stauber, R. H., Wünsch, D., Knauer, S. K. & Fetz, V. An update on the pathobiological relevance of nuclear receptors for cancers of the head and neck. *Histology and Histopathology* **25**(8), 1093–1104 (2010).

41. Unruhe, B., Schroder, E., Wünsch, D. & Knauer, S. K. An Old Flame Never Dies: Survivin in Cancer and Cellular Senescence. *Gerontology* **62**, 173–181, https://doi.org/10.1159/000432398 (2016).
42. Hayden, M. S. & Ghosh, S. Signaling to NF-kappaB. *Genes & development* **18**, 2195–2224, https://doi.org/10.1101/gad.1228704 (2004).
43. Lange, A., McLane, L. M., Mills, R. E., Devine, S. E. & Corbett, A. H. Expanding the Definition of the Classical Bipartite Nuclear Localization Signal. *Traffic (Copenhagen, Denmark)* (2009).
44. Dong, X. *et al*. Structural basis for leucine-rich nuclear export signal recognition by CRM1. *Nature* **458**, 1136–1141 (2009).
45. Wünsch, D. *et al*. Fly versus man: evolutionary impairment of nucleolar targeting affects the degradome of Drosophila's Taspase1. *FASEB J* **29**, 1973–1985, https://doi.org/10.1096/fj.14-262451 (2015).
46. Chen, D. Y. *et al*. Taspase1 functions as a non-oncogene addiction protease that coordinates cancer cell proliferation and apoptosis. *Cancer research* **70**, 5358–5367 (2010).
47. Sherr, C. J. & Roberts, J. M. CDK inhibitors: positive and negative regulators of G1-phase progression. *Genes & development* **13**, 1501–1512 (1999).
48. Romagosa, C. *et al*. p16(Ink4a) overexpression in cancer: a tumor suppressor gene associated with senescence and high-grade tumors. *Oncogene* **30**, 2087–2097, https://doi.org/10.1038/onc.2010.614 (2011).
49. Gupta, A. K. *et al*. Radiation response in two HPV-infected head-and-neck cancer cell lines in comparison to a non-HPV-infected cell line and relationship to signaling through AKT. *Int J Radiat Oncol Biol Phys* **74**, 928–933, https://doi.org/10.1016/j.ijrobp.2009.03.004 (2009).
50. Lassen, P. *et al*. Effect of HPV-associated p16INK4A expression on response to radiotherapy and survival in squamous cell carcinoma of the head and neck. *J Clin Oncol* **27**, 1992–1998, https://doi.org/10.1200/JCO.2008.20.2853 (2009).
51. Stephen, J. K. *et al*. Significance of p16 in Site-specific HPV Positive and HPV Negative Head and Neck Squamous Cell Carcinoma. *Cancer Clin Oncol* **2**, 51–61, https://doi.org/10.5539/cco.v2n1p51 (2013).
52. Li, J., Poi, M. J. & Tsai, M. D. Regulatory mechanisms of tumor suppressor P16(INK4A) and their relevance to cancer. *Biochemistry* **50**, 5566–5582, https://doi.org/10.1021/bi200642e (2011).
53. Malecova, B., Caputo, V. S., Lee, D. F., Hsieh, J. J. & Oelgeschlager, T. Taspase1 processing alters TFIIA cofactor properties in the regulation of TFIID. *Transcription* **6**, 21–32, https://doi.org/10.1080/21541264.2015.1052178 (2015).
54. Knauer, S. K., Bier, C., Habtemichael, N. & Stauber, R. H. The Survivin-Crm1 interaction is essential for chromosomal passenger complex localization and function. *EMBO reports* **7**, 1259–1265 (2006).
55. Knauer, S. K. *et al*. The survivin isoform survivin-3B is cytoprotective and can function as a chromosomal passenger complex protein. *Cell cycle (Georgetown, Tex* **6**, 1502–1509 (2007).
56. Fetz, V., Knauer, S. K., Bier, C., Kriess, J. P. & Stauber, R. H. Translocation Biosensors – Cellular System Integrators to Dissect CRM1-Dependent Nuclear Export by Chemicogenomics. *Sensors* **7**, 5423–5445 (2009).
57. Habtemichael, N. *et al*. Cloning and functional characterization of the guinea pig apoptosis inhibitor protein Survivin. *Gene* **469**, 9–17, https://doi.org/10.1016/j.gene.2010.08.007 (2010).
58. Fetz, V., Knauer, S. K., Bier, C., von Kries, J. P. & Stauber, R. H. Translocation Biosensors - Cellular System Integrators to Dissect CRM1-Dependent Nuclear Export by Chemicogenomics. *Sensors* **9**, 5423–5445, https://doi.org/10.3390/s90705423 (2009).
59. Knauer, S. K. *et al*. Nuclear export is essential for the tumor-promoting activity of survivin. *Faseb J* **21**, 207–216 (2007).
60. Knauer, S. K. & Stauber, R. H. Development of an autofluorescent translocation biosensor system to investigate protein-protein interactions in living cells. *Analytical chemistry* **77**, 4815–4820 (2005).
61. Kramer, O. H. *et al*. *A phosphorylation-acetylation* switch regulates STAT1 signaling. *Genes & development* **23**, 223–235, https://doi.org/10.1101/gad.479209 (2009).

Acknowledgements

This study was supported by grants from the Else-Kröner-Fresenius Foundation, Carl-Zeiss-Foundation, Stiftung Tumorforschung Kopf-Hals, Deutsche Forschungsgemeinschaft, and intramural Funding of the University Medical Center Mainz and the Johannes Gutenberg University Mainz (BiomaTiCS, Impulsfonds Rheinland-Pfalz). The authors thank S. Schneider for excellent technical assistance.

Author Contributions

A.G., A.H., N.H. and M.D. conceived, designed and conducted experiments and analysed the data; A.H., S.S., S.B., and J.H. co-designed the study and revised the manuscript; D.W. conceived and designed the study and wrote the manuscript.

Additional Information

Supplementary information accompanies this paper at https://doi.org/10.1038/s41598-017-14814-x.

Competing Interests: The authors declare that they have no competing interests.

Publisher's note: Springer Nature remains neutral with regard to jurisdictional claims in published maps and institutional affiliations.

II.

Journal of Cancer Research and Clinical Oncology (2020) 146:343–356
https://doi.org/10.1007/s00432-019-03118-4

ORIGINAL ARTICLE – CANCER RESEARCH

Histone deacetylase inhibitors dysregulate DNA repair proteins and antagonize metastasis-associated processes

Nicole Kiweler[1,7] · Désirée Wünsch[2] · Matthias Wirth[3,8] · Nisintha Mahendrarajah[1] · Günter Schneider[3] · Roland H. Stauber[2] · Walburgis Brenner[4,5] · Falk Butter[6] · Oliver H. Krämer[1]

Received: 9 November 2019 / Accepted: 19 December 2019 / Published online: 13 January 2020

Abstract

Purpose We set out to determine whether clinically tested epigenetic drugs against class I histone deacetylases (HDACs) affect hallmarks of the metastatic process.

Methods We treated permanent and primary renal, lung, and breast cancer cells with the class I histone deacetylase inhibitors (HDACi) entinostat (MS-275) and valproic acid (VPA), the replicative stress inducer hydroxyurea (HU), the DNA-damaging agent cis-platinum (L-OHP), and the cytokine transforming growth factor-β (TGFβ). We used proteomics, quantitative PCR, immunoblot, single cell DNA damage assays, and flow cytometry to analyze cell fate after drug exposure.

Results We show that HDACi interfere with DNA repair protein expression and trigger DNA damage and apoptosis alone and in combination with established chemotherapeutics. Furthermore, HDACi disrupt the balance of cell adhesion protein expression and abrogate TGFβ-induced cellular plasticity of transformed cells.

Conclusion HDACi suppress the epithelial–mesenchymal transition (EMT) and compromise the DNA integrity of cancer cells. These data encourage further testing of HDACi against tumor cells.

Keywords Adhesion · EMT · DNA damage · HDACi · MET · TGFβ

Introduction

The formation of metastases that originate from a primary cancer is commonly associated with increased drug resistance and patient death (Fidler and Kripke 2015). EMT and the subsequent transition of cells back to the mesenchymal state have been associated with metastasis for decades (Nieto 2013; Zeisberg and Neilson 2009). However, there is an ongoing dispute whether EMT is a prime event in the metastatic process or whether the mesenchymal phenotype of

Nicole Kiweler and Désirée Wünsch: equal first author contribution.

Electronic supplementary material The online version of this article (https://doi.org/10.1007/s00432-019-03118-4) contains supplementary material, which is available to authorized users.

✉ Oliver H. Krämer
okraemer@uni-mainz.de

1 Department of Toxicology, University Medical Center of the Johannes Gutenberg University Mainz, Obere Zahlbacher Straße 67, 55131 Mainz, Germany

2 Department of Otorhinolaryngology, University Medical Center Mainz, 55131 Mainz, Germany

3 Klinik Und Poliklinik für Innere Medizin II, Technical University of Munich, 81675 Munich, Germany

4 Clinic for Obstetrics and Women's Health, University Medical Center Mainz, 55131 Mainz, Germany

5 Department of Urology, University Medical Center Mainz, 55131 Mainz, Germany

6 Institute of Molecular Biology (IMB), 55128 Mainz, Germany

7 Present Address: Department of Oncology, Luxembourg Institute of Health, 1445 Strassen, Luxembourg

8 Present Address: Hematology and Oncology, Charité-Universitätsmedizin Campus Benjamin Franklin, 12200 Berlin, Germany

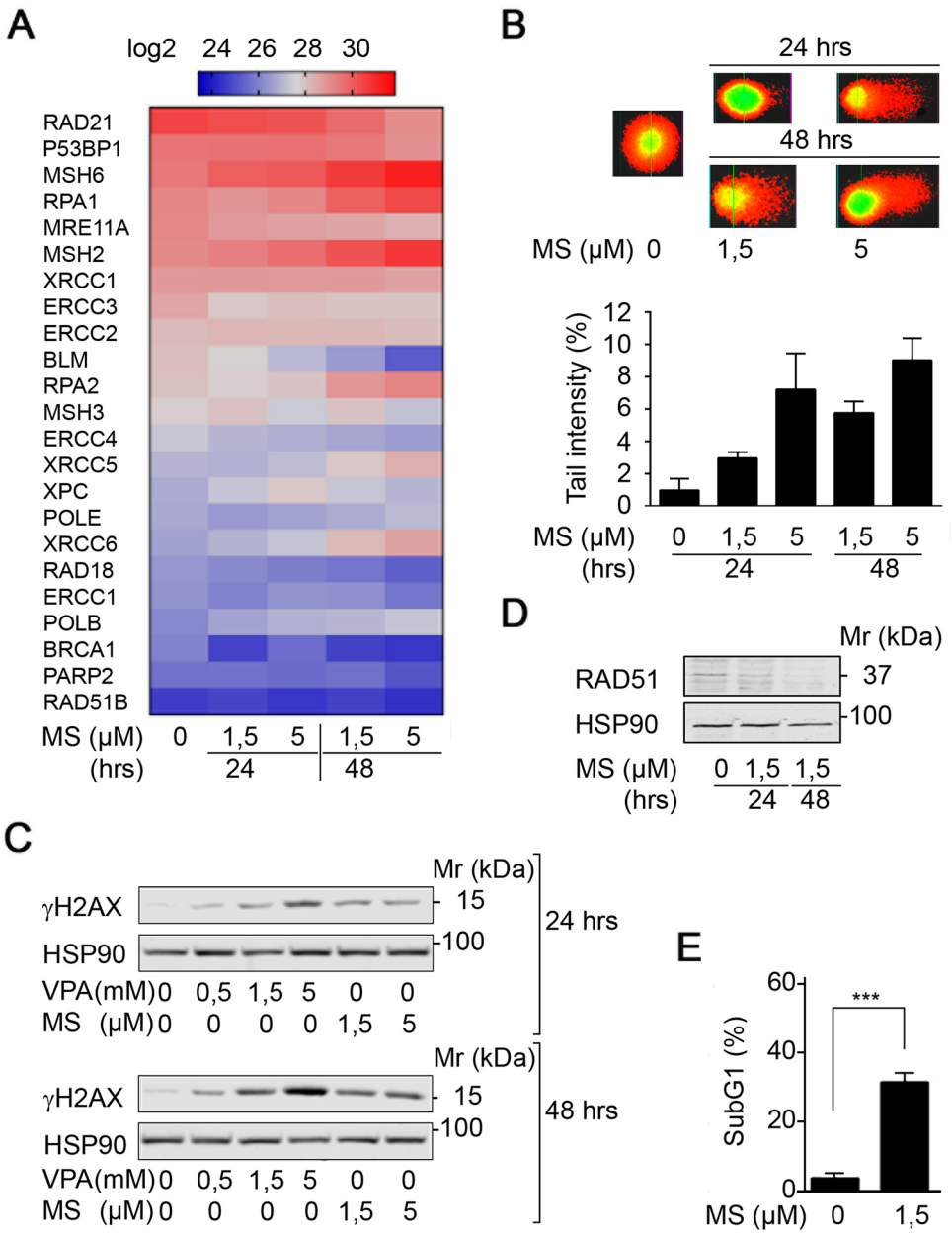

Fig. 1 HDACi trigger replication stress and DNA damage. **a** Renca cells were treated with the indicated concentrations of MS-275 (μM) for 24 to 48 h. Four independent replicates were analyzed for protein expression via LFQ in mass spectrometry. Heatmap depicts changes in LFQ expression levels of proteins with implications for the maintenance of genomic integrity. Statistics regarding changes in protein expression are provided in Supplementary Fig. S1. Several of the proteins are important for various DNA repair pathways and pathway choice. Proteins mainly relevant to DNA repair and HR are RAD21, 53BP1, RPA1, MRE11A, RPA2, XRCC5, POLE, XRCC6, RAD18, POLB, BRCA1, PARP2, RAD51B; critical for MMR are MSH6, MSH2, MSH3; for BER is XRCC1; for NER are ERCC3, ERCC2, BLM, ERCC4, XPC, ERCC1. **b** Renca cells were treated with the indicated concentrations of MS-275 (μM) for 24 h and 48 h. Tail intensity was quantified for $n=2$ independent experiments. **c** Renca cells were treated with the indicated concentrations of MS-275 (μM) and VPA (mM) for 24 h and 48 h, and analyzed for phosphorylation of H2AX (Ser139) by Western blot. HSP90 serves as loading control; Mr (kDa), relative molecular mass in kilo Daltons (kDa). **d** Mz-ccRCC2 cells were treated with 1.5 μM MS-275 for 24 and 48 h. RAD51 expression was analyzed on Western blot. HSP90 served as loading control; Mr (kDa), relative molecular mass in kilo Daltons (kDa). **e** Mz-ccRCC2 cells were treated for 48 h with 1.5 μM MS-275 and cell death was determined as percentage of subG1 population in fixed, PI-stained cells using flow cytometry. Graph shows mean ± SD ($n=5$); two-tailed unpaired t test with Welch's correction, ***p value < 0.001

breast and pancreatic cancer cells represents predominantly an indicator of cellular resistance to DNA damage (Aiello et al. 2017; Brabletz et al. 2018; Fischer et al. 2015; Ye et al. 2017; Zheng et al. 2015). Irrespective of this conceptual conflict, it is undoubted that novel drugs are necessary to combat clinical metastasis formation to enhance patient survival. Such drugs should be analyzed for their impact on both genomic integrity and modulation of EMT.

HDACi are epigenetic drugs that enhance protein acetylation and thereby impact a large number of cellular functions (Bayat Mokhtari et al. 2017; Mrakovcic et al. 2019; Müller and Krämer 2010; Nikolova et al. 2017; Vancurova et al. 2018). Since the Food and Drug Administration has approved four HDACi for the treatment of hematological malignancies, additional research is warranted to demonstrate how a pharmacological inactivation of HDACs affects metastasis formation. To solve this issue, global assays and analyses of various tumor cell types are required. We recently revealed that HDACi did not shift renal cell carcinoma (RCC) cells to a distinct epithelial or mesenchymal phenotype, but rather disrupted functional EMT/MET protein expression signatures and triggered apoptosis of RCC cells (Kiweler et al. 2018). These data are coherent with previous reports that show beneficial effects of HDACi against RCC cells and EMT (Chun 2018; Jones et al. 2009a, b; Juengel et al. 2014; Mao et al. 2017). Furthermore, HDACi counteracted the acquired resistance of RCC cells against the mammalian target of rapamycin-inhibitor everolimus and the glucose-regulating biguanide metformin (Juengel et al. 2014; Wei et al. 2018). In light of the chemoresistance and the poor prognosis of metastatic RCC (Barbieri et al. 2017; Chang et al. 2019), these findings suggest that HDACi pose an interesting therapeutic option for this cancer type.

The analysis of drug-dependent effects on metastasis should also involve conditions that promote this process. The secreted cytokine TGFβ is a tumor suppressor in non-transformed cells through its cell cycle arresting activity. Tumor cells, including those from RCC, are insensitive to this effect of TGFβ and undergo metastasis-promoting EMT and acquire chemotherapy resistance (Hao et al. 2019; Singla et al. 2018; Tretbar et al. 2019). These processes can be abrogated with HDACi in RCC cells. The HDACi trichostatin-A (TSA) and butyrate suppressed TGFβ-induced EMT (Yoshikawa et al. 2007) and VPA prevented the TGFβ-dependent activation of the EMT-associated transcription factor SMAD4 (Mao et al. 2017). Such effects could be particularly relevant to tumors that are or become resistant to standard cancer drugs such as renal and lung tumors (Barbieri et al. 2017; Chang et al. 2019; Dietrich and Gerber 2016; Foy et al. 2017).

In light of the recent discussion on the impact of DNA repair and EMT for the metastatic process and its relation to acquired chemoresistance, and due to the influence of HDACi on the EMT of RCC cells, we set out to investigate if HDACi affect the expression of DNA repair proteins, including p53, and cell adhesion molecules. In addition, we investigated whether HDACi modulate TGFβ-induced cell plasticity and if the combination of HDACi and L-OHP or HU is effective against cancer cells.

Results

HDACi suppress DNA repair protein expression

RCC-derived Renca cells are sensitive to pro-apoptotic effects of class I HDACi (Kiweler et al. 2018). Due to the rising interest in the impact of HDACs and HDACi on DNA replication and DNA integrity, we analyzed the expression levels of proteins that control replicative stress and DNA damage in a previously published proteome database for MS-275-treated Renca cells (Kiweler et al. 2018). This analysis showed that HDAC inhibition by MS-275 decreased the expression of proteins that control homologous recombination (HR), DNA mismatch repair (MMR), nucleotide excision repair (NER), and base excision repair (BER) in Renca cells (Fig. 1a and Supplementary Fig. S1).

To assess if the observed alterations in protein expression result in DNA damage at a global level, we used the comet assay technique, which is also known as single cell electrophoresis assay. MS-275 evoked a time- and dose-dependent increase in DNA tails indicating DNA damage (Fig. 1b).

Due to these findings, we analyzed the phosphorylation of histone H2AX at serine-139 (γH2AX), which is a marker for replication stress, single-/double-strand breaks in DNA, and apoptosis (Nikolova et al. 2017; Rogakou et al. 1998). MS-275 and VPA, which we used as additional class I HDACi (Bradner et al. 2010; Müller and Krämer 2010), induced a time- and dose-dependent accumulation of γH2AX (Fig. 1c).

These data encouraged us to test for a dysregulation of DNA repair factors and DNA injury upon class I HDAC inhibition in primary human RCC cells (Mz-ccRCC2). We found that MS-275 reduced the expression of the recombinase RAD51, which is a key factor for HR-mediated DNA repair (Nikolova et al. 2017), in primary RCC cells (Fig. 1d). This was associated with a highly significantly increased level of DNA fragmentation, which is typically seen in cells undergoing apoptosis (Fig. 1e).

We conclude that the activity of class I HDACs is necessary for the expression of proteins that control genomic integrity. Accordingly, HDACi cause replicative stress and DNA damage in RCC cells.

Status of p53 and its regulation by HDACi in Renca cells

The tumor suppressor p53 determines the fate of HDACi-treated cells (Mrakovcic et al. 2019) and is relevant for DNA replication and HR (Gottifredi and Wiesmüller 2018; Klusmann et al. 2016). As we see replication stress/DNA damage in HDACi-treated cells (Fig. 1), we consequently analyzed the p53 status of and a putative regulation of p53 expression by HDACi in Renca cells. We searched major databases for the characterization of cell lines concerning the p53 status of the Renca cell line. One database provided information that Renca cells carry one R210C exchange in the DNA-binding domain of p53 (Zeitouni et al. 2017). Meta-data analysis of whole-exome sequencing data (WES data; accession no. PRJEB12925) for Renca cells from Mosely et al. (2017) revealed that these cells have one wild-type p53 allele and one allele with the R210C mutation (Supplementary Fig. S2).

The literature does not provide insights into the impact of the R210C mutation on p53 functions and how it might affect a remaining p53 wild-type allele. Therefore, we experimentally assessed p53 in Renca cells. We compared the p53 expression of Renca cells and the pancreatic primary tumor cell line PPT-5436. Both cell lines are of murine origin, but PPT-5436 cells harbor the characterized point mutation $p53^{R172H}$ that results in a stabilized and transcriptionally inactive p53 (Conradt et al. 2012; Freed-Pastor and Prives 2012; Schneider et al. 2010). We noted that the expression of p53 in PPT-5436 cells was about sixfold higher than in Renca cells (Fig. 2a).

These results prompted us to test for an accumulation of p53 in response to genotoxic stress, which indicates wild-type p53 (Schneider et al. 2010). When we analyzed the p53 expression of Renca cells in response to doxorubicin treatment, we found that total p53 protein expression was upregulated in response to this genotoxic stimulus (Fig. 2b).

It is known that HDACi decrease the expression of wild-type and mutant p53 through a transcriptional mechanism in pancreatic and colorectal cancer cells (Göder et al. 2018; Schäfer et al. 2017; Sonnemann et al. 2014; Stojanovic et al. 2017). When we measured the expression of *p53* mRNA in Renca cells, we detected time- and dose-dependent effects of class I HDACi on *p53* mRNA expression. A treatment of

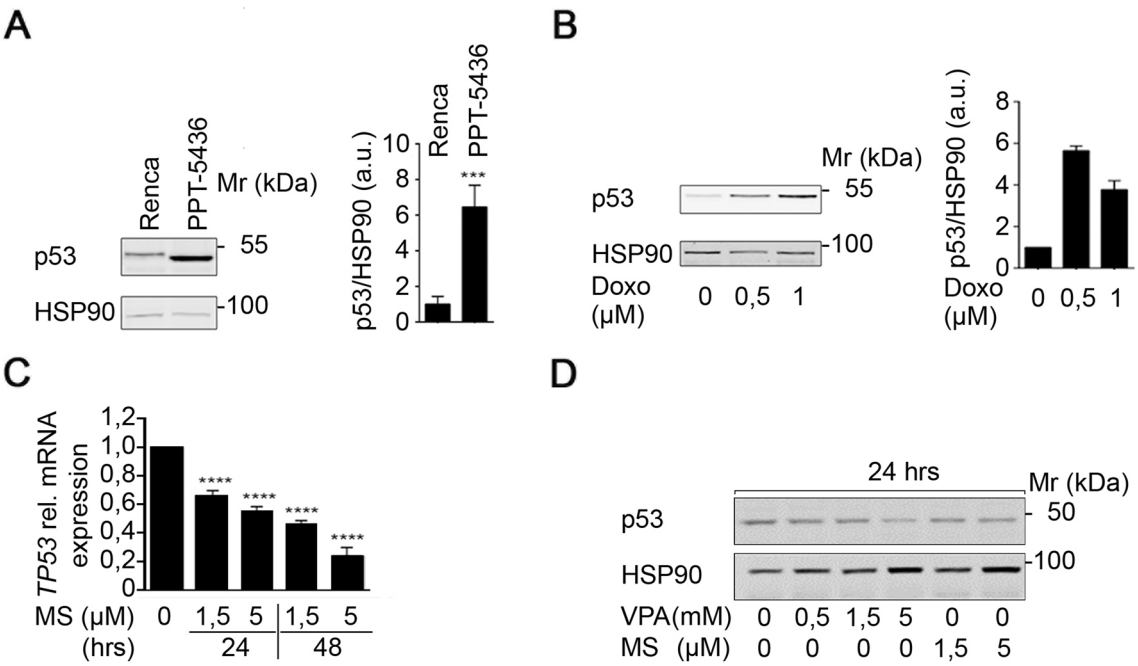

Fig. 2 Status of p53 and regulation through HDACi in Renca cells. **a** Untreated Renca and PPT-5436 cells were analyzed for p53 expression on Western blot. HSP90 served as loading control. Quantification of signal intensities was accomplished by densitometric analysis and subsequent normalization to the respective loading controls. Graph displays mean ± SD ($n = 4$; two-tailed unpaired Student's *t* test, ***p value < 0.001); Mr (kDa), relative molecular mass in kilo Daltons (kDa). **b** Renca cells were treated with the indicated concentrations of doxorubicin for 16 h. Western blot shows p53 and HSP90 as loading control. Quantification of signal intensities was accomplished by densitometric analysis and normalization to the respective loading controls. Graph displays mean ± SD ($n = 2$); Mr (kDa), relative molecular mass in kilo Daltons (kDa). **c** Renca cells were treated with the indicated concentrations of MS-275 for 24 h and 48 h. Independent triplicates were analyzed for *p53* mRNA expression by qPCR analysis. Graph shows mean ± SD ($n = 3$; one-way ANOVA; ****p value < 0.0001). **d** Renca cells were treated with the indicated concentrations of MS-275 (μM) and VPA (mM) for 24 h. Expression of p53 was analyzed by Western blot. HSP90 serves as loading control; Mr (kDa), relative molecular mass in kilo Daltons (kDa)

Renca cells with 1.5 µM MS-275 for 48 h led to a significant reduction of *p53* mRNA to 46.5 ± 1.34% of control levels. This effect was more pronounced at higher doses of MS-275 (Fig. 2c).

Immunoblot analyses revealed that this reduction of the *p53* mRNA translated into reduced levels of the p53 protein after 24-h incubations with MS-275 or VPA (Fig. 2d).

These data suggest that HDACi repress the expression of wild-type p53 and $p53^{R210C}$ in Renca cells.

HDAC inhibition does not promote chemoresistance

Since wild-type p53 is a tumor suppressor (Gottifredi and Wiesmüller 2018; Klusmann et al. 2016), its reduction by HDACi raises concerns that such drugs promote chemoresistance. Furthermore, HDACi-induced alterations in EMT factors (Kiweler et al. 2018) may promote the mesenchymal phenotype that is linked to chemoresistance (Fischer et al. 2015; Zheng et al. 2015). To address these concerns, we incubated Renca cells with combinations of HDACi, and the commonly used chemotherapeutics L-OHP, a DNA crosslinking agent that damages DNA directly, and HU, a ribonucleotide reductase inhibitor that can lead to DNA double-strand breaks secondary to a stalling of replication forks (Nikolova et al. 2017).

Flow cytometric analyses to measure cell death induction showed that Renca cells were resistant to L-OHP and slightly sensitive to HU (Fig. 3a). Such a poor response to chemotherapeutics is a typical feature of RCC (Barbieri et al. 2017; Chang et al. 2019; Piva et al. 2016). Combined treatment of Renca cells with VPA or MS-275 and L-OHP or HU augmented cytotoxic effects of HU significantly (Fig. 3a).

Moreover, the co-treatment with the HDACi and L-OHP or HU reduced the cellular adhesion factor E-cadherin, led to an accumulation of caspase-6, and induced caspase-3 cleavage (Fig. 3b). In addition, MS-275 and VPA slightly increased the accumulation of γH2AX that is caused by L-OHP (Fig. 3b) and this was linked to an abrogated induction of RAD51 by L-OHP and HU in Renca cells (Fig. 3c).

To further extend these findings, we analyzed cells derived from another notoriously chemoresistant tumor, non-small cell lung cancer (NSCLC). We incubated human H1299 lung cancer cells with L-OHP, because platinum compounds are a standard therapy for lung tumors (Foy et al. 2017; Gelsomino et al. 2019). In accordance with the data obtained in renal cancer cell lines, three structurally different HDACi (VPA, MS-275, LBH-589) promoted antiproliferative effects of L-OHP against H1299 cells (Fig. 3d).

We sum up that HDACi do not attenuate drug sensitivity, but rather increase the efficacy of well-established anticancer drugs.

HDACi modulate the expression of adhesion factors

Enhanced chemotherapy resistance and altered cell adhesion and signaling are hallmark features of the metastatic process (Brabletz et al. 2018; Fidler and Kripke 2015; Hao et al. 2019; Nieto 2013; Zeisberg and Neilson 2009). Our analysis of the impact of HDACi on chemosensitivity revealed that class I HDACi in combination with L-OHP and HU attenuated the expression of E-cadherin (Fig. 3b). Therefore, we further analyzed proteome data for the expression of a large number of cell adhesion factors and cytoskeletal proteins. We noted that MS-275 dysregulated a large number of such factors, including E-cadherin [Fig. 4a, b and (Kiweler et al. 2018)].

Proteomics also showed a reduction of integrin-β1 by HDACi (Fig. 4a), which is a key factor for cell adhesion to collagen and the colonization of tumor cells at distant tissues (Chua et al. 2010). Immunoblot analysis verified that 5 µM MS-275 and 5 mM VPA decreased the levels of integrin-β1 (Fig. 4c).

Since overexpression and somatic mutations in the tyrosine kinase ACK1 promote oncogenic signaling, cell proliferation, EMT, and chemoresistance (Chua et al. 2010; Jenkins et al. 2018; Mahajan and Mahajan 2015; Mahajan et al. 2018; Mahendrarajah et al. 2017; Yeh et al. 2012), we additionally tested whether HDACi have an impact on ACK1 in Renca cells. Western blot analyses showed that MS-275 and VPA attenuated ACK1 in a time- and dose-dependent manner (Fig. 4d).

These data demonstrate that HDACi dysregulate proteins that control the metastatic spread to and the colonization of secondary tissues by transformed cells.

HDACi suppress TGFβ-induced cellular plasticity

Cell adhesion and cellular plasticity are key steps in the progression from a local tumor to a distantly spread metastasis. TGFβ promotes EMT, metastasis, and drug resistance of cancer cells (Brabletz et al. 2018; Fidler and Kripke 2015; Hao et al. 2019; Nieto 2013; Zeisberg and Neilson 2009).

As an upregulation of the cell adhesion molecule N-cadherin is a marker for mesenchymal cells and described to be upregulated in epithelial cells as a consequence of EMT induction after TGFβ treatment (Hao et al. 2019; Zeisberg and Neilson 2009), we analyzed N-cadherin expression in HDACi-treated Renca cells. In immunocytochemistry analyses, immunoblot, and mass-spectrometric proteome analyses, we could not detect any N-cadherin expression in resting and TGFβ-treated Renca cells (Fig. 5a and data not shown).

As a substitute, we analyzed N-cadherin levels in mammary epithelial NM18 cells, which represent a standard TGFβ-sensitive cell system (Deckers et al. 2006). Immunocytochemistry of NM18 cells revealed that VPA and MS-275

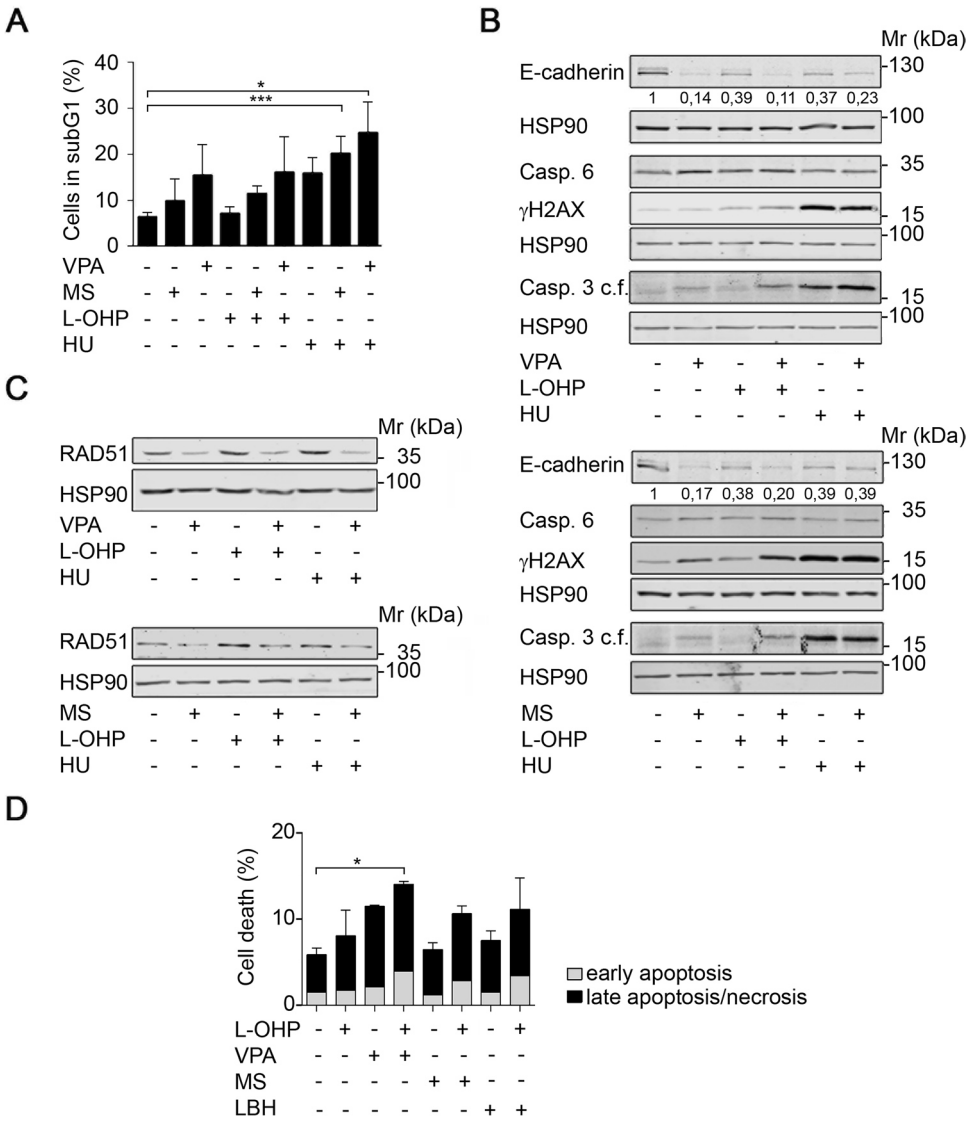

Fig. 3 HDACi interact with chemotherapeutics. **a** Renca cells were pre-treated for 24 h with 1.5 mM VPA or 1.5 µM MS-275 and subsequently treated with 5 µM L-OHP or 1 mM HU for 24 h. Cell death was accessed as % subG1 population in fixed, PI-stained cells using flow cytometry. Graph shows mean ± SD ($n=3$); *p value = 0.0101; ***p value = 0.003; one-way ANOVA. **b** Renca cells were treated with 1.5 mM VPA, 1.5 µM MS-275, 5 µM L-OHP, and 1 mM HU as indicated for 48 h. Expression levels of the indicated proteins were analyzed by Western blot. Band intensities for E-cadherin are indicated, with untreated cells set as 1 ($n=2$). HSP90 serves as loading control; relative molecular mass in kilo Daltons (kDa). **c** Renca cells were pre-treated for 24 h with 1.5 mM VPA or 1.5 µM MS-275 and subsequently treated with 5 µM L-OHP and 1 mM HU for 24 h. Expression of RAD51 was assessed by Western blot. HSP90 serves as loading control; relative molecular mass in kilo Daltons (kDa) ($n=2$). **d** H1299-TO-p53 cells were treated with HDACi (2 µM MS-275, 30 nM LBH-589, 3 mM VPA) and/or oxaliplatin (5 µM L-OHP) for 24-48 h. Annexin V/PI-stained cells were subjected to flow cytometry for cell death analyses; $n=3 \pm$ SD; *p value < 0.05, two-way ANOVA

significantly reduced TGFβ-induced N-cadherin expression (Fig. 5b, c).

Furthermore, we show in primary Mz-ccRCC2 cells that HDACi abolish a basal expression of N-cadherin (Fig. 5d).

These results suggest that HDACi dysregulate the expression of cell adhesion factors and impair TGFβ-induced cell plasticity.

Discussion

Our data illustrate that HDACi promote an induction of replicative stress and DNA damage in cultured cancer cells. This finding is coherent with previously published works, which illustrate that HDACs are required for the expression of factors mediating DNA damage, the recognition and repair of DNA lesions, and for scheduled origin firing

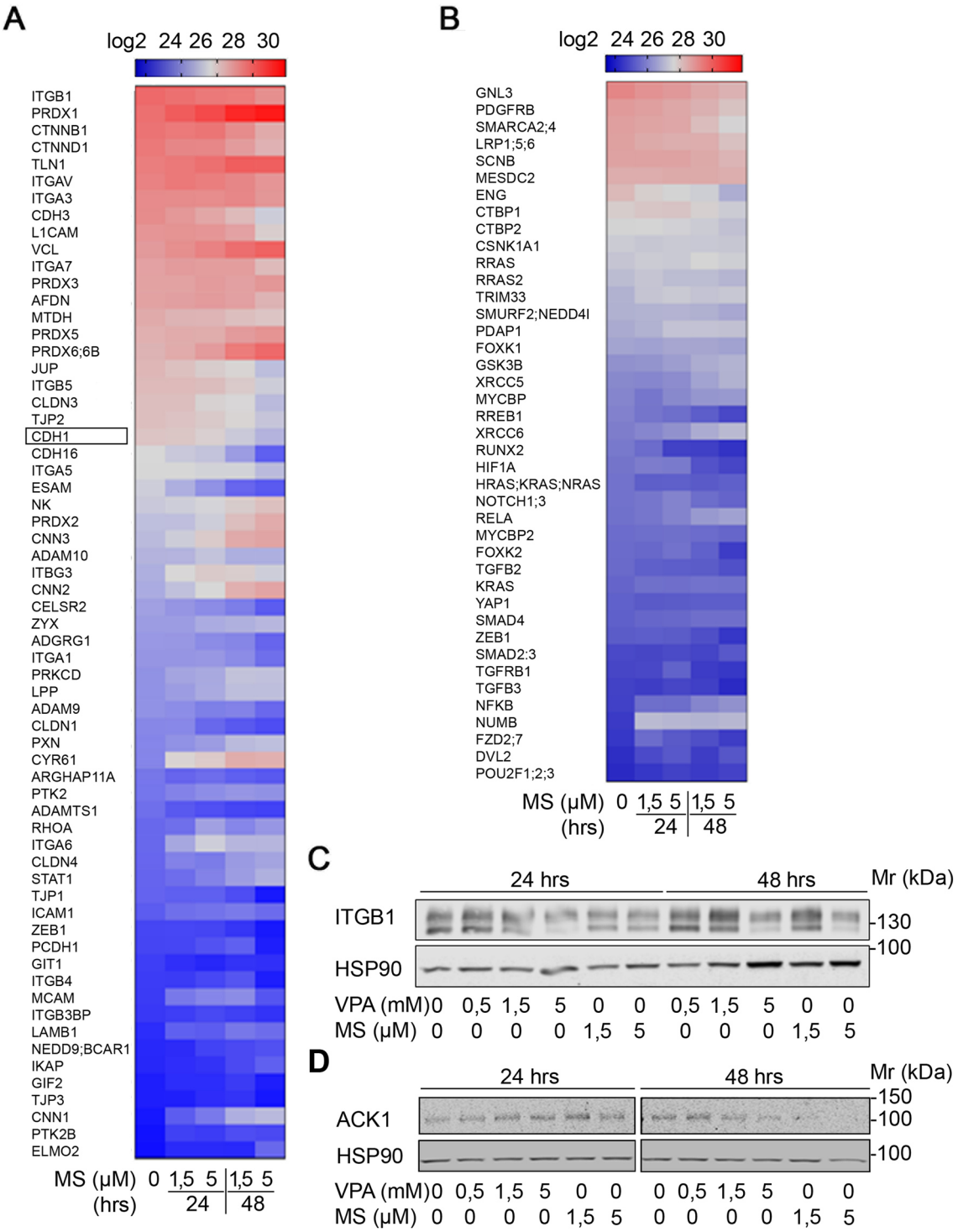

Fig. 4 HDACi decrease EMT-associated protein expression. **a, b** Renca cells were treated with the indicated concentrations of MS-275 (μM) for 24–48 h. Four independent replicates were analyzed for protein expression via LFQ in mass spectrometry (**a** adhesion, **b** epithelial/mesenchymal cell identity). Heatmap depicts changes in LFQ expression levels of the indicated proteins. E-cadherin (also termed CDH1) is marked by a frame in **a**. **c** Renca cells were treated with the indicated concentrations of VPA (mM) and MS-275 (μM) for 24 h and 48 h. ITGB1 expression was analyzed by Western blot. HSP90 serves as loading control. **d** Renca cells were treated with the indicated concentrations of VPA (mM) and MS-275 (μM) for 24 h and 48 h. ACK1 expression was analyzed by Western blot. HSP90 serves as loading control

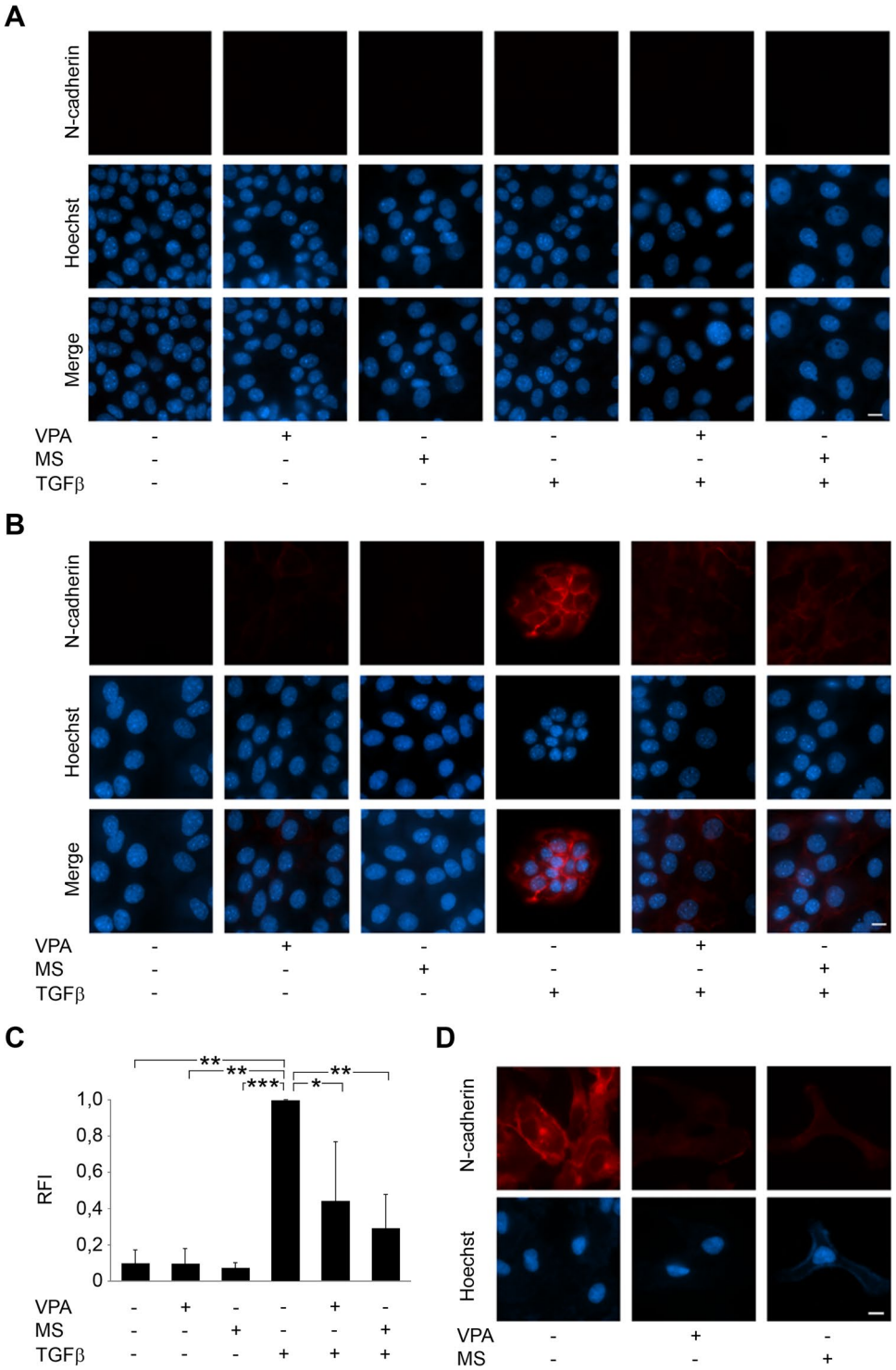

Fig. 5 Abrogation of basal and TGFβ-induced expression in transformed cells. **a** Renca cells were treated with HDACi (1.5 mM VPA, 5 µM MS-275), TGFβ (5 ng/ml), and combinations for 48 h. Immunofluorescence shows absence of N-cadherin (α-N-cadherin Ab (BD Bioscience) and α-mouse Cy3 secondary antibody (Dianova)). Nuclei were marked by Hoechst-33258 dye (blue); scale bar, 10 µm. **b** HDACi prevent N-cadherin (red) induction by TGFβ in NM18 cells from mouse mammary gland. **c** Relative fluorescence intensity (RFI) of N-cadherin staining in NM18 cells was determined from three individual experiments. Mean values are shown; *p value < 0.05; **p value < 0.01; ***p value < 0.001; one-way ANOVA. **d** Levels of N-cadherin in primary human RCC cells (Mz-ccRCC2) that were left untreated or exposed to 1.5 mM VPA or 5 µM MS-275

(Conti et al. 2010; Miller et al. 2010; Nikolova et al. 2017; Noack et al. 2017; Wang et al. 2012; Wells et al. 2013). Our proteomics approach shows that the HDACi-induced accumulation of γH2AX in Renca cells is linked to a disturbed expression of proteins that stabilize DNA replication forks and contribute to DNA damage recognition and repair. For example, we demonstrate that VPA and MS-275 diminish the expression levels of RAD51, which is a key HR protein and a survival factor for cancer cells harboring damaged DNA. These findings are consistent with literature evidence from other tumor-derived cells (Göder et al. 2018; Krumm et al. 2016; Nikolova et al. 2017). The observed correlation between DNA damage and prolonged growth arrest of HDACi-treated Renca cells is coherent with DNA

damage being a major trigger of cell cycle arrest (Kiweler et al. 2018; Lanz et al. 2019; Nikolova et al. 2017). Nevertheless, more investigations are necessary to assess the relative contribution of replication stress/DNA damage to HDACi-induced anti-proliferative effects. For instance, HDACi-induced alterations of proteins that control apoptosis and autophagy are further pathways through which HDACi might restrict tumor cell growth (Koeneke et al. 2015; Mrakovcic et al. 2019; Vancurova et al. 2018). Moreover, our proteome analyses show HDACi-induced alterations of proteins that control immune tolerance (Kiweler et al. 2018), raising the possibility that HDACi combat tumors through immune modulation.

Despite being a frequently used model system to analyze RCC in vitro and in vivo as syngeneic mouse model (Kiweler et al. 2018), the p53 status of Renca cells was undefined. While wild-type p53 is a short-lived protein, the majority of mutations in p53 are missense mutations that lead to the stable expression a p53 protein variant with a prolonged half-life (Conradt et al. 2012; Freed-Pastor and Prives 2012). We observed a strongly diminished expression of total p53 protein in Renca cells in comparison to a cell line expressing a defined mutant p53 isoform. This lower expression of p53 in Renca cells suggests its wild-type status. Our finding of an accumulation of p53 in doxorubicin treated Renca cells supports this notion. Nonetheless, one allele of p53 carries an ill-defined R210C exchange (Zeitouni et al. 2017). In general, p53 wild-type expression in Renca cells would correspond to the majority of cells derived from common renal cancers. *TP53* mutation rates in this disease are exceptionally low in comparison to other cancer types, with 2.5% for renal papillary-cell carcinoma and 2.4% for renal clear-cell carcinoma (Wang et al. 2017).

Since wild-type p53 can suppress tumorigenesis (Gottifredi and Wiesmüller 2018; Klusmann et al. 2016), the reduction of p53 in HDACi-treated Renca cells appears to be counterintuitive with the anti-proliferative effects of HDACi. However, p53 might not be inactivated and its reduction by HDACi is not complete. There is, for example, an accumulation of p21, which is positively regulated by p53, and a repression of survivin, which is negatively regulated by p53 in HDACi-treated Renca cells (Kiweler et al. 2018). Apparently, the reduction of total p53 may not necessarily lead to a suppression of p53 target gene regulation, because p53 is also activated by acetylation. For example, low and very active levels of acetylated p53 can drive the expression of its target genes and apoptosis upon replication stress and DNA damage in colorectal cancer cells (Brandl et al. 2012). On the other hand, we may also detect p53-independent growth arrest and cell death induction by HDACi in Renca cells, as seen in p53-negative colorectal cancer cells (Sonnemann et al. 2014). Moreover, replication stress triggers apoptosis and mitotic catastrophe after HDACi treatment despite a reduced expression of p53 and its target genes (Göder et al. 2018). One should additionally consider that there are even cases in which p53 antagonizes apoptosis induction (Barckhausen et al. 2014) and the HDACi-evoked loss of various DNA repair proteins including p53 may trigger cytotoxic DNA damage. In conclusion, the observed loss of p53 expression in HDACi-treated Renca cells is not linked to diminished cytotoxic responses or an induction of chemoresistance.

Two recent studies point out that the mesenchymal transition of transformed cells ties in with the resistance of pancreatic and breast cancer cells against DNA-damaging agents (Fischer et al. 2015; Zheng et al. 2015). So far, our data illustrate that HDACi themselves attenuate the expression of DNA repair and promote cell death of HU-treated RCC and NSCLC cultures. Studies including small groups of patients treated with HU and HDACi suggest that such combinatorial treatment might be successful (Bug et al. 2005; Müller and Krämer 2010). Undoubtedly, additional in vivo evidence is necessary to clarify the therapeutic validity of HDACi/HU combination treatment schedules. This also applies to the doses that can be achieved without significant toxicity in RCC patients. A recent report found that up to 1.51 µM MS-275 was achieved without gross toxicity in mice, but large variation of maximal plasma concentrations from 4 to 53.1 ± 92.4 and a half-life from 33.4 to 150 h occurred in humans (Connolly et al. 2017; Kurmasheva et al. 2019), indicating unexplained large patient-to-patient variability. The maximum-tolerated dose of VPA was reported to range, for example, from 50 mg/kg daily to 140 mg/kg/day, which is within the therapeutic serum concentrations of VPA from 0.35 to 0.7 mM (Bug et al. 2005; Münster et al. 2007; Phiel et al. 2001).

In addition to the effects of HDACi on replication stress/DNA damage, their impact on EMT needs to be investigated. Preceding work demonstrated a dysregulation of various proteins that control cell adhesion and migratory properties in RCC cells following class I HDAC inhibition (Kiweler et al. 2018) and we verify an HDACi-mediated downregulation of integrin-β1 in Renca cells. This finding is coherent with the literature that reports an inhibition of integrin-α/β expression and their downstream signaling pathways in HDACi-treated RCC cells (Jones et al. 2009b). However, a plethora of additional factors determines EMT in HDACi-treated cells. For example, we see that HDACi decrease RhoA, which regulates EMT and interacts with HDACs (Mertsch and Krämer 2017). Likewise, proteomics suggests an HDACi-induced increase in the inducible transcription factor STAT1 in Renca cells and we found that such an accumulation of STAT1 contributes to apoptosis in HDACi-treated melanoma cells (Krämer et al. 2006). Another example is ACK1, for which evidence collected in various tumor types suggests a pro-tumorigenic role (Chua

et al. 2010; Jenkins et al. 2018; Mahajan and Mahajan 2015; Mahajan et al. 2018). Furthermore, data collected with gastric and liver cancer cells show that ACK1 is overexpressed in primary clinical specimen and that ACK1 promotes the invasive capacity and EMT of such tumor cells through its direct activating effects on AKT kinases (Lei et al. 2015; Xu et al. 2015). AKT also contributes to the spread of RCC cells into bone tissue and a hyperstabilized, mutant ACK1 isoform promotes hallmarks of cancer in RCC cells (Chua et al. 2010). Hence, the reduction of ACK1 by HDACi could cause anti-proliferative, therapeutically relevant effects. We found that HDACi decrease ACK1 by a caspase-dependent mechanism in leukemic cells (Mahendrarajah et al. 2016) and we see that the decline in ACK1 is linked to apoptosis of Renca cells [(Kiweler et al. 2018) and this study]. Accordingly, the loss of ACK1 could occur through caspase-dependent degradation. Additional experiments are necessary to clarify whether ACK1 degradation in renal cancer presents a functional signal for cell growth reduction, cell death induction, and metastasis or poses a downstream marker of cell death.

TGFβ-induced EMT signaling promotes metastasis, chemoresistance, angiogenesis, and immune evasion of tumor cells (Hao et al. 2019). Although the treatment with TGFβ induces N-cadherin in other cell lines (Mikami et al. 2016; Zeisberg and Neilson 2009), Renca cells do not express the TGFβ receptor-II (Engel et al. 1999) and, therefore, fail to accumulate N-cadherin. Such a loss of TGFβ receptor II is also seen in 31 out of 62 RCC patients and correlates with a lower apoptotic index and statistically significant lower survival rates (Miyajima et al. 2003). The expression of E-cadherin, the cytoplasmic localization of β-catenin (Kiweler et al. 2018), and the absence of the mesenchymal marker N-cadherin (this work) verify that Renca cells remain epithelial cells independent of HDACi treatment. In contrast to this, HDACi suppress TGFβ-induced N-cadherin expression in mammary epithelial cells and HDACi decrease basal N-cadherin expression in primary human RCC cells. Our finding that both epithelial (Renca cells) and mesenchymal (Mz-ccRCC2 cells) respond with an induction of cell death to class I HDACi shows that such drugs can kill cells having either differentiation status. Further studies are underway to address if HDACi shift transformed cells to certain molecular signatures of one of the states and thereby eliminate them.

Taken together, our work illustrates that class I HDACi evoke DNA damage and suppress the metastasis-associated phenotype. These data suggest exploiting HDACi further for the treatment of cancer.

Materials and methods

Cell culture conditions and drugs

Fetal calf serum (FCS) was from Gibco Invitrogen Life Technologies, Darmstadt, Germany (catalogue numbers 102270/10270106, EU approved origin: South America, lots. 41Q8207K/42G8258K). Renca cells grow at 37 °C and 5% CO_2 in RPMI medium (Sigma-Aldrich, Munich, Germany) supplemented with 10% FCS, 1% penicillin/streptomycin and 2% glutamine. NM18 and H1299-TO-p53 cells grow at 37 °C and 5% CO_2 in DMEM medium (Sigma-Aldrich, Munich, Germany) supplemented with 10% FCS and 1% penicillin/streptomycin; 1% glutamine and 5 µg/mL insulin were added to NM18 cells. Renca cells were obtained from Prof. W. Wels, GSH Frankfurt/Main, Germany (derived from a spontaneously developed renal cortical adenocarcinoma in a male Balb/c mouse; ATCC® CRL-2947™). PPT-5436 were developed in the group of one of the coauthors (G.S.). These are a low passage cell line from primary pancreatic tumors of a *PTF1a/p48*$^{ex1Cre/+}$*;LSL-KRAS*$^{G12D/+}$*;LSL-p53R172H*$^{+/+}$*;LSL-R26*$^{Tva-lacZ/-}$ mouse. H1299-TO-p53 were given to us by Dr. G. Rohaly, HPI, Hamburg, Germany. These are a derivative of NCI-H1299 (ATCC® CRL-5803™) cells, which are epithelial cells from a metastatic site lymph node of a lung carcinoma of a male patient. NM18 cells are a subclone of NMuMG cells (ATCC® CRL-1636™), which were isolated by their strong response to TGFβ by Deckers et al. (2006). NMuMG cells are epithelial mammary gland cells from a Namru strain mouse. Mz-ccRCC2 renal tumor cells were isolated as described in Haber et al. (2015) from tumor specimens that were obtained shortly after nephrectomy. Tumor tissue was dissociated mechanically and with 1 mg/ml collagenase II, pressed through a cell strainer (70 µm) and centrifuged under sterile conditions. The obtained cells were first cultured in AmnioMAX C100 Basal Medium including AmnioMAX C100 Supplement (Gibco, Life Technologies, Darmstadt, Germany). After the first passage, they were transferred to DMEM medium supplemented with 10% FCS and 1% penicillin/streptomycin and cultured at 37 °C and 5% CO_2; i.e., conditions as for Renca cells. The epithelial origin was confirmed by immunohistochemical cytokeratin staining. For the experiments, the cells were used in passages 2–8. No commonly mischaracterized cells were used and cells were tested free of mycoplasma every 4–8 weeks. TGFβ and VPA were purchased from Sigma-Aldrich, Germany. Entinostat was purchased from Selleckchem, Germany.

Database search for p53 in Renca cells

To search for information on the p53 status of Renca cells, we considered the International Agency for Research on Cancer TP53 Database (IARC, https://p53.iarc.fr/), the Catalogue Of Somatic Mutations In Cancer (COSMIC, https://cancer.sanger.ac.uk/cosmic), the Cancer Cell Line Encyclopedia (CCLE, https://portals.broadinstitute.org/ccle), the American Type Culture Collection (ATCC, https://www.atcc.org), the *TP53 website cell line compendium* (https://p53.fr), and Charles River (Zeitouni et al. 2017). Reanalysis of WES data is based on accession no. PRJEB12925 (Mosely et al. 2017).

Protein lysates, Western blot, densitometric analysis, and antibodies

We have recently summarized the Western blot method used to collect data shown here (Stojanovic et al. 2017). Data acquisition was performed with the Odyssey Infrared Imaging System (Licor), using IRDye® 680RD-coupled or IRDye® 800CW-coupled secondary antibodies. Immunoblots are representative of at least two independent experiments. The following antibodies were used: Cell Signaling Technology (Frankfurt/Main, Germany): cleaved caspase-3/#9661, caspase-6/#9762, E-cadherin/#3195; Enzo Life Sciences (Lörrach, Germany): HSP90/ADI-SPA-830-F; Merck Millipore (Darmstadt, Germany): AB1952; Santa Cruz Biotechnology (Heidelberg, Germany): ACK1/sc-28336, pS139-H2AX/sc-101696 (γH2AX), β-actin/sc-47778, P53/sc81168; Abcam: RAD51/ab63801; BD Bioscience (Heidelberg, Germany): N-cadherin/BD610921.

Cell cycle and cell death analysis

Cells were harvested with trypsin/EDTA and fixed with 80% ethanol. Samples were then stored at − 20 °C for at least 2 h. Thereafter, cells were incubated with RNAse A (Carl Roth; final concentration 20 µg/mL) for 1 h at RT and stained with propidium iodide (PI) (Sigma-Aldrich; final concentration 16.5 µg/mL) for 10 min on ice. Annexin V/PI staining was performed according to the manufacturer's instructions with Annexin V-FITC (Becton Dickinson) and PI at RT for 15 min in the dark. Cells were subjected to flow cytometry with the FACSCanto Flow Cytometer (BD Biosciences). Data were analyzed with the FACSDIVA™ Software (BD Biosciences).

Immunofluorescence to detect N-cadherin

NM18 cells were seeded on chamber coverslips (µ-Slide 8-well, iBidi) and treated with 1.5 mM VPA or 5 µM MS-275, 5 ng/mL TGFβ, or combinations thereof for 48 h. Cells were washed thrice with phosphate-buffered saline (PBS), and fixed for 20 min in 4% paraformaldehyde. After cell permeabilization using 0.1% Triton X-100 in PBS for 10 min, cells were stained for 1 h at RT using α-N-cadherin antibody (BD Bioscience) 1:100 in PBS + 1% FCS. After incubation, slides were washed three times for 5 min in PBS and incubated for 1 h at RT with α-mouse Cy3 secondary antibody (Dianova). DNA/cell nuclei were visualized by staining with 0.5 µg/mL Hoechst-33258 (Sigma-Aldrich). Observation, image acquisition, and analysis of stained cells were performed using AxioVert 200 M, a digital AxioCam CCD camera and Axiovision software (Carl Zeiss, Jena, Germany).

Proteomics and pathway analysis

NuPAGE® LDS Sample Buffer (1×) supplemented with 100 µM DTT was added to treated cells and controls. Lysates were subjected to mass spectrometry (Dejung et al. 2016) for protein detection. Proteins were run on gels and digested with mass spectrometry-grade trypsin (Sigma-Aldrich, St. Louis, Missouri) and purified with a StageTip. Data were analyzed with Maxquant v1.5.2.8 using LFQ, ENSEMBL GRCm38 peptide database (57,751 entries), and custom R scripts. (Dejung et al. 2016). Full proteomics data are available upon scientific request. Preceding statistical analysis by R software version 3.2 using unpaired *t* test (two conditions) or one-way ANOVA (multiple conditions) resulted in an individual set of significantly regulated proteins. The background set was composed of all proteins successfully quantified in the experiment (5812 proteins). For each set of significantly regulated proteins, three hypergeometric tests (for biological processes, for molecular functions, and for cellular components) were performed using the R package "GOstats". By this means, it was determined if the GO terms that were associated with significantly changing genes were over-represented over the defined background (Falcon and Gentleman 2007). For each protein listed, the Entrez gene ID was obtained using the annotation R package "BiomaRt"; see also cells (Kiweler et al. 2018).

Determination of mRNA transcripts

The primer sequences that we used to determine p53 transcript numbers were *AGAGACCGCCGTACAGAAGA* (forward)/*CTGTAGCATGGGCATCCTTT* (reverse); β-actin: *GTCGAGTCGCGTCCACC* (forward)/*GTCATCCATGGCGAACTGGT* (reverse). Isolation of total RNA was carried out by means of the RNeasy Mini-Kit (Qiagen, Hilden, Germany). To quantify the relative gene expression by ΔΔ-Ct method, 20 ng cDNA and 100 nM primer mix (MWG Biotech, Ebersberg, Germany) were mixed together with the Power SybrGreen master mix and applied to the

StepOnePlus real-time PCR device (Applied Biosystems/Thermo Fischer, Frankfurt/Main, Germany). Primer efficiencies were previously determined by the formula $10^{(-1/\text{slope})}$. All experiments were carried out in technical and biological triplicates.

Statistical analysis

One-way ANOVA/two-way ANOVA were used as indicated for the respective experiments (GraphPad Prism Vers.6.01) and corrected for multiple testing using Dunnett's test or Bonferroni's multiple comparisons test. Two-paired *t* test with Welch's correction was used when not more than two conditions were compared and for proteomics as comparison with untreated samples. *p* values are indicated in the legends.

Acknowledgements Open Access funding provided by Projekt DEAL. We thank Franziska Müller, Christina Brachetti, and Andrea Piée-Staffa (ITOX Mainz, Germany) for excellent technical support; Mandy Beyer (ITOX Mainz, Germany) for help with statistics; Dr. Mario Dejung (IMB Mainz, Germany) for help with proteomics. We are indebted to Prof. W. Wels, GSH Frankfurt/Main, Germany, Dr. G. Rohaly, HPI, Hamburg, Germany, and Deckers and colleagues, University Medical Center, Leiden, The Netherlands, for cell lines. This study was mainly supported by grants to OHK from the Wilhelm Sander-Stiftung (#2010.078). The group of OHK is additionally supported by the Deutsche Forschungsgemeinschaft (#KR2291/7-1/8-1/9-1), funded by the Deutsche Forschungsgemeinschaft (DFG, German Research Foundation) – Project-ID 393547839 – SFB 1361, and received intramural funding from the NMFZ Mainz and the University Medical Center Mainz.

Compliance with ethical standards

Conflict of interest The authors declare no conflict of interest.

References

Aiello NM, Brabletz T, Kang Y et al (2017) Upholding a role for EMT in pancreatic cancer metastasis. Nature 547:E7–E8. https://doi.org/10.1038/nature22963

Barbieri CE, Chinnaiyan AM, Lerner SP et al (2017) The emergence of precision urologic oncology: a collaborative review on biomarker-driven therapeutics. Eur Urol 71:237–246. https://doi.org/10.1016/j.eururo.2016.08.024

Barckhausen C, Roos WP, Naumann SC, Kaina B (2014) Malignant melanoma cells acquire resistance to DNA interstrand cross-linking chemotherapeutics by p53-triggered upregulation of DDB2/XPC-mediated DNA repair. Oncogene 33:1964–1974. https://doi.org/10.1038/onc.2013.141

Bayat Mokhtari R, Homayouni TS, Baluch N et al (2017) Combination therapy in combating cancer. Oncotarget 8:38022–38043. https://doi.org/10.18632/oncotarget.16723

Brabletz T, Kalluri R, Nieto MA, Weinberg RA (2018) EMT in cancer. Nature reviews. Cancer 18:128–134. https://doi.org/10.1038/nrc.2017.118

Bradner JE, Mak R, Tanguturi SK et al (2010) Chemical genetic strategy identifies histone deacetylase 1 (HDAC1) and HDAC2 as therapeutic targets in sickle cell disease. Proc Natl Acad Sci USA 107:12617–12622. https://doi.org/10.1073/pnas.1006774107

Brandl A, Wagner T, Uhlig KM et al (2012) Dynamically regulated sumoylation of HDAC2 controls p53 deacetylation and restricts apoptosis following genotoxic stress. J Mol Cell Biol 4:284–293. https://doi.org/10.1093/jmcb/mjs013

Bug G, Ritter M, Wassmann B et al (2005) Clinical trial of valproic acid and all-trans retinoic acid in patients with poor-risk acute myeloid leukemia. Cancer 104:2717–2725. https://doi.org/10.1002/cncr.21589

Chang AJ, Zhao L, Zhu Z et al (2019) The past, present and future of immunotherapy for metastatic renal cell carcinoma. Anticancer Res 39:2683–2687. https://doi.org/10.21873/anticanres.13393

Chua BT, Lim SJ, Tham SC et al (2010) Somatic mutation in the ACK1 ubiquitin association domain enhances oncogenic signaling through EGFR regulation in renal cancer derived cells. Mol Oncol 4:323–334. https://doi.org/10.1016/j.molonc.2010.03.001

Chun P (2018) Therapeutic effects of histone deacetylase inhibitors on kidney disease. Arch Pharmacal Res 41:162–183. https://doi.org/10.1007/s12272-017-0998-7

Connolly RM, Rudek MA, Piekarz R (2017) Entinostat: a promising treatment option for patients with advanced breast cancer. Future Oncol 13:1137–1148. https://doi.org/10.2217/fon-2016-0526

Conradt L, Henrich A, Wirth M et al (2012) Mdm2 inhibitors synergize with topoisomerase II inhibitors to induce p53-independent pancreatic cancer cell death. Int J Cancer. https://doi.org/10.1002/ijc.27916

Conti C, Leo E, Eichler GS et al (2010) Inhibition of histone deacetylase in cancer cells slows down replication forks, activates dormant origins, and induces DNA damage. Cancer Res 70:4470–4480. https://doi.org/10.1158/0008-5472.CAN-09-3028

Deckers M, van Dinther M, Buijs J et al (2006) The tumor suppressor Smad4 is required for transforming growth factor beta-induced epithelial to mesenchymal transition and bone metastasis of breast cancer cells. Cancer Res 66:2202–2209. https://doi.org/10.1158/0008-5472.CAN-05-3560

Dejung M, Subota I, Bucerius F et al (2016) Quantitative proteomics uncovers novel factors involved in developmental differentiation of *Trypanosoma brucei*. PLoS Pathog 12:e1005439. https://doi.org/10.1371/journal.ppat.1005439

Dietrich MF, Gerber DE (2016) Chemotherapy for advanced non-small cell lung cancer. Cancer Treat Res 170:119–149. https://doi.org/10.1007/978-3-319-40389-2_6

Engel JD, Kundu SD, Yang T et al (1999) Transforming growth factor-beta type II receptor confers tumor suppressor activity in murine renal carcinoma (renca) cells. Urology 54:164–170

Falcon S, Gentleman R (2007) Using GOstats to test gene lists for GO term association. Bioinformatics 23:257–258. https://doi.org/10.1093/bioinformatics/btl567

Fidler IJ, Kripke ML (2015) The challenge of targeting metastasis. Cancer Metastasis Rev 34:635–641. https://doi.org/10.1007/s10555-015-9586-9

Fischer KR, Durrans A, Lee S et al (2015) Epithelial-to-mesenchymal transition is not required for lung metastasis but contributes to chemoresistance. Nature 527:472–476. https://doi.org/10.1038/nature15748

Foy V, Schenk MW, Baker K et al (2017) Targeting DNA damage in SCLC. Lung cancer 114:12–22. https://doi.org/10.1016/j.lungcan.2017.10.006

Freed-Pastor WA, Prives C (2012) Mutant p53: one name, many proteins. Genes Dev 26:1268–1286. https://doi.org/10.1101/gad.190678.112

Gelsomino F, Lamberti G, Parisi C et al (2019) The evolving landscape of immunotherapy in small-cell lung cancer: a focus on predictive biomarkers. Cancer Treat Rev 79:101887. https://doi.org/10.1016/j.ctrv.2019.08.003

Göder A, Emmerich C, Nikolova T et al (2018) HDAC1 and HDAC2 integrate checkpoint kinase phosphorylation and cell fate through the phosphatase-2A subunit PR130. Nat Commun 9:764. https://doi.org/10.1038/s41467-018-03096-0

Gottifredi V, Wiesmüller L (2018) The tip of an iceberg: replication-associated functions of the tumor suppressor p53. Cancers. https://doi.org/10.3390/cancers10080250

Haber T, Jöckel E, Roos FC et al (2015) Bone metastasis in renal cell carcinoma is preprogrammed in the primary tumor and caused by AKT and integrin alpha5 signaling. J Urol 194:539–546. https://doi.org/10.1016/j.juro.2015.01.079

Hao Y, Baker D, Ten Dijke P (2019) TGF-beta-mediated epithelial-mesenchymal transition and cancer metastasis. Int J Mol Sci. https://doi.org/10.3390/ijms20112767

Jenkins C, Luty SB, Maxson JE et al (2018) Synthetic lethality of TNK2 inhibition in PTPN11-mutant leukemia. Sci Signal. https://doi.org/10.1126/scisignal.aao5617

Jones J, Juengel E, Mickuckyte A et al (2009a) The histone deacetylase inhibitor valproic acid alters growth properties of renal cell carcinoma in vitro and in vivo. J Cell Mol Med 13:2376–2385. https://doi.org/10.1111/j.1582-4934.2008.00436.x

Jones J, Juengel E, Mickuckyte A et al (2009b) Valproic acid blocks adhesion of renal cell carcinoma cells to endothelium and extracellular matrix. J Cell Mol Med 13:2342–2352. https://doi.org/10.1111/j.1582-4934.2008.00603.x

Juengel E, Nowaz S, Makarevi J et al (2014) HDAC-inhibition counteracts everolimus resistance in renal cell carcinoma in vitro by diminishing cdk2 and cyclin A. Mol Cancer 13:152. https://doi.org/10.1186/1476-4598-13-152

Kiweler N, Brill B, Wirth M et al (2018) The histone deacetylases HDAC1 and HDAC2 are required for the growth and survival of renal carcinoma cells. Arch Toxicol 92:2227–2243. https://doi.org/10.1007/s00204-018-2229-5

Klusmann I, Rodewald S, Müller L et al (2016) p53 activity results in DNA replication fork processivity. Cell Rep 17:1845–1857. https://doi.org/10.1016/j.celrep.2016.10.036

Koeneke E, Witt O, Oehme I (2015) HDAC family members intertwined in the regulation of autophagy: a druggable vulnerability in aggressive tumor entities. Cells 4:135–168. https://doi.org/10.3390/cells4020135

Krämer OH, Baus D, Knauer SK, Stein S, Jäger E, Stauber RH, Grez M, Pfitzner E, Heinzel T (2006) Acetylation of Stat1 modulates NF-kappaB activity. Genes Dev 20(4):473–485

Krumm A, Barckhausen C, Kucuk P et al (2016) Enhanced histone deacetylase activity in malignant melanoma provokes RAD51 and FANCD2-triggered drug resistance. Cancer Res 76:3067–3077. https://doi.org/10.1158/0008-5472.CAN-15-2680

Kurmasheva RT, Bandyopadhyay A, Favours E et al (2019) Evaluation of entinostat alone and in combination with standard-of-care cytotoxic agents against rhabdomyosarcoma xenograft models. Pediatr Blood Cancer 66:e27820. https://doi.org/10.1002/pbc.27820

Lanz MC, Dibitetto D, Smolka MB (2019) DNA damage kinase signaling: checkpoint and repair at 30 years. EMBO J 38:e101801. https://doi.org/10.15252/embj.2019101801

Lei X, Li YF, Chen GD et al (2015) Ack1 overexpression promotes metastasis and indicates poor prognosis of hepatocellular carcinoma. Oncotarget 6:40622–40641. https://doi.org/10.18632/oncotarget.5872

Mahajan K, Mahajan NP (2015) ACK1/TNK2 tyrosine kinase: molecular signaling and evolving role in cancers. Oncogene 34:4162–4167. https://doi.org/10.1038/onc.2014.350

Mahajan NP, Coppola D, Kim J et al (2018) Blockade of ACK1/TNK2 to squelch the survival of prostate cancer stem-like cells. Sci Rep 8:1954. https://doi.org/10.1038/s41598-018-20172-z

Mahendrarajah N, Paulus R, Krämer OH (2016) Histone deacetylase inhibitors induce proteolysis of activated CDC42-associated kinase-1 in leukemic cells. J Cancer Res Clin Oncol 142:2263–2273. https://doi.org/10.1007/s00432-016-2229-x

Mahendrarajah N, Borisova ME, Reichardt S et al (2017) HSP90 is necessary for the ACK1-dependent phosphorylation of STAT1 and STAT3. Cell Signal 39:9–17. https://doi.org/10.1016/j.cellsig.2017.07.014

Mao S, Lu G, Lan X et al (2017) Valproic acid inhibits epithelial–mesenchymal transition in renal cell carcinoma by decreasing SMAD4 expression. Mol Med Rep 16:6190–6199. https://doi.org/10.3892/mmr.2017.7394

Mertsch S, Krämer OH (2017) The interplay between histone deacetylases and rho kinases is important for cancer and neurodegeneration. Cytokine Growth Factor Rev 37:29–45. https://doi.org/10.1016/j.cytogfr.2017.05.006

Mikami S, Oya M, Mizuno R et al (2016) Recent advances in renal cell carcinoma from a pathological point of view. Pathol Int 66:481–490. https://doi.org/10.1111/pin.12433

Miller KM, Tjeertes JV, Coates J et al (2010) Human HDAC1 and HDAC2 function in the DNA-damage response to promote DNA nonhomologous end-joining. Nat Struct Mol Biol 17:1144–1151. https://doi.org/10.1038/nsmb.1899

Miyajima A, Asano T, Seta K et al (2003) Loss of expression of transforming growth factor-beta receptor as a prognostic factor in patients with renal cell carcinoma. Urology 61:1072–1077. https://doi.org/10.1016/s0090-4295(02)02553-0

Mosely SI, Prime JE, Sainson RC et al (2017) Rational selection of syngeneic preclinical tumor models for immunotherapeutic drug discovery. Cancer Immunol Res 5:29–41. https://doi.org/10.1158/2326-6066.CIR-16-0114

Mrakovcic M, Kleinheinz J, Fröhlich LF (2019) p53 at the crossroads between different types of HDAC inhibitor-mediated cancer cell death. Int J Mol Sci. https://doi.org/10.3390/ijms20102415

Müller S, Krämer OH (2010) Inhibitors of HDACs–effective drugs against cancer? Curr Cancer Drug Targets 10:210–228

Münster P, Marchion D, Bicaku E et al (2007) Phase I trial of histone deacetylase inhibition by valproic acid followed by the topoisomerase II inhibitor epirubicin in advanced solid tumors: a clinical and translational study. J Clin Oncol 25:1979–1985. https://doi.org/10.1200/JCO.2006.08.6165

Nieto MA (2013) Epithelial plasticity: a common theme in embryonic and cancer cells. Science 342:1234850. https://doi.org/10.1126/science.1234850

Nikolova T, Kiweler N, Krämer OH (2017) Interstrand crosslink repair as a target for HDAC inhibition. Trends Pharmacol Sci 38:822–836. https://doi.org/10.1016/j.tips.2017.05.009

Noack K, Mahendrarajah N, Hennig D et al (2017) Analysis of the interplay between all-trans retinoic acid and histone deacetylase inhibitors in leukemic cells. Arch Toxicol 91:2191–2208. https://doi.org/10.1007/s00204-016-1878-5

Phiel CJ, Zhang F, Huang EY et al (2001) Histone deacetylase is a direct target of valproic acid, a potent anticonvulsant, mood

stabilizer, and teratogen. J Biol Chem 276:36734–36741. https://doi.org/10.1074/jbc.M101287200

Piva F, Giulietti M, Santoni M et al (2016) Epithelial to mesenchymal transition in renal cell carcinoma: implications for cancer therapy. Mol Diagn Therapy 20:111–117. https://doi.org/10.1007/s40291-016-0192-5

Rogakou EP, Pilch DR, Orr AH et al (1998) DNA double-stranded breaks induce histone H2AX phosphorylation on serine 139. J Biol Chem 273:5858–5868. https://doi.org/10.1074/jbc.273.10.5858

Schäfer C, Göder A, Beyer M et al (2017) Class I histone deacetylases regulate p53/NF-kappaB crosstalk in cancer cells. Cell Signal 29:218–225. https://doi.org/10.1016/j.cellsig.2016.11.002

Schneider G, Henrich A, Greiner G et al (2010) Cross talk between stimulated NF-kappaB and the tumor suppressor p53. Oncogene 29:2795–2806. https://doi.org/10.1038/onc.2010.46

Singla M, Kumar A, Bal A et al (2018) Epithelial to mesenchymal transition induces stem cell like phenotype in renal cell carcinoma cells. Cancer Cell Int 18:57. https://doi.org/10.1186/s12935-018-0555-6

Sonnemann J, Marx C, Becker S et al (2014) p53-dependent and p53-independent anticancer effects of different histone deacetylase inhibitors. Br J Cancer 110:656–667. https://doi.org/10.1038/bjc.2013.742

Stojanovic N, Hassan Z, Wirth M et al (2017) HDAC1 and HDAC2 integrate the expression of p53 mutants in pancreatic cancer. Oncogene 36:1804–1815. https://doi.org/10.1038/onc.2016.344

Tretbar S, Krausbeck P, Müller A et al (2019) TGF-beta inducible epithelial-to-mesenchymal transition in renal cell carcinoma. Oncotarget 10:1507–1524. https://doi.org/10.18632/oncotarget.26682

Vancurova I, Uddin MM, Zou Y, Vancura A (2018) Combination therapies targeting HDAC and IKK in solid tumors. Trends Pharmacol Sci 39:295–306. https://doi.org/10.1016/j.tips.2017.11.008

Wang H, Zhou W, Zheng Z et al (2012) The HDAC inhibitor depsipeptide transactivates the p53/p21 pathway by inducing DNA damage. DNA Repair 11:146–156. https://doi.org/10.1016/j.dnarep.2011.10.014

Wang Z, Peng S, Jiang N et al (2017) Prognostic and clinicopathological value of p53 expression in renal cell carcinoma: a meta-analysis. Oncotarget 8:102361–102370. https://doi.org/10.18632/oncotarget.21971

Wei M, Mao S, Lu G et al (2018) Valproic acid sensitizes metformin-resistant human renal cell carcinoma cells by upregulating H3 acetylation and EMT reversal. BMC Cancer 18:434. https://doi.org/10.1186/s12885-018-4344-3

Wells CE, Bhaskara S, Stengel KR et al (2013) Inhibition of histone deacetylase 3 causes replication stress in cutaneous T cell lymphoma. PLoS ONE 8:e68915. https://doi.org/10.1371/journal.pone.0068915

Xu SH, Huang JZ, Xu ML et al (2015) ACK1 promotes gastric cancer epithelial-mesenchymal transition and metastasis through AKT-POU2F1-ECD signalling. J Pathol 236:175–185. https://doi.org/10.1002/path.4515

Ye X, Brabletz T, Kang Y et al (2017) Upholding a role for EMT in breast cancer metastasis. Nature 547:E1–E3. https://doi.org/10.1038/nature22816

Yeh YC, Lin HH, Tang MJ (2012) A tale of two collagen receptors, integrin beta1 and discoidin domain receptor 1, in epithelial cell differentiation American journal of physiology. Cell Physiol 303:C1207–1217. https://doi.org/10.1152/ajpcell.00253.2012

Yoshikawa M, Hishikawa K, Marumo T, Fujita T (2007) Inhibition of histone deacetylase activity suppresses epithelial-to-mesenchymal transition induced by TGF-beta1 in human renal epithelial cells. J Am Soc Nephrol 18(1):58–65

Zeisberg M, Neilson EG (2009) Biomarkers for epithelial-mesenchymal transitions. J Clin Investig 119:1429–1437. https://doi.org/10.1172/JCI36183

Zeitouni B, Tschuch C, Davis JM et al (2017) Abstract 1840: whole-exome somatic mutation analysis of mouse cancer models and implications for preclinical immunomodulatory drug development. Cancer Res 77(13 Suppl):Abstract nr 1840. doi: 10.1158/1538-7445.AM2017-1840

Zheng X, Carstens JL, Kim J et al (2015) Epithelial-to-mesenchymal transition is dispensable for metastasis but induces chemoresistance in pancreatic cancer. Nature 527:525–530. https://doi.org/10.1038/nature16064

III.

Désirée Gül*, Negusse Habtemichael, Dimo Dietrich, Jörn Dietrich, Dorothee Gößwein, Aya Khamis, Eric Deuss, Julian Künzel, Günter Schneider, Sebastian Strieth and Roland H. Stauber*

Identification of cytokeratin24 as a tumor suppressor for the management of head and neck cancer

https://doi.org/10.1515/hsz-2021-0287
Received June 9, 2021; accepted July 28, 2021;
published online August 27, 2021

Abstract: To improve management of head and neck squamous cell carcinoma patients, we need to increase our understanding of carcinogenesis, to identify biomarkers, and drug targets. This study aimed to identify novel biomarkers by providing transcriptomics profiles of matched primary tumors, lymph node metastasis, and non-malignant tissue of 20 HNSCC patients as well as by bioinformatic analyses of a *TCGA* HNSCC cohort, comprising 554 patients. We provide cancer cell signaling networks differentially expressed in tumors *versus* metastases, such as mesenchymal–epithelial transition, and structural integrity networks. As a proof of principle study, we exploited the data sets and performed functional analyses of a novel cytokeratin, cytokeratin24 (cKRT24), which had not been described as biomarker for tumors before. Survival analysis revealed that low cKRT24 expression correlated with poor overall survival in HNSCC. Experimentally, downregulation of cKRT24 in primary tumors, metastases, and HNSCC cell lines was verified on mRNA and protein level. Cloning and ectopic overexpression of cKRT24 not only affected viability and growth of HNSSC cell lines, but also inhibited tumor growth in murine xenograft studies. We conclude that cKRT24 functions as a tumor suppressor in HNSCC, and may serve as an additional prognostic biomarker and novel target to support current HNSCC treatments.

Keywords: biomarker; carcinogenesis; HNSCC; keratins; metastases; oral cancer.

***Corresponding authors: Désirée Gül and Roland H. Stauber**, Department of Otorhinolaryngology Head and Neck Surgery, Molecular and Cellular Oncology, University Medical Center, D-55131 Mainz, Germany, E-mail: guel@uni-mainz.de (D. Gül), rstauber@uni-mainz.de (R.H. Stauber). https://orcid.org/0000-0002-2446-5756 (R. H. Stauber)

Negusse Habtemichael, Dorothee Gößwein and Aya Khamis, Department of Otorhinolaryngology Head and Neck Surgery, Molecular and Cellular Oncology, University Medical Center, D-55131 Mainz, Germany

Dimo Dietrich, Jörn Dietrich and Sebastian Strieth, Department of Otorhinolaryngology, University Medical Center Bonn, D-53127 Bonn, Germany

Eric Deuss, Department of Otorhinolaryngology Head and Neck Surgery, Molecular and Cellular Oncology, University Medical Center, D-55131 Mainz, Germany; and Department of Otorhinolaryngology Head and Neck Surgery, University Hospital, D-45147 Essen, Germany

Julian Künzel and Günter Schneider, Ear, Nose and Throat Department, University Hospital, D-93053 Regensburg, Germany

Introduction

Head and neck cancer is a heterogeneous disease and accounts for the sixth-most common cancer incidents globally (Beltz et al. 2018, 2019; Bray et al. 2018; Ferlay et al. 2019; Sharma 2020). HNC is typically diagnosed at advanced stages with loco-regional and/or distant metastases resulting in a five-year survival rate of less than 50% (Bray et al. 2018; Deuss et al. 2020; Leemans et al. 2011; Torre et al. 2015). The prevailing form of HNC, head and neck squamous cell carcinoma (HNSCC), is one of the most aggressive and invasive cancer types and includes multiple sites of the upper aerodigestive tract like the nasal cavity, sinuses, lips, mouth, salivary glands, larynx and pharynx (Bray et al. 2018; Deuss et al. 2020; Leemans et al. 2011; Torre et al. 2015). Major risk factors associated with the development of HNSCC are tobacco use, alcohol consumption and high-risk human papilloma virus (HPV) infections (Benson et al. 2014; Marur and Forastiere 2008). If other viruses, as exemplified by the current COVID-19 pandemic, as well as the oropharyngeal microbiome also contribute to malignancy remains to be uncovered (Hoffmann et al. 2021; Siemer et al. 2018). Moreover, the increasing use of 'e-liquids' might need to be considered as an additional risk factor, although conclusive studies are missing so far (Deuss et al. 2020). Despite advances in knowledge and therapy, HNSCC and its treatment still often involve functional impairment and cosmetic deformity of vital functions of the aerodigestive tract (Denaro et al. 2014). Survival rates for HNSCC have not

improved significantly, mainly due to the late disease presentation of the patient, lack of suitable biomarkers and their mechanistic understanding, as well as corresponding drugs for (individually) targeted therapy approaches (Campbell et al. 2018; Cohen 2014; Denaro et al. 2014; Deuss et al. 2020; Rothenberg and Ellisen 2012; Stauber et al. 2012b), including potential nanomedicines (Siemer et al. 2020; Westmeier et al. 2020). Currently, the main prognostic parameters of HNSCC are the location and size of the tumor, the presence of distant metastasis and cervical lymph node metastases, which is not sufficient to evaluate the disease outcome (Ernst et al. 2018; Hamoir et al. 2014; Sessions et al. 2002). The *Union for International Cancer Control* (UICC) staging system mainly considers clinical factors such as tumor size, nodal status and distant metastasis for estimating prognosis, though only the HPV status was recently considered as a relevant biomarker in the new 8th edition of the UICC staging system (Beltz et al. 2018, 2019; Deuss et al. 2020; Laban et al. 2019; Tribius et al. 2019).

Even after more than a decade of different studies there is still need to identify molecular biomarkers with diagnostic relevance to categorize patients into prognostic groups who may benefit from different treatment modalities. Here, mRNA expression profiling technologies have allowed to exploit the whole transcriptome landscape to define new molecular cancer subtypes, undetected by the traditional histopathological parameters. These advancements have facilitated gene expression studies to identify disease-related pathways and clusters of patients (Campbell et al. 2018; van't Veer et al. 2002). Consistently, expression profiling has been used to distinguish between cancer subtypes and predict disease outcome in different types of cancer (Alizadeh et al. 2000; Bittner et al. 2000; Cancer Genome Atlas Network 2015; Huang et al. 2003). Previous studies aimed at the categorization of HNSCC tumors into distinct subtypes (Campbell et al. 2018; Chung et al. 2004), suggested a gene expression signature associated with recurrent disease (Ginos et al. 2004), or confirmed genes with diagnostic or prognostic potential (Campbell et al. 2018; Cancer Genome Atlas Network 2015; Cavalieri et al. 2020; Cromer et al. 2004; El-Naggar et al. 2002; Goesswein et al. 2018; Mendez et al. 2002; Schlingemann et al. 2005). Microarray analysis performed on normal oral epithelium ompared to HNSCC elucidated the roles of microenvironment remodeling and immune responses in survival of HNSCC (Campbell et al. 2018; Thurlow et al. 2010). Clearly, the combination of NGS with other approaches, including analysis by RNA/ExomeSeq, is most promising for the development of clinically relevant, molecular subgroups that may guide treatment (Campbell et al. 2018; Cancer Genome Atlas Network 2015; Sethi et al. 2015).

The focus on defining tumor-specific molecular abnormalities has revealed numerous in HNSCC, including an activation of the proto-oncogene Ras, Survivin, Myc, (epidermal) growth factor receptors and their ligands, proteases such as Taspase1, pro- and anti-apoptotic BCL-2 protein family members, Cyclin D1 and PI3K (Deuss et al. 2020; Engels et al. 2007; Ernst et al. 2018; Feldman et al. 2016; Gammon and Mackenzie 2016; Gribko et al. 2017; Lui et al. 2013; Michaelis et al. 2020; Schweitzer et al. 2008, 2010; Simpson et al. 2015; Stauber et al. 2012a,b; Wunsch et al. 2012), the inactivation of the tumor suppressors TP53 and p16, the expression of angiogenic factors, DNA ploidy, loss of heterozygosity (LOH) at various chromosomal locations, and many more (Bockhorst et al. 2020; Feldman et al. 2016; Gammon and Mackenzie 2016). Additional predictive biomarkers to manage treatment selections are however clearly needed (Cancer Genome Atlas Network 2015; Deuss et al. 2020; Marur and Forastiere 2016).

Notably, cytokeratins (cKRTs) have been identified already in the 80s as major intermediate filaments in squamous epithelium, which form a cytoplasmic network. Notably, cKRTs consist of at >25 unique gene products, are highly conserved during evolution and are critical for cell stabilization, shape, intracellular signaling and transport. Usually keratins are expressed as specific heterodimeric pairs consisting of the acidic type I (K9-K24 and Ha1-8) and the neutral-basic type II (K1-K8 and Hb1-6) polypeptides, both of which are essential for filament formation and function (Moll et al. 2008). As differential (specific) cKRT expression is considered a hallmark of tumor development and progression, many studies aimed to dissect the underlying mechanisms and their predictive value. The expression of cKRTs depends primarily on the epithelial cell type and its degree of differentiation. Hence, the cKRT expression status is useful for distinguishing carcinomas from other types of cancer. Apart from their use as diagnostic tools, the importance of cytokeratins as prognostic markers as well as their role in epithelial tumorigenesis and treatment responsiveness is not understood (Karantza 2011). Also, pan-cytokeratin antibodies are routinely used in diagnostic pathology of the head and neck (Thompson and Bruce 2016), and the immunohistochemical assessment of cKRT4 and cornulin expression in surgical margins of HNSCC patients has been shown to outperform histopathologic grading in predicting the risk for local relapse (Schaaij-Visser et al. 2009). Clearly, modulation of (specific) cKRTs expression levels is considered to interfere with a multitude of intracellular regulation pathways, including kinases, proteases, receptors and pro-/anti-apoptotic proteins, in the majority of cancer cells, including HNSCC (Fazilat-Panah et al. 2020; Majumder et al. 2020; Makarova

et al. 2013; Mehrad et al. 2018; Xu et al. 2018). Here, DNA methylation together with other mechanisms are key epigenetic mechanisms able to control transcriptional processes, including HNC (Bockhorst et al. 2020; Campbell et al. 2018). Also, as shown for many HNC relevant proteins, e.g., p53, inactivating mutations are often found in many cancer types, although limited information is available for cKRTs in general (Campbell et al. 2018; Cancer Genome Atlas Network 2015). cKRTs might play an important role in modulation and control of essential signal transduction events involved in tumor progression, such as Akt and PKCζ activities (Weng et al. 2012). Some studies indicated that overexpression of cKRT8 and 18 was associated with dysplasia grades of tumor precursor lesions and an unfavorable prognosis for patients with HNSCC. In contrast, it was reported that loss of cKRT8 and 18 led to alterations in α6β4-integrin mediated signaling and decreased neoplastic progression (Frohwitter et al. 2016; Kitamura et al. 2017). Collectively, the field agrees that the effects of cKRTs in health and disease are highly complex but far from being understood, together with many partially conflicting data. Based on the obtained expression profiles and their bioinformatic exploitation, we here investigated the expression and tumor relevance of a novel cKRT, cKRT24, which had not been implicated in carcinogenesis before. By comprehensive *in silico* to *in vitro* and *in vivo* studies, we show for the first time that cKRT24 is downregulated in primary tumors and metastases, correlating with poor overall survival of HNSCC patients, exclude methylation or mutations as underlying mechanisms, demonstrate that cKRT24 functions as a tumor suppressor, and thus, conclude to exploit cKRT24 as an additional biomarker/target for HNSCC and potentially other malignancies.

Results

Transcriptomics to identify genes differentially expressed in non-malignant tissue, primary HNSCCs, and corresponding lymph node metastases

HNSCCs show significant heterogeneity in their pathobiological and clinical behavior that currently cannot be reliably predicted using the current array of clinical markers. Hence, the identification of new biomarkers for disease progression and survival predictions would be highly valuable. To identify genes differentially expressed in HNSCC primary tumors (PT) *versus* lymph node metastasis (M) and the corresponding non-malignant tissue (N), tissues were obtained from 20 patients undergoing surgical resection. In contrast to other studies, in which genetic and epigenetic variations present in individual patients require the analysis of a large number of patients to increase the relevance of the obtained data sets, our study design focused on a patient cohort from which N, PT as well as M could be surgically recovered from the same patient. Details on patient demographics are presented in Table 1, and described in "Materials and methods" section.

Although current bioinformatic algorithms seem to facilitate the comparison and (meta) analysis of gene expression data generated by different profiling platforms (Chung et al. 2004; De Cecco et al. 2015), it is fully accepted that optimal results will be obtained by using the same platform, ideally in a single experiment to reduce intrinsic technical variation, which mainly generate 'data noise', potentially occluding data reliability (Irizarry et al. 2003). Consequently, RNA was isolated from forty-five snap-frozen biopsies and all samples were assayed using the *Affymetrix U133A 2.0* gene array, representing 14,500 well-characterized human genes to explore oncogenic disease processes.

Unsupervised data analysis revealed classifiers for HNSCC disease progression

The presence or absence of lymph node metastases is currently one of the most important predictors of disease outcome in HNSCC patients (Kunzel et al. 2014; Marur and Forastiere 2016). However, it is accepted that metastasis is highly complex, influenced by biological, temporal, and anatomical features. In particular, there is evidence that the different subsites of HNSCC origins can contribute to clinical differences (Campbell et al. 2018; Marur and Forastiere 2016). Hence, to analyze the molecular heterogeneity of HNSCC disease progression, the obtained expression data were subjected to unsupervised average-linkage hierarchical clustering using the *GeneSpring* software. Our cluster analysis identified several groups/subtypes within the unfiltered cluster dendrogram. Notably, two-way hierarchical clustering analysis also separated PT from lymph node metastases employing 393 genes (Figure 1A), using the probe sets from the raw data and employing stringent criteria (fold change ≥2.0 and p-value < 0.05). Though, some samples could not be completely separated (PT13 *vs.* M13, PT11 *vs.* M11). This result is not unusual, as M originate from PT and are thus more similar when compared to non-malignant tissue. Still, PT cells need to undergo significant phenotypic and microenvironmental alterations, such as the expansion of immunosuppressive cells, lymphangiogenesis and the upregulation of chemokines and cytokines,

Table 1: Clinical and pathological characteristics of the study group.

#	N/PT/M	Primary site	Age	Sex	T/A	pT	pN	Grading
1	N1/PT1/M1	Hypopharynx	47	F	+/+	2	2	2
2	N2/PT2/M2	Oropharynx	58	F	+/+	3	2	2
3	N3/PT3/M3	Hypopharynx	46	M	+/+	4	1	2
4	N4/PT4/M4	Larynx	68	M	+/+	4	2	2
5	N5/PT5/M5	Oropharynx	56	M	+/+	3	2	2
6	N6/PT6/M6	Hypopharynx	48	M	+/+	3	1	2
7	N7/PT7/M7	Larynx	56	M	+/+	4	3	3
8	N8/PT8/M8	Hypopharynx	58	M	+/+	3	2a	2
9	N9/PT9/M9	Hypopharynx	72	M	+/+	3	2	2
10	N10/PT10/M10	Oropharynx	49	M	+/+	3	1	2
11	N11/PT11/M11	Hypopharynx	57	M	+/+	1	2	3
12	N12/PT12/M12	Oropharynx	53	M	+/+	2	2b	2
13	N13/PT13/M13	Hypopharynx	57	M	+/+	2	3	2
14	N14/PT14/M14	Hypopharynx	47	M	+/+	2	2	2
15	N15/PT15/M15	Hypopharynx	56	M	+/+	2	3	2
16[a]	*PT16*	*Larynx*	*49*	*M*	+/+	*3*	*1*	*2*
17[a]	*N17/PT17*	*Hypopharynx*	*75*	*F*	+/+	*1*	*2*	*1*
18[a]	*PT18*	*Oropharynx*	*53*	*M*	+/+	*2*	*2*	*2*
19[a]	*PT19/M19*	*Hypopharynx*	*63*	*M*	+/+	*2*	*3*	*2*
20[a]	*PT20*	*Oropharynx*	*57*	*M*	+/+	*1*	*2*	*2*

[a](*italic*): excluded from the study due to low RNA quality. T/A: tobacco/alcohol use.

in order to successfully establish lymph node metastases (Leong et al. 2007). As expected, non-malignant tissue and carcinomas grouped separately on a clustering dendrogram employing the complete datasets (data not shown). Thus, HNSCC tumor tissue can be distinguished from corresponding non-malignant tissue and from lymph node metastases using even unsupervised RNA expression signatures. Hence, HNSCC carcinogenesis involves a variety of directly and indirectly deregulated signaling pathways.

Validation of array-based gene expression data

Prerequisite for the data quality obtained by all systematic analytical 'omics' technologies is the reliability of the generated data. Hence, it is of utmost importance to verify differentially expressed genes by independent experimental methods. Consequently, we verified the differential expression of selected genes by RT- or qPCR. For each PT *versus* N and M *versus* PT, 5–6 differentially expressed genes were randomly chosen and validated. As shown in Figure 1B–D, the following genes were analyzed: A. PT *versus* N: *FN1, OSF2, cKRT24, CLCA4, PPR4*; B: PT *versus* M: *SCCA2b, TP73L, C4.4A, FAIM3, ARHGAP25, RASCRP2* in HNSCC compared to metastasis could be validated (Figure 1B and C; and data not shown). Furthermore, the expression of *PRR4* (Figure 1D), *cKRT24* (Figure 3), *FN1* (Figure S2) and *OLR1* (Figure S3) was measured for every patient by qPCR. Collectively, the results obtained by both methods are in excellent accordance, revealing similar expression ratios. These controls underline the quality and reliability of the obtained array data, and their use for bioinformatic exploitation, model building, and most importantly, for subsequent in depth functional and clinical analysis.

Bioinformatic identification of HNSCC disease pathways

In addition to the hierarchical clustering, which is primarily a qualitative tool, we employed the unpaired Student's *t*-test to determine those genes associated with malignancy and invasiveness in statistical fashion. We compared the gene expression profiles of the primary squamous carcinoma samples with those of the matched normal epithelial tissue, the primary carcinoma with those of their corresponding lymph node metastasis and normal tissue mucosae with lymph node metastasis. We identified 650 genes that were significantly differentially expressed between laryngo-oropharyngeal tumors and normal tissue mucosa with 236 genes being upregulated 414 genes being downregulated, 393 genes significantly differentially expressed between primary laryngo-oropharyngeal tumor and their corresponding lymph

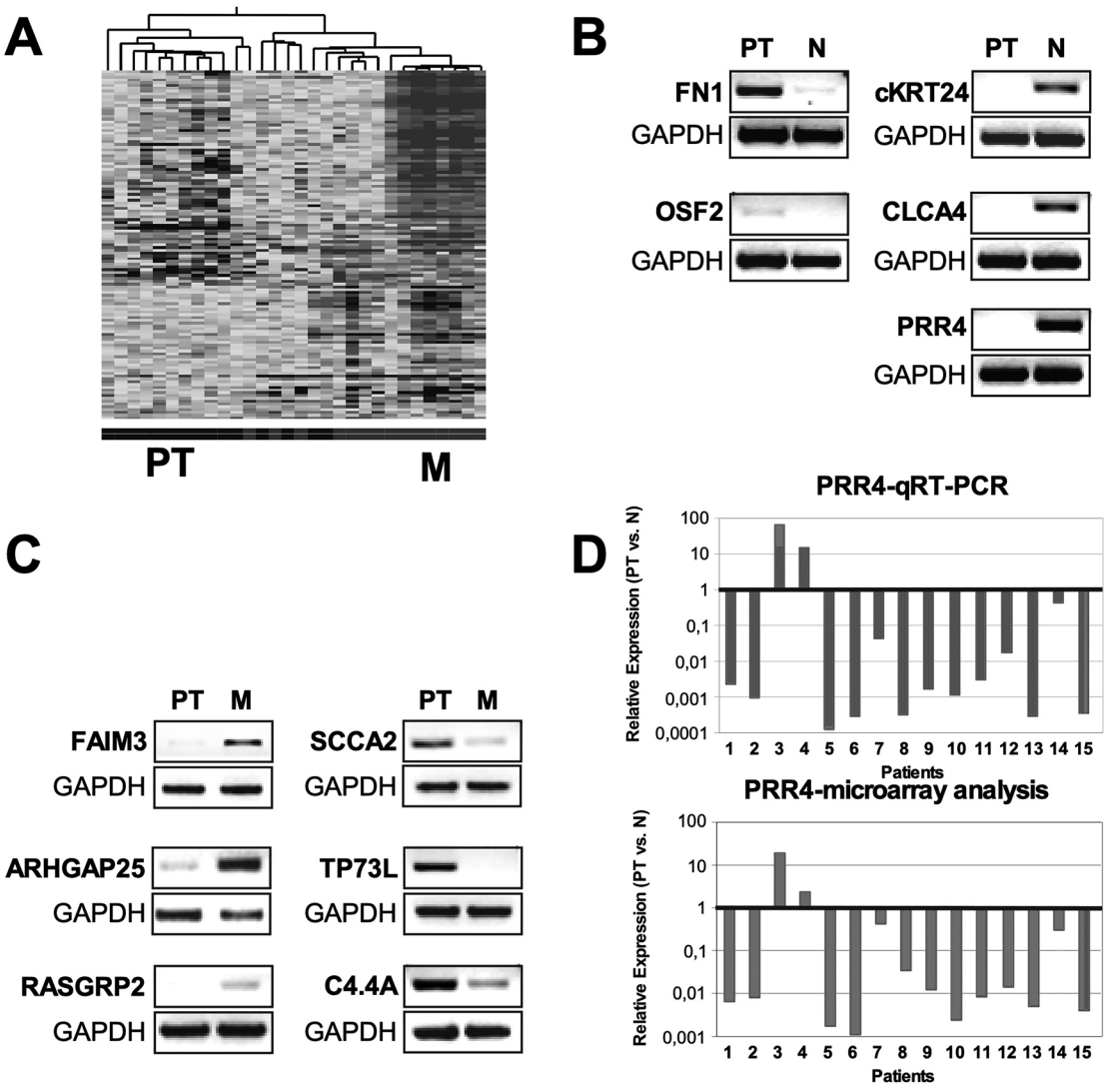

Figure 1: Microarray analyses and validation of expressional data in HNSCC patient cohort.
(A) Bioinformatic cluster analysis of 45 HNSCC expression signatures allows profiling according to disease. Unsupervised two-way hierarchical clustering and gene tree representation of differentially regulated genes (fold change ≥ 2.0 and p-value < 0.05) allow to separate PT and lymph node M (393 deregulated genes). (B–D) Validation of gene expression data obtained by microarray analyses for the indicated genes using either RT-PCR (B, C) or quantitative qRT-PCR (D). For representative genes, differential mRNA levels were analyzed by RT- or qRT-PCR to confirm our microarray data. (A) RT-PCR amplification products of genes that are up- (left) or down- (right) regulated in PT compared to N in our microarray analysis. (B) RT-PCR amplification products of genes that are up (left) or down (right) regulated in M compared to PT in our microarray analysis. (C) Comparison of relative expression levels as obtained by microarray analysis or qRT-PCR for *PRR4*.

node metastasis with 345 being upregulated 48 being down regulated and 1579 genes differentially expressed between normal tissue mucosae with lymph node metastasis 760 genes being upregulated 819 genes being downregulated (significant expression differences determined by applying the filter: $\log_2$(fold-change) ≥2.0; p-value ≤ (0.05). Among the differentially expressed genes in PT and their corresponding M, 29 genes were in common, representing an overlap of 2.8% between the groups. Comparison of differentially expressed genes between PT and N *versus* M and N revealed that 352 genes were expressed in common, representing an overlap of 15% between the entities (visualized by Volcano plot in Figure S1). Tables S2–S5 list the most significant genes that were upregulated or downregulated, ranked by their p-values, respectively along with their *entrez gene* accession number, fold change and p-value.

Next, the 650 genes differentially expressed in PT *versus* N, the 393 genes deregulated in M *versus* PT, and the 1579 genes identified in M *versus* N were analyzed according to their molecular function, pathways, and biological process by using the Onto-Express software (Figures 2, S4

and S5) (Gene Ontology 2015). Molecular functions represent the elemental activities (binding or catalysis) of a gene product at the molecular level, whereas biological processes involve several gene products, operations or sets of molecular events that are essential for the function of cells or tissues (Ashburner et al. 2000).

First, we used the Onto-Pathway analysis tool (Gene Ontology 2015) to identify major signaling pathways that are associated with HNSCC pathogenesis. Figure 2 illustrates the top 10 most significant pathways (p-value < 0.05). The main molecular functions predicted for the identified genes are depicted in Figure S4, and main processes are shown in Figure S5.

Collectively, the most prominent categories detected in primary tumors include ion and molecular binding proteins. Here, the category extracellular matrix (ECM) included mainly upregulated genes, whereas downregulated genes were categorized as enzymes and transporter/channel activity (Figure S5A). In metastasis, enzymes and transcription factors are dominant categories, as well as protein binding and receptor activity for upregulated genes, structural molecular activity and binding proteins for downregulated genes (Figure S5CD). Highly upregulated matrix metalloproteases, integrins, fibronectin, proteoglycans laminin as well as other ECM proteins supports previous studies showing that degradation of the basement membrane and remodelling of the extracellular matrix are essential during the invasion process of a tumour (Goetz et al. 2011; Magan et al. 2020; Paz et al. 2014; Tzanakakis et al. 2018, 2019, 2020; Wahbi et al. 2020). It is accepted that he destruction and remodelling of the extracellular matrix not only drives the mechanical and proteolytic invasion of tumour cells, but also favours metastatic cell reprogramming, behaviour, epithelial to mesenchyme transition, and response to therapy (Goetz et al. 2011; Tzanakakis et al. 2018, 2019, 2020). Specialized Cancer Associated Fibroblasts (CAFs) can degrade various ECM proteins like collagens, basement membrane laminin and fibronectin (Goetz et al. 2011; Magan et al. 2020; Tzanakakis et al. 2018, 2019, 2020; Wahbi et al. 2020) leading to a more aggressive behaviour of the cancer, lymph node metastasis and poor prognosis, as also shown for oral cancers (Lim et al. 2011; Marsh et al. 2011).

Cytokeratin24 (cKRT24) is significantly downregulated in primary and metastatic HNSCC

Clearly, there has been a continuous development in bioinformatics approaches for data analysis and prediction of (novel) disease pathways (De Cecco et al. 2015). Thus, high quality data generated in our study and other (Chung et al. 2004; Cromer et al. 2004; Liu et al. 2008; Nagata et al. 2003), are highly valuable repositories for model and hypothesis building as well as to examine the disease relevance of known genes and pathways for (specific) tumor entities and disease processes. Importantly, such data sets are invaluable resources for the identification of novel proteins and pathways, which have not been considered to potentially contribute to (HNSCC)

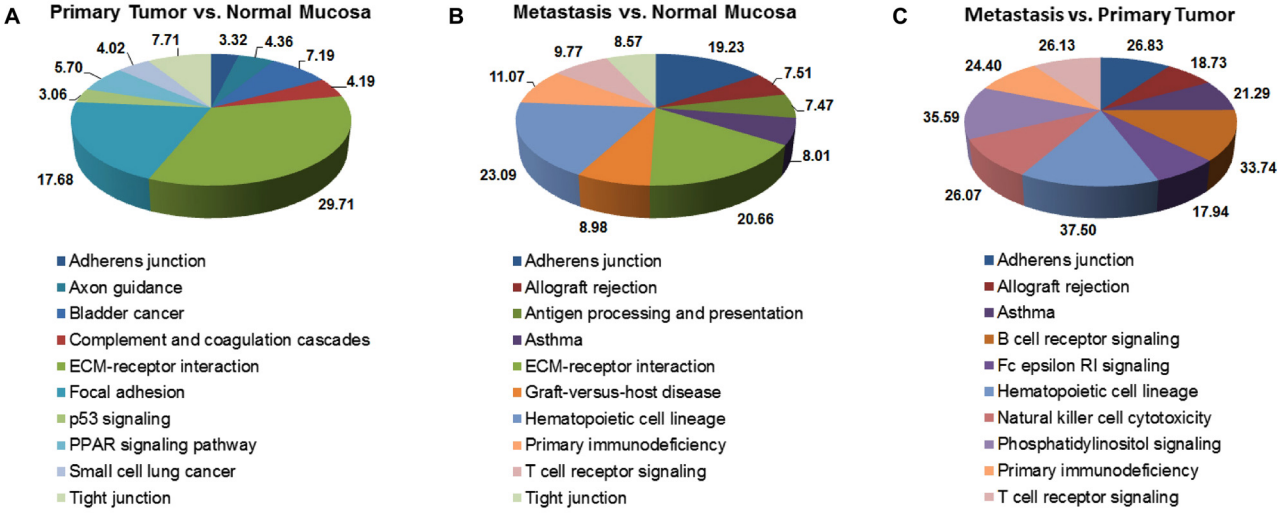

Figure 2: Gene-ontology (GO) pathway data analysis.
Overview of the 10 most prominent signaling categories according to their Onto-Pathway analysis classification in the GO database, ranked by their $-\log_2(p\text{-values})$ for significance. (A) Top 10 signaling pathways of genes deregulated in PT *versus* N. (B) Top 10 signaling pathways of genes deregulated in M *versus* N. (C) Top 10 signaling pathways of genes deregulated in M *versus* PT.

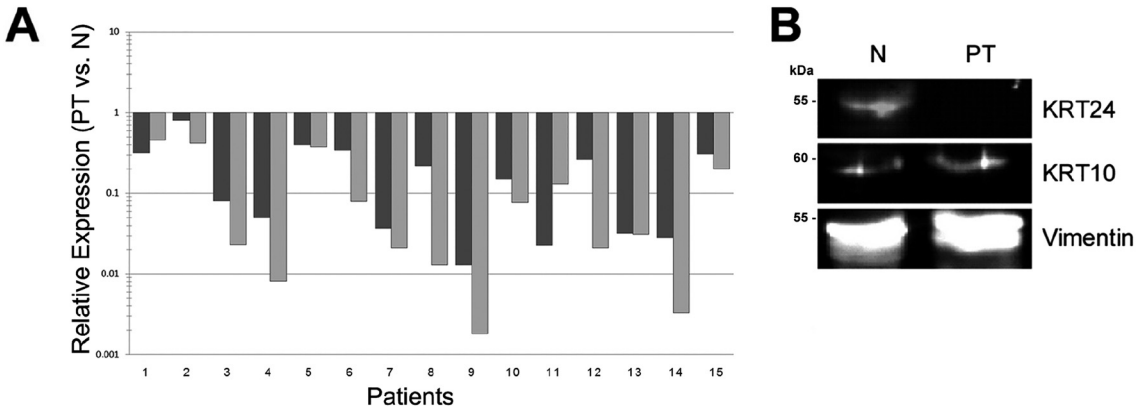

Figure 3: cKRT24 expression is downregulated in HNSCC tumors.
(A) Microarray (dark grey bars) and qRT-PCR (light grey bars) analysis demonstrate significantly reduced *cKRT24* mRNA levels in primary tumors (PT) compared to non-malignant tissue (N) in all patients. (B) Immunoblot analysis confirms reduced cKRT24 protein level in PT compared to N. Vimentin and cKRT10 served as loading controls and remained unchanged. Expression of indicated proteins was detected using verified specific Abs. Molecular weight (kDa) is indicated.

tumorigenesis. However, the 'gold standard' for validation and assessment of the pathobiological and clinical relevance of genes for tumorigenesis and disease progression still remains their in-depth experimental molecular functional and clinical validation. Our GO data indicated an impact of tumor cell differentiation and structural integrity, such as extracellular matrix or focal adhesion together with PI3K-AKT signaling on metastasis, molecular events known to be influenced by cytokeratin networks (Kitamura et al. 2017; Mehrad et al. 2018; Mehrpouya et al. 2019; Weng et al. 2012; Xu et al. 2018; Yang et al. 2008). As numerous cKRTs have been studied before, we selected cKRT24 as a yet unexplored candidate for a subsequent comprehensive functional analysis. Cytokeratins are not only 'simple' structurally relevant components for (epithelial) cell differentiation and maintenance, but also play not fully understood functional roles in the initiation, modulation, and control of essential (tumor) cell processes, including circulating tumor cells (CTCs) (Gribko et al. 2019; Karantza 2011; Kunzel et al. 2019; McGinn et al. 2020; Morales et al. 2018; Siemer et al. 2020; Sprecher et al. 2002). However, in contrast to several other members of the keratin network, such as cKRT 10, 17 or 19 (Kitamura et al. 2017; Mehrad et al. 2018; Mehrpouya et al. 2019; Xu et al. 2018; Yang et al. 2008), neither the expression nor impact of the type I cKRT24 for any type of malignancies, including HNSCC, has been studied before.

To the best of our knowledge, we here demonstrate for the first time that cKRT24 functions as a tumor suppressor in HNSCC. This conclusion is supported by several lines of independent experimental evidence. For one, our transcriptomics data revealed a significant down regulation of cKRT24 in PT or M *versus* the corresponding non-malignant tissue for all patients. Downregulation could be verified independently by qPCR (Figure 3A) and RT-PCR analysis (Figure 1B), also for PT from patients who were not involved in our study (Figure S6). Likewise, RT-PCR analysis demonstrated low or undetectable cKRT24 expression levels in various model HNSCC cell lines widely used in the field, such as FaDu or UM-SCCs (Table S1).

Second, to examine cKRT24 protein expression, ultimately required to evaluate the impact of a specific gene on tumorigenesis and its relevance as a potential biomarker, we next generated peptide-based polyclonal α-cKRT24 antibodies. Antibody-specificity was controlled by using recombinant cKRT24 for immunoblot analysis (data not shown). As shown in Figure 3B, reduced expression of cKRT24 in primary HNSCC compared to non-malignant tissue from the same patient could be verified by immunoblot. Moreover, a significant downregulation of cKRT24 in PT was detectable by immunohistochemistry also in patients, who were not involved in our study. As shown in Figure 4, a significant number of PT tissues had lower cKRT24 levels than non-malignant tissues. Of note, commercially available α-cKRT24 Abs failed to reliably detect cKRT24 expression by immunohistochemistry and thus, were excluded from our study (Figure S7).

To mechanistically understand cKRT24 downregulation, we examined *cKRT24* gene methylation as no studies have been reported for *cKRT24*. As shown by us and others, DNA methylation together with other mechanisms are key epigenetic mechanisms to control transcriptional processes in many cancers, including HNC (Bockhorst et al. 2020; Campbell et al. 2018).

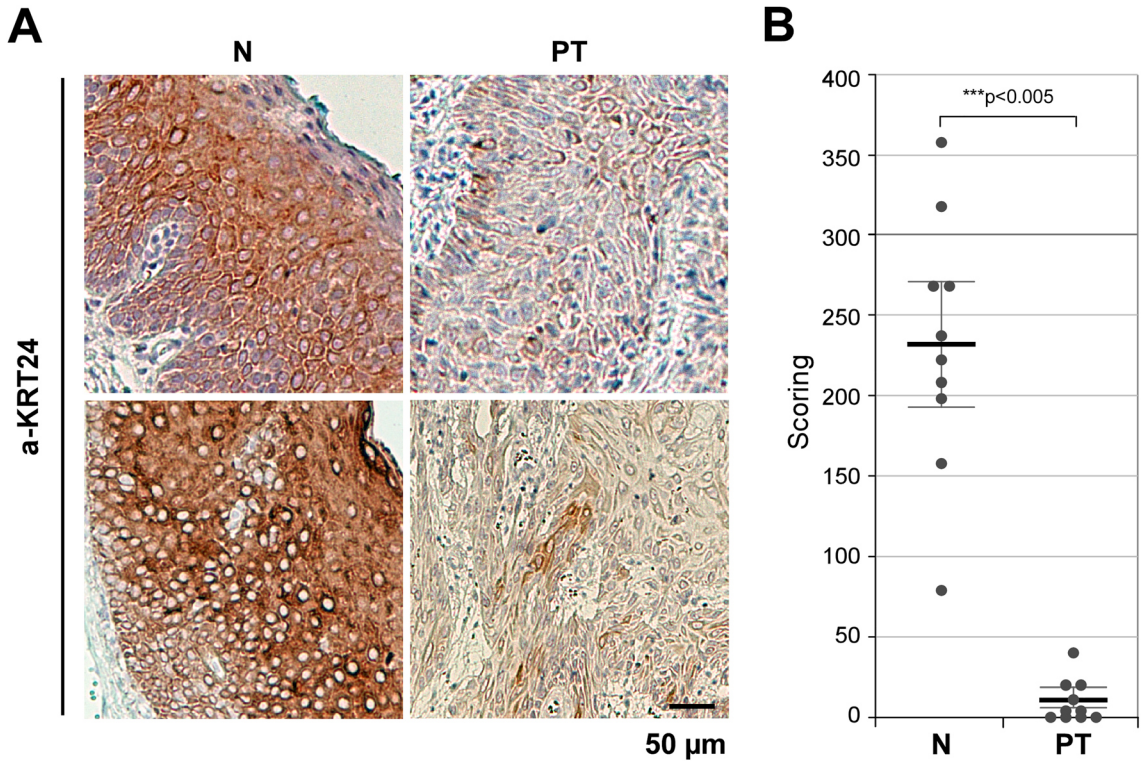

Figure 4: Representative immunohistochemistry images of cKRT24 staining in non-tumor (N) and tumor (PT) tissue samples. (A) Samples were analyzed in a single experiment and images recorded with identical camera settings. Scale bars represent 50 µM. (B) Semi-quantification of cKRT24 protein expression in ten non-tumor *versus* tumor tissue samples. Samples were not part of the transcriptomics study group. cKRT24 levels were significantly lower in tumor compared to non-malignant tissues. *$p < 0.005$. Scoring: Positive cells (%) and staining intensity (scale 0–4) were multiplied.

Transcriptional impact of DNA methylation depends on the CpG site location within the gene. CpG methylations in promoter regions are usually linked to gene silencing, while in gene bodies, it is rather associated with increased transcriptional activity (Bockhorst et al. 2020; Campbell et al. 2018). Notably, DNA methylation of certain genes can be a valid prognostic biomarker in different cancers (Bockhorst et al. 2020; Campbell et al. 2018). To provide a full picture of the *cKRT24* methylation landscape in HNSCC, we analyzed methylation levels at single CpG resolution (cg12564187: CpG 1, cg27316026: CpG 2, cg24340657: CpG 3, cg04219544: CpG 4, cg23737768: CpG 5, cg06899912: CpG 6) in the cohort of HNSCC patients consisting of 528 tumors and 50 normal adjacent tissue, provided by The Cancer Genome Atlas (TCGA) (Campbell et al. 2018; Cancer Genome Atlas Network 2015) (Figure 5). Our study revealed that in the *cKRT24* gene body (CpG 1) and upstream (CpG 6) high methylation levels (mean > 80%) prevail while CpG sites 2–5 located within the transcription start site exhibit lower methylation levels (mean < 50%). Interestingly, when we compared methylation levels in NAT *versus* HNSCC tissue, tumor tissues showed significantly lower methylation levels compared to normal adjacent tissues (Figure 5B). Hence, it is unlikely that gene methylation is significantly responsible for reduced cKRT24 levels. Notably, when analyzing the expression levels of cKRT24 in the *TCGA* HNSCC patient cohort we could independently confirm our results that downregulation of cKRT24 mRNA levels occurred in tumors compared to normal tissue (Figure 5C). Moreover, survival analysis further revealed that low cKRT24 expression correlated with poor overall survival in these patients, further supporting cKRT24's tumor suppressor relevance in the clinical background (Figure 5D).

As shown for many HNC relevant proteins, inactivating mutations are often found in tumor cells, though not reported for *cKRT24* (Campbell et al. 2018; Cancer Genome Atlas Network 2015). Thus, we further investigated the mutation frequency and type in *cKRT24* by exploiting the *BioMutav3.0* database as well as data provided by the TCGA Research Network (Campbell et al. 2018). As illustrated in Supplementary Figure S9, also the analysis of 501 HNSCs from the TCGA cohort only showed six cKRT24 missense mutations in five patients at different positions

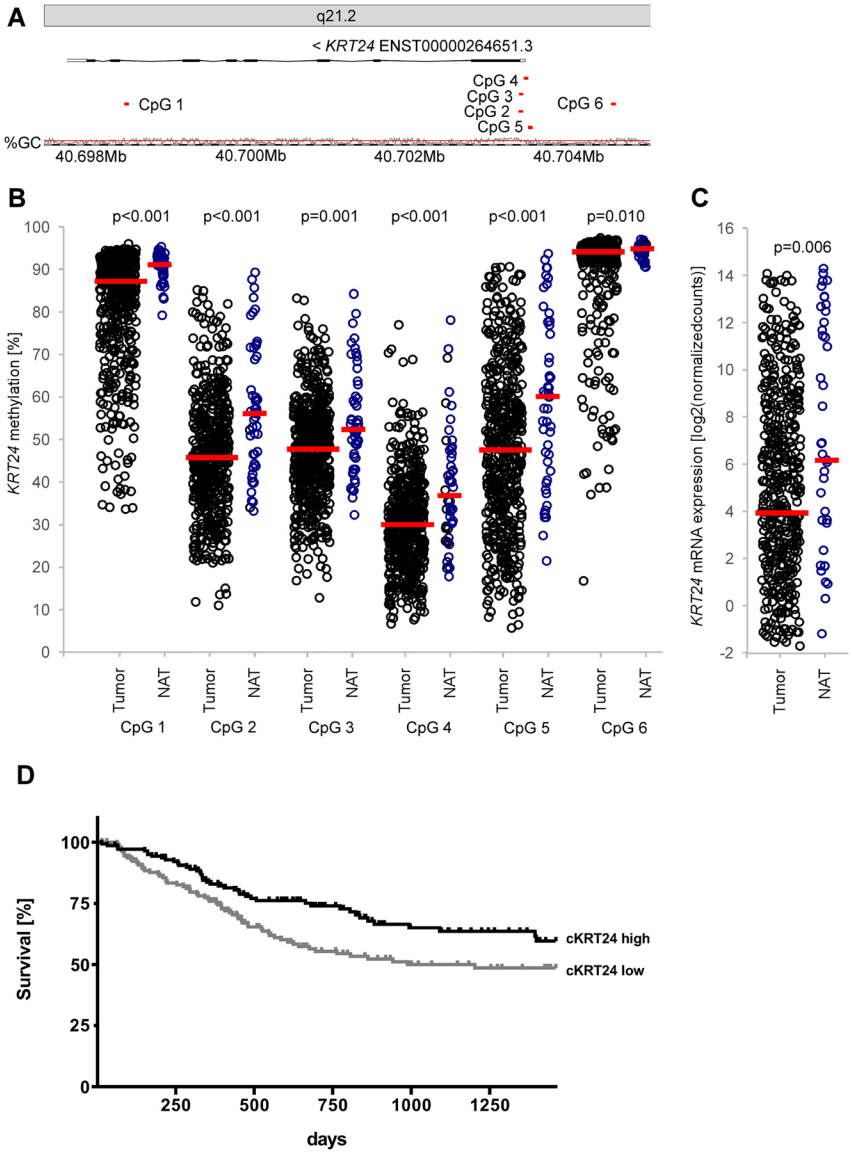

Figure 5: cKRT24 DNA methylation in HNSCC tumors and normal adjacent tissues (NATs).
(A) Illustration of the cKRT24 gene locus, mRNA transcript ENST00000264651.3, GC density, and six analyzed CpG positions (Infinium HumanMethylation450 BeadChip bead cg12564187: CpG 1, cg27316026: CpG 2, cg24340657: CpG 3, cg04219544: CpG 4, cg23737768: CpG 5, cg06899912: CpG 6) are depicted. The modified illustration was exported from www.ensemble.org (release 102, based on Genome Reference Consortium Human Build 38 patch release 13 (GRCh38.p13)). (B) cKRT24 DNA methylation (β values) of six CpG sites in $n = 528$ HNSCC tumors and $n = 50$ NATs from the TCGA cohort. cKRT24 gene body (CpG 1) and upstream (CpG 6) regions show high methylation levels (mean > 80%) while CpG sites 2–5 located within the transcription start site exhibit lower methylation levels (mean < 50%). Tumor tissues showed significantly lower methylation levels compared to normal adjacent tissues (NAT). Red bars represent mean values. *p*-Values refer to Mann–Whitney *U* tests. (C) cKRT24 mRNA expression is significantly ($p = 0.006$) downregulated in HNSCC compared to NAT (cohort described in B). Red bars represent mean values. *p*-Values refer to Mann–Whitney *U* tests. (D) Kaplan Meier plot indicates that low cKRT24 expression levels correlate with reduced survival of HNSCC patients ($n = 282$). $p = 0.016$.

(Campbell et al. 2018). Hence, in contrast to proteins such as p53 (213 mutations in 352 patients of the TCGA HNSC cohort), inactivating mutations in *cKRT24* occur in <1% of analyzed patients and are thus, unlikely to confer loss-of-function of the protein.

cKRT24 overexpression inhibits proliferation of HNSCC tumor cells

Despite the importance of bioinformatic exploitation of 'omics' based data, the cancer relevance of identified

gene-networks needs to be examined and verified by a tiered experimental pipeline. This central aspect is often neglected in most comprehensive 'big data' studies. Consequently, to further investigate and confirm the functional relevance of cKRT24 for tumorigenesis, we were the first to clone the predicted open-reading frame (ORF) from a non-malignant oral mucosa following reverse transcription and amplification of the cDNA. Sequence analysis confirmed that the obtained ORF encodes a polypeptide of 525 amino acids (Figure S9), identical to the predicted sequence (gene bank entry – Gene ID: 192666). Also, when we cloned *cKRT24* from three different PT, we did retrieve an identical sequence (data not shown). As shown in Figure 6A, live-cell microscopy revealed typical mesh-like structures of a cKRT24-GFP fusion also known for other cytokeratins upon ectopic expression in different HNSCC tumor cells lines. Also, ectopically expressed untagged cKRT24 was detectable by immunofluorescence using our polyclonal antibodies (Figure 6B), again underlining the reliability of our reagents. Moreover, a similar localization could be observed for endogenous cKRT24 by immunofluorescence using our polyclonal α-cKRT24 Abs. Here, expression was clearly detectable in the cytoplasm but not the nucleus of epithelial cells isolated from non-malignant oral mucosa (Figure 6B, N), whereas only low amounts of cKRT24 were present in primary larynx (Figure 6B, PT) or hypopharynx tumor cells (data not shown).

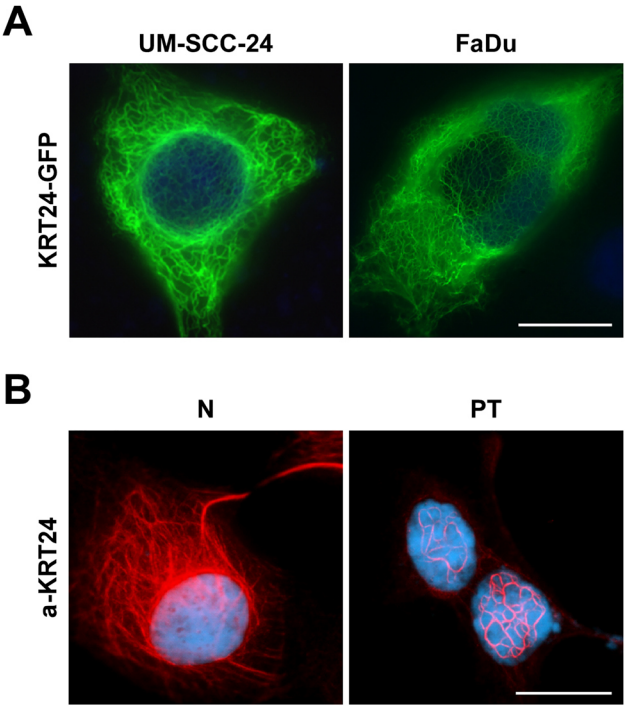

Figure 6: Expression of cKRT24 in head and neck cells.
Live-cell microscopy demonstrates typical cytoplasmic structures of ectopically expressed (A, cKRT24-GFP) or endogenous cKRT24 (B). cKRT24-GFP localization in HNSCC transfectants was visualized by confocal microscopy in living cancer cells. (A) The typical mesh-like structures of cytokeratins are detected in living cells transfected with a cKRT24-GFP fusion protein. Similar localization could be observed for endogenous cKRT24 by immunofluorescence using polyclonal α-cKRT24 antibodies, whereas a strong expression was detectable in primary non-malignant oral mucosa epithelial cells (B, N) primary larynx tumor cells (B, PT) express only low amounts. Signals were recorded with identical CCD camera settings. Scale bars 10 µM.

As transfection efficiencies are often low and vary for HNSCC cell lines, we cloned cKRT24 in a retroviral vector, allowing the simultaneous expression of cKRT24 and GFP from the same mRNA due to the presence of an IRES element. Subsequently, cell lines were transduced, sorted for GFP expression (Figure S8), and proliferation analyzed. Compared to the GFP vector control, MTT assays revealed that cKRT24 overexpression indeed significantly reduced proliferation for all cancer cell lines examined, although to varying degrees (Figure 7), which may (co)depend on their anatomical origin (Table S1).

Hence, HNSCC tumor cell lines of different anatomical origin need to reduce cKRT24 expression levels during the multi-step process of tumorigenesis in order to fulfill the requirements for rapid proliferation and metastasis.

Fourth, employing a xenograft model, we investigated if the tumor-suppressor phenotype observed for cKRT24 *in vitro* is also relevant under the more complex *in vivo* conditions. Here, FaDu cells were freshly transduced with cKRT24-IRES-GFP or the IRES-GFP control, sorted for GFP expression, and subsequently injected into the flanks of nude mice as described (Stauber et al. 2012b). As shown in Figure 8A, growth of cKRT24 overexpressing tumors was significantly reduced compared to the vector control. To verify that cKRT24 expression was not down regulated in the tumor cells *in situ*, *trans* gene expression was confirmed in the resected tumors by RT-PCR (Figure 8B) and immunoblot analysis (Figure 8C).

Collectively, these results strongly suggest that cKRT24 overexpression counteracts the proliferation and potentially metastatic activity of HNSCC tumor cells, providing a rationale why reduced expression of cKRT24 was observed in cancer cells in all patients studied here as well as in widely-used tumor cell models.

Discussion

In this study we analyzed the gene expression profiles of HNSCC tumors *versus* their corresponding normal tissue

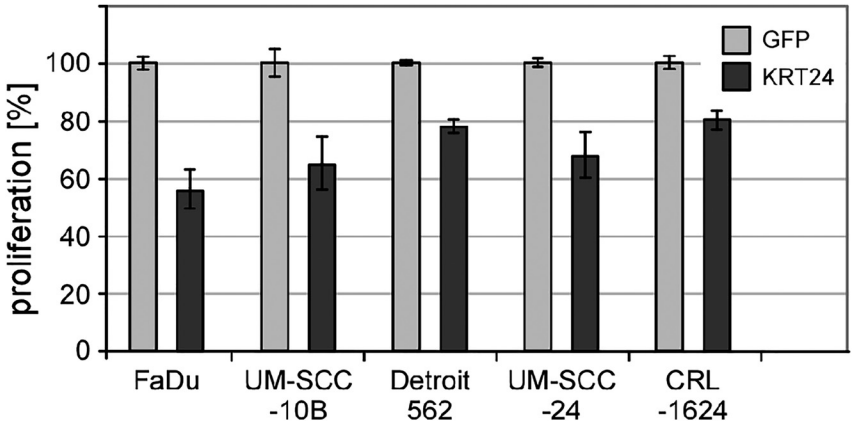

Figure 7: Overexpression of cKRT24 inhibits proliferation in head and neck cancer cell lines.
Indicated HNSCC cell lines were transduced and sorted for GFP expression. Cells were controlled for cKRT24 expression by live cell fluorescence microscopy (upper panel), seeded and proliferation analyzed 48 h later by the MTT assay (lower panel). Compared to the GFP control, cKRT24 overexpression significantly reduced proliferation for all cell lines examined. Proliferation of GFP only expressing controls was set 100%. *$p < 0.01$.

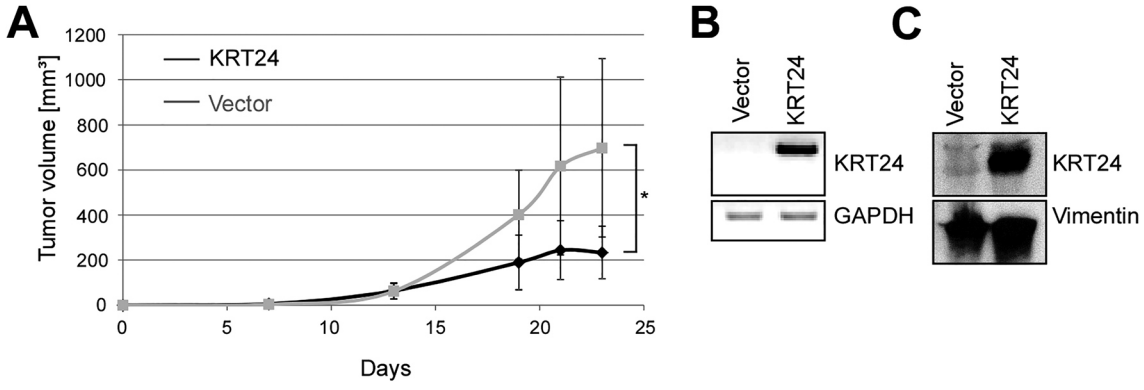

Figure 8: Overexpression of cKRT24 suppresses tumor growth *in vivo*.
(A) Nude mice were inoculated with FaDu tumor cells, either expressing cKRT 24-IRES-GFP or IRES-GFP only. Tumor growth was monitored and mice sacrificed after 23 days. Growth of cKRT24 xenograft tumors was significantly impaired compared to the vector control (p-value < 0.05). One data point represents the mean value from five mice. (B) cKRT24 *trans*gene expression was validated in biopsies from xenograft tumors by RT-PCR. GAPDH served as control. (C) Immunoblot analysis to demonstrate cKRT24 protein expression in xenograft-tumors. Vimentin was used as loading control. Expression of cKRT24 or Vimentin was detected using α-cKRT24 or α-Vimentin antibodies, respectively.

mucosa and lymph node metastasis. Changes in stromal, immune or inflammatory and other components may play an important role in the tumor progression and could potentially be exploited for diagnostic, prognostic or therapeutic purposes. Recently, several profile signatures have been reported to have promising prognostic potential in HNSCC (Eschrich et al. 2009; Hasan et al. 2020; Lohavanichbutr et al. 2013; Wu et al. 2017; Zivicova et al. 2018). Nevertheless, previous microarray-based studies of HNSCC have focused on primary tumor *versus* normal tissue mucosa or primary tumor patterns of expression (Al Moustafa et al. 2002; Alevizos et al. 2001; Cromer et al. 2004; El-Naggar et al. 2002; Kuriakose et al. 2004; Leethanakul et al. 2000; Mendez et al. 2002), while we have included the expression profile of the specific lymph node metastases derived from the primary HNSCC tumors. This delivered us a global insight of the genes differentially expressed between the primary HNSCC and corresponding lymph node metastasis. Our results based on hierarchical clustering analysis show that HNSCC can clearly be distinguished from their corresponding normal tissue mucosa and lymph node metastases. The onset and offset of genes involved in the metastatic progression can be valuable to assess metastatic propensities of developing cancers. Thus, it is important to show genes differentially expressed between normal tissue mucosa *versus* primary HNSCC and *versus* its paired lymph node metastasis from the same patient. Many of the downregulated genes in lymph node metastasis in our microarray data are closely associated with tumo rigenesis and the rest are genes with miscellaneous functions and roles in the human genome. All these genes are potential biomarkers with a prognostic and/or diagnostic

value. For example, micrometastases or occult metastases could be assessed by using these genes. Primary tumors with the property of overexpressing these genes could have already metastasized, since the metastatic behavior of a tumor is based on overexpression of metastasis promoting factors and loss of suppressing factors. Expression profile studies including lymph node metastasis were limited to the comparison of genes differentially expressed in metastatic and non-metastatic primary tumors (Chung et al. 2004; Cromer et al. 2004; Ernst et al. 2018; Liu et al. 2008; Nagata et al. 2003) or non-metastatic, metastatic and lymph node metastases (Roepman et al. 2005).

Genes like fusin (*CXCR4*), Rho GDP dissociation inhibitor (*GDI*) beta, E-NP2 autotaxin (*ATX*), *CCR7*, *CCL9, CR2, RGS1, FUCA1* and *SELL* were shown to be upregulated in metastasizing tumors (Cromer et al. 2004; Liu et al. 2008; Takanami 2003) and were also upregulated in lymph node metastasis from our microarray data. The role of fusin (*CXCR4*) in metastasis has been implicated in neuroblastoma (Geminder et al. 2001), melanoma (Murakami et al. 2002), prostate cancer (Taichman et al. 2002), breast cancer (Kato et al. 2003) and oral squamous cell carcinoma (Uchida et al. 2003, 2004).

CCR7 has been shown to play an important role in tumor cell migration and lymph node metastasis (Wiley et al. 2001). The highly correlated expression of *CCR7* (93% frequency) with its ligand *CCL21* (93% frequency) in lymph node metastasis confirms the reliability of our PathwayExpress analysis which resulted, among others, in a relatively strong involvement of the cytokine–cytokine receptor interaction signaling in the development of metastasis in HNSCC. Other genes involved in the signaling pathways in our list M *versus* PT, directly or indirectly involved in tumorigenesis including colorectal cancer, thyroid cancer, small cell lung cancer and endometrial cancer and could be potential novel drug targets for metastasized tumors.

Many of the upregulated or downregulated genes in primary HNSCC are already known to be involved in carcinogenesis. The upregulation of the ECM-degrading matrix metalloproteinases (MMPs) like *MMP1, MMP3, MMP11, MMP12, MMP13*, urokinase-type plasminogen activator uPa (*PLAU*) and different types of collagens were common for many advanced tumors including HNSCC. The *uPA/uPAR* and *SERPINE1* axis has been associated with tumor resistance and metastasis in HNSCC (Pavon et al. 2006).

Some of the downregulated genes in HNSCC are known to be important enzymes in the xenobiotic metabolic pathway. This includes genes belonging to cytochrome P-450 (*CYP2C9, CYP3A5, CYP4B1*), alcohol dehydrogenase 7, 3A1 (*ADH7* and *ALDH3A1*) and 1C, epoxide dehydrogenase (*EPHX2*), and glutathione s-transferase A2 (*hGST2*). The xenobiotic pathway is of importance in the degradative metabolism of both foreign and/or native toxic and carcinogenic products, although their impact on carcinogenesis is not clear so far (Alevizos et al. 2001; Coles et al. 2001; Garcia-Martin et al. 2002).

Collectively, despite many reports on differentially regulated genes in HNC, there is still a demand to identify *bona fide* genes or gene signatures, which could be used as specific biomarkers for (specific) tumor types, usable for targeted therapies, and/or diagnostic purposes. In contrast to what is sometimes propagated in the field it is unlikely that a single 'magic' HNC biomarker exists. For example, our recent study showed that although expression analyses and targeting of epithelial growth factor receptors has been shown to be beneficial for breast and colon cancer, the success of cetuximab treatment is limited for HNSCC (Deuss et al. 2020). Thus, the pathobiological relevance of identified genes needs to be clearly supported by a comprehensive experimental pipeline. Rational chemo-radiation combination therapies, in addition to immunotherapy, exosomes or nanoparticle-based strategies, are currently considered as the most efficient strategies to combat cancer (Beccard et al. 2020; Campbell et al. 2018; Deuss et al. 2020; Gaipl et al. 2020; Haussmann et al. 2019; Schuler et al. 2017; Siemer et al. 2019; Westmeier et al. 2018a,b, 2020). As the success of these treatments requires a profound molecular knowledge of their underlying mechanisms (Campbell et al. 2018; Leemans et al. 2011), we here focused on the exploration of the function of a yet unexplored downregulated gene, cytokeratin24.

As outlined before, cKRTs are the major intermediate filament structural proteins of epithelial cells and are frequently used to stratify carcinomas into site of origin, tumor subtype, and to predict clinical course and therapy response (Christofori 2006; Li et al. 2020; McGinn et al. 2020; Moll et al. 2008). Our GO data indicated an impact of tumor cell differentiation and structural integrity, such as extracellular matrix or focal adhesion together with PI3K-AKT signaling on metastasis, molecular events known to be influenced by cytokeratin networks (Kitamura et al. 2017; Mehrad et al. 2018; Mehrpouya et al. 2019; Weng et al. 2012; Xu et al. 2018; Yang et al. 2008). As numerous cKRTs have been studied before, we selected cKRT24 as a yet unexplored candidate for a subsequent comprehensive functional analysis. In the current study, we employed comprehensive cell culture and *in vivo* models to demonstrate for the first time that *cKRT24* has tumor suppressive properties in HNSCC. For one, our transcriptomics data revealed a significant down regulation of cKRT24 in PT or M *versus* the corresponding non-malignant tissue for all patients. Second, reduced protein expression of cKRT24 in

primary HNSCC compared to non-malignant tissue from the same patient could be verified by immunoblot as well as immunohistochemistry in patient material. Third, cloning and ectopic expression of cKRT24 demonstrated typical cytokeratin localization by live cell microscopy and cKRT24 expression inhibited proliferation of HNSCC cell lines *in vitro*. Fourth, the tumor suppression activity of cKRT24 could also be verified *in vivo* shown by murine xenograft transplantation studies. Although not further tested, cKRT24 downregulation may also favor metastasis, as we found reduced expression in the distant metastases from the same patients analyzed. Epithelial–mesenchymal transition (EMT), a natural biological process that in cancer cells, leads to loss of intercellular adhesion and enhanced migration and invasion, is classically associated with a transition from some cytokeratins to vimentin intermediate filaments (Shi et al. 2020). Though, expression of simple cKRTs (e.g. 8, 18, 19) to stratified cKRTs (e.g. 5, 17) was observed, the exact roles of specific cKRTs involved are not yet understood (Shi et al. 2020).

Although our data are the first report on cKRT24, previous studies found similar effects for certain cKRT members, underlining the quality and relevance of our study. It is thus impressive that differential cKRTs expression is a hallmark of tumor progression, interfering with a multitude of intracellular regulation pathways, including kinases, receptors, and pro-anti-apoptotic modulator proteins (Frohwitter et al. 2016; Moll et al. 2008). However, these components of the intermediate filaments are highly conserved during evolution and show a high degree of conservation among species, yet they seem to affect tumor-relevant signaling networks quite differentially (Kitamura et al. 2012; Moll et al. 2008). Notably, enhanced expression of high-molecular weight cKRTs 8/18 seems associated with an unfavorable prognosis for HNSCC patients (Frohwitter et al. 2016). Also, increased expression of cKRT19 was associated with high-grade dysplasia and squamous intraepithelial neoplasia and a decreased survival rate of patients with SCCs (Mehrpouya et al. 2019; Noorlag et al. 2017). In contrast to our observation for cKRT24, cKRT19 seems not to be expressed in benign regions of keratinized oral epithelium (Frohwitter et al. 2016; Moll et al. 2008). Moreover, cKRT8/18 and cKRT19 expression had opposing effects on cell cycle regulation (p21), hypoxic stress (HIF-1α and CAIX) or cellular adhesion (α/γ-catenin) (just to name a few networks) (Frohwitter et al. 2016; Moll et al. 2008). cKRT5/cKRT17 dimers facilitate cell junction remodeling (Frohwitter et al. 2016; Kumar et al. 2015; Moll et al. 2008). Whereas nuclear receptor modulating drugs such as retinoids regulate expression of cKRT5, cKRT17, and other stratified cKRT, it might be interesting to also examine their effects on cKRT24 expression and anti-tumoral activity (Frohwitter et al. 2016; Moll et al. 2008; Schweitzer et al. 2010; Schweitzer et al. 2008). In contrast to cKRT24 described here, cKRT8/18 and cKRT19 are not physiologically expressed in normal squamous epithelium, but may be expressed during carcinogenesis and potentially also for metastasis (Moll et al. 2008; Paccione et al. 2008; Toyoshima et al. 2008). Therefore, our results indicate the existence of different pathways in the pathogenesis of HNSCC and other tumor types, which though needs to be resolved. In addition, HNSCC may most likely not be regarded as a homogeneous disease entity, and the alteration in cKRT expression may be a result of tumor dedifferentiation. Based on our preliminary data, one may propose a cross-talk and correlation between cKRT24 and constituents of the ECM (e.g., upregulation of fibronectin expression) and adhesion molecules, which are important players in the pathogenesis of HNSCC. To however to dissect and understand this potential cross-talk additional experimental evidence is needed.

To mechanistically understand cKRT24 downregulation, we examined *cKRT24* gene methylation in the independent TCGA cohort of HNSCC patients. Interestingly, tumor tissues showed significantly lower methylation levels compared to normal adjacent tissues, similar to what we just reported for the immune checkpoint molecule, programmed cell death protein 1 (PD-1, encoded by the *PDCD1* gene) (Bockhorst et al. 2020). Although additional investigations may be needed, our data strongly indicate that gene methylation is unlikely to be responsible for reduced cKRT24 levels observed in tumors. Here, a limitation of the results is the fact that the Infinium HumanMethylation450 BeadChip used by TCGA Research Network only covers a fraction of CpG sites within the region of interest. Therefore, further prospective studies e.g. using bisulfite sequencing may be performed, using matched NAT and tumor tissues.

Likewise, inactivating mutations of proteins are often found in tumor cells, though not reported for *cKRT24* (Campbell et al. 2018; Cancer Genome Atlas Network 2015). Our data shown that in contrast to proteins such as p53 (213 mutations in 352 patients of the TCGA HNSC cohort), inactivating mutations in *cKRT24* occur in <1% of analyzed patients. Also, a low mutation rate was observed for the HNSCC relevant growth factor receptor EGFR (13 mutations in 13 patients of the TCGA HNSC cohort), we reported as a negative prognostic factor in HNSCC (Deuss et al. 2020). Collectively, mutations are unlikely to confer loss-of function of cKRT24 and downregulation seems to be an early event during carcinogenesis.

A limitation of most large ‘omics’ studies is the fact that corresponding non-malignant tissue, PT as well as M

are not always available from the same patient. For example, in the cohort of *The Cancer Genome Atlas* (TCGA) HNSCC cohort, 528 tumors and only 50 normal adjacent tissue (i.e., 10%) were analyzed, which may preclude identification of unknown signaling pathways and/or biomarkers (Campbell et al. 2018; Cancer Genome Atlas Network 2015) (Figure 5). Although we focused on a patient cohort from which N, PT as well as M could be surgically recovered from the same patient, a limitation of our study is its retrospective nature and the low number of patients and FFPE biopsies examined. Also, as this applies to almost all FFPE IHC-based studies, including our previous work (Bier et al. 2012; Deuss et al. 2020; Engels et al. 2007, 2008, 2009a,b; Fetz et al. 2009; Habtemichael et al. 2010; Knauer et al. 2010a; Stauber et al. 2012a), such analyses are semi-quantitative at best. Hence, *in silico* as well as experimental investigations need to also consider existing data repositories and related studies. Also, the cancer relevance of identified gene-networks needs to be examined and verified by a tiered experimental pipeline. A limitation of our study as well most comprehensive 'big data' studies is the fact that such investigations are laborious and time consuming and thus, can mostly be done only on a limited number of genes, as exemplified by confirming the functional relevance of cKRT24 here. Moreover, although our work excluded gene methylation as a major cause for cKRT24 downregulation, we still do not know the signaling networks and molecular events for our observation. Likewise, it would be important to define the type of biological, chemical or physical signals (e.g. toxic agents in tobacco, HPV, DNA damage, oncogenes ect.) that cause downregulation and triggers the activation of its tumor suppressor functions in disease and in its physiological environment. Though, studies on proteins downregulated in tumor cells are clearly more challenging that overexpression studies. From what has been discussed in the literature, cKRTs seem to influence various pathways, including differentiation, proliferation, inhibition, metabolic stress, activation of Toll like receptors, senescence, apoptosis and migration in normal physiology (e.g., keratinocyte differentiation) and disease (Aymard et al. 2011; Fortier et al. 2013; Kim and Coulombe 2007). Although cKRTs are recognized as multi-faceted effectors, it is striking that even for cKRTs used for diagnostic purposes for decades the detailed mechanistic knowledge is still missing. Given the fact that we here report the relevance of cKRT24 for the first time this limitation is expected and need to be resolved in future studies. We feel that our study may stimulate the field to curate our lack of knowledge, which may allow to better use cKRTs as biomarkers and potential targets for chemico-genetic therapeutics. Clearly, cKRT24's pathological and clinical relevance concerning disease progression and therapy responses need to be examined in large prospective studies. In addition to the limited number of biopsies examined here, large IHC-based investigation of cKRT24 as a prognostic marker need to follow by retro-/prospective studies also addressing the HPV-status and treatments. Also, we do not wish to postulate that cKRT24 is 'the' unique biomarker for HNSCC but needs to be considered in the context of other biomarkers reported so far. Despite these limitations, we feel that our transcriptomics data set are a valuable resource and our results corroborate our hypothesis that cKRT24 may serve as a biomarker and may be exploited as a target to support current HNSCC treatments to improve management of HNSCC patients.

Materials and methods

Study population

Investigation has been conducted in accordance with the ethical standards according to the Declaration of Helsinki and according to local, national, and international guidelines as described (Deuss et al. 2020). Tissue samples were obtained from patients undergoing surgical resection at the department of otolaryngology of the Universities of Mainz. The study protocol has been approved by the local ethics committee (#83756604) after obtaining the patients' informed consent to participate in the study and was processed anonymously. All cases were diagnosed histopathologically as HNSCC and staged according to the TNM classification of malignant tumors recommended by the 'Union International Contre le Cancer' UICC. All experiments were performed in accordance with relevant laws and the University Medical Center Mainz Guidelines and approved by the institutional ethics committee at the University Medical Center Mainz. In this study, tumor specimens, corresponding non-malignant tissue, and lymph node metastasis were analyzed. All of the primary tumors that we analyzed had positive clinical as well as pathological lymph node metastasis status. Specimens included oropharyngeal and laryngopharyngeal carcinoma of different tumor size (T1–T4), lymph node status (N0–2), no distant metastasis (M0) and grading G1–G3. However, we excluded five patients from the study due to insufficient mRNA quality isolated from either N, PT or M. The median age of patients was 56 years, and 86% were males. Six of the resected tumors were classified as stage II (40%), nine as stage III (60%); 13 (86%) of them had a moderate (G2) tumor differentiation grade and two (15%) a poor differentiation grade. Twelve patients had a lymph node status of N1/2 (80%), and three of N3 (20%). The majority of cancers were located in the hypopharynx (60%), 13% in the larynx, and 27% in the oropharynx.

Upon resection samples were immediately placed on ice and snap-frozen in liquid nitrogen within 30 min. Histological analyses were performed to ensure that each specimen contained >70% tumor tissue and <10% necrotic debris. Samples not meeting these criteria were rejected. Data of $n = 50$ normal adjacent tissue (NAT) and $n = 528$

HNSCC tissue samples were included from The Cancer Genome Atlas (TCGA) Research Network (http://cancergenome.nih.gov/). The TCGA Research Network included patients in accordance with the guidelines of the Declaration of Helsinki of 1975 and all patients provided signed informed consent.

Tissue sampling and primary cell isolation

For the isolation of primary cancer cells or epithelial cell from non-malignant tissue, specimens were cut into pieces and enzymatically digested with collagenase typeI/hyaluronidase (Sigma Aldrich, Munich, Germany) in RPMI-1640 (Invitrogen, Karlsruhe, Germany) at 37 °C overnight. Following digestion, dissociated cells were passed through a cell strainer, and epithelial cells were isolated by MACS® separation using CD326 (EpCAM) MicroBeads (Miltenyi Biotec GmbH, Bergisch Gladbach, Germany) according to the manufacturer's recommendations. Cells were propagated for one week as described (Knauer et al. 2007b, 2013; Stauber et al. 2012b) and subjected to analysis.

RNA extraction

Frozen tissue samples (30–50 mg) were collected in 1 mL Trizol (Invitrogen, Karlsruhe, Germany) and dispersed using an Ultra-Turrax T25 tissue homogenizer (IKA Werke, Staufen, Germany). Total RNA was extracted according to the recommendations given by the manufacturer's Trizol protocol and further purified on RNeasy Mini spin columns (Qiagen, Hilden, Germany). Integrity and purity of total RNA were assessed on a Bioanalyzer 2100 (Agilent Technologies, Boeblingen, Germany) using a RNA 6000 Nano LabChip Kit (Agilent) according to the manufacturer's instructions (Knauer et al. 2007a).

Target preparation and hybridization for Affymetrix GeneChip Arrays

Total RNA (5 µg) was used to prepare biotinylated cRNAs for hybridization, following the guidelines given in the Affymetrix GeneChip Expression Analysis Technical Manual. cRNA clean-up was performed on RNeasy Mini filters (Qiagen). In all, 10 µg of fragmented, labelled cRNA were hybridized to Affymetrix HG-U133A arrays (Affymetrix, Santa Clara, CA, USA) using standard conditions (16 h, 45 °C). Arrays were washed and stained in a Fluidics Station 400 (Affymetrix) and scanned on a Gene Array Scanner 2500 (Agilent), as recommended by Affymetrix. Raw fluorescence intensities from all hybridizations were normalized applying variance stabilization with additional scaling. Additionally, MAS5 as well as gcRMA expression values were calculated.

Microarray data processing, pathway analysis and bioinformatics

Data and cluster analyses were performed using Affymetrix Microarray Suite 5.0 (MAS5) and GeneSpring GX software (Agilent Technologies, Santa Clara, USA). All samples were normalized to the median of control samples. Each measurement for each gene in those specific samples was divided by the median of that gene's measurements in the corresponding control samples. The gene list was subjected to a Student's *t*-test (p-value < 0.05). The resulting list was further filtered for confidence using a Benjamini–Hochberg false discovery rate correction. A 2.0-fold cut-off filter was then applied to identify genes that were preferentially up- or downregulated. Heatplots are used for visualizing gene expression: yellow indicates no change in expression, red enhanced expression (upregulated), and blue suppressed expression (downregulated). Volcano plot analysis was used to show the distribution of significance (corrected p-value ≤ 0.05) to magnitude ($\log_2$ratio ≥ twofold) of N to PT or M, as well as PT to M. Onto-Express software (http://vortex.cs.wayne.edu/projects.htm) was used for the analysis of Gene-Ontology (GO) and pathways. Probe set lists of the differentially expressed genes were used to browse through the GO terms organized in tree structure. Significance was assessed by using the hypergeometric distribution. Genome wide information of *cKRT24* mutations were obtained from the *BioMutav3.0* database as well as by the TCGA Research Network data provided by (Campbell et al. 2018). Further analyses were performed on the TCGA Research Network generated methylation raw data using the Infinium HumanMethylation450 BeadChip (Illumina, Inc., San Diego, CA, USA). We included six beads that target CpG sites within the gene body, the transcription start site, and upstream of the *cKRT24* gene (cg12564187: CpG 1, cg27316026: CpG 2, cg24340657: CpG 3, cg04219544: CpG 4, cg23737768: CpG 5, cg06899912). Raw data were downloaded from the UCSC Xena browser (www.xena.ucsc.edu). Methylation levels (β-values) were calculated: β-value = (Intensity_Methylated_Signal)/(Intensity_Methylated_Signal + Intensity_Unmethylated_Signal) × 100%. Means of groups were compared using Mann–Whitney U test.

Survival data sets were also obtained from the TCGA network. A total of $n = 282$ patients were included. Data was assessed via the USCS Xena server and patients grouped according to genomic expression of cKRT24 (quartiles, i.e. high > 7.893; low < 1.367). Final visualizations and statistics were performed with graphpad Prism.

Reverse transcription (RT)-PCR and quantitative real-time PCR analysis

RT-PCR was performed using specific primer sets for *OSF2, FN1, cKRT24, CLCA4, PRR4, SCCA2b, TP73L, C4.4A, FAIM3, ARHGAP25, RASGRP2* and *GAPDH* genes (Table S9) as described (Knauer et al. 2007b, 2013). *GAPDH* was used to control the amounts of cDNA generated from each sample. First-strand cDNA synthesis was carried out using a cDNA synthesis kit for RT-PCR (Superscript II, Invitrogen life technologies). 1 µg of total RNA was converted to cDNA and 1 µL of the 20 µL RT product was amplified for 30 cycles (initial denaturation at 95 °C for 3 min, 30 s at 95 °C, 30 s at a variable temperature for annealing and 1 min at 72 °C) followed by an extension of 5 min at 72 °C. RT-PCR amplification products were analyzed on 2% agarose gel stained with ethidium bromide.

For selected genes, changes in mRNA levels detected in microarray experiments were evaluated by reverse transcription (RT) and quantitative real-time PCR analysis, using the iCycler (BioRad, Munich, Germany). One µg of total RNA was converted to cDNA using Superscript II (Invitrogen Corporation) and oligo (dT) primer according to manufacturer's specifications. PCR reaction mixtures consisted of 12.5 µL of 2x iQ™ SYBER® Green Supermix (Abgene, UK), 0.5 µL of each 10 µM target primer, 1 µL (1:10) cDNA template in a final scaled down reaction volume of 25 µL. Thermal cycling conditions comprised an initial denaturation step at 95 °C for 15 min, 40 cycles at 95 °C for 30 s

and variable annealing temperatures for 30 s depending on the respective set of target primers. Cumulative fluorescence was measured at the end of the extension phase of each cycle. Specific amplicon formation with each primer pair was confirmed by dissociation curve analysis and by visualization of a single band on a 2% agarose gel. To define the relative expression of the genes, the PCR product results from each tumor sample were compared with the results from normal tissue or lymph node metastasis from the same patient. The relative expression ratio (R) of target gene is calculated using the equation: Ratio = $(E_{\text{target}})^{\Delta \text{Cp target(control-sample)}}/(E_{\text{ref}})^{\Delta \text{Cpref(control-sample)}}$ based on its real-time PCR efficiencies (E) and the crossing point (CP) difference of an unknown sample *versus* a control and expressed relative to the non-regulated housekeeping gene glyceraldehyde-3-phosphate dehydrogenase gene (GAPDH), as described (Knauer et al. 2007a, 2013; Stauber et al. 2012b).

Plasmids

The cKRT24 coding sequence was amplified from cDNA obtained from non-malignant oral mucosa or head and neck tumors. mRNA preparation and cDNA synthesis from tumor tissue was performed as described (Engels et al. 2007; Knauer et al. 2013). Cloning of the cKRT24 coding sequence into expression vectors pc3 or pc3-GFP using BamHI/EcoRI- or BamHI/NheI-restriction sites, respectively, allowed the expression of cKRT24, alone or as a fusion with the green fluorescent protein as described (Engels et al. 2007; Knauer et al. 2013). cKRT24 was also cloned in a retroviral vector (IRES-GFP), allowing the simultaneous expression of cKRT24 and GFP from the same mRNA due to the presence of an IRES element.

Cells, cell culture, and proliferation assays

Authenticated and characterized cell lines were purchase from the *ATCC* repository, expanded, stocks prepared at early passages, and frozen stocks kept in liquid nitrogen. Thawed cells were routinely monitored by visual inspection and growth-curve analyses to keep track of cell-doubling times, and were used for a maximum of 20 passages for all experiments. Depending on passage number from purchase, cell line authentication was further performed at reasonable intervals by short tandem repeat (STR) profiling. Cell lines (Supplementary Table S2) were maintained and transfected with Lipofectamine 2000 (Invitrogen, Karlsruhe, Germany) as described (Fetz et al. 2009; Knauer et al. 2007a, 2013; Schrenk et al. 2018; Westmeier et al. 2018a). Proliferation was assessed by MTT assays as described (Knauer et al. 2013; Stauber et al. 2012b). Data shown are calculated from the mean values of three independent experiments.

Retrovirus production and infection

Production of retroviral stocks and viral titer determination were carried out as previously described (Engels et al. 2007). Transduction was monitored by FACS analysis or fluorescence microscopy using IRES-GFP according to standard protocols (Stauber et al. 1998). To generate cells stably expressing cKRT24, FaDu cells were transduced with cKRT24-IRES-GFP expressing retroviruses. Fluorescent cells were isolated by two rounds of fluorescence activated cell sorting as described (Engels et al. 2007; Knauer et al. 2013).

Animals and xenograft tumors

All animal work has been conducted according to relevant national and international guidelines. For animal studies, TE671 (2×10^6) cells were implanted into both flanks of four-week-old female MRI *nu/nu* mice (Harlan Winkelmann, Hamburg, Germany) as described (Stauber et al. 2006, 2012b). Mice were randomized into groups (5 mice/group). Tumor growth was monitored using calipers to calculate tumor volumes with the formula: length $\times$ π width^2 $\times$ 0.52. Animals were euthanized at the end of the study and the tumors were processed for Western blot analysis. All animal experiments were approved by the Institutional Animal Care and Use Committee at the University of Mainz.

Protein extraction and immunoblot analysis

Preparation of whole lysates from cells or tissue and immunoblotting were carried out as described (Knauer et al. 2013; Stauber et al. 2012b; Wunsch et al. 2015a,b). Briefly, tissues (~50 mg) were homogenized in 300 µL lysis buffer (10 mM *Tris*-HCl, pH7.5, 1 mM $MgCl_2$, 1 mM EGTA, 0.5% CHAPS, 10% glycerol (v/v), 5 mM mercaptoethanol, 0.1 mM phenylmethylsulfonyl flouoride and Complete Protease Inhibitor Cocktail EDTA-free from Roche Diagnostics, Mannheim, Germany) using an Ultra-Turrax-T25 homogenizer (IKA Labortechnik, Staufen, Germany) as described (Fetz et al. 2009; Knauer et al. 2013; Stauber et al. 2012b). Equal loading of lysates was controlled by reprobing blots for GAPDH/Vimentin as described previously (Knauer et al. 2013; Stauber et al. 2012b).

Immunohistochemistry (IHC)

Formalin-fixed and paraffin-embedded tissue blocks from tumors, normal tissue or lymph node metastasis were used for immunohistochemistry (IHC) staining. 5 µM tissue sections were deparaffined with xylene and dehydrated with sequential washes of 100, 90, 80, and 70% isopropanol, and endogenous peroxidase activity was blocked with a 3% hydrogen peroxidase solution as described (Engels et al. 2007; Haussmann et al. 2019; Stauber et al. 2012b). For cKRT24, the samples were digested with Proteinase K and then steamed for antigen retrieval with citrate buffer (pH 7.0) for 30 min and treated with 0.1% Triton in PBS for 10min at room temperature. After blocking, polyclonal antibodies against cKRT24 (1:200) were added and incubated at 4 °C overnight. Detection was performed with the Envision/horseradish peroxidase system (Dako-Cytomation, Denmark) as described (Engels et al. 2007; Stauber et al. 2012b). Slides were finally counterstained with 50% hematoxylin and examined by light microscopy on a Leica microscope at 100× magnification. Images were recorded with identical camera settings. Semi-quantification of protein expression was defined by a scoring system, for which the positive cells (%) and staining intensity (scale 0–4) were evaluated, and then multiplied to yield a score from 0 to 400. In order to maintain consistency, the same qualified pathologist gave interpretations for all IHC data.

Fluorescence microscopy, confocal laser scanning microscopy (CLSM), immunofluorescence, and image processing

Observation, quantitation, image analysis and presentation were performed as described (Bier et al. 2011; Habtemichael et al. 2010; Tenzer et al. 2013). CLSM images were acquired using Leica LAS AF software on a Leica TCS SP8 system equipped with four lasers (UV 405 nm, Ar 458/476/488/496/514 nm, DPSS 561 nm, HeNe 633 nm) and a HCX-PL APO 63x/1.20 water lens (Leica). To avoid crosstalk between different dyes, emission signals were collected independently in serial mode. Images were taken at constant laser power, with a pinhole size of 1 Airy Disk, a line average of three, and a frame average of one. Cells were seeded in 35 mm glass bottom dishes (MatTek). For detection of cytokeratins, cultures were washed twice with PBS and fixed with ice-cold methanol for 5 min. Fixed cells were washed once with PBS and rehydrated in PBS containing 2% bovine serum for 30 min before being further processed for immunofluorescence microscopy. Following overnight incubation with the primary antibody at 4 °C (dilution of 1:50 for cKRT24 in PBS/10% bovine serum), cells were washed with PBS buffer, and incubated for 1 h at room temperature with fluorescent-labeled secondary antibodies (dilution of 1:200). After washing again for three times with PBS, cell nuclei were stained with 0.5 µg/mL Hoechst 33342 (excitation: 405 nm; emission: 430–480 nm). For visualization of the multi-layer structure of cytokeratins, fluorescence channels were subtracted from the transmission light image using Photoshop CS6 (Adobe Systems) as described (Knauer et al. 2010b).

Acknowledgments: The authors thank Sandra Olf for excellent technical assistance, Ludger Klein-Hitpass for support with microarray analyses, Wilfried Roth and the University Medical Center Mainz biobank-initiative, and Jan Hagemann for support.

Author contributions: All the authors have accepted responsibility for the entire content of this submitted manuscript and approved submission.

Research funding: This study was supported by Else-Kröner Foundation, Stiftung Tumorforschung Kopf-Hals, DAAD/TransMed, DFG, and the Science Support Program of the University Hospital Mainz.

Conflict of interest statement: The authors declare that the research was conducted in the absence of any commercial or financial relationships that could be construed as a potential conflict of interest.

References

Alevizos, I., Mahadevappa, M., Zhang, X., Ohyama, H., Kohno, Y., Posner, M., Gallagher, G.T., Varvares, M., Cohen, D., Kim, D., et al. (2001). Oral cancer *in vivo* gene expression profiling assisted by laser capture microdissection and microarray analysis. Oncogene 20: 6196–6204.

Alizadeh, A.A., Eisen, M.B., Davis, R.E., Ma, C., Lossos, I.S., Rosenwald, A., Boldrick, J.C., Sabet, H., Tran, T., Yu, X., et al. (2000). Distinct types of diffuse large B-cell lymphoma identified by gene expression profiling. Nature 403: 503–511.

Al Moustafa, A.E., Alaoui-Jamali, M.A., Batist, G., Hernandez-Perez, M., Serruya, C., Alpert, L., Black, M.J., Sladek, R., and Foulkes, W.D. (2002). Identification of genes associated with head and neck carcinogenesis by cDNA microarray comparison between matched primary normal epithelial and squamous carcinoma cells. Oncogene 21: 2634–2640.

Ashburner, M., Ball, C.A., Blake, J.A., Botstein, D., Butler, H., Cherry, J.M., Davis, A.P., Dolinski, K., Dwight, S.S., Eppig, J.T., et al. (2000). Gene ontology: tool for the unification of biology. Gene Ontol. Consortium Nat. Genet. 25: 25–29.

Aymard, E., Barruche, V., Naves, T., Bordes, S., Closs, B., Verdier, M., and Ratinaud, M.H. (2011). Autophagy in human keratinocytes: an early step of the differentiation? Exp. Dermatol. 20: 263–268.

Beccard, I.J., Hofmann, L., Schroeder, J.C., Ludwig, S., Laban, S., Brunner, C., Lotfi, R., Hoffmann, T.K., Jackson, E.K., Schuler, P.J., et al. (2020). Immune suppressive effects of plasma-derived exosome populations in head and neck cancer. Cancers (Basel) 12, https://doi.org/10.3390/cancers12071997.

Beltz, A., Gosswein, D., Zimmer, S., Stauber, R.H., Hagemann, J., Strieth, S., Matthias, C., and Kunzel, J. (2018). Staging of oropharyngeal carcinomas: new TNM classification as a challenge for head and neck cancer centers. HNO 66: 375–382.

Beltz, A., Gosswein, D., Zimmer, S., Limburg, I., Wunsch, D., Gribko, A., Deichelbohrer, M., Hagemann, J., Stauber, R.H., and Kunzel, J. (2019). Staging of oropharyngeal squamous cell carcinoma of the head and neck: prognostic features and power of the 8th edition of the UICC staging manual. Eur. J. Surg. Oncol. 45: 1046–1053.

Benson, E., Li, R., Eisele, D., and Fakhry, C. (2014). The clinical impact of HPV tumor status upon head and neck squamous cell carcinomas. Oral Oncol. 50: 565–574.

Bier, C., Knauer, S.K., Docter, D., Schneider, G., Kramer, O.H., and Stauber, R.H. (2011). The importin-alpha/nucleophosmin switch controls taspase1 protease function. Traffic 12: 703–714.

Bier, C., Knauer, S.K., Wunsch, D., Kunst, L., Scheiding, S., Kaiser, M., Ottmann, C., Kramer, O.H., and Stauber, R.H. (2012). Allosteric inhibition of Taspase1's pathobiological activity by enforced dimerization *in vivo*. FASEB J. 26: 3421–3429.

Bittner, M., Meltzer, P., Chen, Y., Jiang, Y., Seftor, E., Hendrix, M., Radmacher, M., Simon, R., Yakhini, Z., Ben-Dor, A., et al. (2000). Molecular classification of cutaneous malignant melanoma by gene expression profiling. Nature 406: 536–540.

Bockhorst, C., Dietrich, J., Vogt, T.J., Stauber, R.H., Strieth, S., Bootz, F., Dietrich, D., and Vos, L. (2020). The DNA methylation landscape of PD-1 (PDCD1) and adjacent lncRNA AC131097.3 in head & neck squamous cell carcinoma. Epigenomics 13: 113–127.

Bray, F., Ferlay, J., Soerjomataram, I., Siegel, R.L., Torre, L.A., and Jemal, A. (2018). Global cancer statistics 2018: GLOBOCAN estimates of incidence and mortality worldwide for 36 cancers in 185 countries. CA Canc. J. Clin. 68: 394–424.

Campbell, J.D., Yau, C., Bowlby, R., Liu, Y., Brennan, K., Fan, H., Taylor, A.M., Wang, C., Walter, V., Akbani, R., et al. (2018). Genomic, pathway network, and immunologic features distinguishing squamous carcinomas. Cell Rep. 23: 194–212 e196.

Cancer Genome Atlas Network. (2015). Comprehensive genomic characterization of head and neck squamous cell carcinomas. Nature 517: 576–582.

Cavalieri, S., De Cecco, L., Brakenhoff, R.H., Serafini, M.S., Canevari, S., Rossi, S., Lanfranco, D., Hoebers, F.J.P., Wesseling, F.W.R., Keek, S., et al. (2020). *Development of a multiomics database for personalized prognostic forecasting in head and neck cancer: the big data to decide EU project*. Head Neck.

De Cecco, L., Nicolau, M., Giannoccaro, M., Daidone, M.G., Bossi, P., Locati, L., Licitra, L., and Canevari, S. (2015). Head and neck cancer subtypes with biological and clinical relevance: meta-analysis of gene-expression data. Oncotarget 6: 9627–9642.

Christofori, G. (2006). New signals from the invasive front. Nature 441: 444–450.

Chung, C.H., Parker, J.S., Karaca, G., Wu, J., Funkhouser, W.K., Moore, D., Butterfoss, D., Xiang, D., Zanation, A., Yin, X., et al. (2004). Molecular classification of head and neck squamous cell carcinomas using patterns of gene expression. Canc. Cell 5: 489–500.

Cohen, R.B. (2014). Current challenges and clinical investigations of epidermal growth factor receptor (EGFR)- and ErbB family-targeted agents in the treatment of head and neck squamous cell carcinoma (HNSCC). Canc. Treat Rev. 40: 567–577.

Coles, B.F., Morel, F., Rauch, C., Huber, W.W., Yang, M., Teitel, C.H., Green, B., Lang, N.P., and Kadlubar, F.F. (2001). Effect of polymorphism in the human glutathione S-transferase A1 promoter on hepatic GSTA1 and GSTA2 expression. Pharmacogenetics 11: 663–669.

Cromer, A., Carles, A., Millon, R., Ganguli, G., Chalmel, F., Lemaire, F., Young, J., Dembele, D., Thibault, C., Muller, D., et al. (2004). Identification of genes associated with tumorigenesis and metastatic potential of hypopharyngeal cancer by microarray analysis. Oncogene 23: 2484–2498.

Denaro, N., Russi, E.G., Adamo, V., and Merlano, M.C. (2014). State-of-the-art and emerging treatment options in the management of head and neck cancer: news from 2013. Oncology 86: 212–229.

Deuss, E., Gosswein, D., Gul, D., Zimmer, S., Foersch, S., Eger, C.S., Limburg, I., Stauber, R.H., and Kunzel, J. (2020). Growth factor receptor expression in oropharyngeal squamous cell cancer: Her1–4 and c-Met in Conjunction with the clinical features and human papillomavirus (p16) status. Cancers (Basel) 12(11), https://doi.org/10.3390/cancers12113358.

El-Naggar, A.K., Kim, H.W., Clayman, G.L., Coombes, M.M., Le, B., Lai, S., Zhan, F., Luna, M.A., Hong, W.K., and Lee, J.J. (2002). Differential expression profiling of head and neck squamous carcinoma: significance in their phenotypic and biological classification. Oncogene 21: 8206–8219.

Engels, K., Knauer, S.K., Metzler, D., Simf, C., Struschka, O., Bier, C., Mann, W., Kovacs, A.F., and Stauber, R.H. (2007). Dynamic intracellular survivin in oral squamous cell carcinoma: underlying molecular mechanism and potential as an early prognostic marker. J. Pathol. 211: 532–540.

Engels, K., du Bois, A., Harter, P., Fisseler-Eckhoff, A., Kommoss, F., Stauber, R., Kaufmann, M., Nekljudova, V., and Loibl, S. (2009a). VEGF-A and i-NOS expression are prognostic factors in serous epithelial ovarian carcinomas after complete surgical resection. J. Clin. Pathol. 62: 448–454.

Engels, K., Knauer, S.K., Loibl, S., Fetz, V., Harter, P., Schweitzer, A., Fisseler-Eckhoff, A., Kommoss, F., Hanker, L., Nekljudova, V., et al. (2008). NO signaling confers cytoprotectivity through the survivin network in ovarian carcinomas. Cancer Res 68: 5159–5166.

Engels, K., Stauber, R., Magnussen, H., Kirsten, D., Wirtz, H., and Watz, H. (2009b). Angiomyolipomas are indicator lesions for sporadic lymphangioleiomyomatosis in women. Eur Urol, 55: 755–756.

Ernst, B.P., Mikstas, C., Stover, T., Stauber, R., and Strieth, S. (2018). Association of eIF4E and SPARC expression with lymphangiogenesis and lymph node metastasis in hypopharyngeal cancer. Anticancer Res. 38: 699–706.

Eschrich, S., Zhang, H., Zhao, H., Boulware, D., Lee, J.H., Bloom, G., and Torres-Roca, J.F. (2009). Systems biology modeling of the radiation sensitivity network: a biomarker discovery platform. Int. J. Radiat. Oncol. Biol. Phys. 75: 497–505.

Fazilat-Panah, D., Vakili Ahrari Roudi, S., Keramati, A., Fanipakdel, A., Sadeghian, M.H., Homaei Shandiz, F., Shahidsales, S., and Javadinia, S.A. (2020). Changes in cytokeratin 18 during neoadjuvant chemotherapy of breast cancer: a prospective study. Iran J Pathol 15: 117–126.

Feldman, R., Gatalica, Z., Knezetic, J., Reddy, S., Nathan, C.A., Javadi, N., and Teknos, T. (2016). Molecular profiling of head and neck squamous cell carcinoma. Head Neck 38: E1625–E1638.

Ferlay, J., Colombet, M., Soerjomataram, I., Mathers, C., Parkin, D.M., Pineros, M., Znaor, A., and Bray, F. (2019). Estimating the global cancer incidence and mortality in 2018: GLOBOCAN sources and methods. Int. J. Canc. 144: 1941–1953.

Fetz, V., Bier, C., Habtemichael, N., Schuon, R., Schweitzer, A., Kunkel, M., Engels, K., Kovacs, A.F., Schneider, S., Mann, W., et al. (2009). Inducible NO synthase confers chemoresistance in head and neck cancer by modulating survivin. Int. J. Canc. 124: 2033–2041.

Fortier, A.M., Asselin, E., and Cadrin, M. (2013). Keratin 8 and 18 loss in epithelial cancer cells increases collective cell migration and cisplatin sensitivity through claudin1 up-regulation. J. Biol. Chem. 288: 11555–11571.

Frohwitter, G., Buerger, H., Van Diest, P.J., Korsching, E., Kleinheinz, J., and Fillies, T. (2016). Cytokeratin and protein expression patterns in squamous cell carcinoma of the oral cavity provide evidence for two distinct pathogenetic pathways. Oncol. Lett. 12: 107–113.

Gaipl, U.S., Multhoff, G., Pockley, A.G., and Rodel, F. (2020). Editorial: radioimmunotherapy-translational opportunities and challenges. Front. Oncol. 10: 190.

Gammon, L. and Mackenzie, I.C. (2016). Roles of hypoxia, stem cells and epithelial-mesenchymal transition in the spread and treatment resistance of head and neck cancer. J. Oral Pathol. Med. 45: 77–82.

Garcia-Martin, E., Martinez, C., Ladero, J.M., Gamito, F.J., Rodriguez-Lescure, A., and Agundez, J.A. (2002). Influence of cytochrome P450 CYP2C9 genotypes in lung cancer risk. Canc. Lett. 180: 41–46.

Geminder, H., Sagi-Assif, O., Goldberg, L., Meshel, T., Rechavi, G., Witz, I.P., and Ben-Baruch, A. (2001). A possible role for CXCR4 and its ligand, the CXC chemokine stromal cell-derived factor-1, in the development of bone marrow metastases in neuroblastoma. J. Immunol. 167: 4747–4757.

Gene Ontology, C. (2015). Gene ontology consortium: going forward. Nucl. Acids Res. 43: D1049–D1056.

Ginos, M.A., Page, G.P., Michalowicz, B.S., Patel, K.J., Volker, S.E., Pambuccian, S.E., Ondrey, F.G., Adams, G.L., and Gaffney, P.M.

(2004). Identification of a gene expression signature associated with recurrent disease in squamous cell carcinoma of the head and neck. Canc. Res. 64: 55–63.

Goesswein, D., Habtemichael, N., Gerhold-Ay, A., Mazur, J., Wunsch, D., Knauer, S.K., Kunzel, J., Matthias, C., Strieth, S., and Stauber, R.H. (2018). Expressional analysis of disease-relevant signalling-pathways in primary tumours and metastasis of head and neck cancers. Sci. Rep. 8: 7326.

Goetz, J.G., Minguet, S., Navarro-Lerida, I., Lazcano, J.J., Samaniego, R., Calvo, E., Tello, M., Osteso-Ibanez, T., Pellinen, T., Echarri, A., et al. (2011). Biomechanical remodeling of the microenvironment by stromal caveolin-1 favors tumor invasion and metastasis. Cell 146: 148–163.

Gribko, A., Hahlbrock, A., Strieth, S., Becker, S., Hagemann, J., Deichelbohrer, M., Hildebrandt, A., Habtemichael, N., and Wunsch, D. (2017). Disease-relevant signalling-pathways in head and neck cancer: taspase1's proteolytic activity fine-tunes TFIIA function. Sci. Rep. 7: 14937.

Gribko, A., Kunzel, J., Wunsch, D., Lu, Q., Nagel, S.M., Knauer, S.K., Stauber, R.H., and Ding, G.B. (2019). Is small smarter? Nanomaterial-based detection and elimination of circulating tumor cells: current knowledge and perspectives. Int. J. Nanomed. 14: 4187–4209.

Habtemichael, N., Heinrich, U.R., Knauer, S.K., Schmidtmann, I., Bier, C., Docter, D., Brochhausen, C., Helling, K., Brieger, J., Stauber, R.H., et al. (2010). Expression analysis suggests a potential cytoprotective role of Birc5 in the inner ear. Mol. Cell. Neurosci. 45: 297–305.

Hamoir, M., Schmitz, S., and Gregoire, V. (2014). The role of neck dissection in squamous cell carcinoma of the head and neck. Curr. Treat. Options Oncol. 15: 611–624.

Hasan, F., Yadav, V., Katiyar, T., Yadav, S., Pandey, R., Mehrotra, D., Hadi, R., Singh, S., Bhatt, M.L.B., and Parmar, D. (2020). Validation of gene expression profiles of candidate genes using low density array in peripheral blood of tobacco consuming head and neck cancer patients and auto/taxi drivers with preneoplastic lesions. Genomics 112: 513–519.

Haussmann, J., Tamaskovics, B., Bolke, E., Djiepmo-Njanang, F.J., Kammers, K., Corradini, S., Hautmann, M., Ghadjar, P., Maas, K., Schuler, P.J., et al. (2019). Addition of chemotherapy to hyperfractionated radiotherapy in advanced head and neck cancer-a meta-analysis. Strahlenther. Onkol. 195: 1041–1049.

Hoffmann, T.K., Greve, J., Laban, S., and Schuler, P.J. (2021). *Treatment of patients with head and neck cancer during the COVID-19 pandemic*, 1st ed. 69. HNO, Germany, pp. 14–16.

Huang, E., Cheng, S.H., Dressman, H., Pittman, J., Tsou, M.H., Horng, C.F., Bild, A., Iversen, E.S., Liao, M., Chen, C.M., et al. (2003). Gene expression predictors of breast cancer outcomes. Lancet 361: 1590–1596.

Irizarry, R.A., Hobbs, B., Collin, F., Beazer-Barclay, Y.D., Antonellis, K.J., Scherf, U., and Speed, T.P. (2003). Exploration, normalization, and summaries of high density oligonucleotide array probe level data. Biostatistics 4: 249–264.

Karantza, V. (2011). Keratins in health and cancer: more than mere epithelial cell markers. Oncogene 30: 127–138.

Kato, M., Kitayama, J., Kazama, S., and Nagawa, H. (2003). Expression pattern of CXC chemokine receptor-4 is correlated with lymph node metastasis in human invasive ductal carcinoma. Breast Canc. Res. 5: R144–R150.

Kim, S. and Coulombe, P.A. (2007). Intermediate filament scaffolds fulfill mechanical, organizational, and signaling functions in the cytoplasm. Genes Dev. 21: 1581–1597.

Kitamura, R., Toyoshima, T., Tanaka, H., Kawano, S., Kiyosue, T., Matsubara, R., Goto, Y., Hirano, M., Oobu, K., and Nakamura, S. (2012). Association of cytokeratin 17 expression with differentiation in oral squamous cell carcinoma. J. Canc. Res. Clin. Oncol. 138: 1299–1310.

Kitamura, R., Toyoshima, T., Tanaka, H., Kawano, S., Matsubara, R., Goto, Y., Jinno, T., Maruse, Y., Oobu, K., and Nakamura, S. (2017). Cytokeratin 17 mRNA as a prognostic marker of oral squamous cell carcinoma. Oncol. Lett. 14: 6735–6743.

Knauer, S.K., Bier, C., Schlag, P., Fritzmann, J., Dietmaier, W., Rodel, F., Klein-Hitpass, L., Kovacs, A.F., Doring, C., Hansmann, M.L., et al. (2007a). The survivin isoform survivin-3B is cytoprotective and can function as a chromosomal passenger complex protein. Cell Cycle 6: 1502–1509.

Knauer, S.K., Kramer, O.H., Knosel, T., Engels, K., Rodel, F., Kovacs, A.F., Dietmaier, W., Klein-Hitpass, L., Habtemichael, N., Schweitzer, A., et al. (2007b). Nuclear export is essential for the tumor-promoting activity of survivin. FASEB J. 21: 207–216.

Knauer, S.K., Heinrich, U.R., Bier, C., Habtemichael, N., Docter, D., Helling, K., Mann, W.J., and Stauber, R.H. (2010a). An otoprotective role for the apoptosis inhibitor protein survivin. Cell Death Dis. 1: e51.

Knauer, S.K., Heinrich, U.R., Bier, C., Habtemichael, N., Docter, D., Helling, K., Mann, W.J., and Stauber, R.H. (2010b). An otoprotective role for the apoptosis inhibitor protein survivin. Cell Death Dis. 1: e51.

Knauer, S.K., Unruhe, B., Karczewski, S., Hecht, R., Fetz, V., Bier, C., Friedl, S., Wollenberg, B., Pries, R., Habtemichael, N., et al. (2013). Functional characterization of novel mutations affecting survivin (BIRC5)-mediated therapy resistance in head and neck cancer patients. Hum. Mutat. 34: 395–404.

Kumar, V., Bouameur, J.E., Bar, J., Rice, R.H., Hornig-Do, H.T., Roop, D.R., Schwarz, N., Brodesser, S., Thiering, S., Leube, R.E., et al. (2015). A keratin scaffold regulates epidermal barrier formation, mitochondrial lipid composition, and activity. J. Cell Biol. 211: 1057–1075.

Kunzel, J., Psychogios, G., Mantsopoulos, K., Grundtner, P., Waldfahrer, F., and Iro, H. (2014). Lymph node ratio as a predictor of outcome in patients with oropharyngeal cancer. Eur. Arch. Oto-Rhino-Laryngol. 271: 1171–1180.

Kunzel, J., Gribko, A., Lu, Q., Stauber, R., and Wunsch, D. (2019). Nanomedical detection and downstream analysis of circulating tumor cells in head and neck patients. Biol. Chem. 400: 1465–1479.

Kuriakose, M.A., Chen, W.T., He, Z.M., Sikora, A.G., Zhang, P., Zhang, Z.Y., Qiu, W.L., Hsu, D.F., McMunn-Coffran, C., Brown, S.M., et al. (2004). Selection and validation of differentially expressed genes in head and neck cancer. Cell. Mol. Life Sci. 61: 1372–1383.

Laban, S., Gangkofner, D.S., Holzinger, D., Schroeder, L., Eichmuller, S.B., Zornig, I., Jager, D., Wichmann, G., Dietz, A., Broglie, M.A., et al. (2019). Antibody responses to cancer antigens identify patients with a poor prognosis among HPV-positive and HPV-negative head and neck squamous cell carcinoma patients. Clin. Canc. Res. 25: 7405–7412.

Leemans, C.R., Braakhuis, B.J., and Brakenhoff, R.H. (2011). The molecular biology of head and neck cancer. Nat. Rev. Canc. 11: 9–22.

Leethanakul, C., Patel, V., Gillespie, J., Pallente, M., Ensley, J.F., Koontongkaew, S., Liotta, L.A., Emmert-Buck, M., and Gutkind, J.S. (2000). Distinct pattern of expression of differentiation and growth-related genes in squamous cell carcinomas of the head and neck revealed by the use of laser capture microdissection and cDNA arrays. Oncogene 19: 3220–3224.

Leong, S.P., Cady, B., Jablons, D.M., Garcia-Aguilar, J., Reintgen, D., Werner, J.A., and Kitagawa, Y. (2007). Patterns of metastasis in human solid cancers. Canc. Treat Res. 135: 209–221.

Li, Q., Jiang, M., Han, X., Yang, Z., Shu, W., and Ding, X. (2020). Induction chemotherapy for unresectable Stage III non-small-cell lung cancer may improve survival of induction chemotherapy responders as predicted by elevated levels of carcinoembryonic antigen and cytokeratin fragment 19 and classification as stage N3 cancer. J. Canc. Res. Therapeut. 16: 222–229.

Lim, K.P., Cirillo, N., Hassona, Y., Wei, W., Thurlow, J.K., Cheong, S.C., Pitiyage, G., Parkinson, E.K., and Prime, S.S. (2011). Fibroblast gene expression profile reflects the stage of tumour progression in oral squamous cell carcinoma. J. Pathol. 223: 459–469.

Liu, C.J., Liu, T.Y., Kuo, L.T., Cheng, H.W., Chu, T.H., Chang, K.W., and Lin, S.C. (2008). Differential gene expression signature between primary and metastatic head and neck squamous cell carcinoma. J. Pathol. 214: 489–497.

Lohavanichbutr, P., Mendez, E., Holsinger, F.C., Rue, T.C., Zhang, Y., Houck, J., Upton, M.P., Futran, N., Schwartz, S.M., Wang, P., et al. (2013). A 13-gene signature prognostic of HPV-negative OSCC: discovery and external validation. Clin. Canc. Res. 19: 1197–1203.

Lui, V.W., Hedberg, M.L., Li, H., Vangara, B.S., Pendleton, K., Zeng, Y., Lu, Y., Zhang, Q., Du, Y., Gilbert, B.R., et al. (2013). Frequent mutation of the PI3K pathway in head and neck cancer defines predictive biomarkers. Canc. Discov. 3: 761–769.

Magan, M., Wiechec, E., and Roberg, K. (2020). CAFs affect the proliferation and treatment response of head and neck cancer spheroids during co-culturing in a unique in vitro model. Canc. Cell Int. 20: 599.

Majumder, A., Jagani, R., and Basu, A. (2020). Double-positive in triple-negative? How significant is basal cytokeratin expression in breast cancer? Med. J. Armed Forces India 76: 63–70.

Makarova, G., Bette, M., Schmidt, A., Jacob, R., Cai, C., Rodepeter, F., Betz, T., Sitterberg, J., Bakowsky, U., Moll, R., et al. (2013). Epidermal growth factor-induced modulation of cytokeratin expression levels influences the morphological phenotype of head and neck squamous cell carcinoma cells. Cell Tissue Res. 351: 59–72.

Marsh, D., Suchak, K., Moutasim, K.A., Vallath, S., Hopper, C., Jerjes, W., Upile, T., Kalavrezos, N., Violette, S.M., Weinreb, P.H., et al. (2011). Stromal features are predictive of disease mortality in oral cancer patients. J. Pathol. 223: 470–481.

Marur, S. and Forastiere, A.A. (2008). Head and neck cancer: changing epidemiology, diagnosis, and treatment. Mayo Clin. Proc. 83: 489–501.

Marur, S. and Forastiere, A.A. (2016). Head and neck squamous cell carcinoma: update on epidemiology, diagnosis, and treatment. Mayo Clin. Proc. 91: 386–396.

McGinn, O., Ward, A.V., Fettig, L.M., Riley, D., Ivie, J., Paul, K.V., Kabos, P., Finlay-Schultz, J., and Sartorius, C.A. (2020). Cytokeratin 5 alters beta-catenin dynamics in breast cancer cells. Oncogene 39: 2478–2492.

Mehrad, M., Dupont, W.D., Plummer, W.D., Jr., and Lewis, J.S., Jr. (2018). Expression and significance of cytokeratin 7, a squamocolumnar junction marker, in head and neck squamous cell carcinoma. Head Neck Pathol. 12: 448–454.

Mehrpouya, M., Pourhashem, Z., Yardehnavi, N., and Oladnabi, M. (2019). Evaluation of cytokeratin 19 as a prognostic tumoral and metastatic marker with focus on improved detection methods. J. Cell. Physiol. 234: 21425–21435.

Mendez, E., Cheng, C., Farwell, D.G., Ricks, S., Agoff, S.N., Futran, N.D., Weymuller, E.A., Jr., Maronian, N.C., Zhao, L.P., and Chen, C. (2002). Transcriptional expression profiles of oral squamous cell carcinomas. Cancer 95: 1482–1494.

Michaelis, M., Voges, Y., Rothweiler, F., Weipert, F., Zia-Ahmad, A., Cinatl, J., von Deimling, A., Westermann, F., Rodel, F., Wass, M.N., et al. (2020). Testing of the survivin suppressant YM155 in a large panel of drug-resistant neuroblastoma cell lines. Cancers (Basel) 12, https://doi.org/10.3390/cancers12030577.

Moll, R., Divo, M., and Langbein, L. (2008). The human keratins: biology and pathology. Histochem. Cell Biol. 129: 705–733.

Morales, S., Velasco, A., Gasol, A., Cordoba, F., Vidal, J., Serrate, A., Valls, J., Samame, J.C., Gisbert, R., Moral, D., et al. (2018). Circulating tumor cells (CTCs) and cytokeratin 19 (CK19) mRNA as prognostic factors in heavily pretreated patients with metastatic breast cancer. Canc. Treat. Res. Commun. 16: 13–17.

Murakami, T., Maki, W., Cardones, A.R., Fang, H., Tun Kyi, A., Nestle, F.O., and Hwang, S.T. (2002). Expression of CXC chemokine receptor-4 enhances the pulmonary metastatic potential of murine B16 melanoma cells. Canc. Res. 62: 7328–7334.

Nagata, M., Fujita, H., Ida, H., Hoshina, H., Inoue, T., Seki, Y., Ohnishi, M., Ohyama, T., Shingaki, S., Kaji, M., et al. (2003). Identification of potential biomarkers of lymph node metastasis in oral squamous cell carcinoma by cDNA microarray analysis. Int. J. Canc. 106: 683–689.

Noorlag, R., van Es, R.J.J., de Bree, R., and Willems, S.M. (2017). Cytokeratin 19 expression in early oral squamous cell carcinoma and their metastasis: inadequate biomarker for one-step nucleic acid amplification implementation in sentinel lymph node biopsy procedure. Head Neck 39: 1864–1868.

Paccione, R.J., Miyazaki, H., Patel, V., Waseem, A., Gutkind, J.S., Zehner, Z.E., and Yeudall, W.A. (2008). Keratin down-regulation in vimentin-positive cancer cells is reversible by vimentin RNA interference, which inhibits growth and motility. Mol. Canc. Therapeut. 7: 2894–2903.

Pavon, N., Martin, A.B., Mendialdua, A., and Moratalla, R. (2006). ERK phosphorylation and FosB expression are associated with L-DOPA-induced dyskinesia in hemiparkinsonian mice. Biol. Psychiatr. 59: 64–74.

Paz, H., Pathak, N., and Yang, J. (2014). Invading one step at a time: the role of invadopodia in tumor metastasis. Oncogene 33: 4193–4202.

Roepman, P., Wessels, L.F., Kettelarij, N., Kemmeren, P., Miles, A.J., Lijnzaad, P., Tilanus, M.G., Koole, R., Hordijk, G.J., van der Vliet, P.C., et al. (2005). An expression profile for diagnosis of lymph node metastases from primary head and neck squamous cell carcinomas. Nat. Genet. 37: 182–186.

Rothenberg, S.M. and Ellisen, L.W. (2012). The molecular pathogenesis of head and neck squamous cell carcinoma. J. Clin. Invest. 122: 1951–1957.

Schaaij-Visser, T.B., Graveland, A.P., Gauci, S., Braakhuis, B.J., Buijze, M., Heck, A.J., Kuik, D.J., Bloemena, E., Leemans, C.R., Slijper, M., et al. (2009). Differential proteomics identifies protein biomarkers that predict local relapse of head and neck squamous cell carcinomas. Clin. Canc. Res. 15: 7666–7675.

Schlingemann, J., Habtemichael, N., Ittrich, C., Toedt, G., Kramer, H., Hambek, M., Knecht, R., Lichter, P., Stauber, R., and Hahn, M. (2005). Patient-based cross-platform comparison of oligonucleotide microarray expression profiles. Lab. Invest. 85: 1024–1039.

Schrenk, C., Fetz, V., Vallet, C., Heiselmayer, C., Schroder, E., Hensel, A., Hahlbrock, A., Wunsch, D., Goesswein, D., Bier, C., et al. (2018). TFIIA transcriptional activity is controlled by a 'cleave-and-run' Exportin-1/Taspase 1-switch. J. Mol. Cell Biol. 10: 33–47.

Schuler, P.J., Laban, S., Doescher, J., Bullinger, L., and Hoffmann, T.K. (2017). Novel treatment options in head and neck cancer. Oncol. Res. Treat. 40: 342–346.

Schweitzer, A., Knauer, S.K., and Stauber, R.H. (2008). Therapeutic potential of nuclear receptors. Expert Opin. Ther. Pat. 18: 861–888.

Schweitzer, A., Knauer, S.K., and Stauber, R.H. (2010). Nuclear receptors in head and neck cancer: current knowledge and perspectives. Int. J. Canc. 15: 801–809.

Sessions, D.G., Spector, G.J., Lenox, J., Haughey, B., Chao, C., and Marks, J. (2002). Analysis of treatment results for oral tongue cancer. Laryngoscope 112: 616–625.

Sethi, N., MacLennan, K., Wood, H.M., and Rabbitts, P. (2015). Past and future impact of next-generation sequencing in head and neck cancer. Head Neck 38: E2395–E2402.

Sharma, R. (2020). Descriptive epidemiology of incidence and mortality of primary liver cancer in 185 countries: evidence from GLOBOCAN 2018. Jpn. J. Clin. Oncol., https://doi.org/10.1093/jjco/hyaa130.

Shi, R., Liu, L., Wang, F., He, Y., Niu, Y., Wang, C., Zhang, X., Zhang, X., Zhang, H., Chen, M., et al. (2020). Downregulation of cytokeratin 18 induces cellular partial EMT and stemness through increasing EpCAM expression in breast cancer. Cell. Signal. 76: 109810.

Siemer, S., Hahlbrock, A., Vallet, C., McClements, D.J., Balszuweit, J., Voskuhl, J., Docter, D., Wessler, S., Knauer, S.K., Westmeier, D., et al. (2018). Nanosized food additives impact beneficial and pathogenic bacteria in the human gut: a simulated gastrointestinal study. NPJ Sci. Food 2: 22.

Siemer, S., Westmeier, D., Barz, M., Eckrich, J., Wunsch, D., Seckert, C., Thyssen, C., Schilling, O., Hasenberg, M., Pang, C., et al. (2019). Biomolecule-corona formation confers resistance of bacteria to nanoparticle-induced killing: implications for the design of improved nanoantibiotics. Biomaterials 192: 551–559.

Siemer, S., Wunsch, D., Khamis, A., Lu, Q., Scherberich, A., Filippi, M., Krafft, M.P., Hagemann, J., Weiss, C., Ding, G.B., et al. (2020). Nano meets micro-translational nanotechnology in medicine: nano-based applications for early tumor detection and therapy. Nanomaterials (Basel) 10(2), https://doi.org/10.3390/nano10020383.

Simpson, D.R., Mell, L.K., and Cohen, E.E. (2015). Targeting the PI3K/AKT/mTOR pathway in squamous cell carcinoma of the head and neck. Oral Oncol. 51: 291–298.

Sprecher, E., Itin, P., Whittock, N.V., McGrath, J.A., Meyer, R., DiGiovanna, J.J., Bale, S.J., Uitto, J., and Richard, G. (2002). Refined mapping of Naegeli–Franceschetti–Jadassohn syndrome to a 6 cm interval on chromosome 17q11.2-q21 and investigation of candidate genes. J. Invest. Dermatol. 119: 692–698.

Stauber, R.H., Rabenhorst, U., Rekik, A., Engels, K., Bier, C., and Knauer, S.K. (2006). Nucleocytoplasmic shuttling and the biological activity of mouse survivin are regulated by an active nuclear export signal. Traffic 7: 1461–1472.

Stauber, R.H., Afonina, E., Gulnik, S., Erickson, J., and Pavlakis, G.N. (1998). Analysis of intracellular trafficking and interactions of cytoplasmic HIV-1 Rev mutants in living cells. Virology 251: 38–48.

Stauber, R.H., Bier, C., and Knauer, S.K. (2012a). Targeting Taspase1 for cancer therapy – letter. Canc. Res. 72: 2912–2913.

Stauber, R.H., Knauer, S.K., Habtemichael, N., Bier, C., Unruhe, B., Weisheit, S., Spange, S., Nonnenmacher, F., Fetz, V., Ginter, T., et al. (2012b). A combination of a ribonucleotide reductase inhibitor and histone deacetylase inhibitors downregulates EGFR and triggers BIM-dependent apoptosis in head and neck cancer. Oncotarget 3: 31–43.

Taichman, R.S., Cooper, C., Keller, E.T., Pienta, K.J., Taichman, N.S., and McCauley, L.K. (2002). Use of the stromal cell-derived factor-1/CXCR4 pathway in prostate cancer metastasis to bone. Canc. Res. 62: 1832–1837.

Takanami, I. (2003). Overexpression of CCR7 mRNA in nonsmall cell lung cancer: correlation with lymph node metastasis. Int. J. Canc. 105: 186–189.

Tenzer, S., Docter, D., Kuharev, J., Musyanovych, A., Fetz, V., Hecht, R., Schlenk, F., Fischer, D., Kiouptsi, K., Reinhardt, C., et al. (2013). Rapid formation of plasma protein corona critically affects nanoparticle pathophysiology. Nat. Nanotechnol. 8: 772–781.

Thompson, L.D.R.W. and Bruce, M. (2016). *Diagnostic pathology: head and neck*. Elsevier, Netherlands.

Thurlow, J.K., Pena Murillo, C.L., Hunter, K.D., Buffa, F.M., Patiar, S., Betts, G., West, C.M., Harris, A.L., Parkinson, E.K., Harrison, P.R., et al. (2010). Spectral clustering of microarray data elucidates the roles of microenvironment remodeling and immune responses in survival of head and neck squamous cell carcinoma. J. Clin. Oncol. 28: 2881–2888.

Torre, L.A., Bray, F., Siegel, R.L., Ferlay, J., Lortet-Tieulent, J., and Jemal, A. (2015). Global cancer statistics, 2012. CA Canc. J. Clin. 65: 87–108.

Toyoshima, T., Vairaktaris, E., Nkenke, E., Schlegel, K.A., Neukam, F.W., and Ries, J. (2008). Cytokeratin 17 mRNA expression has potential for diagnostic marker of oral squamous cell carcinoma. J. Canc. Res. Clin. Oncol. 134: 515–521.

Tribius, S., Wurdemann, N., Laban, S., Hoffmann, T.K., Sharma, S.J., and Klussmann, J.P. (2019). Update on HPV-associated head and neck cancer-highlights from the 2019 ASCO annual meeting. HNO 67: 912–917.

Tzanakakis, G., Kavasi, R.M., Voudouri, K., Berdiaki, A., Spyridaki, I., Tsatsakis, A., and Nikitovic, D. (2018). Role of the extracellular matrix in cancer-associated epithelial to mesenchymal transition phenomenon. Dev. Dynam. 247: 368–381.

Tzanakakis, G., Neagu, M., Tsatsakis, A., and Nikitovic, D. (2019). Proteoglycans and immunobiology of cancer-therapeutic implications. Front. Immunol. 10: 875.

Tzanakakis, G., Giatagana, E.M., Kuskov, A., Berdiaki, A., Tsatsakis, A.M., Neagu, M., and Nikitovic, D. (2020).

Proteoglycans in the pathogenesis of hormone-dependent cancers: mediators and effectors. Cancers (Basel) 12(9), https://doi.org/10.3390/cancers12092401.

Uchida, D., Begum, N.M., Almofti, A., Nakashiro, K., Kawamata, H., Tateishi, Y., Hamakawa, H., Yoshida, H., and Sato, M. (2003). Possible role of stromal-cell-derived factor-1/CXCR4 signaling on lymph node metastasis of oral squamous cell carcinoma. Exp. Cell Res. 290: 289–302.

Uchida, D., Begum, N.M., Tomizuka, Y., Bando, T., Almofti, A., Yoshida, H., and Sato, M. (2004). Acquisition of lymph node, but not distant metastatic potentials, by the overexpression of CXCR4 in human oral squamous cell carcinoma. Lab. Invest. 84: 1538–1546.

van't Veer, L.J., Dai, H., van de Vijver, M.J., He, Y.D., Hart, A.A., Mao, M., Peterse, H.L., van der Kooy, K., Marton, M.J., Witteveen, A.T., et al. (2002). Gene expression profiling predicts clinical outcome of breast cancer. Nature 415: 530–536.

Wahbi, W., Naakka, E., Tuomainen, K., Suleymanova, I., Arpalahti, A., Miinalainen, I., Vaananen, J., Grenman, R., Monni, O., Al-Samadi, A., et al. (2020). The critical effects of matrices on cultured carcinoma cells: human tumor-derived matrix promotes cell invasive properties. Exp. Cell Res. 389: 111885.

Weng, Y.R., Cui, Y., and Fang, J.Y. (2012). Biological functions of cytokeratin 18 in cancer. Mol. Canc. Res. 10: 485–493.

Westmeier, D., Hahlbrock, A., Reinhardt, C., Frohlich-Nowoisky, J., Wessler, S., Vallet, C., Poschl, U., Knauer, S.K., and Stauber, R.H. (2018a). Nanomaterial-microbe cross-talk: physicochemical principles and (patho)biological consequences. Chem. Soc. Rev. 47: 5312–5337.

Westmeier, D., Posselt, G., Hahlbrock, A., Bartfeld, S., Vallet, C., Abfalter, C., Docter, D., Knauer, S.K., Wessler, S., and Stauber, R.H. (2018b). Nanoparticle binding attenuates the pathobiology of gastric cancer-associated *Helicobacter pylori*. Nanoscale 10: 1453–1463.

Westmeier, D., Siemer, S., Vallet, C., Steinmann, J., Docter, D., Buer, J., Knauer, S.K., and Stauber, R.H. (2020). Boosting nanotoxicity to combat multidrug-resistant bacteria in pathophysiological environments. Nanoscale Adv. 2: 5428–5440.

Wiley, H.E., Gonzalez, E.B., Maki, W., Wu, M.T., and Hwang, S.T. (2001). Expression of CC chemokine receptor-7 and regional lymph node metastasis of B16 murine melanoma. J. Natl. Canc. Inst. 93: 1638–1643.

Wu, S., Law, A., and Whipple, M.E. (2017). A Bayesian network model of head and neck squamous cell carcinoma incorporating gene expression profiles. Stud. Health Technol. Inf. 245: 634–638.

Wunsch, D., Fetz, V., Heider, D., Tenzer, S., Bier, C., Kunst, L., Knauer, S., and Stauber, R. (2012). Chemico-genetic strategies to inhibit the leukemic potential of threonine aspartase-1. Blood Canc. J. 2: e77.

Wunsch, D., Hahlbrock, A., Heiselmayer, C., Backer, S., Heun, P., Goesswein, D., Stocker, W., Schirmeister, T., Schneider, G., Kramer, O.H., et al. (2015a). Fly *versus* man: evolutionary impairment of nucleolar targeting affects the degradome of Drosophila's Taspase1. FASEB J. 29: 1973–1985.

Wunsch, D., Hahlbrock, A., Heiselmayer, C., Bäcker, S., Schrenk, C., Benne, F., and Knauer, S. (2015b). Evolutionary divergence of Threonine Aspartase1 leads to species-specific substrate recognition. Biol. Chem. 396: 367–376.

Xu, E.S., Yang, M.H., Liu, C.Y., Liu, K.W., Yang, T.T., Chou, T.Y., Hwang, T.Z., and Hsu, C.T. (2018). Decreasing cytokeratin 17 expression in head and neck cancer predicts nodal metastasis and poor prognosis: the first evidence. Clin. Otolaryngol. 43(4): 1010–1018.

Yang, X.R., Xu, Y., Shi, G.M., Fan, J., Zhou, J., Ji, Y., Sun, H.C., Qiu, S.J., Yu, B., Gao, Q., et al. (2008). Cytokeratin 10 and cytokeratin 19: predictive markers for poor prognosis in hepatocellular carcinoma patients after curative resection. Clin. Canc. Res. 14: 3850–3859.

Zivicova, V., Gal, P., Mifkova, A., Novak, S., Kaltner, H., Kolar, M., Strnad, H., Sachova, J., Hradilova, M., Chovanec, M., et al. (2018). Detection of distinct changes in gene-expression profiles in specimens of tumors and transition zones of tenascin-positive/-negative head and neck squamous cell carcinoma. Anticanc. Res. 38: 1279–1290.

Supplementary Material: The online version of this article offers supplementary material (https://doi.org/10.1515/hsz-2021-0287).

IV.

cancers

MDPI

Article

Impact of Secretion-Active Osteoblast-Specific Factor 2 in Promoting Progression and Metastasis of Head and Neck Cancer

Désirée Gül [1,*], Andrea Schweitzer [1], Aya Khamis [1,2], Shirley K. Knauer [3], Guo-Bin Ding [4], Laura Freudelsperger [1], Ioannis Karampinis [5], Sebastian Strieth [6], Jan Hagemann [1] and Roland H. Stauber [1,4,*]

1 Department of Otorhinolaryngology, Head and Neck Surgery, Molecular and Cellular Oncology, University Medical Center, 55131 Mainz, Germany; andrea.schweitzer@gmx.de (A.S.); ayakhamis@uni-mainz.de (A.K.); laura.freudelsperger@unimedizin-mainz.de (L.F.); jan.hagemann@unimedizin-mainz.de (J.H.)
2 Oral Pathology Department, Faculty of Dentistry, Alexandria University, El Azareta, Alexandria, Egypt
3 Institute for Molecular Biology, Centre for Medical Biotechnology (ZMB), University Duisburg-Essen, Universitätsstraße, 45117 Essen, Germany; shirley.knauer@uni-due.de
4 Institute of Biotechnology, The Key Laboratory of Chemical Biology and Molecular Engineering of Ministry of Education, Shanxi University, Taiyuan 030006, China; dinggb2012@sxu.edu.cn
5 Academic Thoracic Center, University Medical Center, 55131 Mainz, Germany; ioannis.karampinis@unimedizin-mainz.de
6 Department of Otorhinolaryngology, University Medical Center Bonn, 53127 Bonn, Germany; sebastian.strieth@ukbonn.de
* Correspondence: guel@uni-mainz.de (D.G.); rstauber@uni-mainz.de (R.H.S.); Tel.: +49-0-6131176030 (D.G.)

Simple Summary: Head and neck cancers (HNC) exhibit poor survival due to metastases. Our study identified osteoblast-specific factor 2 (OSF-2) as overexpressed in primary tumors, lymph node metastases, and the tumor microenvironment. High OSF-2 levels correlate with metastatic disease and reduced survival of HPV-negative HNC patients. OSF-2's active secretion signal seems to promote metastases by supporting the tumor microenvironment via the ß1 integrin-induced PI3K and Akt/PKB signaling pathway. We suggest OSF-2 as a potential biomarker and drug target to control (HPV-negative) HNC metastasis and disease management.

Abstract: Treatment success of head and neck cancer (HNC) is still hampered by tumor relapse due to metastases. Our study aimed to identify biomarkers by exploiting transcriptomics profiles of patient-matched metastases, primary tumors, and normal tissue mucosa as well as the *TCGA* HNC cohort data sets. Analyses identified osteoblast-specific factor 2 (OSF-2) as significantly overexpressed in lymph node metastases and primary tumors compared to normal tissue. High OSF-2 levels correlate with metastatic disease and reduced overall survival of predominantly HPV-negative HNC patients. No significant correlation was observed with tumor localization or therapy response. These findings were supported by the fact that OSF-2 expression was not elevated in cisplatin-resistant HNC cell lines. OSF-2 was strongly expressed in tumor-associated fibroblasts, suggesting a tumor microenvironment-promoting function. Molecular cloning and expression studies of OSF-2 variants from patients identified an evolutionary conserved bona fide protein secretion signal (^{1}MIPFLPMFSLLLLLIVNPINA^{21}). OSF-2 enhanced cell migration and cellular survival under stress conditions, which could be mimicked by the extracellular administration of recombinant protein. Here, OSF-2 executes its functions via ß1 integrin, resulting in the phosphorylation of PI3K and activation of the Akt/PKB signaling pathway. Collectively, we suggest OSF-2 as a potential prognostic biomarker and drug target, promoting metastases by supporting the tumor microenvironment and lymph node metastases survival rather than by enhancing primary tumor proliferation or therapy resistance.

Keywords: metastases; HPV; biomarker; therapy resistance; methylation; oral cancer; protein secretion

Citation: Gül, D.; Schweitzer, A.; Khamis, A.; Knauer, S.K.; Ding, G.-B.; Freudelsperger, L.; Karampinis, I.; Strieth, S.; Hagemann, J.; Stauber, R.H. Impact of Secretion-Active Osteoblast-Specific Factor 2 in Promoting Progression and Metastasis of Head and Neck Cancer. *Cancers* **2022**, *14*, 2337. https://doi.org/10.3390/cancers14092337

Academic Editors: Eldad Zacksenhaus and Sean Egan

Received: 17 March 2022
Accepted: 5 May 2022
Published: 9 May 2022

1. Introduction

Head and neck cancers (HNC) are among the most common malignant neoplasms in humans [1,2]. The most common entity of HNC is solid squamous cell carcinoma (HNSCC) which is the sixth most malignant tumor worldwide with 890,000 new cases yearly and 450,000 deaths in 2018 [3]. Major risk factors associated with the development of HNC are tobacco use, alcohol consumption, and high-risk human papillomavirus infections (HPV) [2]. HNC occurs in 50% of patients with locoregional invasion and lymph node metastases [4]. Along with the late disease presentation, lack of suitable biomarkers, and corresponding drugs for individually targeted therapy approaches this is the reason that survival rates for HNC have not improved significantly within the last years [5–7]. In cases of developed distant metastases, HNC patients have a 5-year survival rate of less than 20% [8]. Furthermore, it is presumed that the presence of micrometastases leads to enhanced mortality and morbidity. A huge number of cancer deaths are caused by the haematogenous spread of cancer cells into distant organs in combination with metastases development [9,10]. Metastatic spread was often described as a late process in malignant progression, but recent work about breast cancer progression suggested that the dissemination of primary cancer cells to distant sites seems to be an early event [11,12]. Thus, the early formation of micrometastases might also play an important role in HNC tumorigenesis and progression, which need to be understood on the molecular and clinical levels.

The main prognostic parameters of head and neck squamous cell carcinoma are the location and size of the tumor, the presence of distant metastases, and the presence of cervical lymph node metastases [13]. However, since the prognosis according to the TNM classification is not sufficient to evaluate the disease outcome [14], there is a need to identify molecular biomarkers with prognostic and diagnostic relevance. Microarray gene expression studies suggested gene expression signatures associated with recurrent disease in HNC [15], or genes with diagnostic or prognostic potential [1,7,16–18].

A variety of factors, genetic as well as epigenetic, have been associated with the complex process of (HNC) metastasis. For example, among the list of frequently altered genes by methylation in HNC are also proteins responsible for cellular adhesion, migration, and extracellular matrix degradation such as APC, CDH1, SPP1, and TIMP3 [19,20]. We refer the interested reader to some detailed reviews [11,21–25]. Enhancing tumor metastasis can be influenced by increasing (local) tumor cell proliferation or/and by increasing the cell's capability to migrate and survive in distant 'hostile' microenvironments. Here, a variety of proteases, anti-apoptotic proteins, and matricellular proteins, such as osteopontin have been suggested to impact metastasis [26–30]. However, in most cases, such proteins are not solely involved in metastasis but also impact tumorigenesis.

Regarding the tumor microenvironment, so called 'niche proteins' regulate various functions in the tumor-associated bed [31–35]. Cancer cells detach from the primary solid tumor and intravasate into the peripheral blood system to form new metastatic sites. Moreover, tumor cells in the bone marrow seem to form an important reservoir of cancer cells from which they also may re-circulate into other distant organs [36].

In this study, we identified OSF-2 up-regulation in a series of human HNC tumors and their corresponding metastases and normal tissue. The 93 kDa glycoprotein OSF-2 was originally identified as an adhesion molecule involved in bone formation, regulating differentiation of osteoblasts, and preferentially expressed in periosteum in bone tissues [37,38]. The OSF-2 protein was described to be composed of an N-terminal EMI domain (EMILIN family domain, cysteine-rich), a tandem repeat of four fas1 domains allowing binding of integrins, and glycans [39], and a carboxyl-terminal domain that includes a heparin-binding site [40]. Due to structure and sequence homologies, OSF-2 was classified as a member of the fasciclin 1 family [38]. In addition to OSF-2, the group of FAS1-similar proteins contains also βigh3 [41], stabilin I and II [42], and periostin-like-factor (PLF) [43]. However, the molecular functions of the predicted domains are not fully understood. In addition, OSF-2 was also found to be under- or overexpressed in various human cancers and other diseases [44–47]. Despite its history, the tumor-promoting or tumor-suppressing functional

relevance of OSF-2 in cancer development and metastasis in the quite heterogeneous field of solid and liquid malignancies is still controversially discussed.

Here, our bioinformatic results regarding *OSF-2* up-regulation in HNC were independently verified on the mRNA and protein levels. To investigate the source of OSF-2 production, we isolated human HNC cancer cells and tumor-associated fibroblasts and found OSF-2 expression significantly upregulated in tumor-associated fibroblasts. We further analyzed OSF-2 isoform expression signatures in tumors, their corresponding lymph node metastases, and normal tissue as well as expression signatures in tumor cells and corresponding tumor-associated fibroblasts. We identified OSF-2 as a secreted protein, crucial for cell migration and survival under stress conditions via ß1 integrin-induced PI3K and Akt/PKB signaling pathway, classifying OSF-2 as a 'tumor niche' protein' in HNC.

2. Materials and Methods

2.1. Antibodies, Chemicals, and Reagents

Ab used: α-OSF-2 (Biovendor, Heidelberg, Germany), α-GAPDH (sc-47724; Santa Cruz Biotechnology, Heidelberg, Germany), α-GFP (sc-8334; Santa Cruz Biotechnology, Heidelberg, Germany) α-Lamin B1 (NEB, Darmstadt, Germany), anti-Actin (A2066; Sigma Aldrich, Munich, Germany), anti-Vimentin (V9; Fisher Scientific, Schwerte, Germany), anti-p-Akt (9271; NEB, Darmstadt, Germany), anti-γH2AX (A300-081A, Bethyl Laboratories, Montgomery, TX, USA). Appropriate HRP-, Cy3- or FITC-conjugated secondary antibodies (Sigma Aldrich, Munich, Germany; Santa Cruz Biotechnology, Heidelberg, Germany) were used. Recombinant OSF-2 (RD1720450, sequence in Supplementary Table S5) was purchased from BioVendor, Heidelberg, Germany. PI3K-inhibitor (LY294002, Cat. No. 9901) was purchased from Cell Signalling Technology, Danvers, MA, USA. Reagents, such as cisplatin were from Sigma (Sigma Aldrich, Munich, Germany) or MSC (MSC UG&CoKG, Mainz, Germany) unless stated otherwise.

2.2. Cell Culture and OSF-2 Secretion

Authenticated and characterized cell lines (Fadu, SU8686, 1624, HOB18, Pancl, Carey24, MG63, HeLa, HEK293T were purchased from the *ATCC* repository, expanded, stocks prepared at early passages, and frozen stocks kept in liquid nitrogen. Thawed cells were routinely monitored by visual inspection and growth-curve analyses to keep track of cell-doubling times, and were used for a maximum of 20 passages for all experiments. Depending on the passage number from purchase, cell line authentication was further performed at reasonable intervals by short tandem repeat (STR) profiling. The Pica cell line was initially established from laryngeal squamous cell carcinoma as described by Siemer et al. [48]. The HNSCCUM-02T squamous cell carcinoma cell line was established by Welkoborsky et al. [49] and maintained as described before [50]. To avoid contamination Hela and HEK293T cells are cultivated and maintained physically separately. For primary tumor cell and CAF isolation, ethical approval has been obtained for the collection and use of HNC tumor biopsies. Primary tumor cells and CAFs were isolated from an independent patient cohort. For the isolation of primary cancer cells or CAFs, specimens were cut into pieces and enzymatically digested with collagenase type I/hyaluronidase (Sigma Aldrich, Munich, Germany) in RPMI-1640 (Invitrogen, Karlsruhe, Germany) at 37 °C overnight. Following digestion, dissociated cells were passed through a cell strainer, and epithelial cells were isolated by MACS®separation using CD326 (EpCAM) MicroBeads (Miltenyi Biotec GmbH, Bergisch Gladbach, Germany) according to the manufacturer's recommendations. Cells were propagated for one week as [1] and subjected to analysis.

For the detection of secreted OSF-2 protein, HEK293T cells were grown in a normal medium until 70% confluency. Twelve hours after OSF-2-transfection cells were washed and the medium was replaced by 1% FCS containing medium for 24 h. The medium was harvested and analyzed by immunoblot.

To prepare the conditioned medium, HEK293T cells were transfected with OSF-2, incubated for 12 h, and the medium was exchanged containing 1% FCS. After 24 h incubation, the conditioned medium was collected, either used directly or stored at −80 °C.

2.3. Microarray Analysis

Global examination of gene expression was performed with an Affymetrix HG-U133A array (Affymetrix, Santa Clara, CA, USA) using standard conditions (16 h, 45 °C) as described [1,2]. Arrays were washed and stained in a Fluidics Station 400 (Affymetrix) and scanned on a Gene Array Scanner 2500 (Agilent, Santa Clara, CA, USA). Raw fluorescence intensities from all hybridizations were normalized by applying variance stabilization with additional scaling. MAS5 and gcRMA expression values were calculated. Data and cluster analyses were performed using Affymetrix Microarray Suite 5.0 (MAS5) and GeneSpring GX software. Probes were made from total RNA following the guidelines given in the Affymetrix GeneChip Expression Analysis Technical Manual. An amount of 10 µg of fragmented, labelled cDNA was used for hybridization [1,2].

2.4. Clinical Data Analysis

Publicly available gene expression and survival data sets were obtained from the Cancer Genome Atlas (TCGA) filtering for patients with HNCs (TCGA HNSC). A total of n = 612 patients were included, and data were analyzed as described before [48]. For detailed patient characteristics, see also Supplementary Table S2. Data was assessed via the USCS Xena server [51] and patients were grouped according to indicated phenotypic or clinical characteristics. Final visualizations and statistical analyses were performed with Graphpad Prism. Furthermore, methylation analysis was performed using the MEXPRESS online tool [52]. Analysis of single-nucleotide variations was performed with the BioMuta v4.0 online tool [53].

2.5. Microscopy, Fluorescence Imaging, and Quantitation of Cells

Observation, quantitation, image analysis, and presentation were performed using Axiovert 200 M fluorescence microscope (Zeiss, Jena, Germany) as described [48,54,55]. To determine the average number of cells showing p-Akt staining, at least 200 fluorescent cells from three separate images were examined, visually inspected, and counted. Immunofluorescence staining of γH2AX was performed as reported in detail [48].

2.6. RNA Extraction, Reverse Transcription (RT)-PCR, and Quantitative Real-Time PCR Analysis

Total RNA was purified, and first-strand cDNA synthesis was carried out using a cDNA synthesis kit (Superscript II, Invitrogen life technologies). An amount of 1 µg of total RNA was converted to cDNA and 1 µL of the produced cDNA was amplified for 30 cycles (initial denaturation at 95 °C for 3 min, 30 s at 95 °C, 30 s at a variable temperature for annealing, and 1 min at 72 °C) followed by an extension of 5 min at 72 °C (for primer sequences please see Table S4). RT-PCR amplification products were analyzed on 2% agarose gels stained with ethidium bromide. GAPDH was used as a control.

Quantitative real-time PCR analysis was performed using the LightCycler® 1.5 (Roche, Switzerland). PCR reaction mixtures consisted of 4 µL of LC FastStart DNA Master^{plus} SYBER® Green Supermix (Roche, Basel, Switzerland), 50 ng of each target primer, and 2 µL cDNA template in a final reaction volume of 20 µL. Thermal cycling for OSF-2 was performed as follows: (95 °C, 600 s; 40 × (95 °C, 10 s; 62 °C, 5 s; 72 °C, 5 s); 72 °C to 95 °C melting curve analysis). Thermal cycling for RNA-PolII (housekeeping gene control) was performed as follows: (95 °C, 600 s; 40 × (95 °C, 10 s; 60 °C, 15 s; 72 °C, 15 s); 72 °C to 95 °C melting curve analysis). Cumulative fluorescence was measured at the end of the extension phase of each cycle. Specific amplicon formation with each primer pair was confirmed by melting curve analysis and by visualization of a single band on a 2% agarose gel. For primer sequences please see Table S4.

To define the relative expression of OSF-2 in CAFs, the results from the CAF sample were compared with the results from primary tumor cells. The relative expression ratio (R) of OSF-2 is calculated using the equation: Ratio = $(E_{target})^{\Delta Cp\ target(control-sample)} / (E_{ref})^{\Delta Cpref(control-sample)}$ based on its real-time PCR efficiencies (E = 1.5) and the crossing point (CP) difference of CAF sample versus PT and expressed relative to the non-regulated housekeeping gene (PolII), as described.

2.7. Study Population, Tissue Preparation, and Immunohistochemistry (IHC)

Investigations were conducted in accordance with the ethical standards according to the Declaration of Helsinki as well as according to local, national, and international guidelines as described [14]. Tissue samples were obtained from patients undergoing surgical resection at the department of otolaryngology of the Universities of Mainz. The study protocol has been approved by the local ethics committee (#83756604) after obtaining the patients' informed consent to participate in the study and was processed anonymously. Cases were clinically and histologically diagnosed according to established criteria including grading and TNM classification [14]. All experiments were performed in accordance with relevant laws and the University Medical Center Mainz Guidelines and approved by the institutional ethics committee. In this study, tumor specimens, corresponding non-malignant tissue, and lymph node metastases were analyzed. Tissue samples were fixed and paraffin-embedded (FFPE) as described [56]. Tissues were processed for IHC as described [57,58]. Antigen retrieval was performed in a pressure cooker (sodium citrate, 10 mM, pH 6.0). For visualization of human OSF-2 protein (polyclonal α-OSF-2 Ab-diluted 1:150), the EnVision® detection system (Dako GmbH) was used as described [57,58]. Sections were counterstained with hematoxylin. Negative control slides without primary Ab were included for each staining [56].

2.8. Plasmids and Sequence Analyses

To construct an OSF-2 expression plasmid, cDNA was isolated out of HNC cancer cell lines, and the full open reading frame of human OSF-2 cDNA was cloned into pcDNA3.1 mammalian expression vector (Invitrogen) with C-terminal GFP-tag (for primer sequences please see Table S4). The cloned variant of OSF-2 (referred to as full-length) corresponds to published isoform3 (Q15063-3) lacking exons 17 and 21. The plasmid was introduced into cells as described before [56,58]. Secretion-GFP was generated by the insertion of the OSF-2 secretion signal (aa1-21) into pc3-GFP. The OSF-2 secretion mutant ΔSec-GFP was amplified from full-length OSF-2-GFP and cloned into pc3-GFP using SacII/NheI-restriction sites. For sequencing the C-terminus of OSF-2, cDNA was amplified (for 5′-CACCTGACACCAGGAGTTTTC-3′; rev 5′-AAAGCTAGCCTGAGAACGACCTTCCCTTAATC-3′), cloned in a pGEM T easy Vector System (Promega, Madison, WI, USA), and several clones were sequenced (Genterprise, Mainz). RNA sequencing (RNASeq) was then performed as described in [59] and visualizations were achieved with the help of Graphpad Prism.

2.9. Protein Extraction, Immunoblot Analysis

Preparation of whole cell lysates was carried out as described using a low salt lysis buffer (50 mM Tris pH8.0, 150 mM NaCl, 5 mM EDTA, 0.5%NP-40, 1 mM DTT, 1 mM PMSF, complete EDTA-free from Roche Diagnostics, Mannheim, Germany) [58]. Preparation of cell lysates for phospho-staining was carried out according to the supplier's recommendation. Subcellular fractionation was performed using the Qproteome Cell Compartment Kit (Qiagen, Valencia, CA, USA) according to the supplier's recommendation. Fractions were analyzed by Western blotting. The purity of the fractions was determined using α-lamin B1 (nucleus), α-GAP-DH (cytosol), and α-Vimentin (membrane, cytoskeleton) Abs. equal loading of lysates was controlled by reprobing blots for housekeeping genes (actin, GAPDH). At least $n = 2$ biological replicates were performed and representative results are shown. Results of densitometric analyses of all Western blots can be found in the supplementary.

2.10. Cellular Assays

The scratch assay was performed using Ibidi culture inserts and the TScratch-software. Briefly, 7×10^3 cells were seeded into each insert chamber, and after 24 h the insert was removed, the medium was replaced and pictures of the dish were taken every 30 min for 12 h.

To measure cell viability, cells were incubated with 100 ng/mL of-2 in 1% FCS-containing medium or 1% FCS-containing medium for 4 days. The medium was replaced every 24 h and cell viability was examined using the CellTiter-Glo Luminescent Cell Viability Assay (Roche, Mannheim) according to the manufacturer's instruction. Luminescent signals were recorded using a Tecan Spark® (Tecan, Männedorf, Switzerland) and normalized to untreated controls. For 3D assays, spheroids were grown in 96-well round bottom, ultra-low adhesion cell culture plates (Corning, New York, NY, USA; 1000 cells/well), and initial spheroid formation was allowed for 3 days. Spheroids were either treated (n = 4) with cisplatin and viability probed as described above, or observed for 10 days to determine clonogenicity.

For colony formation assay, 100 cells per ml were seeded in T-25 flasks (n = 24) and grown for 8–10 days. Colonies were fixed with 4% PFA, stained with Giemsa for 5 h at RT, washed with water, and counted using COLCOUNT™ (Oxford Optronix).

Matrigel invasion assay was performed using transiently transfected HeLa cells. A volume of 50–100 µL diluted matrigel (BD Bioscience, Billerica, MA, USA) was pipetted into the upper chamber of the 24-well transwell (Falcon BD, 8 µm pore size). Twenty-four hours after transfection, 1×10^5 cells were seeded in 100 µL of cell suspension in a medium with 1% FCS into the upper chamber of the transwell. After gelling at 37 °C for at least 4–5 h, the lower chamber was filled with 10% FCS medium and incubated at 37 °C. Cells were observed for 4 days.

2.11. Xenograft Experiments

All animal work has been conducted according to relevant national and international guidelines. All animal experiments were approved by the Institutional Animal Care and Use Committee at the University of Mainz. Equal numbers (1×10^6/animal) of stably OSF-2-GFP-expressing A431 cells and control cells were subcutaneously injected into both flanks of four-week-old female MRI nu/nu mice (Harlan Winkelmann, Hamburg, Germany) as described [1,60,61]. Six mice per group were used for three groups (Vector control/OSF-GFP wt/ΔSec-OSF-GFP). Tumor growth was monitored using calipers to calculate tumor volumes with the formula: length $\times$ π width^2 $\times$ 0.52. Animals were euthanized at the end of the study.

2.12. Statistical Analysis

Statistical analyses were performed using Graphpad Prism (version 9.3.1) as described before [48]. Survival data were assessed via the USCS Xena server, visualized, and analyzed by Graphpad Prism (Log-rank/Mantel-Cox test; Hazard Ratio (Mantel-Haenszel)). For two groups, a paired or unpaired Student's t-test, for more groups analysis of variance (ANOVA) was performed. Unless stated otherwise, p values represent data obtained from two independent experiments performed in triplicate. Statistical significance is represented in figures as follows: * $p < 0.05$, ** $p < 0.01$, *** $p < 0.001$, **** $p < 0.0001$, and n.s. indicates not significant. A p-value that was less than 0.05 was considered statistically significant.

3. Results

3.1. OSF-2 Is Overexpressed in HNC Primary Tumors and Lymph Node Metastases

HNC shows huge heterogeneity in their pathobiological and clinical behavior, which cannot yet be reliably predicted using current biomarkers. Hence, the identification of new biomarkers/drug targets to monitor disease progression, survival predictions, and therapies is of key interest [1,7,48,61,62].

To identify genes differentially expressed in HNC primary tumors (PT) versus lymph node metastases (LN M) and the corresponding non-malignant tissue (N), we report transcriptomics data from 15 patients undergoing surgical resection (for clinical and pathological characteristics and a list of differentially expressed genes see Supplementary Tables S1 and S3). In contrast to other studies, in which variations in individual patients require the analysis of a large number of unmatched samples to increase the relevance of the obtained data sets, our study focused on a patient cohort from which PT, N, and LN M could be obtained from the same patient. Notably, although the TCGA HNC data set comprises in total of 528 tumor tissues and 82 non-matched non-malignant tissues, the collection contains full experimental data from only two LN M, limiting the bioinformatic identification of pathways relevant for metastases.

In our data set, OSF-2 was identified among the top genes significantly up-regulated in PT versus N and LN M (Table S3; Figure 1A). Microarray results showed a metastases/normal (LN M/N) ratio that was even higher than the tumor/normal (PT/N) ratio (Figure 1A), suggesting the relevance of OSF-2 for metastases. We did not observe an additional increase in OSF-2 levels in PT/LN M, indicating that OSF-2 function seems to be important to maintain rather than to initiate metastatic growth. Although bioinformatic results are the first important step for the identification of potential biomarkers, it is necessary to carefully confirm obtained insights through independent experiments on the RNA and protein levels. Thus, RT-PCR, as well as Western blot analysis, was performed in tissues of our cohort used for microarray analyses, confirming OSF-2 up-regulation (Figure 1C,D).

When we further analyzed the expression and clinical relevance of OSF-2 by exploiting the *TCGA* HNC data set, comprising 612 cancer patients of various disease states and clinical backgrounds, we also found OSF-2 significantly upregulated in PT versus N (Supplementary Figure S1). As the HPV status influences clinical response and overall survival, we examined HPV-negative versus HPV-positive patients. Interestingly, high OSF-2 expression correlated with poor overall survival of HPV-negative HNC patients ($n = 75$; $p = 0.05$) (Figure 1B). Of note, these data support the transcriptomics data, which were also obtained from HPV-negative patients. In contrast, high OSF-2 expression did not correlate with poor survival in HPV-positive HNC patients (data not shown, $n = 39$; $p < 0.05$). However, caution is advised in this conclusion due to the small sample size available for the statistical analysis. We recommend additional investigations in larger patient cohorts in follow-up studies to evaluate the impact of HPV infection on OSF-2 expression and pathobiology.

Despite the wealth of clinical data, the TCGA HNC data set comprises transcriptomics data from only two LN M (patients are classified as N2a). Still, comparing OSF-2 levels in these samples supports our hypothesis that OSF-2 function seems to be important to maintain rather than drive metastatic growth (OSF-2 levels: TCGA-KU-A6H7-01 (PT) 9.56; TCGA-KU-A6H7-06 (matched LN M) 9.108; TCGA-UF-A71A-01 (PT) 14.23; TCGA-UF-A71A-06 (matched LN M) 13.63).

Interestingly, survival analysis indicated a correlation of OSF-2 expression with the HPV status of the tumor. OSF-2 was significantly increased in HPV negative compared to positive tumors (Figure 2A). Moreover, high OSF-2 expression correlated with markers of metastatic diseases, such as increased perineural infiltration, extracapsular spread, or lymph node metastases (pathological status; pLNx) (Figure 2B–D). Here, patients classified with pLN3 express significantly higher amounts of OSF-2 compared to pLN0 patients (Figure 2D). In contrast, OSF-2 expression did not correlate with HNC tumor localization, such as oral cavity, larynx, oro-, or hypopharynx (Supplementary Figure S2).

As DNA methylation belongs to crucial epigenetic mechanisms controlling transcriptional processes in many cancers, including HNC [20,63], we bioinformatically examined the OSF-2 gene methylation status. Using the MEXPRESS analysis tool [52], the data from the six CpG sites covered in the *TCGA* cohort ($n = 612$; PT = 528; LN M = 2; N = 82), demonstrated that PT showed significantly lower methylation levels compared to N correlating with increased OSF-2 expression in PT versus N (Supplementary Figure S3A). Further-

more, the OSF-2 methylation status correlated with the HPV status of the patients. Here, HPV-positive tumors exhibited increased CpG methylation (Supplementary Figure S3B). These results suggest that reduced gene methylation may at least be partially responsible for increased OSF-2 levels in HPV negative HNC tumors and non-malignant tissue.

In addition to OSF-2, also other matricellular proteins, such as osteopontin (SPP1), were suggested to impact HNC tumorigenesis and metastases [28,29]. However, in contrast to OSF-2, we did not observe a significant correlation between osteopontin expression with overall patient survival (Supplementary Figure S4). Consequently, we here focused on OSF-2 in our experimental pipeline.

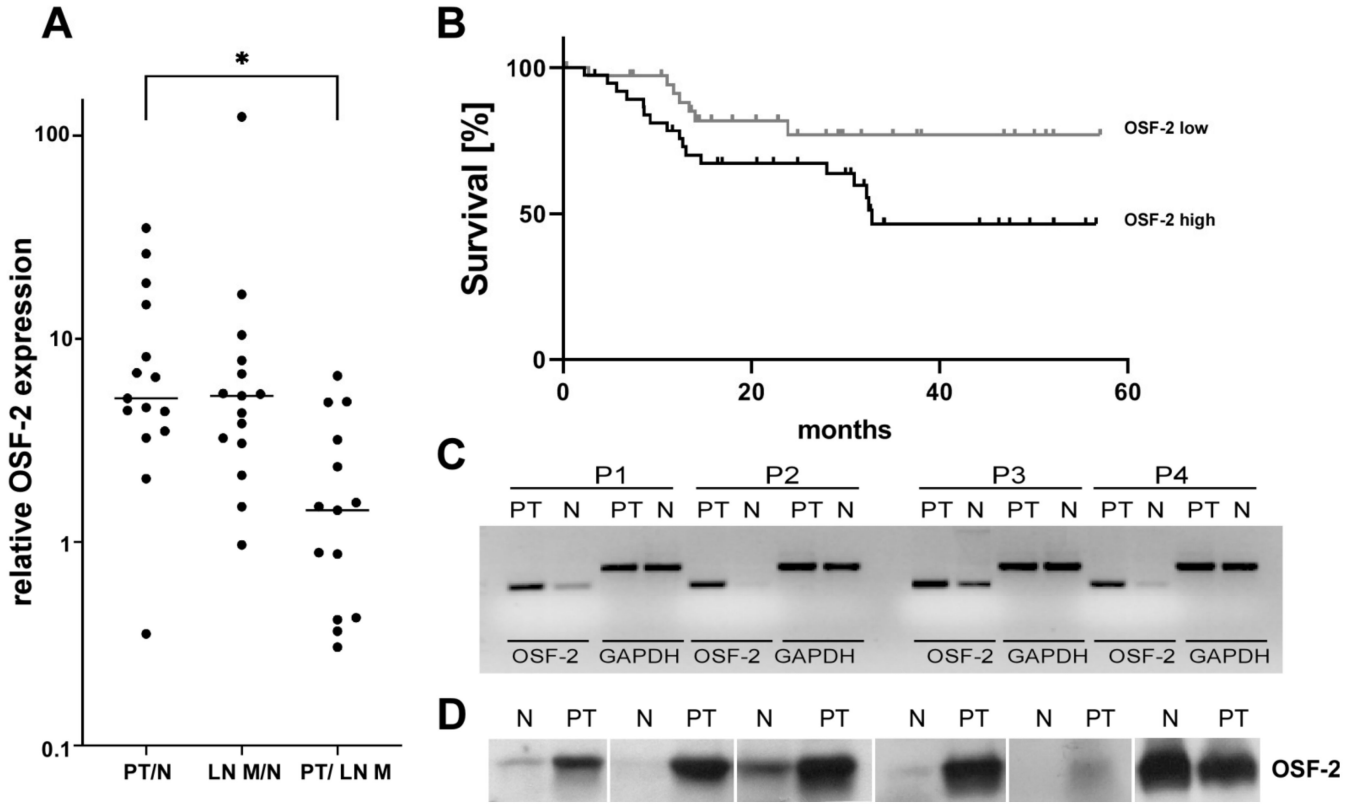

Figure 1. OSF-2 is significantly overexpressed in primary and metastatic HNCs. (**A**) RNA microarray analyses revealed at least 5-fold median overexpression of OSF-2 in the primary tumor (PT) versus normal tissue (N), as well as in lymph node metastases (LN M) versus N. PT versus LN M ratio indicated no further increase in OSF-2 expression in LN M (left). $n = 15$, * $p < 0.05$. (**B**) Survival analysis demonstrates that high OSF-2 expression levels correlate with reduced overall survival of HPV negative HNC patients; $n = 75$; $p < 0.05$. Hazard Ratio (Mantel-Haenszel) = 2.230. OSF-2 low < 12.3 (median), and OSF-2 high $\geq$ 12.3. (**C**) OSF-2 overexpression in PT versus N was confirmed by RT-PCR. OSF-2 up-regulation is shown in four representative cases (demographics see Table S1). GAPDH was used as a control. (**D**) Verification of OSF-2 microarray results on the protein level ($n = 6$). Higher expression of OSF-2 protein was found in PT versus N in five out of six representative cases. The uncropped western blot figures were presented in Figure S9.

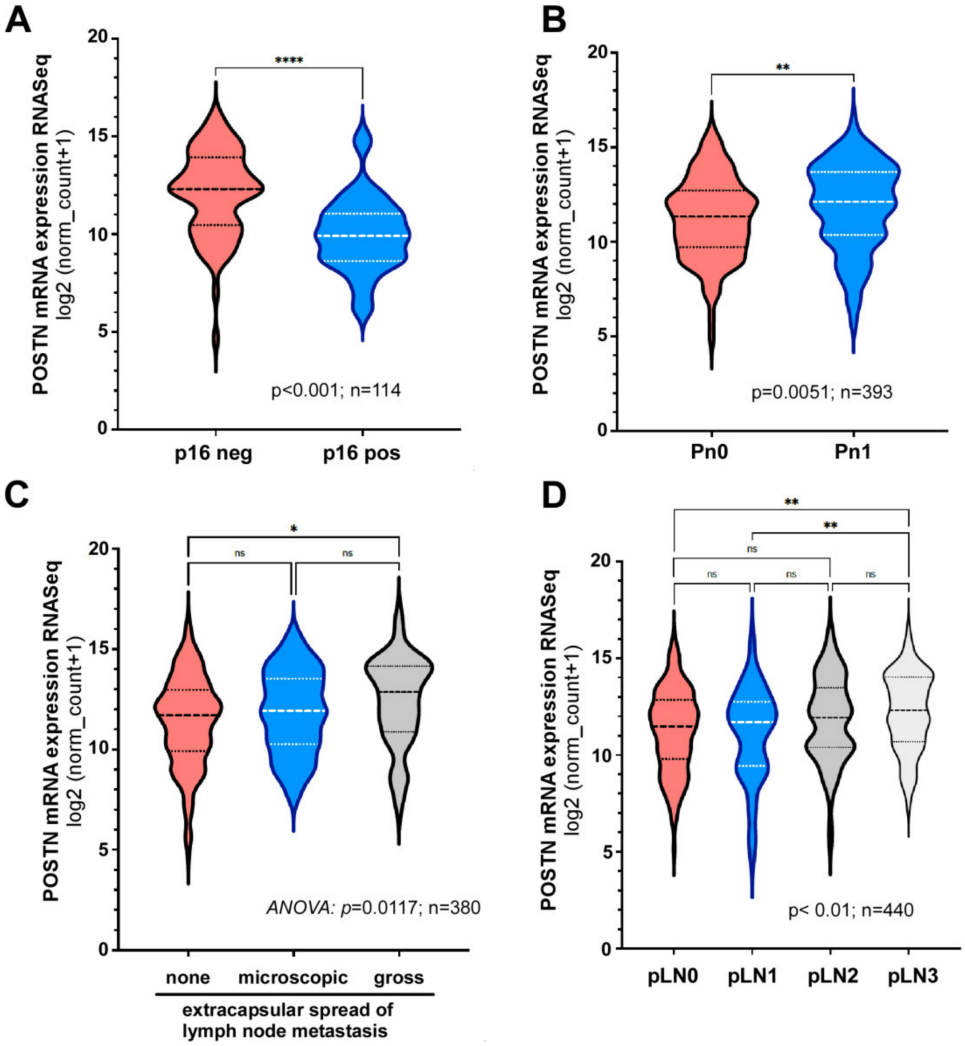

Figure 2. OSF-2 expression correlates with HPV status and markers of metastatic disease. Bioinformatic analysis of the *TCGA* HNC patient cohort (n = 612). High OSF-2 expression significantly correlates with (**A**) HPV status, (**B**) perineural infiltration, (**C**) extracapsular spread (ECE), and (**D**) pathological lymph node status (pLNx) for p16 negative or unknown. N2a/b/c and N3a/b are pooled, respectively; AJCC 8th Edition. p-values and sample size (n) as indicated. * $p < 0.05$, ** $p < 0.01$, **** $p < 0.0001$, and ns indicates not significant.

3.2. OSF-2 Expression Does Not Directly Contribute to Therapy Resistance

First-line chemotherapy in HNC is mainly cisplatin-based [2,48,64–66]. It has been suggested that OSF-2 also contributes to the development of cisplatin resistance in cancer, such as lung cancer [67], although the underlying mechanisms are not understood. To experimentally investigate the potential impact of OSF-2 on chemoresistance in HNC, we established two cisplatin-resistant HNC cell lines allowing the comparison of cisplatin-sensitive versus -resistant cells ($Pica_{Cis}$ and $FaDu_{Cis}$; Figure 3). Although the cells were highly resistant to cisplatin, as shown in 2D (Figure 3A) as well as 3D spheroid cultures (Supplementary Figure S5), NGS RNA sequencing transcriptomics did not reveal an up-regulation of OSF-2 in resistant versus the sensitive parental HNC cell lines (Figure 3C). Moreover, bioinformatic analysis of the HNC *TCGA* patient cohort failed to identify a correlation of OSF-2 expression with residual disease after first-line, predominantly platinum-based, chemo(radio)therapy (Figure 3D). These data strongly suggest that OSF-2 expression appears not to directly contribute to therapy resistance in HNC. However, we cannot exclude indirect effects, e.g., by up-regulation of anti-apoptotic protein, such as Survivin [57,68,69].

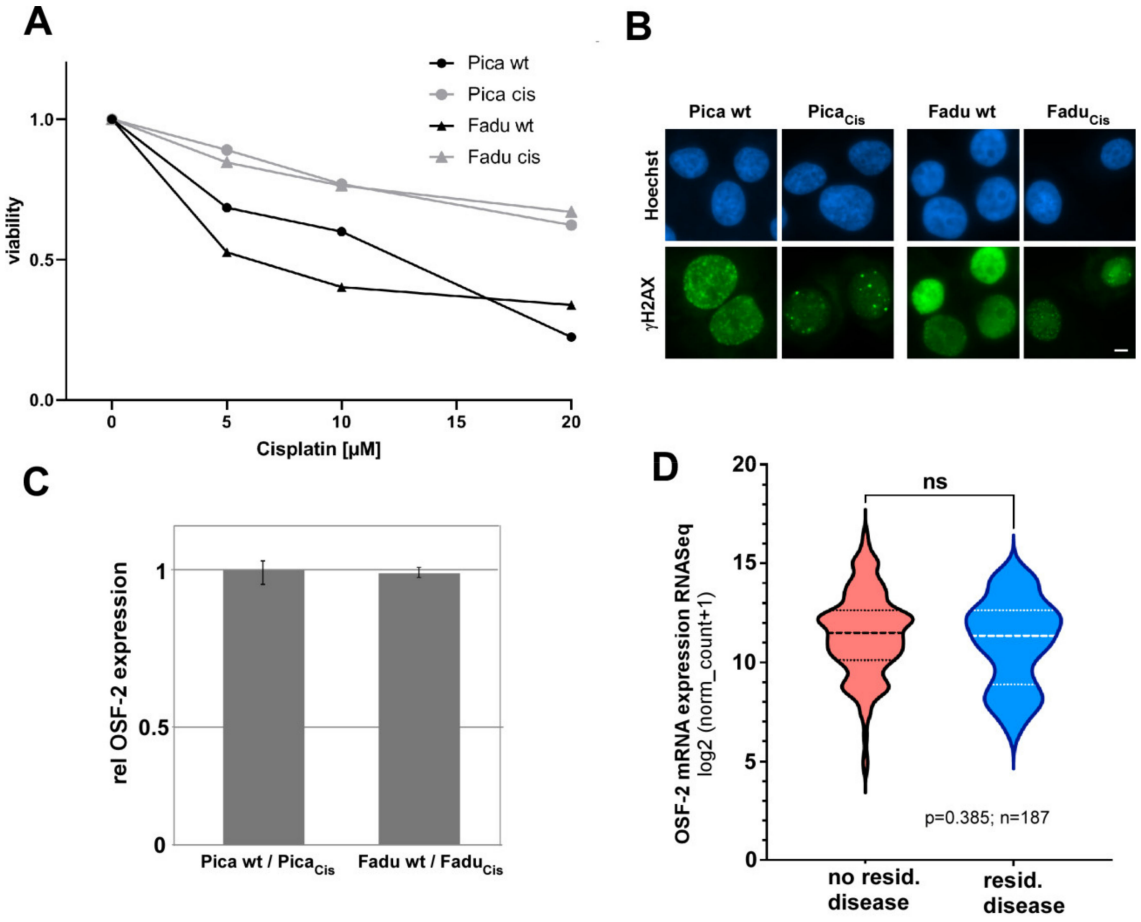

Figure 3. OSF-2 expression does not directly contribute to cisplatin therapy resistance. (**A**) Selected cisplatin-resistant Pica$_{Cis}$ and FaDu$_{Cis}$ cells (grey) are highly resistant. Cells were treated with indicated cisplatin concentrations for 48 h and viability normalized to untreated controls. (**B**) Resistant Pica$_{Cis}$ and FaDu$_{Cis}$ cells show a lower number of cisplatin-induced DNA damage foci (γH2AX) compared to wt Pica/FaDu cells. Cells were treated with 20 µM cisplatin and analyzed by fluorescence microscopy after 24 h. Scale bar, 5 µm. (**C**) OSF-2 is not overexpressed in resistant Pica$_{Cis}$/FaDu$_{Cis}$ versus sensitive wt cells. OSF-2 expression was quantified by RNASeq transcriptomics; relative mRNA expression is shown. (**D**) OSF-2 expression does not correlate with locoregional remission status after primary therapy (*disease after curative treatment)* in the *TCGA* HNC patient cohort. *p*-value and sample size (*n*) as indicated.

3.3. OSF-2 Is Overexpressed in the Tumor Microenvironment

To further examine OSF-2 expression on the protein level, we performed immunohistochemical (IHC) staining of HNC tissue sections (Figure 4). Interestingly, IHC staining detected OSF-2 not only in the cytoplasm and the granulae in tumor cells (Figure 4(A1)) but also in the surrounding stroma (Figure 4(A3,A4)). Moreover, high OSF-2 levels were also detectable in the intercellular space, indicating protein secretion (Figure 4(A2)). Indeed, when we examined cancer-associated fibroblasts (CAFs) by quantitative RT-PCR, and real-time PCR, we found a more than 20-fold overexpression of OSF-2 (relative expression ratio R = 21.18) in CAFs compared to tumor cells, supporting our hypothesis that OSF-2 expression/secretion appears to generate a tumor-friendly microenvironment (Figure 4B,C).

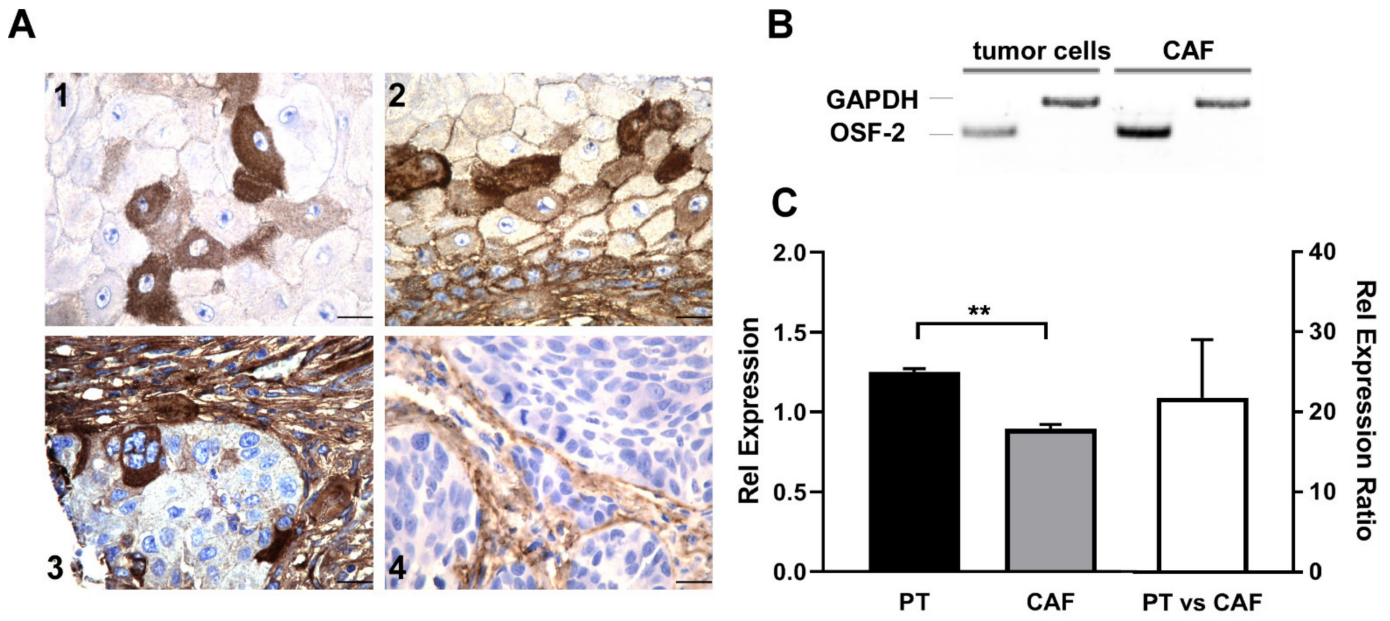

Figure 4. OSF-2 is expressed in the tumor microenvironment. (**A**) Immunohistochemical analysis of OSF-2 expression in primary HNC tissue. Intense staining was observed in cancer cells (**1**,**2**), but also in the juxtatumoral stroma (**3**,**4**). Scale bars, 20 µm. (**B**) RT-PCR of primary tumor cells and CAFs revealed higher expression of OSF-2 in CAFs. GAPDH was used as a control. (**C**) Up-regulation of *OSF-2* in CAFs compared to primary tumor cells was confirmed by quantitative real-time-PCR. Up-regulation is shown by lower C_T values and thus, a lower relative expression for CAFs. OSF-2 expression in primary tumor cells (PT, black) and CAFs (grey) is shown compared to RNA-Pol II expression (OSF-2/RNA-Pol II; left axis), and as relative expression ratio R (right axis). R = 21.18, $n = 2$, ** $p < 0.005$. The uncropped western blot figures were presented in Figure S10.

3.4. HNC Patients Express Various OSF-2 Isoforms

Although a 'canonical' coding sequence for OSF-2 (Q15063-1) has been deposited [38], there is an ongoing debate if alternative isoforms, potentially executing additional functions, are expressed in (HNC) tumor patients. To address this question, we cloned OSF-2 coding sequences from primary tissues. Interestingly, sequence analysis revealed that the OSF-2 isoforms we found significantly differ from other variants previously reported for other tumor types [37,38,70] (Figure 5). To further examine isoform expression signatures, we analyzed the sequence of the OSF-2 C-terminus (exon 13-21, aa 569-789) in different cell lines, primary tumor tissue, corresponding lymph node metastases, normal tissue, and tumor-associated fibroblasts (Figure 5).

Surprisingly, we did not detect the 'canonical' sequence of OSF-2 (Q15063-1) in the analyzed samples, but instead, 12 OSF-2 isoforms exhibited deletion of exon 17 and/or exon 20 and thus, differing in their C-terminus. The distribution of isoforms was not specific for malignant versus normal cells. Interestingly, an inspection of the proposed OSF-2 protein domain structure suggested that these deletions within the C-terminal domain (CTD) may affect postulated OSF-2 functions, such as regulation of extracellular matrix and multimerization [71,72]. However, these proposed functions are not yet understood mechanistically. The wide appearance of these isoforms in patients' tissue however indicates the relevance of the CTD domain, which needs to be clarified in future studies. Our findings indicate also for the field that when studying molecular OSF-2 functions, caution may be advised to exclusively focus on the 'canonical' OSF-2 sequence (Q15063-1) but underline the need to investigate OSF-2 forms really expressed in the respective disease tissues. Notably, one may suggest probing the biological functions of OSF-2 variants by means of recombinant proteins. The commercially available recombinant OSF-2 protein (rOSF-2) used here is produced in *E. coli* and was also used in other studies [73,74]. rOSF-2

is comparable to natural occurring OSF-2 variants we found in HNC tumors also lacking exons 17 and 20 (Figure 5). Potentially, one could consider using rOSF-2, encoding the isoforms we identified in our study, to (fine)map so far unknown biological functions of OSF-2, e.g., of the CTD domain. However, as OSF-2 is glycosylated (FAS1 domain) in cells, we advise caution that rOSF-2 produced in *E. coli* will be the most adequate tool to identify all potential functions.

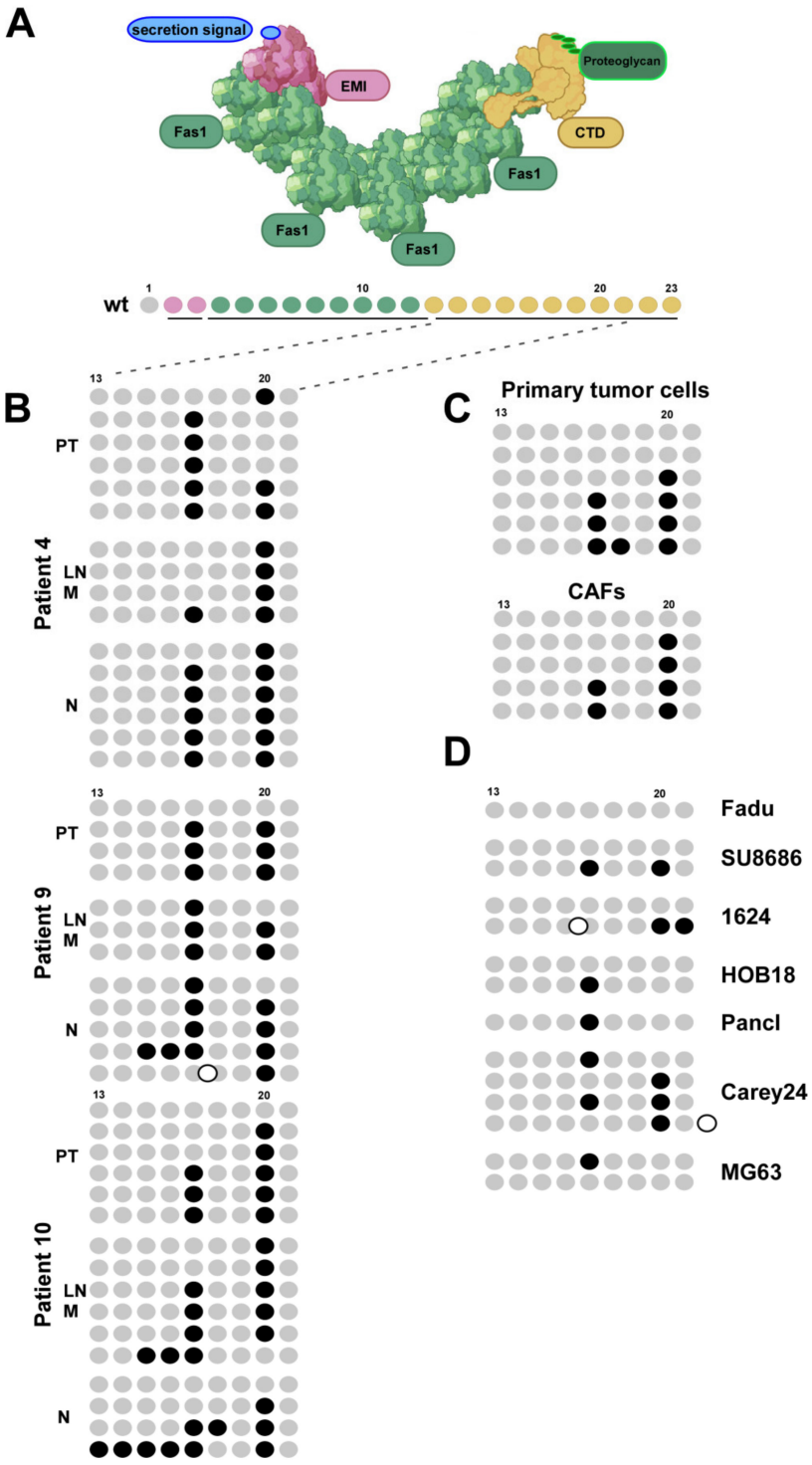

Figure 5. HNC patients express various OSF-2 isoforms differing in their C-terminal domain. (**A**) Proposed protein domain organization of OSF-2 (modified from [40]). The canonical sequence (wt) consists

of 23 exons building the N-terminal secretion signal (blue, identified in this study), the EMI domain (red, exon 2–3), four Fas1 domains (green, exons 3–13), and the variable C-terminal domain (CTD, yellow, exons 13–23). (**B**) Expression of OSF-2 isoforms was examined by sequence analyses of the OSF-2 C-terminus (exon 13–21), and compared to the 'canonical' sequence (wt). In total, 12 isoforms were identified. Grey dots represent verified exons, black dots lack exons (deletions), and white dots have additional exons (insertions). OSF-2 isoform distribution was analyzed in multiple clones of 3 patients (PT, LN M, N) from our study cohort (**B**), isolated primary tumor cells and corresponding CAFs (**C**), as well as in different HNC tumor cell lines (**D**).

As shown for many HNC-relevant proteins, (in)activating mutations are often found in tumor cells. Thus, we further investigated the mutation frequency and type in OSF-2 by exploiting the BioMutav3.0 database and data provided by the TCGA HNC collection. Here, the analysis of 507 HNCs from the TCGA cohort showed a low number of mutations in patients, indicating again that various OSF-2 isoforms may be active in cancer patients (Supplementary Figure S6).

3.5. OSF-2 Isoforms of HNC Patients Contain an Evolutionary Conserved, Functional Secretion Signal

As IHC analysis revealed high amounts of extra/inter-cellular OSF-2, suggesting active protein secretion, we searched for a potential secretion signal in the OSF-2 protein sequence. Global protein alignment of homologous OSF-2 proteins from *Homo sapiens*, *Pan troglodytes* (chimpanzee), *Sus scrofa* (pig), *Bos taurus* (cattle), *Mus musculus* (mouse), and *Canis familaris* (dog) revealed overall protein similarity ranging between 90 and 96.5% and proposed the first ~21 aa as a putative secretion signal (Figure 6A). However, bioinformatic predictions need to be confirmed experimentally. Hence, we first engineered a GFP-tagged full-length OSF-2 protein (OSF-GFP), the isolated proposed secretion signal fused to GFP (aa1-21; Sec-GFP), and a full-length mutant lacking the signal (OSF-ΔSec-GFP). The functionality of the suggested signal in living tumor cells was demonstrated by independent evidence: First, expression of OSF-2-GFP in different tumor cell lines showed a cytoplasmic granular localization, typical for secreted proteins (Figure 6B). No OSF-GFP was present in the nucleus. Second, no secretion vesicles were evident upon expression of the OSF-ΔSec-GFP secretion mutant. Third, the expression of the signal alone fused to GFP (aa1-21; Sec-GFP) was sufficient for the formation of secretion vesicles (Figure 6C). Moreover, in subcellular fractionation experiments, only OSF-GFP was detectable in the membrane fraction of secretion vesicles and the supernatant (Figure 6D,E). In contrast, the OSF-ΔSec-GFP secretion mutant failed to be incorporated into vesicles or to be secreted. Thus, we here identified the OSF-2 aa 1-21 (^{1}MIPFLPMFSLLLLLIVNPINA^{21}) as its *bona fide* secretion signal.

3.6. OSF-2 Does Not Affect Tumor Cell Proliferation but Is Crucial for Cell Migration and Cellular Survival under Stress Conditions

Enhancing tumor metastasis can be influenced by increasing (local) tumor cell proliferation or/and by increasing the cell's capability to migrate and survive in distant 'hostile' microenvironments. Thus, we performed in vitro and in vivo proliferation and scratch assays. Intriguingly, the administration of recombinant OSF-2 (100 ng/mL) did not affect cell proliferation (Figure 7A). Likewise, ectopic OSF-2 overexpression in transfectants did not affect local tumor growth in xenograft models (Supplementary Figure S7). In addition, ectopic expression of secretion active versus secretion-deficient OSF-2 did not significantly enhance invasion in matrigel assays (Supplementary Figure S8). In contrast, the administration of recombinant OSF-2 significantly increased cell migration (Figure 7B) and cellular survival under serum starvation 'stress' conditions (Figure 7C). To further mimic 'hostile' metastases microenvironments, we employed clonogenic 3D-spheroid formation assays (Figure 7D–F). Here, OSF-2 expressing, patient-derived primary HNC tumor cells (characterized in Figures 4B,C and 5C), as well as two HNC cell lines, were cultivated as

3D-spheroids (Figure 7D,E). Treatment with recombinant OSF-2 significantly increased the number of formed spheroid colonies (Figure 7F).

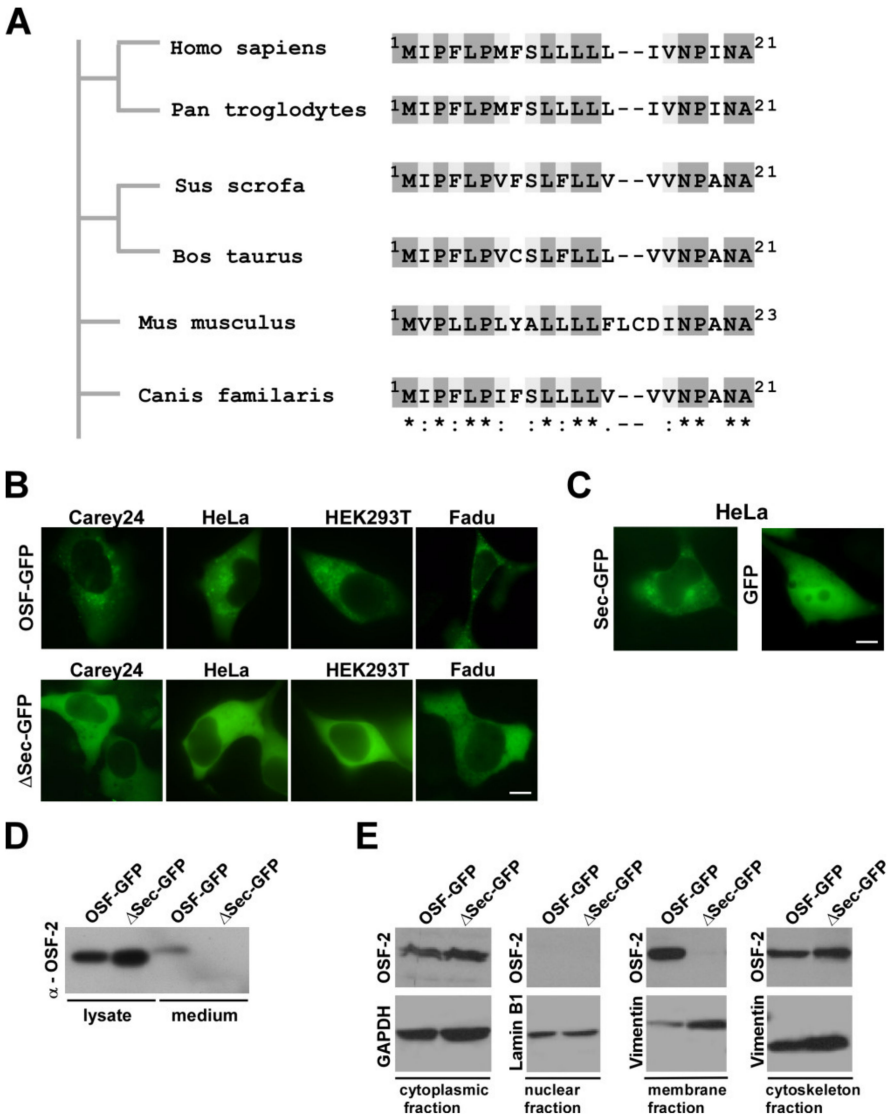

Figure 6. OSF-2 contains an evolutionarily conserved secretion signal. (**A**) Alignment of predicted secretion sequences in various OSF-2 homologs. Phylogram constructed on the basis of amino acid sequence similarities depicting the evolutionary relationships among OSF-2 proteins of different species. The sequence of the predicted human secretion signal (aa1-21) is conserved in all compared homologs. * Identical residues (dark grey), conserved substitutions/similar characteristic (light grey), semi-conserved substitution/similar shape (white). Organisms and amino acid positions are indicated. (**B**) OSF-2-GFP transfection in different tumor cell lines revealed a cytoplasmic granular localization. No secretion granulae were observed upon expression of the secretion mutant, ΔSec-GFP. (**C**) Expression of the signal alone fused to GFP (aa1-21; Sec-GFP) was sufficient for the formation of secretion vesicles. GFP expression served as the negative control. Scale bars, 5 µm. (**D**) Western blot confirming OSF-2 secretion. (**E**) Immunoblot analysis of cell fractions from OSF-2-GFP and ΔSec-GFP HEK293T transfectants. Only OSF-GFP was detectable in the membrane fraction of secretion vesicles and the supernatant. In contrast, the OSF-ΔSec-GFP secretion mutant failed to be incorporated into vesicles or to be secreted. Probing with anti-GAPDH (cytoplasm), anti-Vimentin (membrane, cytoskeleton), and anti-Lamin B1 (nuclear) Abs served as controls for lysate preparation. Representative results for $n = 2$ are shown. The uncropped western blot figures were presented in Figures S11 and S12.

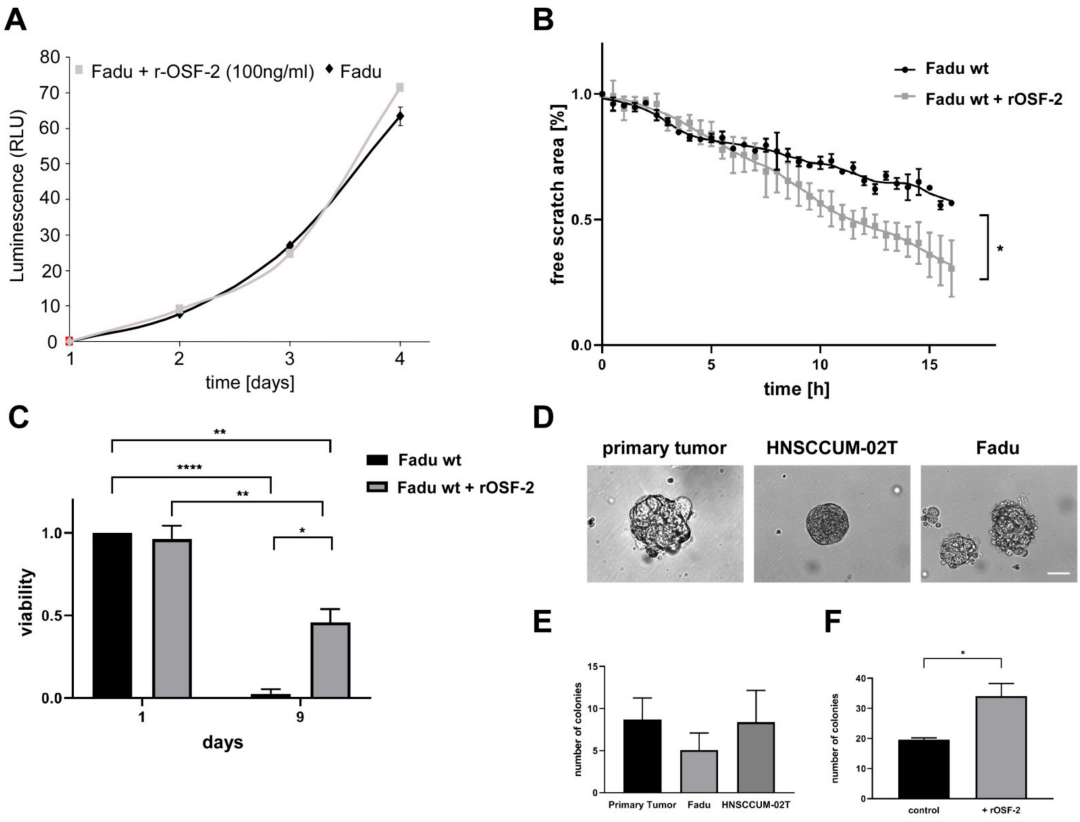

Figure 7. OSF-2 promotes cell migration and cellular survival under stress conditions. Administration of recombinant OSF-2 (100 ng/mL) did not affect HNC cell (FaDu) proliferation (**A**), but resulted in increased cell migration (**B**), and improved survival under serum deprivation (**C**). (**D**,**E**) Spheroid and colony formation assays revealed clonogenicity of three OSF-2 overexpressing HNC cell lines (controls without treatment). Scale bar, 100 µm. (**F**) Presence of recombinant OSF-2 increases the number of formed colonies using Fadu cells. *p*-values of unpaired *t*-testing as indicated. * $p < 0.05$, ** $p < 0.01$, **** $p < 0.0001$.

Collectively, in contrast to other factors such as matrix proteases, promoting metastasis by enhancing invasion, these results strongly suggest that OSF-2 (over)expression promotes metastasis in head and neck cancer by acting on cancer cells and/or CAFs ectopically rather than by stimulating invasion or proliferation pathways intrinsically.

3.7. OSF-2 Promotes Cells by β1-Integrin-Induced Activation of the PI3-Kinase/Akt/PKB Pathway

To define the mechanisms of how OSF-2 promotes cellular migration and survival, we examined cancer-relevant signaling pathways. It has been suggested that OSF-2 stimulates Wnt signaling in breast cancer [75]. However, when we examined Wnt expression in metastases we did not detect a significant up-regulation. Whereas no differential expression of Wnt1 or Wnt3A could be detected we even found a down-regulation of Wnt-5A or -5B M versus N as well as LN M versus PT (see Supplementary File microarray analysis all). Moreover, Wnt expression did not correlate with patterns of metastatic disease in the HNC TCGA cohort.

Next, we examined ECM/focal adhesion receptors in HNC. Notably, we found that β1-integrin, but not α3/α5- or β3-integrins was induced by the addition of rOSF-2 (Figure 8A,B), suggesting its potential role as an 'OSF-2 receptor'. Indeed, treatment with a conditioned medium from engineered OSF-2 overexpressing cells as well as recombinant OSF-2 (r-OSF-2) did not only increase β1-integrin expression (Figure 8A) but also activated the Akt/PKB signaling pathway, as shown by immunofluorescence staining of phosphorylated Akt1/PKBα (Ser473) (Figure 8 C,D). Phosphorylation, indicative of Akt

activation, was independently confirmed by Western blot analysis (Figure 8E). Furthermore, the positive effect of r-OSF-2 treatment on cellular survival under stress conditions could be counteracted by treatment with the PI3K-inhibitor LY294002 (Figure 8F). These results demonstrate that the effects of OSF-2 on cell migration and survival depend (at least) on integrin-mediated Akt/PKB signaling. Of note, serum OSF-2 levels in the range of 100 ng/mL have been reported [76–78]. Hence, although the exact local OSF-2 concentrations in the tumor microenvironment in vivo are not known, 10/100 ng/mL rOSF-2 represent realistic physiological doses, underlining the relevance of our findings.

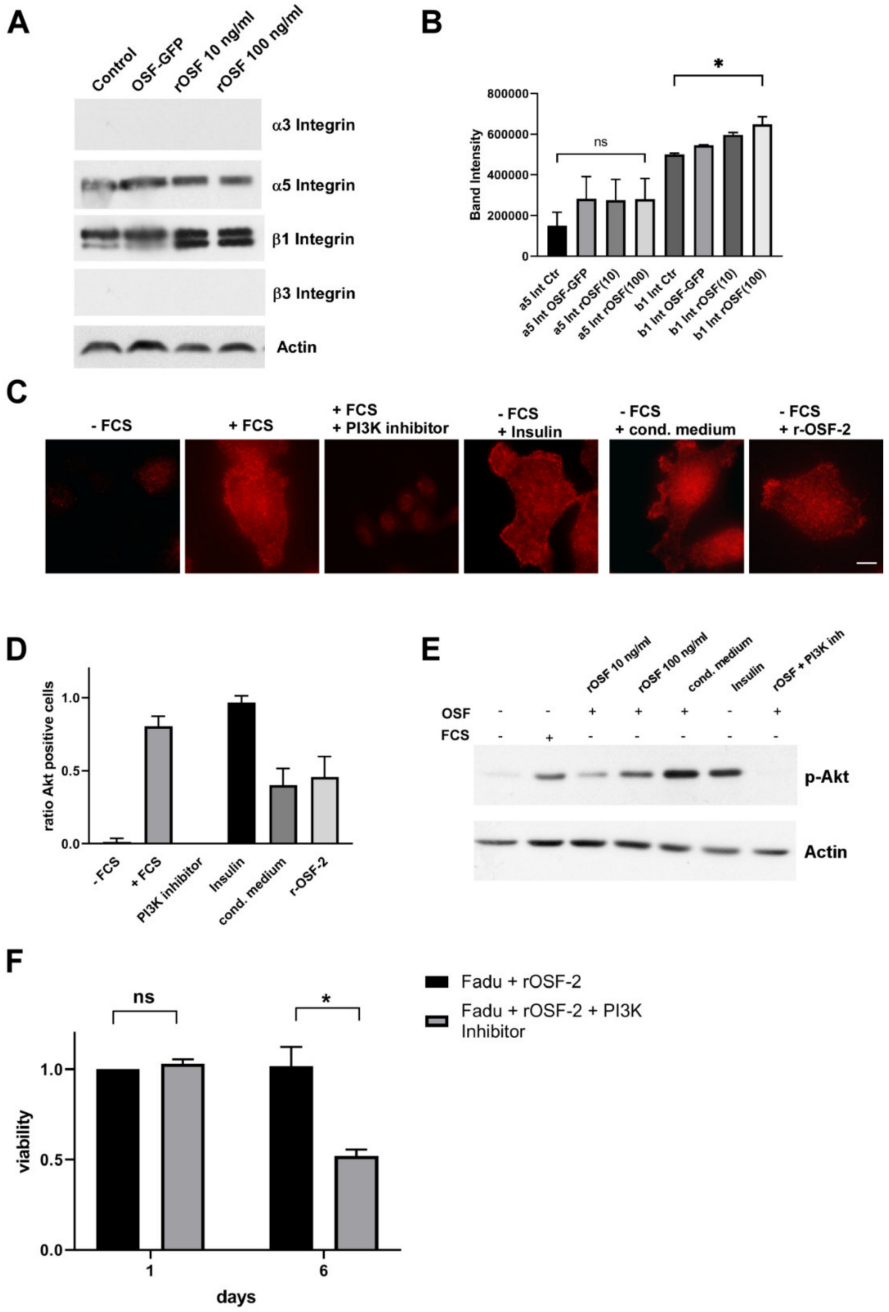

Figure 8. OSF-2 stimulates the Akt/PKB pathway via integrin-dependent PI3-Kinase activation. (**A**,**B**) β1-integrin, but not α5 integrin is induced by the addition of rOSF-2 (10, 100 ng/mL). Integrin receptor expression was analyzed by Western blot in HNSCCUM-02T cells. Actin served as the loading control. Representative results (n = 2) are shown. Densitometric analysis of detected bands is

shown in (**B**). (**C**) Specific phosphorylation of Akt1/PKBα on Ser473 was detected in HNSCCUM-02T cells. Insulin and serum-containing medium (+FCS) served as positive, serum deprivation (−FCS), and PI3K-inhibitor (LY294002; +FCS) treatment as negative controls for staining. Scale bar, 5 µm. (**D**) Quantification of p-Akt positive cells. At least 200 cells from three separate images were examined, visually inspected, and counted as p-Akt positive or negative. Ratio of p-Akt positive cells (= #pAkt positive/all counted cells) is shown for indicated treatments. All treatments, except PI3K-inhibitor, and +FCS, were performed under serum starvation conditions. (**E**) Akt1/PKBα phosphorylation was confirmed by Western blot analysis using HNSCCUM-02T cells. Akt1/PKBα phosphorylation was induced by recombinant OSF-2 (rOSF-2) and conditioned medium under serum-free conditions. OSF-2-induced phosphorylation was prevented by PI3K inhibition. Actin served as the loading control. Representative results (n = 2) are shown. (**F**) HNC cancer cell (Fadu) survival was reduced after treatment with r-OSF-2 and a PI3K-inhibitor (LY294002). ns: $p > 0.05$; * $p \leq 0.05$. The uncropped western blot figures were presented in Figure S13.

4. Discussion

OSF-2 is investigated as a relevant multifunctional protein exhibiting executing various biological functions in health and disease, including cancer/metastasis, development, repair, and/or (bio)material tolerance [28,79]. However, since both tumor-promoting, as well as tumor-suppressive activities have been reported, their relevance and functional role in (head and neck) cancer are still controversially discussed. Thus, this study aimed at a clinical and functional characterization of OSF-2 in a cohort of metastatic head and neck tumors to assess its potential as a prognostic/diagnostic biomarker and/or as a target for novel therapeutic interventions.

First, our bioinformatic analyses revealed OSF-2 not only as significantly upregulated in primary tumors, as well as lymph node metastases, but also suggests OSF-2 as a potential prognostic biomarker for HPV negative head and neck tumors. Although it is widely accepted that HPV negativity correlates with poor survival, there is still a lack of robust biomarkers and molecular understanding for this subgroup. Interestingly, Martinez et al. proposed potential biomarkers correlating with patients' HPV status [80]. Inspection of these data revealed that OSF-2 was among the differentially expressed genes, independently underlining the relevance of our finding. In contrast to OSF-2, another potential promotor of metastases we found upregulated in HPV negative tumors, osteopontin (*SPP1*), seems to play only a minor role in the clinical outcome of these patients. Our finding that high OSF-2 correlates with clinical parameters of high tumor aggressiveness in HNC, such as lymph node status and perineural infiltration, seems to be relevant also for other entities [44,81,82].

Additionally, we analyzed *OSF-2* gene methylation in the TCGA cohort of HNC patients to mechanistically understand OSF-2 up-regulation in primary tumors and metastases. Here, tumor tissues showed significantly lower methylation levels compared to normal solid tissues which are consistent with other methylation studies of HNC [1,20]. Thus, our data indicate that reduced gene methylation might at least be partially responsible for increased OSF-2 levels observed in tumors. However, due to the very small sample size of metastatic (lymph node) tissue in this cohort (n = 2), we could not draw conclusions about the up-regulation of OSF-2 in distant metastases. Results might also be limited due to the use of the *Infinium Human Methylation450 BeadChip* by *TCGA* Research Network which only covers a fraction of CpG sites within the region of interest. Further prospective studies applying additional experimental methods are needed, ideally exploiting matched normal, tumor, as well as metastatic tissues, also from distant sites, which though rare, are in HNC.

It has been suggested that OSF-2 (in)directly contributes to cisplatin resistance in lung cancer cells via activation of Stat3, Akt, and up-regulation of the anti-apoptotic protein survivin [67]. Furthermore, the contribution of OSF-2 to chemoresistance was indicated for ovarian carcinoma [83–85], and osteosarcoma [86]. Interestingly, whereas it has been indicated that OSF-2 affects to radioresistance of HNC cells [79], to our knowledge there are no studies about the role of OSF-2 in cisplatin-resistance of HNC. In contrast, the matricellular protein osteopontin was already suggested to be involved in cisplatin

resistance and poor clinical outcomes of oral cell carcinoma [30]. However, our study revealed that OSF-2 expression was neither increased in two engineered cisplatin-resistant HNC cell lines nor correlated with residual disease after first-line therapy in the *TCGA* cohort. Of note, such controlled approaches have not been performed for other tumor types [67,79,83–86], precluding to conclude that OSF-2 directly causes therapy resistances. Our results suggest that OSF-2 does not directly induce therapy resistance (in HNC).

The tumor microenvironment does not only consist of neoplastic tumor cells but also of non-neoplastic stromal cells including fibroblasts, cancer-associated fibroblasts (CAFs), endothelial cells, pericytes, and inflammatory cells. Here, CAFs are building up the majority of the cellular tumor stroma and play an important role in tumor initiation, progression, and metastasis [87]. Especially for HNC, it has been reported that CAFs are key players in invasion, cancer relapse, treatment resistance, and poor patient outcomes [88]. It is still under debate if secreted OSF-2 is predominantly expressed directly by tumor cells or tumor stromal cells [89]. In vivo, two reports demonstrated that *OSF-2* overexpression in tumor cell lines increases metastases and angiogenesis in nude mice and reduces stress-induced apoptosis [44,90], while another report provided evidence that OSF-2 suppresses lung metastasis of mouse melanoma cell line B16-F10 [91]. Although OSF-2 overexpression does not seem to be systematic in human tumors, studies agree on the low level of OSF-2 expression in most tumor cell lines [91–95]. Lower levels of *OSF-2* expression in tumor cell lines compared to tumor tissues are in agreement with studies showing the production of OSF-2 by stromal cells—and not cancer cells—in tumors [81,82,96,97]. However, the nature of OSF-2-producing cells in tumors is another matter of controversy as separate in situ hybridization experiments suggested that *OSF-2* mRNA is detected in the cytoplasm of cancer cells [45,90]. Thus, in this study, we did not only analyze patient tumor samples but also isolated primary tumor cells, as well as CAFs to characterize OSF-2 expression and localization in different cell types. By immunohistochemical analyses we identified OSF-2 expression in both, tumor and stromal cells, the latter exhibiting more than 20-fold higher OSF-2 levels compared to tumor cells. It has to be mentioned that OSF-2 expression shows high variations between different cells. However, in contrast to other studies [45,81,82,96–98], it can be postulated that both tumor cells and tumor stromal cells contribute to the overall OSF-2 expression of HNC tumors. It will be relevant to further examine OSF-2 expression in CAFs and cancer cells also in samples of lymph node metastases via IHC in larger cohorts in a comprehensive follow-up study, including its impact on HNC disease.

Although the expression of OSF-2 isoforms produced by alternative splicing has been reported [38], little is known about their specific biological functions and the existence of cell/tissue-specific expression patterns. Here, we identified 12 isoforms of OSF-2 protein differing in their C-terminus. Importantly, we could not determine a cancer cell-specific expression signature of OSF-2 in HNC patients, primary cells, or cancer cell lines, but the deletion of exons 17 and 20 occurred with high incidence. The in-frame insertions and deletions of the detected isoforms suggest their generation via alternative splicing mechanisms as described before [37,38]. The fact that we did not detect expression of the postulated 'canonical' or wild-type sequence of OSF-2 (Q15063-1) consisting of 23 exons in all analyzed samples strongly suggests that this isoform does not represent the biologically active, predominant variant. Our findings indicate for the field that when studying molecular OSF-2 functions, caution may be advised to exclusively focus on the 'canonical' OSF-2 sequence (Q15063-1) but investigate OSF-2 expression signatures in the respective disease phenotype. Of note, recombinant OSF-2 protein used in this study also lacks exons 17 and 20 and thus, is comparable to natural occurring OSF-2 variants in HNC tumors.

Determining its subcellular localization and thus also its biological functions, the functional protein domains of OSF-2 were analyzed. Bioinformatic analyses suggest that OSF-2 contains an N-terminal secretory signal peptide, followed by a cysteine-rich domain, four internal homologous Fas1 repeats, and a C-terminal hydrophilic domain. Interestingly, we could show an abundance of OSF-2 in the intercellular space suggesting secretion of

OSF-2 which we proved in this study for the first time also biochemically by secretion-deficient mutants. Additionally, subcellular localization studies revealed that deletion of the N-terminal secretion signal results in cytoplasmic and cytoskeletal localization, but not in membranous localization of OSF-2. Thus, we could prove that the secretion signal is exclusive and indispensable for the secretion of OSF-2 into the intercellular space. It has to be mentioned that the recombinant OSF-2 protein used in our study lacks the identified N-terminal secretion signal. However, for the conducted experiments the lacking secretion signal is negligible because ectopically rOSF-2 treatment mimics the naturally occurring secretion process of endogenous OSF-2 by tumor cells and/or CAFs. Interestingly, OSF-2 was identified as a protein-enriched also in exosomes secreted by metastatic breast cancer cells [99,100]. These results suggest that OSF-2 might execute its pro-migratory functions not only directly via up-regulation in (metastatic) cancer cells, and direct secretion into the intercellular space, but also by exosomal transfer to recipient cells. However, we did not detect OSF-2 protein in isolated exosomes from head and neck cancer cell lines (data not shown). Nevertheless, future analyses of OSF-2 abundance in exosomes derived from HNC cancer patients and other malignancies may help to evaluate its clinical relevance as a novel 'liquid biopsy' marker for metastatic disease [24,50].

Tumor metastasis can be influenced by a variety of factors, such as increasing (local) tumor cell proliferation, enhancing cancer cells' invasiveness, increasing the cells' capability to migrate, or, as only recently accepted, the ability to survive in distant 'hostile' microenvironments. However, in contrast to cancer-associated proteases, OSF-2 does not perform enzymatic proteolytic degradation per se. Though, there is indeed an intense discussion that OSF-2 promotes invasion indirectly by cross-talk with various signaling pathways, such as WNT, fibronectin, and TGFβ, thereby promoting angiogenesis and micrometastatic outgrowth [75,101]. The relevance of ectopic OSF-2 for the tumor microenvironment was supported by our studies on cell migration, clonogenic 3D-spheroid formation assays, and survival under stress conditions. Here, the data strongly suggest that OSF-2 overexpression acts on cancer cells and/or CAFs extrinsically via stimulation of integrin receptors, rather than by activating proliferation and pro-survival pathways, such as Akt/PKB signaling intrinsically (Figure 9). We propose that OSF-2-mediated regulation of the tumor microenvironment occurs especially under stress conditions (such as hypoxia, nutrient deprivation, pH changes, or reduced vascularization) by integrin-mediated activation of Akt/PKB pathways and downstream signaling.

It has been suggested that OSF-2 stimulates Wnt signaling in breast cancer (stem) cells [75]. However, when we examined Wnt expression in metastases we neither detected a significant up-regulation, nor a correlation with patterns of metastatic disease in the HNC TCGA cohort. Indeed, whereas breast cancer is a highly metastatic disease particularly also to distant organs, metastases of HNC are mainly found in local lymph nodes and metastases to distant organs are rare. Moreover, in contrast to breast cancer, we clearly detected OSF-2 overexpression also in primary tumor cells. Thus, OSF-2 induction of Wnt might be different in breast cancer versus HNC but clearly may deserve future investigations.

Due to its proposed multiple functions in proliferation, survival, stress response, invasion, and chemoresistance, OSF-2 also represents a promising therapeutic target for novel anti-cancer therapies. Small molecules directly targeting OSF-2 or integrin receptors and/or secretion inhibitors might be used to inhibit OSF-2-mediated metastasis and/or chemoresistance. However, such compounds still await their identification, and the field may be stimulated by the findings reported here. Moreover, to our knowledge, no small molecules altering OSF-2 expression have been reported. For breast cancer models, different approaches have been studied to inhibit OSF-2 activity. Lee et al. suggested that DNA aptamers directed against human OSF-2, and could efficiently block tumor growth and cell dissemination in a xenograft mouse model [102]. Recently, a peptide antagonist was engineered to overcome OSF-2-mediated tumor-promoting effects including chemoresistance in breast cancer [103]. Additionally, anti-OSF-2 antibodies have been used to inhibit tumor growth in vivo [104]. However, the mechanistic effects of these approaches are not always

fully understood, and potential side effects on regenerating non-malignant tissues/bones need to be monitored carefully.

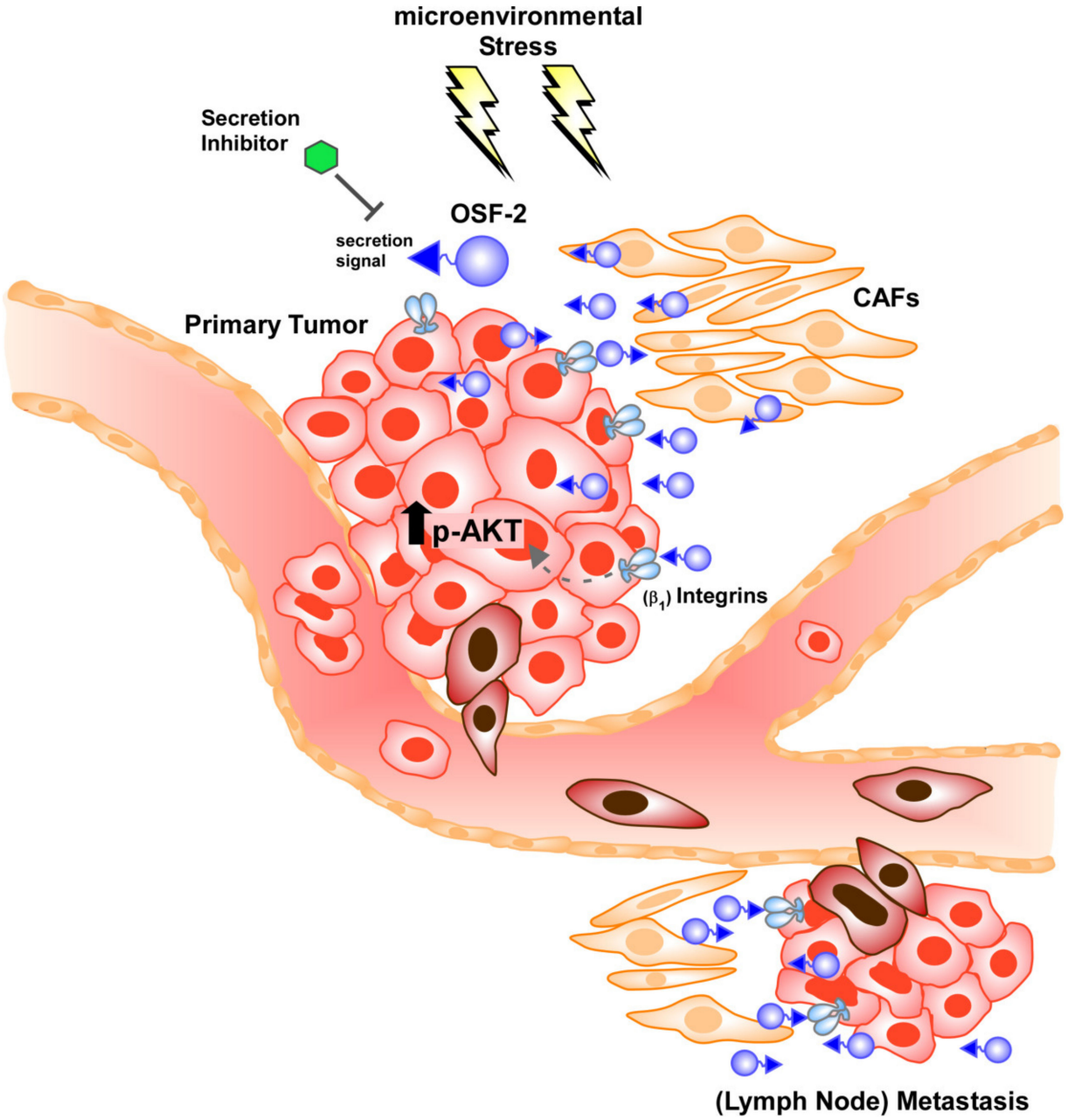

Figure 9. Proposed OSF-2 function in promoting (lymph node) metastases by regulating the tumor microenvironment and cellular survival. OSF-2 is overexpressed in tumor cells, as well as in cancer-associated fibroblasts (CAFs) at the primary tumor and lymph node metastatic sites in HNC. Though, it is likely that these mechanisms are also relevant for distant site metastases in other cancer types. Due to the conserved N-terminal secretion signal, OSF-2 seems to execute its tumor-promoting functions not mainly intracellularly, but extracellularly in the tumor microenvironment. Here, secretion inhibitors could be therapeutically relevant. OSF-2 modulates the tumor microenvironment by integrin-dependent activation of Akt/PKB pathways and downstream signaling, particularly critical under stress conditions.

5. Conclusions

Metastasis is the main cause of cancer-related deaths and is responsible for about 90% of cancer mortality, including HNC. Our study demonstrates the (clinical) relevance of the

osteoblast-specific factor 2 (OSF-2), predominantly for HPV-negative HNC patients. We show that OSF-2 executes its tumor-promoting functions mainly via the tumor microenvironment, rather than by stimulating proliferation and pro-survival pathways intrinsically. By identifying a secretion signal, we suggest not only exploiting OSF-2 as a potential prognostic biomarker for head and neck cancers but also targeting its tumor microenvironment reservoir by secretion inhibitors.

Supplementary Materials: The following are available online at https://www.mdpi.com/article/10.3390/cancers14092337/s1, Supplementary Figure S1: OSF-2 (POSTN) is significantly up-regulated in TCGA HNSCC patient cohort (n = 566) comparing N vs PT; Figure S2: OSF-2 expression did not correlate with tumor localization in TCGA HNSCC patient cohort (n = 538); Figure S3: OSF-2 DNA methylation of six CpG sites in n = 528 HNSCC tumors and n = 82 normal tissue samples from the TCGA cohort; Figure S4: Osteopontin (SPP1) is significantly upregulated in HPV negative vs. positive tumors of the TCGA HNSCC patient cohort (n = 114); Figure S5: Spheroids of cisplatin-resistant pica cell line (PicaCis) exhibit significant chemoresistance towards different concentrations of cisplatin compared to wt cell line; Figure S6: Mutational analysis of OSF-2 gene using TCGA database (n = 493); Figure S7: Overexpression of OSF-2 in head and neck cancer cells did not alter tumor growth after subcutaneous injection into nude mice; Figure S8: OSF-2 secretion has no effect on cancer cell invasion. Figures S9–S13 Uncropped western blot figures. Supplementary Table S1: Clinical and histopathological characteristics of microarray cohort; Table S2: Clinical characteristics of TCGA Head and Neck Cancer (HNSC) cohort (n = 612); Table S3: Top 30 list of significantly up-regulated genes in PT vs. N (log2FC > 1.5, p-value < 0.0001); Table S4: List of used primers for RT-PCR, quantitative Real-Time PCR, and cloning; Table S5: Sequence of recombinant OSF-2 (BioVendor).

Author Contributions: Conceptualization, D.G., A.S. and R.H.S.; Data curation, D.G., A.S., A.K. and L.F.; Formal analysis, D.G. and A.S.; Funding acquisition, D.G., J.H. and R.H.S.; Investigation, D.G., A.S., L.F. and J.H.; Methodology, D.G., A.S., A.K. and G.-B.D.; Project administration, D.G., S.S., J.H. and R.H.S.; Resources, D.G., J.H. and R.H.S.; Supervision, D.G., S.S. and R.H.S.; Validation, D.G. and A.S.; Visualization, D.G., A.S., J.H. and R.H.S.; Writing—original draft, D.G., A.S., S.K.K., J.H. and R.H.S.; Writing—review & editing, D.G., A.S., A.K., S.K.K., G.-B.D., L.F., I.K., S.S. and R.H.S. All authors have read and agreed to the published version of the manuscript.

Funding: This study was supported by Else-Kröner Fresenius Foundation (2015_A233), Stiftung Tumorforschung Kopf-Hals (TF-OSF), DAAD/TransMed (ST35), Deutsche Forschungsgemeinschaft (STR 1014; HA8065), and the Science Support Program of the University Hospital Mainz.

Institutional Review Board Statement: The investigation has been conducted in accordance with the ethical standards according to the Declaration of Helsinki and according to local, national, and international guidelines, as exemplified by the ARRIVE guidelines (https://arriveguidelines.org/arrive-guidelines; accessed on 2 March 2021). Tissue samples were obtained from patients undergoing surgical resection at the department of otolaryngology/pathology of the University of Mainz after obtaining the patients' informed consent to participate in the study and were processed anonymously. All animal procedures were approved by the Institutional Animal Care and Use Committee at the University of Mainz. Publicly available gene expression data was obtained from The Cancer Genome Atlas (TCGA) Research Network (http://cancergenome.nih.gov/, accessed on 17 March 2022). The TCGA Research Network included patients in accordance with the guidelines of the Declaration of Helsinki of 1975 and all patients provided signed informed consent.

Informed Consent Statement: Written informed consent was obtained from all subjects involved in the study.

Data Availability Statement: The datasets supporting the findings of this study are indicated in the article and are available from the corresponding author on request.

Acknowledgments: The authors thank Sandra Olf for excellent technical assistance, Negusse Habtemichael, and Ludger Klein-Hitpass for support and microarray analyses.

Conflicts of Interest: The authors declare that the research was conducted in the absence of any commercial or financial relationships that could be construed as a potential conflict of interest.

References

1. Gul, D.; Habtemichael, N.; Dietrich, D.; Dietrich, J.; Gosswein, D.; Khamis, A.; Deuss, E.; Kunzel, J.; Schneider, G.; Strieth, S.; et al. Identification of cytokeratin24 as a tumor suppressor for the management of head and neck cancer. *Biol. Chem.* 2021, *Epub ahead of print*. [CrossRef]
2. Alsahafi, E.; Begg, K.; Amelio, I.; Raulf, N.; Lucarelli, P.; Sauter, T.; Tavassoli, M. Clinical update on head and neck cancer: Molecular biology and ongoing challenges. *Cell Death Dis.* **2019**, *10*, 540. [CrossRef]
3. Ferlay, J.; Colombet, M.; Soerjomataram, I.; Mathers, C.; Parkin, D.M.; Pineros, M.; Znaor, A.; Bray, F. Estimating the global cancer incidence and mortality in 2018: GLOBOCAN sources and methods. *Int. J. Cancer* **2019**, *144*, 1941–1953. [CrossRef]
4. Ferlito, A.; Shaha, A.R.; Silver, C.E.; Rinaldo, A.; Mondin, V. Incidence and sites of distant metastases from head and neck cancer. *ORL J. Oto-Rhino-Laryngol. Its Relat. Spec.* **2001**, *63*, 202–207. [CrossRef]
5. Cohen, R.B. Current challenges and clinical investigations of epidermal growth factor receptor (EGFR)- and ErbB family-targeted agents in the treatment of head and neck squamous cell carcinoma (HNSCC). *Cancer Treat. Rev.* **2014**, *40*, 567–577. [CrossRef]
6. Denaro, N.; Russi, E.G.; Adamo, V.; Merlano, M.C. State-of-the-art and emerging treatment options in the management of head and neck cancer: News from 2013. *Oncology* **2014**, *86*, 212–229. [CrossRef]
7. Deuss, E.; Gosswein, D.; Gul, D.; Zimmer, S.; Foersch, S.; Eger, C.S.; Limburg, I.; Stauber, R.H.; Kunzel, J. Growth Factor Receptor Expression in Oropharyngeal Squamous Cell Cancer: Her1-4 and c-Met in Conjunction with the Clinical Features and Human Papillomavirus (p16) Status. *Cancers* **2020**, *12*, 3358. [CrossRef]
8. Jemal, A.; Siegel, R.; Ward, E.; Hao, Y.; Xu, J.; Murray, T.; Thun, M.J. Cancer statistics, 2008. *CA Cancer J. Clin.* **2008**, *58*, 71–96. [CrossRef]
9. Eccles, S.A.; Welch, D.R. Metastasis: Recent discoveries and novel treatment strategies. *Lancet* **2007**, *369*, 1742–1757. [CrossRef]
10. Kunzel, J.; Gribko, A.; Lu, Q.; Stauber, R.H.; Wunsch, D. Nanomedical detection and downstream analysis of circulating tumor cells in head and neck patients. *Biol. Chem.* **2019**, *400*, 1465–1479. [CrossRef]
11. Hu, Y.; Yu, X.; Xu, G.; Liu, S. Metastasis: An early event in cancer progression. *J. Cancer Res. Clin. Oncol.* **2017**, *143*, 745–757. [CrossRef]
12. Rocken, M. Early tumor dissemination, but late metastasis: Insights into tumor dormancy. *J. Clin. Investig.* **2010**, *120*, 1800–1803. [CrossRef]
13. Jou, A.; Hess, J. Epidemiology and Molecular Biology of Head and Neck Cancer. *Oncol. Res. Treat.* **2017**, *40*, 328–332. [CrossRef]
14. Beltz, A.; Gosswein, D.; Zimmer, S.; Limburg, I.; Wunsch, D.; Gribko, A.; Deichelbohrer, M.; Hagemann, J.; Stauber, R.H.; Kunzel, J. Staging of oropharyngeal squamous cell carcinoma of the head and neck: Prognostic features and power of the 8th edition of the UICC staging manual. *Eur. J. Surg. Oncol.* **2019**, *45*, 1046–1053. [CrossRef]
15. Ginos, M.A.; Page, G.P.; Michalowicz, B.S.; Patel, K.J.; Volker, S.E.; Pambuccian, S.E.; Ondrey, F.G.; Adams, G.L.; Gaffney, P.M. Identification of a gene expression signature associated with recurrent disease in squamous cell carcinoma of the head and neck. *Cancer Res.* **2004**, *64*, 55–63. [CrossRef]
16. Alevizos, I.; Mahadevappa, M.; Zhang, X.; Ohyama, H.; Kohno, Y.; Posner, M.; Gallagher, G.T.; Varvares, M.; Cohen, D.; Kim, D.; et al. Oral cancer in vivo gene expression profiling assisted by laser capture microdissection and microarray analysis. *Oncogene* **2001**, *20*, 6196–6204. [CrossRef]
17. El-Naggar, A.K.; Kim, H.W.; Clayman, G.L.; Coombes, M.M.; Le, B.; Lai, S.; Zhan, F.; Luna, M.A.; Hong, W.K.; Lee, J.J. Differential expression profiling of head and neck squamous carcinoma: Significance in their phenotypic and biological classification. *Oncogene* **2002**, *21*, 8206–8219. [CrossRef]
18. Mendez, E.; Cheng, C.; Farwell, D.G.; Ricks, S.; Agoff, S.N.; Futran, N.D.; Weymuller, E.A., Jr.; Maronian, N.C.; Zhao, L.P.; Chen, C. Transcriptional expression profiles of oral squamous cell carcinomas. *Cancer* **2002**, *95*, 1482–1494. [CrossRef]
19. Castilho, R.M.; Squarize, C.H.; Almeida, L.O. Epigenetic Modifications and Head and Neck Cancer: Implications for Tumor Progression and Resistance to Therapy. *Int. J. Mol. Sci.* **2017**, *18*, 1506. [CrossRef]
20. Bockhorst, C.; Dietrich, J.; Vogt, T.J.; Stauber, R.H.; Strieth, S.; Bootz, F.; Dietrich, D.; Vos, L. The DNA methylation landscape of PD-1 (PDCD1) and adjacent lncRNA AC131097.3 in head and neck squamous cell carcinoma. *Epigenomics* **2021**, *13*, 113–127. [CrossRef]
21. Zacksenhaus, E.; Egan, S.E. Progression to Metastasis of Solid Cancer. *Cancers* **2021**, *13*, 717. [CrossRef] [PubMed]
22. Allen, C.T.; Law, J.H.; Dunn, G.P.; Uppaluri, R. Emerging insights into head and neck cancer metastasis. *Head Neck* **2013**, *35*, 1669–1678. [CrossRef] [PubMed]
23. Bottos, A.; Hynes, N.E. Cancer: Staying together on the road to metastasis. *Nature* **2014**, *514*, 309–310. [CrossRef] [PubMed]
24. Gribko, A.; Kunzel, J.; Wunsch, D.; Lu, Q.; Nagel, S.M.; Knauer, S.K.; Stauber, R.H.; Ding, G.B. Is small smarter? Nanomaterial-based detection and elimination of circulating tumor cells: Current knowledge and perspectives. *Int. J. Nanomed.* **2019**, *14*, 4187–4209. [CrossRef] [PubMed]
25. Mehlen, P.; Puisieux, A. Metastasis: A question of life or death. *Nat. Rev.* **2006**, *6*, 449–458. [CrossRef]
26. Zacksenhaus, E.; Shrestha, M.; Liu, J.C.; Vorobieva, I.; Chung, P.E.D.; Ju, Y.; Nir, U.; Jiang, Z. Mitochondrial OXPHOS Induced by RB1 Deficiency in Breast Cancer: Implications for Anabolic Metabolism, Stemness, and Metastasis. *Trends Cancer* **2017**, *3*, 768–779. [CrossRef]
27. Mason, S.D.; Joyce, J.A. Proteolytic networks in cancer. *Trends Cell Biol.* **2011**, *21*, 228–237. [CrossRef]

28. Gonzalez-Gonzalez, L.; Alonso, J. Periostin: A Matricellular Protein With Multiple Functions in Cancer Development and Progression. *Front. Oncol.* **2018**, *8*, 225. [CrossRef]
29. Le, Q.T.; Sutphin, P.D.; Raychaudhuri, S.; Yu, S.C.; Terris, D.J.; Lin, H.S.; Lum, B.; Pinto, H.A.; Koong, A.C.; Giaccia, A.J. Identification of osteopontin as a prognostic plasma marker for head and neck squamous cell carcinomas. *Clin. Cancer Res.* **2003**, *9*, 59–67.
30. Luo, S.D.; Chen, Y.J.; Liu, C.T.; Rau, K.M.; Chen, Y.C.; Tsai, H.T.; Chen, C.H.; Chiu, T.J. Osteopontin Involves Cisplatin Resistance and Poor Prognosis in Oral Squamous Cell Carcinoma. *BioMed Res. Int.* **2015**, *2015*, 508587. [CrossRef]
31. Liu, Y.; Huang, Z.; Cui, D.; Ouyang, G. The Multiaspect Functions of Periostin in Tumor Progression. *Adv. Exp. Med. Biol.* **2019**, *1132*, 125–136. [CrossRef] [PubMed]
32. Wu, T.; Dai, Y. Tumor microenvironment and therapeutic response. *Cancer Lett.* **2017**, *387*, 61–68. [CrossRef] [PubMed]
33. Watermann, C.; Pasternack, H.; Idel, C.; Ribbat-Idel, J.; Bragelmann, J.; Kuppler, P.; Offermann, A.; Jonigk, D.; Kuhnel, M.P.; Schrock, A.; et al. Recurrent HNSCC Harbor an Immunosuppressive Tumor Immune Microenvironment Suggesting Successful Tumor Immune Evasion. *Clin. Cancer Res.* **2021**, *27*, 632–644. [CrossRef] [PubMed]
34. Ritchie, K.E.; Nor, J.E. Perivascular stem cell niche in head and neck cancer. *Cancer Lett.* **2013**, *338*, 41–46. [CrossRef] [PubMed]
35. Chen, S.M.Y.; Krinsky, A.L.; Woolaver, R.A.; Wang, X.; Chen, Z.; Wang, J.H. Tumor immune microenvironment in head and neck cancers. *Mol. Carcinog* **2020**, *59*, 766–774. [CrossRef] [PubMed]
36. Pantel, K.; Alix-Panabieres, C. Bone marrow as a reservoir for disseminated tumor cells: A special source for liquid biopsy in cancer patients. *Bonekey Rep.* **2014**, *3*, 584. [CrossRef]
37. Horiuchi, K.; Amizuka, N.; Takeshita, S.; Takamatsu, H.; Katsuura, M.; Ozawa, H.; Toyama, Y.; Bonewald, L.F.; Kudo, A. Identification and characterization of a novel protein, periostin, with restricted expression to periosteum and periodontal ligament and increased expression by transforming growth factor beta. *J. Bone Miner. Res.* **1999**, *14*, 1239–1249. [CrossRef]
38. Takeshita, S.; Kikuno, R.; Tezuka, K.; Amann, E. Osteoblast-specific factor 2: Cloning of a putative bone adhesion protein with homology with the insect protein fasciclin I. *Biochem. J.* **1993**, *294 Pt 1*, 271–278. [CrossRef]
39. Elkins, T.; Hortsch, M.; Bieber, A.J.; Snow, P.M.; Goodman, C.S. Drosophila fasciclin I is a novel homophilic adhesion molecule that along with fasciclin III can mediate cell sorting. *J. Cell Biol.* **1990**, *110*, 1825–1832. [CrossRef]
40. Zhu, D.; Zhou, W.; Wang, Z.; Wang, Y.; Liu, M.; Zhang, G.; Guo, X.; Kang, X. Periostin: An Emerging Molecule With a Potential Role in Spinal Degenerative Diseases. *Front. Med.* **2021**, *8*, 694800. [CrossRef]
41. Kim, J.E.; Kim, S.J.; Lee, B.H.; Park, R.W.; Kim, K.S.; Kim, I.S. Identification of motifs for cell adhesion within the repeated domains of transforming growth factor-beta-induced gene, betaig-h3. *J. Biol. Chem.* **2000**, *275*, 30907–30915. [CrossRef] [PubMed]
42. Kzhyshkowska, J.; Gratchev, A.; Martens, J.H.; Pervushina, O.; Mamidi, S.; Johansson, S.; Schledzewski, K.; Hansen, B.; He, X.; Tang, J.; et al. Stabilin-1 localizes to endosomes and the trans-Golgi network in human macrophages and interacts with GGA adaptors. *J. Leukoc. Biol.* **2004**, *76*, 1151–1161. [CrossRef] [PubMed]
43. Ruan, K.; Bao, S.; Ouyang, G. The multifaceted role of periostin in tumorigenesis. *Cell. Mol. Life Sci.* **2009**, *66*, 2219–2230. [CrossRef] [PubMed]
44. Bao, S.; Ouyang, G.; Bai, X.; Huang, Z.; Ma, C.; Liu, M.; Shao, R.; Anderson, R.M.; Rich, J.N.; Wang, X.F. Periostin potently promotes metastatic growth of colon cancer by augmenting cell survival via the Akt/PKB pathway. *Cancer Cell* **2004**, *5*, 329–339. [CrossRef]
45. Baril, P.; Gangeswaran, R.; Mahon, P.C.; Caulee, K.; Kocher, H.M.; Harada, T.; Zhu, M.; Kalthoff, H.; Crnogorac-Jurcevic, T.; Lemoine, N.R. Periostin promotes invasiveness and resistance of pancreatic cancer cells to hypoxia-induced cell death: Role of the beta4 integrin and the PI3k pathway. *Oncogene* **2007**, *26*, 2082–2094. [CrossRef]
46. Yu, B.; Wu, K.; Wang, X.; Zhang, J.; Wang, L.; Jiang, Y.; Zhu, X.; Chen, W.; Yan, M. Periostin secreted by cancer-associated fibroblasts promotes cancer stemness in head and neck cancer by activating protein tyrosine kinase 7. *Cell Death Dis.* **2018**, *9*, 1082. [CrossRef]
47. Ye, D.; Zhou, C.; Wang, S.; Deng, H.; Shen, Z. Tumor suppression effect of targeting periostin with siRNA in a nude mouse model of human laryngeal squamous cell carcinoma. *J. Clin. Lab. Anal.* **2019**, *33*, e22622. [CrossRef]
48. Siemer, S.; Fauth, T.; Scholz, P.; Al-Zamel, Y.; Khamis, A.; Gul, D.; Freudelsperger, L.; Wollenberg, B.; Becker, S.; Stauber, R.H.; et al. Profiling Cisplatin Resistance in Head and Neck Cancer: A Critical Role of the VRAC Ion Channel for Chemoresistance. *Cancers* **2021**, *13*, 4831. [CrossRef]
49. Welkoborsky, H.J.; Jacob, R.; Riazimand, S.H.; Bernauer, H.S.; Mann, W.J. Molecular biologic characteristics of seven new cell lines of squamous cell carcinomas of the head and neck and comparison to fresh tumor tissue. *Oncology* **2003**, *65*, 60–71. [CrossRef]
50. Gribko, A.; Stiefel, J.; Liebetanz, L.; Nagel, S.M.; Künzel, J.; Wandrey, M.; Hagemann, J.; Stauber, R.H.; Freese, C.; Gül, D. IsoMAG—An Automated System for the Immunomagnetic Isolation of Squamous Cell Carcinoma-Derived Circulating Tumor Cells. *Diagnostics* **2021**, *11*, 2040. [CrossRef]
51. Goldman, M.J.; Craft, B.; Hastie, M.; Repecka, K.; McDade, F.; Kamath, A.; Banerjee, A.; Luo, Y.; Rogers, D.; Brooks, A.N.; et al. Visualizing and interpreting cancer genomics data via the Xena platform. *Nat. Biotechnol.* **2020**, *38*, 675–678. [CrossRef] [PubMed]
52. Koch, A.; De Meyer, T.; Jeschke, J.; Van Criekinge, W. MEXPRESS: Visualizing expression, DNA methylation and clinical TCGA data. *BMC Genom.* **2015**, *16*, 636. [CrossRef] [PubMed]
53. Dingerdissen, H.M.; Torcivia-Rodriguez, J.; Hu, Y.; Chang, T.C.; Mazumder, R.; Kahsay, R. BioMuta and BioXpress: Mutation and expression knowledgebases for cancer biomarker discovery. *Nucleic. Acids Res.* **2018**, *46*, D1128–D1136. [CrossRef] [PubMed]

54. Habtemichael, N.; Wunsch, D.; Bier, C.; Tillmann, S.; Unruhe, B.; Frauenknecht, K.; Heinrich, U.R.; Mann, W.J.; Stauber, R.H.; Knauer, S.K. Cloning and functional characterization of the guinea pig apoptosis inhibitor protein Survivin. *Gene* **2010**, *469*, 9–17. [CrossRef] [PubMed]
55. Bier, C.; Knauer, S.K.; Klapthor, A.; Schweitzer, A.; Rekik, A.; Kramer, O.H.; Marschalek, R.; Stauber, R.H. Cell-based Analysis of Structure-Function Activity of Threonine Aspartase 1. *J. Biol. Chem.* **2011**, *286*, 3007–3017. [CrossRef]
56. Knauer, S.K.; Heinrich, U.R.; Bier, C.; Habtemichael, N.; Docter, D.; Helling, K.; Mann, W.J.; Stauber, R.H. An otoprotective role for the apoptosis inhibitor protein survivin. *Cell Death Dis.* **2010**, *1*, e51. [CrossRef]
57. Engels, K.; Knauer, S.K.; Loibl, S.; Fetz, V.; Harter, P.; Schweitzer, A.; Fisseler-Eckhoff, A.; Kommoss, F.; Hanker, L.; Nekljudova, V.; et al. NO signaling confers cytoprotectivity through the survivin network in ovarian carcinomas. *Cancer Res.* **2008**, *68*, 5159–5166. [CrossRef]
58. Fetz, V.; Bier, C.; Habtemichael, N.; Schuon, R.; Schweitzer, A.; Kunkel, M.; Engels, K.; Kovacs, A.F.; Schneider, S.; Mann, W.; et al. Inducible NO synthase confers chemoresistance in head and neck cancer by modulating survivin. *Int. J. Cancer* **2009**, *124*, 2033–2041. [CrossRef]
59. Trothe, J.; Ritzmann, D.; Lang, V.; Scholz, P.; Pul, U.; Kaufmann, R.; Buerger, C.; Ertongur-Fauth, T. Hypotonic stress response of human keratinocytes involves LRRC8A as component of volume-regulated anion channels. *Exp. Dermatol.* **2018**, *27*, 1352–1360. [CrossRef]
60. Stauber, R.H.; Rabenhorst, U.; Rekik, A.; Engels, K.; Bier, C.; Knauer, S.K. Nucleocytoplasmic shuttling and the biological activity of mouse survivin are regulated by an active nuclear export signal. *Traffic* **2006**, *7*, 1461–1472. [CrossRef]
61. Stauber, R.H.; Knauer, S.K.; Habtemichael, N.; Bier, C.; Unruhe, B.; Weisheit, S.; Spange, S.; Nonnenmacher, F.; Fetz, V.; Ginter, T.; et al. A combination of a ribonucleotide reductase inhibitor and histone deacetylase inhibitors downregulates EGFR and triggers BIM-dependent apoptosis in head and neck cancer. *Oncotarget* **2012**, *3*, 31–43. [CrossRef] [PubMed]
62. Stauber, R.H.; Bier, C.; Knauer, S.K. Targeting Taspase1 for cancer therapy—letter. *Cancer Res.* **2012**, *72*, 2912. [CrossRef] [PubMed]
63. Campbell, J.D.; Yau, C.; Bowlby, R.; Liu, Y.; Brennan, K.; Fan, H.; Taylor, A.M.; Wang, C.; Walter, V.; Akbani, R.; et al. Genomic, Pathway Network, and Immunologic Features Distinguishing Squamous Carcinomas. *Cell Rep.* **2018**, *23*, 194–212.e6. [CrossRef]
64. Price, K.A.; Cohen, E.E. Current treatment options for metastatic head and neck cancer. *Curr. Treat. Options Oncol.* **2012**, *13*, 35–46. [CrossRef] [PubMed]
65. Oosting, S.F.; Haddad, R.I. Best Practice in Systemic Therapy for Head and Neck Squamous Cell Carcinoma. *Front. Oncol.* **2019**, *9*, 815. [CrossRef]
66. Siemer, S.; Bauer, T.A.; Scholz, P.; Breder, C.; Fenaroli, F.; Harms, G.; Dietrich, D.; Dietrich, J.; Rosenauer, C.; Barz, M.; et al. Targeting Cancer Chemotherapy Resistance by Precision Medicine-Driven Nanoparticle-Formulated Cisplatin. *ACS Nano* **2021**, *15*, 18541–18556. [CrossRef] [PubMed]
67. Hu, W.; Jin, P.; Liu, W. Periostin Contributes to Cisplatin Resistance in Human Non-Small Cell Lung Cancer A549 Cells via Activation of Stat3 and Akt and Upregulation of Survivin. *Cell. Physiol. Biochem.* **2016**, *38*, 1199–1208. [CrossRef] [PubMed]
68. Engels, K.; du Bois, A.; Harter, P.; Fisseler-Eckhoff, A.; Kommoss, F.; Stauber, R.; Kaufmann, M.; Nekljudova, V.; Loibl, S. VEGF-A and i-NOS Expression are Prognostic Factors in Serous Epithelial Ovarian Carcinomas after Complete Surgical Resection. *J. Clin. Pathol.* **2009**, *62*, 448–454. [CrossRef]
69. Engels, K.; Knauer, S.K.; Metzler, D.; Simf, C.; Struschka, O.; Bier, C.; Mann, W.; Kovacs, A.F.; Stauber, R.H. Dynamic intracellular survivin in oral squamous cell carcinoma: Underlying molecular mechanism and potential as an early prognostic marker. *J. Pathol.* **2007**, *211*, 532–540. [CrossRef]
70. Litvin, J.; Selim, A.H.; Montgomery, M.O.; Lehmann, K.; Rico, M.C.; Devlin, H.; Bednarik, D.P.; Safadi, F.F. Expression and function of periostin-isoforms in bone. *J. Cell. Biochem.* **2004**, *92*, 1044–1061. [CrossRef]
71. Khurshid, Z.; Mali, M.; Adanir, N.; Zafar, M.S.; Khan, R.S.; Latif, M. Periostin: Immunomodulatory Effects on Oral Diseases. *Eur. J. Dent.* **2020**, *14*, 462–466. [CrossRef] [PubMed]
72. Kii, I. Periostin Functions as a Scaffold for Assembly of Extracellular Proteins. *Adv. Exp. Med. Biol.* **2019**, *1132*, 23–32. [CrossRef] [PubMed]
73. Kikuchi, Y.; Kunita, A.; Iwata, C.; Komura, D.; Nishiyama, T.; Shimazu, K.; Takeshita, K.; Shibahara, J.; Kii, I.; Morishita, Y.; et al. The niche component periostin is produced by cancer-associated fibroblasts, supporting growth of gastric cancer through ERK activation. *Am. J. Pathol.* **2014**, *184*, 859–870. [CrossRef] [PubMed]
74. Kudo, Y.; Iizuka, S.; Yoshida, M.; Nguyen, P.T.; Siriwardena, S.B.; Tsunematsu, T.; Ohbayashi, M.; Ando, T.; Hatakeyama, D.; Shibata, T.; et al. Periostin directly and indirectly promotes tumor lymphangiogenesis of head and neck cancer. *PLoS ONE* **2012**, *7*, e44488. [CrossRef]
75. Malanchi, I.; Santamaria-Martinez, A.; Susanto, E.; Peng, H.; Lehr, H.A.; Delaloye, J.F.; Huelsken, J. Interactions between cancer stem cells and their niche govern metastatic colonization. *Nature* **2011**, *481*, 85–89. [CrossRef]
76. Cho, J.H.; Kim, K.; Yoon, J.W.; Choi, S.H.; Sheen, Y.H.; Han, M.; Ono, J.; Izuhara, K.; Baek, H. Serum levels of periostin and exercise-induced bronchoconstriction in asthmatic children. *World Allergy Organ. J.* **2019**, *12*, 100004. [CrossRef]
77. Kanno, A.; Satoh, K.; Masamune, A.; Hirota, M.; Kimura, K.; Umino, J.; Hamada, S.; Satoh, A.; Egawa, S.; Motoi, F.; et al. Periostin, secreted from stromal cells, has biphasic effect on cell migration and correlates with the epithelial to mesenchymal transition of human pancreatic cancer cells. *Int. J. Cancer* **2008**, *122*, 2707–2718. [CrossRef]

78. Ma, H.; Wang, J.; Zhao, X.; Wu, T.; Huang, Z.; Chen, D.; Liu, Y.; Ouyang, G. Periostin Promotes Colorectal Tumorigenesis through Integrin-FAK-Src Pathway-Mediated YAP/TAZ Activation. *Cell Rep.* **2020**, *30*, 793–806.e6. [CrossRef]
79. Park, J.J.; Hah, Y.S.; Ryu, S.; Cheon, S.Y.; Cho, H.Y.; Kim, J.P.; Won, S.J.; Lee, J.S.; Hwa, J.S.; Seo, J.H.; et al. Periostin Plays a Key Role in Radioresistance of Head and Neck Cancer Cells Via Epithelial-to-Mesenchymal Transition. *Anticancer Res.* **2020**, *40*, 2627–2635. [CrossRef]
80. Martinez, I.; Wang, J.; Hobson, K.F.; Ferris, R.L.; Khan, S.A. Identification of differentially expressed genes in HPV-positive and HPV-negative oropharyngeal squamous cell carcinomas. *Eur. J. Cancer* **2007**, *43*, 415–432. [CrossRef]
81. Sasaki, H.; Yu, C.Y.; Dai, M.; Tam, C.; Loda, M.; Auclair, D.; Chen, L.B.; Elias, A. Elevated serum periostin levels in patients with bone metastases from breast but not lung cancer. *Breast Cancer Res. Treat.* **2003**, *77*, 245–252. [CrossRef] [PubMed]
82. Erkan, M.; Kleeff, J.; Gorbachevski, A.; Reiser, C.; Mitkus, T.; Esposito, I.; Giese, T.; Buchler, M.W.; Giese, N.A.; Friess, H. Periostin creates a tumor-supportive microenvironment in the pancreas by sustaining fibrogenic stellate cell activity. *Gastroenterology* **2007**, *132*, 1447–1464. [CrossRef] [PubMed]
83. Chu, L.; Wang, F.; Zhang, W.; Li, H.F.; Xu, J.; Tong, X.W. Periostin Secreted by Carcinoma-Associated Fibroblasts Promotes Ovarian Cancer Cell Platinum Resistance Through the PI3K/Akt Signaling Pathway. *Technol. Cancer Res. Treat.* **2020**, *19*, 1533033820977535. [CrossRef]
84. Sung, P.L.; Jan, Y.H.; Lin, S.C.; Huang, C.C.; Lin, H.; Wen, K.C.; Chao, K.C.; Lai, C.R.; Wang, P.H.; Chuang, C.M.; et al. Periostin in tumor microenvironment is associated with poor prognosis and platinum resistance in epithelial ovarian carcinoma. *Oncotarget* **2016**, *7*, 4036–4047. [CrossRef] [PubMed]
85. Sterzynska, K.; Kazmierczak, D.; Klejewski, A.; Swierczewska, M.; Wojtowicz, K.; Nowacka, M.; Brazert, J.; Nowicki, M.; Januchowski, R. Expression of Osteoblast-Specific Factor 2 (OSF-2, Periostin) Is Associated with Drug Resistance in Ovarian Cancer Cell Lines. *Int. J. Mol. Sci.* **2019**, *20*, 3927. [CrossRef] [PubMed]
86. Xu, C.; Wang, Z.; Zhang, L.; Feng, Y.; Lv, J.; Wu, Z.; Yang, R.; Wu, T.; Li, J.; Zhou, R.; et al. Periostin promotes the proliferation and metastasis of osteosarcoma by increasing cell survival and activates the PI3K/Akt pathway. *Cancer Cell Int.* **2022**, *22*, 34. [CrossRef]
87. Xouri, G.; Christian, S. Origin and function of tumor stroma fibroblasts. *Semin. Cell Dev. Biol.* **2010**, *21*, 40–46. [CrossRef]
88. New, J.; Arnold, L.; Ananth, M.; Alvi, S.; Thornton, M.; Werner, L.; Tawfik, O.; Dai, H.; Shnayder, Y.; Kakarala, K.; et al. Secretory Autophagy in Cancer-Associated Fibroblasts Promotes Head and Neck Cancer Progression and Offers a Novel Therapeutic Target. *Cancer Res.* **2017**, *77*, 6679–6691. [CrossRef]
89. Choi, K.U.; Yun, J.S.; Lee, I.H.; Heo, S.C.; Shin, S.H.; Jeon, E.S.; Choi, Y.J.; Suh, D.S.; Yoon, M.S.; Kim, J.H. Lysophosphatidic acid-induced expression of periostin in stromal cells: Prognoistic relevance of periostin expression in epithelial ovarian cancer. *Int. J. Cancer* **2011**, *128*, 332–342. [CrossRef]
90. Shao, R.; Bao, S.; Bai, X.; Blanchette, C.; Anderson, R.M.; Dang, T.; Gishizky, M.L.; Marks, J.R.; Wang, X.F. Acquired expression of periostin by human breast cancers promotes tumor angiogenesis through up-regulation of vascular endothelial growth factor receptor 2 expression. *Mol. Cell. Biol.* **2004**, *24*, 3992–4003. [CrossRef]
91. Kim, C.J.; Yoshioka, N.; Tambe, Y.; Kushima, R.; Okada, Y.; Inoue, H. Periostin is down-regulated in high grade human bladder cancers and suppresses in vitro cell invasiveness and in vivo metastasis of cancer cells. *Int. J. Cancer* **2005**, *117*, 51–58. [CrossRef] [PubMed]
92. Ismail, R.S.; Baldwin, R.L.; Fang, J.; Browning, D.; Karlan, B.Y.; Gasson, J.C.; Chang, D.D. Differential gene expression between normal and tumor-derived ovarian epithelial cells. *Cancer Res.* **2000**, *60*, 6744–6749. [PubMed]
93. Gonzalez, H.E.; Gujrati, M.; Frederick, M.; Henderson, Y.; Arumugam, J.; Spring, P.W.; Mitsudo, K.; Kim, H.W.; Clayman, G.L. Identification of 9 genes differentially expressed in head and neck squamous cell carcinoma. *Arch. Otolaryngol.-Head Neck Surg.* **2003**, *129*, 754–759. [CrossRef]
94. Yoshioka, N.; Fuji, S.; Shimakage, M.; Kodama, K.; Hakura, A.; Yutsudo, M.; Inoue, H.; Nojima, H. Suppression of anchorage-independent growth of human cancer cell lines by the TRIF52/periostin/OSF-2 gene. *Exp. Cell Res.* **2002**, *279*, 91–99. [CrossRef] [PubMed]
95. Tai, I.T.; Dai, M.; Chen, L.B. Periostin induction in tumor cell line explants and inhibition of in vitro cell growth by anti-periostin antibodies. *Carcinogenesis* **2005**, *26*, 908–915. [CrossRef]
96. Sasaki, H.; Dai, M.; Auclair, D.; Fukai, I.; Kiriyama, M.; Yamakawa, Y.; Fujii, Y.; Chen, L.B. Serum level of the periostin, a homologue of an insect cell adhesion molecule, as a prognostic marker in nonsmall cell lung carcinomas. *Cancer* **2001**, *92*, 843–848. [CrossRef]
97. Sasaki, H.; Lo, K.M.; Chen, L.B.; Auclair, D.; Nakashima, Y.; Moriyama, S.; Fukai, I.; Tam, C.; Loda, M.; Fujii, Y. Expression of Periostin, homologous with an insect cell adhesion molecule, as a prognostic marker in non-small cell lung cancers. *Jpn. J. Cancer Res.* **2001**, *92*, 869–873. [CrossRef]
98. Shao, R.; Guo, X. Human microvascular endothelial cells immortalized with human telomerase catalytic protein: A model for the study of in vitro angiogenesis. *Biochem. Biophys. Res. Commun.* **2004**, *321*, 788–794. [CrossRef]
99. Vardaki, I.; Ceder, S.; Rutishauser, D.; Baltatzis, G.; Foukakis, T.; Panaretakis, T. Periostin is identified as a putative metastatic marker in breast cancer-derived exosomes. *Oncotarget* **2016**, *7*, 74966–74978. [CrossRef]
100. Paolillo, M.; Schinelli, S. Integrins and Exosomes, a Dangerous Liaison in Cancer Progression. *Cancers* **2017**, *9*, 95. [CrossRef]

101. Ghajar, C.M.; Peinado, H.; Mori, H.; Matei, I.R.; Evason, K.J.; Brazier, H.; Almeida, D.; Koller, A.; Hajjar, K.A.; Stainier, D.Y.; et al. The perivascular niche regulates breast tumour dormancy. *Nat. Cell Biol.* **2013**, *15*, 807–817. [CrossRef] [PubMed]
102. Lee, Y.J.; Kim, I.S.; Park, S.A.; Kim, Y.; Lee, J.E.; Noh, D.Y.; Kim, K.T.; Ryu, S.H.; Suh, P.G. Periostin-binding DNA aptamer inhibits breast cancer growth and metastasis. *Mol. Ther.* **2013**, *21*, 1004–1013. [CrossRef] [PubMed]
103. Oo, K.K.; Kamolhan, T.; Soni, A.; Thongchot, S.; Mitrpant, C.; Thuwajit, C.; Thuwajit, P. Development of an engineered peptide antagonist against periostin to overcome doxorubicin resistance in breast cancer. *BMC Cancer* **2021**, *21*, 65. [CrossRef] [PubMed]
104. Kyutoku, M.; Taniyama, Y.; Katsuragi, N.; Shimizu, H.; Kunugiza, Y.; Iekushi, K.; Koibuchi, N.; Sanada, F.; Oshita, Y.; Morishita, R. Role of periostin in cancer progression and metastasis: Inhibition of breast cancer progression and metastasis by anti-periostin antibody in a murine model. *Int. J. Mol. Med.* **2011**, *28*, 181–186. [CrossRef]

V.

diagnostics

MDPI

Article

IsoMAG—An Automated System for the Immunomagnetic Isolation of Squamous Cell Carcinoma-Derived Circulating Tumor Cells

Alena Gribko [1,†], Janis Stiefel [2,†], Lana Liebetanz [2], Sophie Madeleine Nagel [1], Julian Künzel [3], Madita Wandrey [1], Jan Hagemann [1], Roland H. Stauber [1], Christian Freese [2,*] and Désirée Gül [1,*]

1 Department of Otorhinolaryngology, University Medical Center Mainz, Langenbeckstr. 1, 55131 Mainz, Germany; algribko@uni-mainz.de (A.G.); sophiemadeleine.nagel@web.de (S.M.N.); wandrey@uni-mainz.de (M.W.); jan.hagemann@unimedizin-mainz.de (J.H.); rstauber@uni-mainz.de (R.H.S.)
2 Fraunhofer Institute for Microengineering and Microsystems IMM, Carl-Zeiss-Str. 18-20, 55129 Mainz, Germany; Janis.Stiefel@imm.fraunhofer.de (J.S.); lana-liebetanz@web.de (L.L.)
3 Department of Otorhinolaryngology, University Hospital Regensburg, Franz-Josef-Strauß-Allee 11, 93053 Regensburg, Germany; julian.kuenzel@ukr.de
* Correspondence: Christian.freese@imm.fraunhofer.de (C.F.); guel@uni-mainz.de (D.G.)
† These authors contributed equally.

Abstract: Background: detailed information about circulating tumor cells (CTCs) as an indicator of therapy response and cancer metastasis is crucial not only for basic research but also for diagnostics and therapeutic approaches. Here, we showcase a newly developed IsoMAG IMS system with an optimized protocol for fully automated immunomagnetic enrichment of CTCs, also revealing rare CTC subpopulations. Methods: using different squamous cell carcinoma cell lines, we developed an isolation protocol exploiting highly efficient EpCAM-targeting magnetic beads for automated CTC enrichment by the IsoMAG IMS system. By FACS analysis, we analyzed white blood contamination usually preventing further downstream analysis of enriched cells. Results: 1 µm magnetic beads with tosyl-activated hydrophobic surface properties were found to be optimal for automated CTC enrichment. More than 86.5% and 95% of spiked cancer cells were recovered from both cell culture media or human blood employing our developed protocol. In addition, contamination with white blood cells was minimized to about 1200 cells starting from 7.5 mL blood. Finally, we showed that the system is applicable for HNSCC patient samples and characterized isolated CTCs by immunostaining using a panel of tumor markers. Conclusion: Herein, we demonstrate that the IsoMAG system allows the detection and isolation of CTCs from HNSCC patient blood for disease monitoring in a fully-automated process with a significant leukocyte count reduction. Future developments seek to integrate the IsoMAG IMS system into an automated microfluidic-based isolation workflow to further facilitate single CTC detection also in clinical routine.

Keywords: automation; liquid biopsy; circulating tumor cells; head and neck squamous cell carcinoma; immunomagnetic particle-based detection; metastasis

Citation: Gribko, A.; Stiefel, J.; Liebetanz, L.; Nagel, S.M.; Künzel, J.; Wandrey, M.; Hagemann, J.; Stauber, R.H.; Freese, C.; Gül, D. IsoMAG—An Automated System for the Immunomagnetic Isolation of Squamous Cell Carcinoma-Derived Circulating Tumor Cells. *Diagnostics* **2021**, *11*, 2040. https://doi.org/10.3390/diagnostics11112040

Academic Editor: Gustavo Baldassarre

Received: 20 September 2021
Accepted: 1 November 2021
Published: 4 November 2021

1. Introduction

Cancer is the second major cause of death in modern society. Besides improved treatment strategies, the development of innovative diagnostics is indispensible for long-term improvement of diagnosis and treatment of cancer patients. The lymph-/hematogenous spread of cancer cells into distant organs and their subsequent growth to overt metastases is the most fatal complication of solid tumors, such as squamous cell carcinoma of the head and neck (HNSCC) [1,2]. Moreover, therapy resistance and associated relapses are common and associated with high patient morbidity [3,4]. The classical view is that metastatic spread is a late process in malignant progression, but today it is accepted that

blood circulation and dissemination of primary cancer cells to distant sites is already an early event [5,6].

The fact that these circulating tumor cells (CTCs) are detectable in the peripheral blood of cancer patients months to years after complete removal of the primary tumor in a period called "metastatic cancer dormancy" supports the idea that these cells circulate between metastatic sites [7]. Since their early discovery in the 19th century [8], CTCs have been demonstrated to be clinically recognized and present in the blood circulation of many cancer types including colon [9], lung [10], ovarian [11], breast [12], melanoma [13], prostate [14] and head and neck cancer [15]. Clinical studies present a correlation between the progression of cancer disease and the number of detected CTCs [16–18]. A high number of detected CTCs can give information about tumor burden, recurrence and usually represents a poor prognosis. In detail, the determination of CTCs before and after resection also opens up the possibility for monitoring therapeutic response [19] in combination with analyses of circulating tumor DNA (ctDNA) [20]. Hence, the detection and characterization of CTCs as a part of minimal invasive "liquid biopsy" has gained (pre)clinical considerable attention over the last decade [21,22].

However, the capture and detection of CTCs are extremely challenging because of their rarity, the property to move as individual cells or as multi-cellular clumps, and their heterogeneity regarding size and biological and molecular changes during the epithelial-to-mesenchymal transition (EMT) processes. These challenges require the ability to handle a very small number of cells by isolation methods with high efficiency in an acceptable time scale [23]. Various techniques that are based on physical or immunological properties have been developed [24], and different materials with their unique properties according to their shape, size and surface were applied in this field [25–27]. Only a few systems are available on the liquid biopsy market but have been shown to isolate CTCs in a proper way. Thereby, these methods often dictate an exact protocol to the user, taking away application flexibility. In contrast to that, researchers aim for process-adaptable platforms as the disciplines of liquid biopsy expand permanently, concerning various sample types such as tissue-derived single cell suspensions or adjustable sample sizes.

All techniques developed for CTC enrichment have their advantages and disadvantages. In contrast to immunomagnetic separation, physical separation methods (e.g., Parsortix® technology, Angle, Surrey, UK) allow label-free isolation but lack cell distinction due to overlapping sizes of CTCs and white blood cells [28]. A microstructure-based enrichment is limited in throughput and sieve-shaped technologies, error-prone to complex liquids such as whole blood, are consequently at risk of clogging in automated lab solutions. Though it has drawbacks in target selectivity, immunomagnetic enrichment is often the method of choice because it is easily automatable and enables a high sample throughput. Since the establishment of the "Food and Drug Administration" (FDA)-approved CellSearch® system, which is held as the gold standard of automated immunomagnetic enrichment and staining platforms, the sensitivity of CTC detection has markedly improved [29,30]. CellSearch® relies on the expression of the epithelial cell adhesion molecule (EpCAM) for the quantification of CTCs in different tumor types [31]. Although this optical detection method have been used in numerous studies, the cost for instruments (220,000 dollars), sample preparations and analysis are still laborious and relatively high (approx. 1000 dollars/run) [32]. Consequently, such assays did not succeed in establishing in clinical routine as a low-cost diagnostic test. Due to the above-mentioned obstacles, fully automated, easy-to-use platforms will demonstrate future solutions to improve cancer diagnostics and therapies as well as basic scientific knowledge of tumor development.

The Fraunhofer CTCelect unit has been developed to meet the need of such a fully automated, easy-to-use platform for CTC isolation out of 7.5 mL whole blood samples. Herein, we characterized the IsoMAG IMS device as the core unit of such a platform applying fully automated immunomagnetic enrichment of rare cells with flexibly selectable antigen targets. In this proof-of-principle study, we established a robust protocol for the automated isolation of an EpCAM- and CSV (cell surface vimentin)-positive subpopulation

of cells with a concomitant reduction of background white blood cells as a prerequisite for implementation of the device into the CTCelect unit allowing downstream analyses on a single cell level. Furthermore, we proved feasibility of the method for two squamous cell carcinoma cell lines and HNSCC patient samples.

2. Materials and Methods

2.1. Cell Lines

The SCL-1 squamous cell carcinoma line was established by Dr. Petra Boukamp (DKFZ, Heidelberg, DE, Germany) [33] and kept in Gibco™ DMEM (low glucose, pyruvate) medium supplemented with 10% FCS. HNSCCUM-02T squamous cell carcinoma cell line was established by Welkoborsky et al. (UMC Mainz, DE, Germany) [34], and kept in DMEM:F-12 (cc-pro) medium supplemented with 10% FCS and 1% L-glutamine. Cell lines were cultured at subconfluence and incubated at 37 °C in a 5% CO_2 humidified atmosphere. Other cell lines (A431, HEK293T, MV3, BLM) were received from cell line collections (DSMZ, ATCC) and handled as described before [35–37].

2.2. Blood Samples

All blood samples were obtained from the University Medical Center Mainz, DE. To quantify leukocyte contamination, whole blood bags (500 mL CompoFlex, Fresenius Kabi, Bad Homburg, Germany) from healthy donors were purchased at the local Blood Transfusion Center. Whole blood from HNSCC patients was collected at the Department of Otorhinolaryngology in compliance with ethical guidelines [38].

2.3. Immobilization of EpCAM Antibodies on Immunomagnetic Beads

Immunomagnetic beads at different sizes and surface properties (Table 1) were purchased at Thermo Fisher Scientific, Darmstadt, DE and coated with biotinylated monoclonal mouse anti-human EpCAM (CD326) antibody 1B7 (20 µg/mL, eBioscience, GB) or anti-human CSV antibody (clone 84-1, Abnova, Taiwan) for 1 h as described by the manual. Free streptavidin binding sites on anti-EpCAM beads were then saturated with a biotin/PBS solution for 30 min. Anti-EpCAM beads were stored at 4 °C for several weeks.

Table 1. Overview of tested Dynabeads.

Beads	Size	Surface Functionalization
Dynabeads MyOne Streptavidin T1	1 µm	Tosyl-activated, hydrophobic
Dynabeads MyOne Streptavidin C1	1 µm	Carboxylic acid, hydrophilic
Dynabeads M-270 Streptavidin	2.8 µm	Carboxylic acid, hydrophilic
Dynabeads M-280 Streptavidin	2.8 µm	Tosyl-activated, hydrophobic

2.4. Manual Cell Isolation by Immunomagnetic Beads

To compare the performance of the IsoMAG IMS unit it was also necessary to establish a standard protocol for manual cell isolation. Cells (SCL-1, HNSCCUM-02T) were released from culture flasks and stained using the CellTrace™ CFSE Cell Proliferation Kit (CFSE) according to the manufacturer's protocol. A defined number of stained single cells were aspirated with a 10 µL pipette from a 1:100 diluted cell suspension in a petri dish and spiked into 7.5 mL sample volume consisting of cell culture medium, or blood of healthy donors. Next, 100 or 150 µL (depending on medium or blood) of anti-EpCAM Dynabeads MyOne Streptavidin were added (see Table 1) and incubated for 30 min with slow rotation of the tube. Next, the bead-bound cells were magnetically separated for 10 min by using DynaMag-15 (Invitrogen, Thermo Fisher Scientific, Dreieich, Germany) and resuspended in 5 mL washing buffer. Washing steps and magnetic separation were repeated three times using a decreased incubation time of 5 min and resuspension in washing buffer with decreasing volumes (ranging from 5 mL, 4 mL up to 1 mL).

2.5. Automated CTC Enrichment Using the IsoMAG Device

For the establishment of a standard protocol using the IsoMAG IMS unit, antibody-coupled beads were added to a 7.5 mL sample volume consisting of cell culture medium, blood of healthy donors or patient blood samples with spiked EpCAM+ SCL-1 or patient-derived HNSCC cells (HNSCCUM-02T). Before initiating the assay in the software, five tubes containing the input sample and washing buffers were placed in the tube holder carousel and a 10 mL pipet tip was put in the holder of the IsoMAG device as described in Table S1. The sample was incubated for 30 min. After incubation, bead-bound CTCs were magnetically separated alternately with several washing steps in decreasing volumes from 5 mL to 1 mL (see Supplementary Table S1 for detailed protocol).

2.6. Characterization of Leukocyte Contamination in IsoMAG Isolates

To quantify analysis-disrupting white blood cell (WBC) contamination in tumor cell isolates, CD45+ cell count after manual and automated IMS was determined by flow cytometry. Therefore, we established a double staining protocol for leukocytes using a CD45-PE antibody targeting the specific surface protein of WBCs (1:50 dilution; Miltenyi Biotec, Bergisch Gladbach, DE, Germany) and nuclear stain RedDot™ (Biotium, Fremont, CA, USA). Wash buffers were set up in the IsoMAG IMS unit and 150 µL EpCAM beads were added to 7.5 mL whole blood before initiating the automated protocol. Manual enrichment was performed in parallel. The final samples were separated in a magnet separator, the supernatant was discarded and the bead cell pellet was stained with the above-mentioned solutions. Dual-positive cells [CD45+/RedDot+] were analyzed by FACS using the BD Accuri C6 flow cytometer. Cell counts after IMS were measured in four samples of different healthy donors and the average WBC contamination with standard deviation (SD) was calculated.

2.7. Immunostaining of IsoMAG Isolated CTCs

To assess possible tumor origin of isolated cells, the final 1 mL sample was administered several staining steps. First, isolated cells were stained with fluorescent CD45-FITC antibody (1:1000 dilution) to label leukocytes. Subsequently, the sample was washed three times with PBS in a magnetic separator and transferred to an ibidi 8-well slide (ibidi GmbH, Gräfelfing, Germany) after the last separation step. Cells were centrifuged to the bottom of the slide by a CytoSpin device and fixed in 4% paraformaldehyde for 10 min. After further washing steps, cells were permeabilized (0.1% Triton X in PBS, 5 min) and stained with nuclear dye Hoechst33342 (1:1000 dilution) for 20 min. Following further washing steps, unspecific binding was blocked for 30 min using 0.5% BSA in PBS and staining with fluorescent anti-pan-Cytokeratin-PE antibody (1:200 dilution, overnight) was performed.

2.8. Statistical Analysis

Each experiment was repeated at least three times. Data are shown as means with SD and statistical analysis was performed using GraphPad PRISM for Windows (GraphPad Software v9.1.2.226, San Diego, CA, USA, www.graphpad.com, accessed on 13 July 2021). *p*-values were reported as significant when * $p \leq 0.05$.

3. Results

3.1. Optimization of Biofunctionalized Beads for Cell Enrichment

The selection of magnetic beads and immobilized antibodies on the bead surface are decisive factors in terms of cell-specific enrichment. First, EpCAM-biotin antibodies were immobilized on the streptavidin-biofunctionalized beads. To identify a proper CTC model to characterize IsoMAG, manual immunomagnetic enrichment of various epithelial cancer cell lines, such as cutaneous squamous cell carcinoma cells (SCL-1, SCL-2), and A431 was performed (Supplementary Figure S1). We determined the highest recovery rates for EpCAM beads using SCL-1 (85%, $n = 3$) and A431 cells (100 ± 20%, $n = 3$). As controls, we were also able to isolate melanoma cells (MV3, BLM) targeting melanoma-associated

chondroitin sulfate proteoglycan (MCSP), but not HEK293T (Supplementary Figure S1B). Being an appropriate squamous epithelial-derived model close to HNSCC, we therefore chose to proceed with the characterization of IsoMAG using the combination of EpCAM beads and SCL-1 cells. For this cell line, high expression of epithelial marker EpCAM is described. EpCAM mRNA expression in SCL-1 cells was confirmed on a single cell level using RT-qPCR (Supplementary Figure S2).

Since there are numerous commercially available beads with different surface modifications and sizes, the next step was to investigate their potential to enrich EpCAM-positive cells spiked into cell culture medium. In this context, four different types of magnetic beads varying in size and surface properties were tested (Table 1). Therefore, 20 fluorescently labeled SCL-1 cells were spiked into 7.5 mL cell culture medium and functionalized magnetic beads were added. After incubation, these cells were manually enriched with a magnetic separator. We obtained the best recovery rates by using 1 µm T1 beads and 2.8 µm M280 beads (Figure 1A). Using these beads, the cell recovery rate was 88.3% (±2.9% SD) whereas the use of 1 µm C1 or 2.8 µm M270 beads resulted in less than 50% cell recovery.

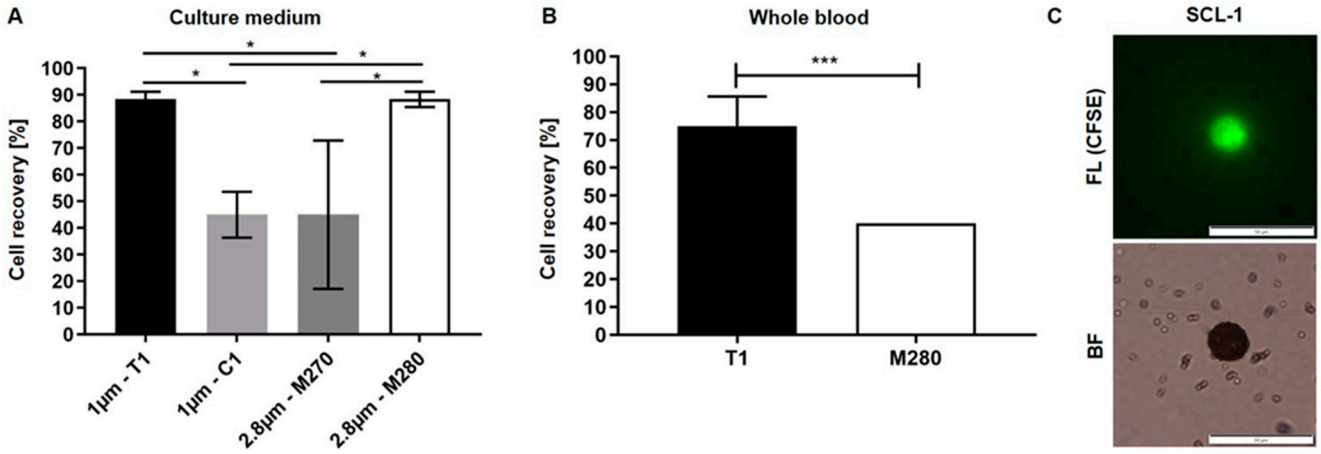

Figure 1. Enrichment of HNSCC cells from cell culture medium (**A**) and whole blood (**B**) differs depending on size and type of functionalized magnetic beads. Values are displayed as means of recovered cells using antibody-coupled magnetic beads with specific sizes and surface modifications. Twenty fluorescently labelled SCL-1 cells were spiked into 7.5 mL cell culture medium (**A**) or 7.5 mL full blood samples (**B**), and manually enriched by using EpCAM antibody coupled magnetic beads. (**A**) Welch's *t*-test, $n = 3$, *: $p < 0.05$ (one-way ANOVA test with Tukey's *t*-test); (B) Welch's *t*-test, $n = 6$ (T1), $n = 2$ (M280), ***: $p < 0.002$; (**C**) recovered, CFSE-stained SCL-1 cells were analyzed by fluorescence microscopy (FL). Corresponding bright-field image (BF) shows beads bound to cell and freely distributed in the medium. Scale bar, 50 µm.

Subsequently, the performance of T1 and M280 beads was investigated in blood samples of healthy donors. Again, 20 fluorescently labeled SCL-1 cells were spiked into 7.5 mL blood and were manually enriched using the same protocol. As depicted in Figure 1B, the number of recovered cells is significantly higher using T1 beads compared to M280 beads (75 vs. 40%). Microscopic analysis of isolated cells in the counting chamber revealed that cells are densely covered by magnetic beads which are also freely distributed in the enrichment medium (Figure 1C).

Regarding our previous results, T1 beads were chosen for establishment of the automated cell isolation using the IsoMAG IMS demonstrator (Figure 2A). The centerpiece of the benchtop device is a rotatable tube holder carousel with max. 6 reagent slots (Figure 2B). The different positions of the carousel and the 10 mL pipet tip holder to pick up the pipet tip and perform the enrichment are driven by a pipetting robot on a vertical and horizontal axis. The magnet arm is moveable at a swivel joint to capture bead bound cells and free beads in the pipet tip while reducing the sample volume by discarding the supernatant wash buffers. Macrofluidic sample pipetting is directed pneumatically with a syringe pump. The 7.5 mL starting sample is placed into the first position of the carousel. Posi-

tions 2–5 are subsequently filled with washing buffers in a decreasing volume and the assay is initiated in the software on an external computer (for detailed protocol see also Supplementary Table S1).

The results obtained with the IsoMAG IMS unit were directly compared to manually enriched cells with the same batch of magnetic beads. Automated isolation resulted in 86.9% cell recovery while 88.8% of the spiked cells could be detected by manual isolation. This means that in our spiking experiments more than 17 out of 20 cells were recovered from a volume of 7.5 mL by both manual enrichment and the fully automated protocol without significant difference. Statistical analysis of recovery rates showed a slightly lower SD of 2.4% (n = 4) after automated isolation compared to manual enrichment (4.8% SD; n = 4), indicating a reproducible automation.

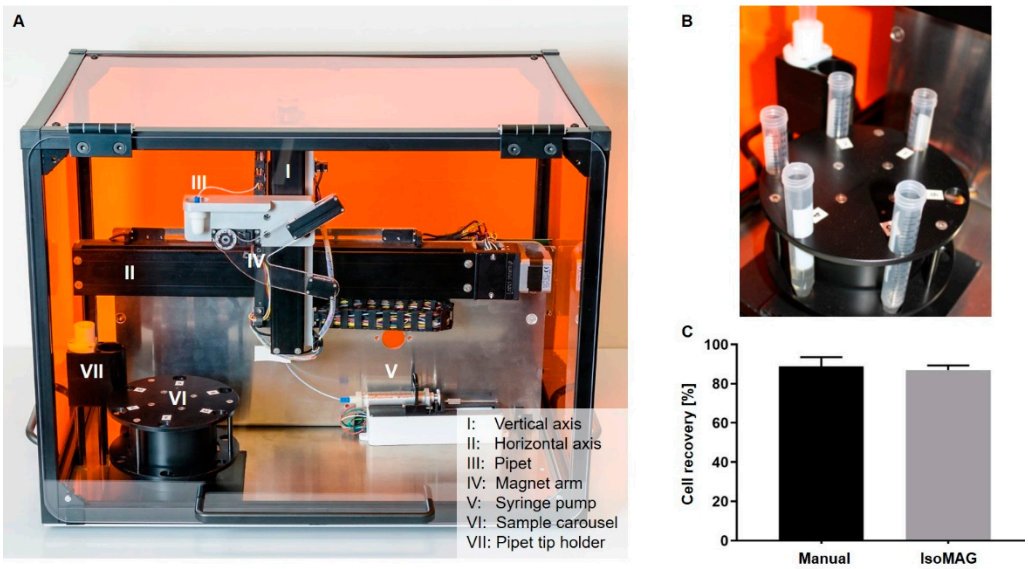

Figure 2. Establishment of automated cell recovery using IsoMAG IMS unit. (**A**) IsoMAG IMS demonstrator with horizontal and vertical axis driving the pipet unit and magnet arm; (**B**) the carousel as tube holder for prestorage of sample and wash buffers; (**C**) 20 fluorescently labelled cells were spiked into 7.5 mL cell culture medium and enriched by using EpCAM antibody coupled T1 (1 µm) magnetic beads. The sample was processed manually or automated using the IsoMAG IMS system. Welch's t-test, n = 4, ns: $p > 0.1234$.

3.2. Reduction of Blood Cell Contamination

Besides a robust protocol and an easy-to-handle automated system, it is crucial to reduce the number of "background" WBCs to enable high quality downstream analyses. In preliminary work we already established the basic isolation process, including optimization of necessary washing steps (data not shown). In this study, the automated assay was characterized regarding washing buffers to minimize the unspecific carryover of dual-positive leukocytes [CD45+/RedDot+]. Samples were analyzed by FACS to determine WBC contamination. Gates were set with CD45-PE/RedDot^{TM}-stained blood dilution as positive control and stained beads as negative control. The results presented in Figure 3A show that the number of leukocytes after the automated isolation process was about 1200 cells. Comparable results were achieved after manual enrichment (5123 dual-positive cells). However, we observed a broad scattering of WBC counts with a standard deviation of almost 4900 cells in manually enriched samples. Thus, an automated protocol has been developed considering both a high efficiency of cell recovery as well as a low rate of WBC contamination.

A

Enrichment	Total cell count	RedDot+/CD45+	Mean [RedDot+/CD45+]	SD
Automated	1,059,336	1202	**1202**	-
Manual	1,212,269	83	**5123**	±4888
	1,265,018	1813		
	1,476,892	5810		
	1,661,907	12,786		

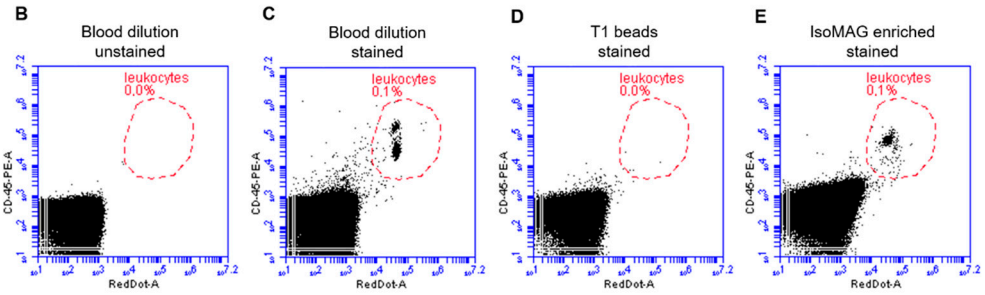

Figure 3. Automated immunomagnetic enrichment procedure exhibits a significantly lower amount of leukocyte contamination compared to manual cell isolation. (**A**) Summary of enrichment processes and quantification of leukocyte contamination. (**B**–**E**) After the automated enrichment process, cells were stained with CD45-PE antibody and nucleic staining reagent RedDot^{TM}. Blood dilution (1:1000) shows a dual-positive cell population (**B**,**C**). After the enrichment process, this gating was used to quantify the leukocyte contamination (**E**) while showing no staining of the free beads themselves (**D**).

3.3. Automated Enrichment of Head and Neck Cancer Cells

We applied the method to a second cancer entity originating from squamous cell tissue with an epithelial, EpCAM-positive phenotype as proof-of-principle. Thus, enrichment experiments were also performed with an epithelial cell line model derived from head and neck squamous cell carcinoma (HNSCCUM-02T). HNSCCUM-02T cells show high EpCAM expression allowing enrichment with our system (Supplementary Figure S3A).

Automated enrichment (spike-in) experiments with HNSCCUM-02T cells were conducted as described before and demonstrated applicability of the IsoMAG IMS unit using blood samples, both from healthy donors and patient blood (Figures 4 and 5). In total, 95% (±15) of spiked cells were recovered (Figure 4A), quantified by fluorescence microscopy after intracellular staining of epithelial tumor marker pan-cytokeratin (pan-CK) [39] and CD45 (Figure 4B). Isolated tumor cells were identified by expression of cytokeratin [Hoechst+/CD45−/panCK+] and could be differentiated from CD45-positive leukocytes [Hoechst+/CD45+/panCK−] appearing at low frequency after enrichment.

As dynamic EMT and MET processes seem to modulate primary tumors, metastases and CTCs disease- and patient-dependently, detection systems allowing the use of variable CTC/cancer markers are highly desirable. To underline the advantage and full flexibility of our device to also isolate cells by using variable cancer markers, we here targeted cell-surface vimentin (CSV) as an additional proof-of-concept example. As shown in Figure 4C, we performed spike-in experiments using engineered CSV-coupled immunomagnetic beads to isolate HNSCCUM-02T cancer cells from human blood. Expression of CSV was verified by Western blot analysis and immunofluorescent staining (Supplementary Figure S3C,D). Importantly, automated isolation of spiked HNSCCUM-02T cells using CSV-coupled beads also resulted in high recovery rates of ±95% (Figure 4C).

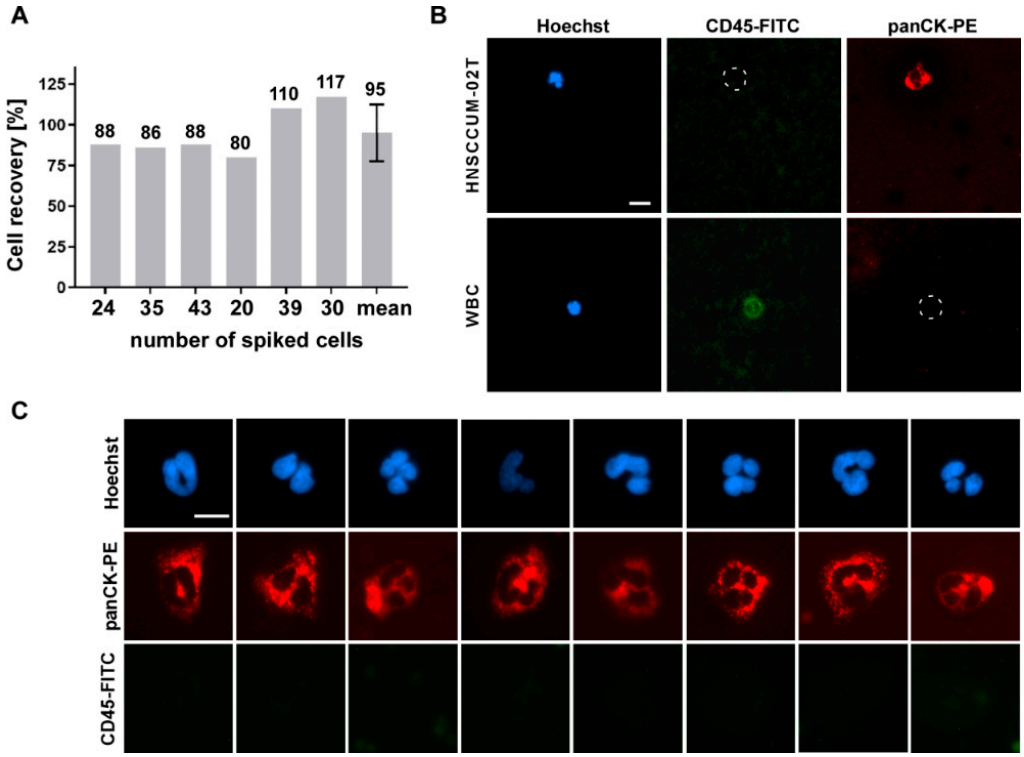

Figure 4. Cell isolation by the IsoMAG System resulted in high recovery rates for head and neck cancer cells. (**A**) Different numbers of HNSCCUM-02T cells were spiked in blood samples and enriched by EpCAM-coupled T1-beads using the IsoMAG unit. (**B**) For cell counting, recovered cells were stained with Hoechst dye, cytokeratin (panCK-PE) and CD45-FITC antibodies and quantified by fluorescence microscopy. [Hoechst+/CD45−/panCK+) cells were classified as HNSCCUM-02T cells, [Hoechst+/CD45+/panCK−] cells as leukocytes (WBC). Scale bar, 10 µm. (**C**) Examples of cells enriched by CSV-coupled T1-beads. Cells were stained as described in (**B**). Scale bar, 10 µm.

3.4. CTC Screening Using Blood of HNSCC Patients

Finally, three HNSCC patients were screened for CTCs applying our established protocol for the IsoMAG IMS system. The results shown in Figure 5 impressively demonstrate the clinical applicability of the system. All cells positive for cytokeratin but negative for CD45 expression [Hoechst+/CD45−/panCK+] were counted and classified as potential CTCs (Figure 5B). Here, we were able to isolate 74 to 93 potential CTCs with an epithelial-like character from patients suffering from different head–neck tumor subtypes (hypo- and oropharynx cancers with lymph node metastasis, see Figure 5A). We also captured preliminary data on isolation of CTCs out of patient blood using a combination of EpCAM and CSV beads (Supplementary Figure S4). However, these results obtained from a small and heterogeneous group of patients are preliminary and have to be confirmed by larger studies and further analysis methods, e.g., sequencing.

A

#	Localization	Clinical TNM	pTNM	p16 status	HPV status	Detected CTCs
1	Hypopharynx	cT4a cN3b cM0	n.a.	n.a.	-	**93**
2	Oropharynx	cT3 cN1 cM0	pT2pN1 G3	+	+	**74**
3	Oropharynx	cT2 cN0 cMx	pT3pN1 G3	-	-	**86**

B

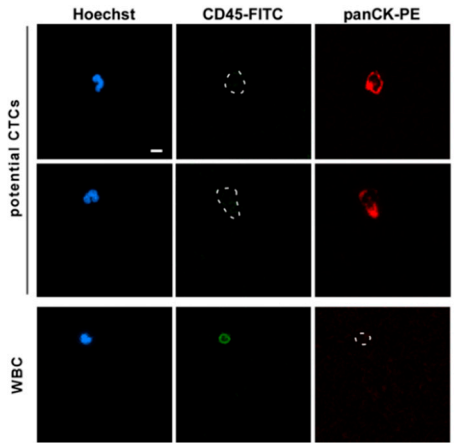

Figure 5. Potential circulating tumor cells (CTCs) could be enriched from head and neck cancer patient blood. (**A**) Clinical parameters and numbers of detected CTCs for three patients suffering from hypo- or oropharyngeal cancers including lymph node metastases. (**B**) 7.5 mL of patient blood was mixed with EpCAM-coupled T1 beads and placed into the IsoMAG unit for automatic enrichment of CTCs. For cell counting, enriched cells were stained with Hoechst dye, cytokeratin (panCK-PE), and CD45-FITC antibodies and quantified by fluorescence microscopy. [Hoechst+/CD45−/panCK+] cells were classified as potential CTCs, [Hoechst+/CD45+/panCK−] cells as leukocytes (WBC). Scale bar, 10 µm.

4. Discussion

Personalized cancer therapy will benefit from analysis of single solid and circulating tumor cells in the future. In order to develop a fully automated system for the enrichment and isolation of single tumor cells, the reduction in sample volume plays a pivotal role. Thus, excellent performance is required for the enrichment step depending on the developed system but also on the developed protocol.

In the present study, we successfully established a robust protocol for the automated isolation of CTCs by the IsoMAG IMS device, a core unit of the CTCelect platform. As a first step, we developed a suitable CTC model system to establish the protocol for squamous cell carcinoma. Although we also achieved high recovery rates for the epithelial A431 cells, we decided to use SCL-1 and HNSCCUM-02T cell lines as squamous epithelial-derived models close to HNSCC. Of note, we are aware of variable EpCAM expression in "primary CTCs" versus established cancer cell lines. However, for the development and comparison of CTC selection procedures and devices, CTC models with defined EpCAM levels are mandatory. Using this model, we demonstrated improved performance of 1 µm tosyl-activated, hydrophobic magnetic beads (T1) which thus were chosen for our final protocol. In addition to their advantageous characteristics for automated applications, such as a low sedimentation rate and faster reaction kinetics compared to M-280/M-270 beads, our results are in line with other studies showing improved capture efficiency and specificity of 1 µm T1 beads for magnetic cell detection [40,41].

Downstream analyses of isolated cells by fluorescence microscopy not only confirmed expression of relevant cancer markers, but also revealed tight binding of magnetic beads to the cell surface (see also Figure 1C). Regarding the size of the used T1 beads (1 µm) and an average diameter of CTCs between 10–12 µm [28], the surface of a cancer cell could theoretically be covered with 300–450 magnetic beads suggesting severe consequences for cell integrity and viability. However, we observed that isolated CTCs are not completely

covered with beads, and preliminary studies revealed that re-attachment and cultivation of isolated cells is not excluded, albeit very challenging (see Supplementary Figure S5). Here, additional washing and bead detachment steps, as well as careful adjustments of cell cultivation, such as the use of preconditioned medium and collagen-coated slides, are necessary to receive viable and proliferating cells. Due to the highly versatile construction and design of the device, it is possible to implement such additional purification steps to the automated IsoMAG protocol. Moreover, the biocompatibility of micro/nanocarriers may be affected by biomolecule corona formation [26,42,43]. It is accepted that when micro/nanocarriers enter physiological environments, proteins and other biomolecules bind to their surfaces, leading to the rapid formation of a biomolecule corona [44]. The corona may be critically co-defining the biological, medical, biotechnological and pathophysiological identity of micro/nanocarriers, although the mechanistic details have not been resolved in detail [45,46].

As an additional relevant factor, reduction of background white blood cells is mandatory for the establishment of a reliable protocol allowing downstream single-cell analysis. In summary, our study shows that using the optimized protocol for IsoMAG tumor cells from patient samples can be enriched and detected in a semi-automated process combined with a reduction of white blood cells (WBC) starting from a large volume (7.5 mL). The broad scattering of WBC counts we observed could depend on a naturally different blood cell count between healthy individuals. It is conceivable that the WBC count could be a hindrance to nucleic acid-based downstream applications at this point due to enforced background noise. A purity of at least 50% is recommended for proper genomic analysis, whereas in our small patient screening, a vast percentage of total output cells was WBCs. On an average, we were able to isolate 84 potential CTCs from three patient samples, while EpCAM-based enrichment entailed a bycatch of ~1200 WBCs. Nevertheless, the relatively low number of 10^3 WBCs (compared to 10^7 WBCs/mL in healthy adults) enabled immunofluorescent assessment of the patient isolates and marker-based distinction between potential CTCs and WBCs to deliver a ready-to-use assay in an otorhinolaryngology lab environment. In comparison, a similar WBC bycatch of over 800 cells/sample was described for CellSearch® [47], whereas size-based Parsortix® delivers purity grades ranging from 29–97% depending on the study [48,49].

To address downstream analysis, subsequent microfluidic cell sorting of the IsoMAG isolates, manual cell picking or aspiration technologies such as the ALS CellCelector™ are appropriate tools to improve signal-to-noise ratio for transcriptomic analysis. We already started implementing IsoMAG in an in-house developed microfluidic single-cell-sorting workflow resulting in a purity of $\geq$75% (Supplementary Figure S6). By aspirating only dispensed droplets that contain fluorescent cells for RNA isolation, we obtained promising PCR results detecting even small numbers of EpCAM+ tumor cells with low WBC background signal. These findings underline that (immunomagnetic) pre-enrichment of the CTCs by IsoMAG is an indispensable prerequisite for microfluidic cell sorting and downstream CTC analysis.

Interestingly, during protocol establishment we observed cell recovery rates of >100%. This was likely due to false positive panCK or false negative CD45 staining which has been optimized during establishment. However, our automated protocol combines both a high efficiency of cell recovery as well as a low rate of WBC contamination.

Furthermore, in the presented study we could also show that the established method is adaptable to the detection of EpCAM-, as well as CSV-positive subpopulation of CTCs. Typically, immunomagnetic cell isolation devices use epithelial markers, mostly EpCAM, for CTC detection neglecting the fact that cancer cells undergo morphological changes during epithelial-to-mesenchymal transition (EMT) and the reverse process (MET). Importantly EMT/MET which takes place during entry and transport in the blood stream is accompanied by up- and downregulation of surface markers used for CTC detection, such as EpCAM, N-/E-Cadherine, and cell-surface vimentin [50]. Thus, in contrast to other commercial systems we are able to capture cells exhibiting not only epithelial, but

also mesenchymal and/or an intermediate phenotype. Preliminary data combining beads targeting EpCAM as wells as CSV for automated cell enrichment were also promising but have to be confirmed in larger studies to assess the added value of using multiple markers for HNSCC.

In our small patient screening study, we were able to isolate 74 to 93 potential CTCs with the optimized protocol. Previous studies applying different methods for CTCs detection in HNSCC revealed a broad range of enumerated cells. Whereas Grisanti et al. detected 0–2 CTCs in 16–40% of the patients using the CellSearch® platform [51], manual enumeration of immunofluorescent stained cells resulted in higher CTC numbers (0–37 CTCs/1000 PBMC) [18]. Despite the broad ranges of detected CTCs, the obtained results of our IsoMAG IMS unit are in the order of previous studies combined with low numbers of leukocyte contamination. We could also observe a slight tendency for an increasing CTC number in T4 staged tumors compared to T1–3 as described previously [16,18]. Of course, these results have to be interpreted with caution because the small number of patients does not allow reliable assessment. This observation and the fact that a high mortality rate of HNSCC patients correlates to late diagnosis show the necessity of an early and reliable detection method of CTCs. Semi-automated detection of CTCs such as IsoMAG has the potential to be related as a standardized part of liquid biopsy with the advantages of real-time personalized analysis in combination with non-invasiveness and individual prognostic therapy [15].

Taken together, there are several findings of this study underlining the advantages of the IsoMAG device compared to other immunomagnetic isolation methods. Whereas CellSearch® is marketed relying only on epithelial targeting of preserved cells in the CELLTRACKS® AUTOPREP® System and requires centrifugation [52], the IsoMAG protocol allows highly flexible targeting of viable CTCs without blood pre-processing. Implementation into the CTCelect workflow in future will allow downstream single-cell analysis and cell cultivation. The general major advantage of automated cell isolation in contrast to manual enrichment consists of standardizing protocols and preventing human errors while reducing costs and hands-on time. Commercial magnetic cell separation devices, i.e., an autoMACS® Separator (Miltenyi Biotec, Bergisch Gladbach, Germany) were strongly improved over the last few years but were mostly marketed to isolate abundant cell populations, rather than rare cells such as CTCs. With regard to the long-term goal of a low-cost diagnostic test, IsoMAG was characterized with in-house functionalized EpCAM beads minimizing material expenses to 35 EUR per 7.5 mL blood compared to 102 EUR for Miltenyi StraightFrom® Whole Blood CD326 MicroBeads. Conclusively, the overall aim of our study is the implementation of IsoMAG IMS unit as a core unit of the CTCelect for the fully automated isolation of single CTCs without sample preparation. Due to urgently needed low cost minimally invasive diagnostics methods in the clinical routine, allowing the sensitive and reliable detection of tumor components in patients' blood, the establishment of our IsoMAG IMS unit of CTCelect also represents a technology for single cell isolation and comprehensive downstream "omics"-based analyses. Such approaches will deepen our understanding of CTC pathobiology, a prerequisite for improved treatments and management of cancer patients in the future.

5. Conclusions

Here, the automated IsoMAG IMS unit was thoroughly characterized as a reliable, economic, and straightforward technology for automated and reproducible CTC detection and enrichment. In addition, the IsoMAG IMS system was shown to allow the use of variable cancer/CTC markers, such as cell surface vimentin. Its flexibility can be tailored to the user's specific needs for various malignancies and/or cell types. Future developments aim to combine immunomagnetic separation with microfluidic devices to further improve the power of automated immunomagnetic cell isolation devices for research and the clinics.

Supplementary Materials: The following are available online at https://www.mdpi.com/article/10.3390/diagnostics11112040/s1: Figure S1: Recovery rates of different cancer cell lines; Figure S2: Gel

electrophoresis of EpCAM RT-qPCR products from SCL-1 single cell RNA; Figure S3: Expression of EpCAM protein (A and B) and CSV (C and D) in HNSCCUM-02T; Figure S4: Potential CTCs could be enriched from whole blood of a HNSCC patient using EpCAM- and CSV beads; Figure S5: Brightfield microscopic images of HNSCCUM-02T cells cultivated after immunomagnetic isolation; Figure S6: Establishment of CTCelect unit improves purity of isolated tumor cells from whole blood; Table S1: Detailed protocol of IsoMAG isolation procedure.

Author Contributions: Conceptualization, A.G., J.S., C.F. and D.G.; methodology, A.G., J.S., L.L., S.M.N. and J.H.; validation and formal analysis, A.G., J.S., M.W., C.F. and D.G.; investigation, A.G., J.S., L.L., S.M.N. and M.W.; resources, R.H.S., C.F. and D.G.; data curation, A.G., J.S., C.F. and D.G.; writing, review and editing, A.G., J.S., M.W., J.K., J.H., R.H.S., C.F. and D.G.; visualization, A.G., J.S., C.F. and D.G.; project supervision and administration, R.H.S., C.F. and D.G.; funding acquisition, A.G. and D.G. All authors have read and agreed to the published version of the manuscript.

Funding: The work was supported by the Brigitte and Konstanze Wegener Stiftung, DFG, STFKH, intramural Funding of the University Medical Center Mainz, and by the Federal Ministry of Education and Research (131A020B; 03VP01061).

Institutional Review Board Statement: The study was conducted according to the guidelines of the Declaration of Helsinki, and approved by the local ethics committee (ref.no. 837.485.15 (10253); date 01/29/2016).

Informed Consent Statement: Informed consent was obtained from all subjects involved in the study.

Data Availability Statement: The data presented in this study are available on request from the corresponding authors.

Acknowledgments: The authors acknowledge Michael Baßler, Sabine Alebrand and all the team members of Fraunhofer IMM involved in the development of the *IsoMAG* IMS device. The authors would like to thank Ralf Himmelreich and Lisa Schott for their work, and Tom Teichmann for the preliminary experiments.

Conflicts of Interest: The authors declare no conflict of interest.

References

1. Kunzel, J.; Gribko, A.; Lu, Q.; Stauber, R.H.; Wunsch, D. Nanomedical detection and downstream analysis of circulating tumor cells in head and neck patients. *Biol. Chem.* **2019**, *400*, 1465–1479. [CrossRef] [PubMed]
2. Gül, D.; Habtemichael, N.; Dietrich, D.; Dietrich, J.; Gößwein, D.; Khamis, A.; Deuss, E.; Künzel, J.; Schneider, G.; Strieth, S.; et al. Identification of cytokeratin24 as a tumor suppressor for the management of head and neck cancer. *Biol. Chem.* **2021**. [CrossRef] [PubMed]
3. Siemer, S.; Fauth, T.; Scholz, P.; Al-Zamel, Y.; Khamis, A.; Gül, D.; Freudelsperger, L.; Wollenberg, B.; Becker, S.; Stauber, R.H.; et al. Profiling Cisplatin Resistance in Head and Neck Cancer: A Critical Role of the VRAC Ion Channel for Chemoresistance. *Cancers* **2021**, *13*, 4831. [CrossRef]
4. Beltz, A.; Gosswein, D.; Zimmer, S.; Limburg, I.; Wunsch, D.; Gribko, A.; Deichelbohrer, M.; Hagemann, J.; Stauber, R.H.; Kunzel, J. Staging of oropharyngeal squamous cell carcinoma of the head and neck: Prognostic features and power of the 8th edition of the UICC staging manual. *Eur. J. Surg. Oncol.* **2019**, *45*, 1046–1053. [CrossRef] [PubMed]
5. Kiweler, N.; Wunsch, D.; Wirth, M.; Mahendrarajah, N.; Schneider, G.; Stauber, R.H.; Brenner, W.; Butter, F.; Kramer, O.H. Histone deacetylase inhibitors dysregulate DNA repair proteins and antagonize metastasis-associated processes. *J. Cancer Res. Clin. Oncol.* **2020**, *146*, 343–356. [CrossRef]
6. Hu, Y.; Yu, X.; Xu, G.; Liu, S. Metastasis: An early event in cancer progression. *J. Cancer Res. Clin. Oncol.* **2017**, *143*, 745–757. [CrossRef] [PubMed]
7. Park, S.-Y.; Nam, J.-S. The force awakens: Metastatic dormant cancer cells. *Exp. Mol. Med.* **2020**, *52*, 569–581. [CrossRef]
8. Ashworth, T.R. A case of cancer in which cells similar to those in the tumours were seen in the blood after death. *Australas. Med. J.* **1869**, *14*, 146–147.
9. Murray, N.P.; Albarran, V.; Perez, G.; Villalon, R.; Ruiz, A. Secondary Circulating Tumor Cells (CTCs) but not Primary CTCs are Associated with the Clinico-Pathological Parameters in Chilean Patients With Colo-Rectal Cancer. *Asian Pac. J. Cancer Prev.* **2015**, *16*, 4745–4749. [CrossRef] [PubMed]
10. Wendel, M.; Bazhenova, L.; Boshuizen, R.; Kolatkar, A.; Honnatti, M.; Cho, E.H.; Marrinucci, D.; Sandhu, A.; Perricone, A.; Thistlethwaite, P.; et al. Fluid biopsy for circulating tumor cell identification in patients with early-and late-stage non-small cell lung cancer: A glimpse into lung cancer biology. *Phys. Biol.* **2012**, *9*, 016005. [CrossRef]

11. Engel, H.; Kleespies, C.; Friedrich, J.; Breidenbach, M.; Kallenborn, A.; Schondorf, T.; Kolhagen, H.; Mallmann, P. Detection of circulating tumour cells in patients with breast or ovarian cancer by molecular cytogenetics. *Br. J. Cancer* **1999**, *81*, 1165–1173. [CrossRef]
12. Jaeger, B.A.; Jueckstock, J.; Andergassen, U.; Salmen, J.; Schochter, F.; Fink, V.; Alunni-Fabbroni, M.; Rezai, M.; Beck, T.; Beckmann, M.W.; et al. Evaluation of two different analytical methods for circulating tumor cell detection in peripheral blood of patients with primary breast cancer. *Biomed. Res. Int.* **2014**, *2014*, 491459. [CrossRef] [PubMed]
13. Mocellin, S.; Hoon, D.; Ambrosi, A.; Nitti, D.; Rossi, C.R. The prognostic value of circulating tumor cells in patients with melanoma: A systematic review and meta-analysis. *Clin. Cancer Res.* **2006**, *12*, 4605–4613. [CrossRef] [PubMed]
14. de Bono, J.S.; Scher, H.I.; Montgomery, R.B.; Parker, C.; Miller, M.C.; Tissing, H.; Doyle, G.V.; Terstappen, L.W.; Pienta, K.J.; Raghavan, D. Circulating tumor cells predict survival benefit from treatment in metastatic castration-resistant prostate cancer. *Clin. Cancer Res.* **2008**, *14*, 6302–6309. [CrossRef]
15. Zhou, S.; Wang, L.; Zhang, W.; Liu, F.; Zhang, Y.; Jiang, B.; Wang, J.; Yuan, H. Circulating Tumor Cells Correlate With Prognosis in Head and Neck Squamous Cell Carcinoma. *Technol. Cancer Res. Treat.* **2021**, *20*, 1533033821990037. [CrossRef]
16. Kulasinghe, A.; Perry, C.; Jovanovic, L.; Nelson, C.; Punyadeera, C. Circulating tumour cells in metastatic head and neck cancers. *Int. J. Cancer* **2015**, *136*, 2515–2523. [CrossRef]
17. Muller, V.; Stahmann, N.; Riethdorf, S.; Rau, T.; Zabel, T.; Goetz, A.; Janicke, F.; Pantel, K. Circulating tumor cells in breast cancer: Correlation to bone marrow micrometastases, heterogeneous response to systemic therapy and low proliferative activity. *Clin. Cancer Res.* **2005**, *11*, 3678–3685. [CrossRef]
18. Weller, P.; Nel, I.; Hassenkamp, P.; Gauler, T.; Schlueter, A.; Lang, S.; Dountsop, P.; Hoffmann, A.C.; Lehnerdt, G. Detection of circulating tumor cell subpopulations in patients with head and neck squamous cell carcinoma (HNSCC). *PLoS ONE* **2014**, *9*, e113706. [CrossRef] [PubMed]
19. Pantel, K.; Alix-Panabieres, C. Circulating tumour cells in cancer patients: Challenges and perspectives. *Trends Mol. Med.* **2010**, *16*, 398–406. [CrossRef]
20. Pérez-Barrios, C.; Nieto-Alcolado, I.; Torrente, M.; Jiménez-Sánchez, C.; Calvo, V.; Gutierrez-Sanz, L.; Palka, M.; Donoso-Navarro, E.; Provencio, M.; Romero, A. Comparison of methods for circulating cell-free DNA isolation using blood from cancer patients: Impact on biomarker testing. *Transl. Lung Cancer Res.* **2016**, *5*, 665–672. [CrossRef] [PubMed]
21. Cristofanilli, M.; Broglio, K.R.; Guarneri, V.; Jackson, S.; Fritsche, H.A.; Islam, R.; Dawood, S.; Reuben, J.M.; Kau, S.W.; Lara, J.M.; et al. Circulating tumor cells in metastatic breast cancer: Biologic staging beyond tumor burden. *Clin. Breast Cancer* **2007**, *7*, 471–479. [CrossRef]
22. Tinhofer, I.; Staudte, S. Circulating tumor cells as biomarkers in head and neck cancer: Recent advances and future outlook. *Expert Rev. Mol. Diagn.* **2018**, *18*, 897–906. [CrossRef] [PubMed]
23. Satelli, A.; Mitra, A.; Brownlee, Z.; Xia, X.; Bellister, S.; Overman, M.J.; Kopetz, S.; Ellis, L.M.; Meng, Q.H.; Li, S. Epithelial-mesenchymal transitioned circulating tumor cells capture for detecting tumor progression. *Clin. Cancer Res.* **2015**, *21*, 899–906. [CrossRef] [PubMed]
24. Reisbeck, M.; Richter, L.; Helou, M.J.; Arlinghaus, S.; Anton, B.; van Dommelen, I.; Nitzsche, M.; Baßler, M.; Kappes, B.; Friedrich, O.; et al. Hybrid integration of scalable mechanical and magnetophoretic focusing for magnetic flow cytometry. *Biosens. Bioelectron.* **2018**, *109*, 98–108. [CrossRef]
25. Gribko, A.; Kunzel, J.; Wunsch, D.; Lu, Q.; Nagel, S.M.; Knauer, S.K.; Stauber, R.H.; Ding, G.B. Is small smarter? Nanomaterial-based detection and elimination of circulating tumor cells: Current knowledge and perspectives. *Int. J. Nanomed.* **2019**, *14*, 4187–4209. [CrossRef]
26. Siemer, S.; Wunsch, D.; Khamis, A.; Lu, Q.; Scherberich, A.; Filippi, M.; Krafft, M.P.; Hagemann, J.; Weiss, C.; Ding, G.B.; et al. Nano Meets Micro-Translational Nanotechnology in Medicine: Nano-Based Applications for Early Tumor Detection and Therapy. *Nanomaterials* **2020**, *10*, 383. [CrossRef]
27. Rauscher, H.; Sokull-Kluttgen, B.; Stamm, H. The European Commission's recommendation on the definition of nanomaterial makes an impact. *Nanotoxicology* **2013**, *7*, 1195–1197. [CrossRef]
28. Shashni, B.; Ariyasu, S.; Takeda, R.; Suzuki, T.; Shiina, S.; Akimoto, K.; Maeda, T.; Aikawa, N.; Abe, R.; Osaki, T.; et al. Size-Based Differentiation of Cancer and Normal Cells by a Particle Size Analyzer Assisted by a Cell-Recognition PC Software. *Biol. Pharm. Bull.* **2018**, *41*, 487–503. [CrossRef]
29. Nichols, A.C.; Lowes, L.E.; Szeto, C.C.; Basmaji, J.; Dhaliwal, S.; Chapeskie, C.; Todorovic, B.; Read, N.; Venkatesan, V.; Hammond, A.; et al. Detection of circulating tumor cells in advanced head and neck cancer using the CellSearch system. *Head Neck* **2012**, *34*, 1440–1444. [CrossRef]
30. Riethdorf, S.; Fritsche, H.; Muller, V.; Rau, T.; Schindlbeck, C.; Rack, B.; Janni, W.; Coith, C.; Beck, K.; Janicke, F.; et al. Detection of circulating tumor cells in peripheral blood of patients with metastatic breast cancer: A validation study of the CellSearch system. *Clin. Cancer Res.* **2007**, *13*, 920–928. [CrossRef] [PubMed]
31. Riethdorf, S.; O'Flaherty, L.; Hille, C.; Pantel, K. Clinical applications of the CellSearch platform in cancer patients. *Adv. Drug Deliv. Rev.* **2018**, *125*, 102–121. [CrossRef]
32. Obayashi, K.; Akatsuka, J.; Endo, Y.; Takeda, H.; Hayashi, T.; Toyama, Y.; Suzuki, Y.; Hamasaki, T.; Kimura, G.; Ohnaga, T.; et al. Initial detection of circulating tumor cells from metastatic prostate cancer patients with a novel small device. *Prostate Int.* **2019**, *7*, 131–138. [CrossRef]

33. Boukamp, P.; Tilgen, W.; Dzarlieva, R.T.; Breitkreutz, D.; Haag, D.; Riehl, R.K.; Bohnert, A.; Fusenig, N.E. Phenotypic and genotypic characteristics of a cell line from a squamous cell carcinoma of human skin. *J. Natl. Cancer Inst.* **1982**, *68*, 415–427.
34. Welkoborsky, H.J.; Jacob, R.; Riazimand, S.H.; Bernauer, H.S.; Mann, W.J. Molecular biologic characteristics of seven new cell lines of squamous cell carcinomas of the head and neck and comparison to fresh tumor tissue. *Oncology* **2003**, *65*, 60–71. [CrossRef]
35. Gribko, A.; Hahlbrock, A.; Strieth, S.; Becker, S.; Hagemann, J.; Deichelbohrer, M.; Hildebrandt, A.; Habtemichael, N.; Wunsch, D. Disease-relevant signalling-pathways in head and neck cancer: Taspase1's proteolytic activity fine-tunes TFIIA function. *Sci. Rep.* **2017**, *7*, 14937. [CrossRef] [PubMed]
36. Goesswein, D.; Habtemichael, N.; Gerhold-Ay, A.; Mazur, J.; Wunsch, D.; Knauer, S.K.; Kunzel, J.; Matthias, C.; Strieth, S.; Stauber, R.H. Expressional analysis of disease-relevant signalling-pathways in primary tumours and metastasis of head and neck cancers. *Sci. Rep.* **2018**, *8*, 7326. [CrossRef]
37. Wünsch, D.; Hahlbrock, A.; Heiselmayer, C.; Backer, S.; Heun, P.; Goesswein, D.; Stocker, W.; Schirmeister, T.; Schneider, G.; Kramer, O.H.; et al. Fly versus man: Evolutionary impairment of nucleolar targeting affects the degradome of Drosophila's Taspase1. *FASEB J.* **2015**, *29*, 1973–1985. [CrossRef] [PubMed]
38. Deuss, E.; Gosswein, D.; Gul, D.; Zimmer, S.; Foersch, S.; Eger, C.S.; Limburg, I.; Stauber, R.H.; Kunzel, J. Growth Factor Receptor Expression in Oropharyngeal Squamous Cell Cancer: Her1-4 and c-Met in Conjunction with the Clinical Features and Human Papillomavirus (p16) Status. *Cancers* **2020**, *12*, 3358. [CrossRef] [PubMed]
39. Barak, V.; Goike, H.; Panaretakis, K.W.; Einarsson, R. Clinical utility of cytokeratins as tumor markers. *Clin. Biochem.* **2004**, *37*, 529–540. [CrossRef]
40. Foddai, A.; Elliott, C.T.; Grant, I.R. Maximizing capture efficiency and specificity of magnetic separation for Mycobacterium avium subsp. paratuberculosis cells. *Appl. Environ. Microbiol.* **2010**, *76*, 7550–7558. [CrossRef] [PubMed]
41. Foddai, A.C.G.; Grant, I.R. A novel one-day phage-based test for rapid detection and enumeration of viable Mycobacterium avium subsp. paratuberculosis in cows' milk. *Appl. Microbiol. Biotechnol.* **2020**, *104*, 9399–9412. [CrossRef] [PubMed]
42. Siemer, S.; Westmeier, D.; Barz, M.; Eckrich, J.; Wunsch, D.; Seckert, C.; Thyssen, C.; Schilling, O.; Hasenberg, M.; Pang, C.; et al. Biomolecule-corona formation confers resistance of bacteria to nanoparticle-induced killing: Implications for the design of improved nanoantibiotics. *Biomaterials* **2018**, *192*, 551–559. [CrossRef] [PubMed]
43. Hussain, T.; Gellrich, D.; Siemer, S.; Reichel, C.A.; Eckrich, J.; Dietrich, D.; Knauer, S.K.; Stauber, R.H.; Strieth, S. TNF-alpha-Inhibition Improves the Biocompatibility of Porous Polyethylene Implants In Vivo. *Tissue Eng. Regen. Med.* **2021**, *18*, 297–303. [CrossRef]
44. Westmeier, D.; Siemer, S.; Vallet, C.; Steinmann, J.; Docter, D.; Buer, J.; Knauer, S.K.; Stauber, R.H. Boosting nanotoxicity to combat multidrug-resistant bacteria in pathophysiological environments. *Nanoscale Adv.* **2020**, *2*, 5428–5440. [CrossRef]
45. Stauber, R.H.; Siemer, S.; Becker, S.; Ding, G.B.; Strieth, S.; Knauer, S.K. Small Meets Smaller: Effects of Nanomaterials on Microbial Biology, Pathology, and Ecology. *ACS Nano* **2018**, *12*, 6351–6359. [CrossRef]
46. Stauber, R.H.; Westmeier, D.; Wandrey, M.; Becker, S.; Docter, D.; Ding, G.B.; Thines, E.; Knauer, S.K.; Siemer, S. Mechanisms of nanotoxicity—Biomolecule coronas protect pathological fungi against nanoparticle-based eradication. *Nanotoxicology* **2020**, *14*, 1157–1174. [CrossRef]
47. Sieuwerts, A.M.; Kraan, J.; Bolt-de Vries, J.; van der Spoel, P.; Mostert, B.; Martens, J.W.; Gratama, J.W.; Sleijfer, S.; Foekens, J.A. Molecular characterization of circulating tumor cells in large quantities of contaminating leukocytes by a multiplex real-time PCR. *Breast Cancer Res. Treat.* **2009**, *118*, 455–468. [CrossRef]
48. Chudziak, J.; Burt, D.J.; Mohan, S.; Rothwell, D.G.; Mesquita, B.; Antonello, J.; Dalby, S.; Ayub, M.; Priest, L.; Carter, L.; et al. Clinical evaluation of a novel microfluidic device for epitope-independent enrichment of circulating tumour cells in patients with small cell lung cancer. *Analyst* **2016**, *141*, 669–678. [CrossRef]
49. Ciccioli, M.; Bravo-Santano, N.; Davis, A.; Lewis, J.; Malcolm, R.; Pailhes-Jimenez, A.S. Mesenchymal markers: The new avenue for circulating tumor cells detection. In Proceedings of the ANGLE plc AACR 2021, Virtual Meeting, 9–14 April 2021.
50. Grover, P.K.; Cummins, A.G.; Price, T.J.; Roberts-Thomson, I.C.; Hardingham, J.E. Circulating tumour cells: The evolving concept and the inadequacy of their enrichment by EpCAM-based methodology for basic and clinical cancer research. *Ann. Oncol.* **2014**, *25*, 1506–1516. [CrossRef]
51. Grisanti, S.; Almici, C.; Consoli, F.; Buglione, M.; Verardi, R.; Bolzoni-Villaret, A.; Bianchetti, A.; Ciccarese, C.; Mangoni, M.; Ferrari, L.; et al. Circulating tumor cells in patients with recurrent or metastatic head and neck carcinoma: Prognostic and predictive significance. *PLoS ONE* **2014**, *9*, e103918. [CrossRef]
52. Menarini Silicon Biosystems Inc. Available online: https://documents.cellsearchctc.com/pdf/e631600006/e631600006_EN.pdf (accessed on 10 October 2021).

8. APPENDIX

8.1 List of Figures and Tables

8.2 Abbreviations and units

aa	amino acids
Akt	protein kinase B
CDKN2A	cyclin dependent kinase inhibitor 2A
cKRT	cytokeratin
CSV	cell surface vimentin
CTC	circulating tumor cell
DNA	deoxyribonucleic acid
ECM	extracellular matrix
e.g.	for example
EGFR	epithelial growth factor receptor
EMT	epithelial-mesenchymal transition
EpCAM	epithelial cell adhesion molecule
FACS	fluorescence activated cell sorting
FDA	Food and Drug Administration
GFP	green fluorescent protein
GST	glutathione-S-transferase
HDAC	histone deacetylase
HDACi	histone deacetylase inhibitor
HNC	head and neck cancer
HNSCC	head and neck squamous cell carcinoma
HPV	human papilloma virus
IAP	inhibitors of apoptosis
i.e.	*lat.*, id est
IF	intermediate filament
MET	mesenchymal-epithelial transition
MLL	mixed lineage leukemia
mRNA	messenger RNA

NES	nuclear export signal
NLS	nuclear localization signal
OSF-2	osteoblast-specific factor 2
PI3K	phosphoinositide-3 kinase
POSTN	periostin
RNA	ribonucleic acid
RT-PCR	reverse transcriptase polymerase chain reaction
SV40	simian virus 40
Taspase1	Threonin Aspartase 1
TFIIA	transcription factor II A
UICC	Union for International Cancer Control
USF2	upstream transcription factor 2

Units and measures

Da	Dalton	k	kilo (10^3)
m	meter	µ	mikro (10^{-6})

Amino acids

A	Ala	alanine
C	Cys	cysteine
D	Asp	aspartic acid
E	Glu	glutamic acid
F	Phe	phenylalanine
G	Gly	glycine
H	His	histidine
I	Ile	isoleucine
K	Lys	lysine
L	Leu	leucine
M	Met	methionine
N	Asn	asparagine
P	Pro	proline
Q	Gln	glutamine
R	Arg	arginine
S	Ser	serine
T	Thr	threonine
V	Val	valine
W	Trp	tryptophan
Y	Tyr	tyrosin